Equilibrium and Uptake Kinetics of Copper and Cadmium ions by the Microalgae, *Chlorella vulgaris* and *Scenedesmus obliquus*

A Thesis submitted to Newcastle University for the Degree of Doctor of Philosophy

by

James Hockaday

School of Engineering

Newcastle University, United Kingdom

March 2021

Abstract

The removal of heavy metals from wastewater is an important step in a wastewater treatment process. Some metals are essential minerals, but others such as copper and cadmium are toxic when consumed. Microalgae have been identified as organisms that can tolerate and accumulate heavy metals. This tolerance offers a potential mechanism for metal removal that is cheaper and more efficient than current conventional methods.

In this research, two species of microalgae, *C. vulgaris* and *S. obliquus* were exposed to water that was contaminated with copper and cadmium at concentrations of 0.25, 0.5, 0.75 and 2.5mg.L^{-1}. The binding capacity of the microalgae biomass to the metal ions increased linearly with the size of the ratio of the initial concentration of the metal ions to the initial concentration of the microalgae. The total metal ion removal from solution appeared to be independent of initial concentrations however, with *C. vulgaris* removing between 88% and 90% of the copper with all concentration combinations investigated.

Based on equilibrium studies, the Freundlich Isotherm was concluded to best represent the experimental data. The linear Freundlich isotherms had R^2 values greater than 0.98 for all experiments, and the Freundlich Isotherm assumptions relate more to the heterogeneity of the algae surface. The Langmuir isotherm showed a stronger linear correlation with R^2 values greater than 0.99 in all cases, but did not produce realistic model parameters for the adsorption of copper by *C. vulgaris*.

The adsorption kinetics of the metals were investigated and compared by fitting the Lagergren, Second-order model, the Elovich model and a kinetic expression derived from the Langmuir Isotherm to the experimental data. The second order model was found to fit experimental data more accurately than the Elovich and the Lagergren models when parameters were obtained by linearising the data. The Langmuir rate equation was approximated to the Lagergren model and the second order model, and based on the analysis the Lagergren model with parameters derived from the Langmuir Isotherm was most appropriate to model metal adsorption by *S. obliquus*.

The current study analysed techniques used to compare the binding capacities of *C. vulgaris* and *S. obliquus*, and determined that both species were successful adsorbents for copper and cadmium. It was concluded from the rate expressions that *C. vulgaris* adsorbed the metal ions at a faster rate than *S. obliquus*, and has a higher capacity to both metal species. This would suggest that out of the two species of microalgae, *C. vulgaris* would be most suitable for metal removal for wastewater treatment purposes.

Acknowledgements

First and foremost I'd like to express my gratitude to my parents, Colin Hockaday and Dr Ruth Hardstaff without whom I would not have had the opportunity to return to university to study undergraduate Chemical Engineering and would have been unable to pursue this PhD. An extra thanks should be awarded to them for putting up with me during this tumultuous year where I have been writing my thesis from the safety of Australia while the rest of the world struggled with the Covid-19 pandemic.

Secondly, to my supervisors. In alphabetical order, Professor Adam Harvey; of all the memories of the PhD process the most vivid will always be the playing of dominos in Beamish Museum and watching him let off steam by hoop-trundling in a 19th century school playground. Adam's grounded and relaxed demeanour and advice helped ease my anxiety and self-doubt over many occasions during my PhD experience. Without his calm guidance I do not think I could have completed this PhD.

In chronological order, working with Dr Sharon Velasquez-Orta has taken me to Mexico, provided funding to pursue a PhD, and directed towards the opportunity to work with industry. These are among the most significant moments of my life and it is difficult to express how valuable these three experiences have been. If it was not for Dr Velasquez-Orta, this project would not have happened and my life would be unrecognisable. I sincerely hope my efforts and work has done her justice for the opportunities she has provided.

Shortly before lockdown, I regained contact with my old Pharmacology project partner, Atefeh Beigi. Since then she has provided invaluable support throughout my writeup period, and has shown me unparalleled patience. Her encouragement and support have kept me going for the final twelve months of this process and I look forward to many years of repaying my gratitude.

I also would like to thank Dr Gary Caldwell, Dr Isaac Nava Bravo, Matthew Pickersgill and the MEng student who contributed to this work, Alex Hunt. Dr Gary Caldwell has offered invaluable support, while not being a member of my supervisory team,

and has accommodated me in his labs. Isaac took me under his wing when I was a masters student, and looked after me while I was in Mexico. I dearly hope to be able to work with him in future. Matt Pickersgill supported me on while on placement at Bran Sands, where I helped initiate a pilot scale project. Thanks to his patience and trust, I was able to get hands on experience in industry. Finally, Ian Hockaday who was supportive and offered advice and helped me iron out bugs in MS Word when writing this thesis.

My experience over the previous four years has enhanced my motivation, and has provided me with the ambition to pursue future projects that address the questions and other research areas highlighted by this project.

Contents

Table of Figures

List of Tables

Chapter 1 Introduction

1.1 Background and Motivation

When heavy metals are released into the environment, they are conserved as there are no mechanisms for their breakdown. The metals can be transformed or can form complexes with organic compounds, but once they enter the food chain they are retained and conserved, passed on from prey to predator causing irreparable damage [1-3].

Any metalloid can be classed as a heavy metal if it has the potential to be bioaccumulated [4]. Some of these metals are essential components of metabolic processes, while metals such as cadmium, mercury and lead are toxic both aquatic and terrestrial life [4].

These metals are often present in industrial effluents that require treatment before release to the environment. Conventionally, both chemical and biological methods are utilised in the wastewater treatment process [5]. Usually the removal of metal from waste effluent is a quaternary process and the final stage prior to release back into the environment. The addition of potassium hydroxide is a cost effective method for settling metals out of solution for metal concentrations above 10mg.L^{-1} [6].

For metals such as cadmium and mercury, to meet effluent consent the concentration of these metals have to be reduced considerably lower than 10mg.L^{-1}. Technologies such as ion exchange or electrowinning can be used to reduce metal ion concentrations to below these levels, but these technologies incur considerable operating costs and are prone to fouling [6]. The reduction of heavy metal concentrations to parts per billion levels ($\times 10^{-3}$ mg.L^{-1}) at large scale incurs considerable processing costs [4].

Microalgae have evolved sensitive mechanisms to obtain nutrient metals that are present in trace quantities from their environment [7]. As well as the ability to be able to remove nutrient metals, microalgae have been shown to be able to bind

non-essential metals such as cadmium [8, 9]. Microalgae are also able to consume compounds that can cause eutrophication such as phosphorous and nitrogenous compounds, so offer the opportunity to remove numerous harmful pollutants in a single process [10, 11].

There have been few previous studies that have investigated the kinetics of metal removal by microalgae, with three early papers recognising the dual process of fast adsorption followed by a slower metabolically driven internalisation of the metals [7, 12, 13], while more recent papers focus primarily on the initial, fast adsorption process by applying the Lagergren and second order model to the data [14-17]. The majority of metal sorption studies using microalgae mainly investigate the final bioaccumulation of the algal biomass, focussing primarily on equilibrium studies [18-27].

Technology that utilises algae biomass has been developed specifically for the purpose of metal removal from contaminated waters. AlgaSORB® utilises dead algae or cyanobacteria that has been fixed in a bio-resin [28]. This has an advantage of reusability in that it has been shown to be effective for multiple adsorption/desorption cycles over a two-year period, but as this uses deactivated microalgae it does not have the advantages of being a self-replenishing biosorbent.

The benefit of cultivating microalgae in the presence of the heavy metals copper and cadmium have been observed by Yang et al (2015), showing that the presence of these metals enhanced the lipid production by the microalgae *Chlorella minutissima* [29]. This demonstrated the potential that live microalgae has for the heavy metal removal from solution, while producing important energy precursors for the production of biofuels [30]. This current study investigates the kinetics of adsorption of copper and cadmium by two species of microalgae, *Chlorella vulgaris* and *Scenedesmus obliquus*, using kinetic models that have been applied to other biosorbents in literature, and attempts to put the models into theoretical context by applying the scarcely used Langmuir kinetic model to the adsorption data. This will provide a mechanism to compare the species of microalgae when designing processes that remove metals from contaminated water, that use microalgae.

1.2 Aims and Objectives

The overall aim of this project is to evaluate the suitability of two species of microalgae, *Chlorella vulgaris* and *Scenedesmus obliquus* for the purpose of metal removal from contaminated waste water. To determine their suitability, and number of outcomes are necessary.

1. Determine which species has the highest metal binding capacity.
2. Determine whether there are any effects caused by fluctuations in metal concentration.
3. Investigate whether adsorption isotherms could be fitted to equilibrium data.
4. Determine which algae has the highest metal uptake rate by fitting rate expressions to the experimental data.

To achieve these outcomes, copper and cadmium were selected for study and a number of objectives were set.

Objective 1: to cultivate microalgae and devise experiments that capture the time profiles for the removal of metal ions from contaminated water. This would involve

- Cultivation of stocks of *Chlorella vulgaris* and *Scenedesmus obliquus* and to create standard curves that can be used to measure microalgae biomass concentration by UV-vis.
- Develop a protocol for stabilising metal solutions and samples for analysis by ICP-OES and ICP-MS.
- Undertake experiments to record the metal the variation over time in metal concentration of a solution exposed to microalgae biomass.

Objective 2: to record and compare the capacity of the algae *Chlorella vulgaris* and *S. obliquus* has to copper and cadmium. This would involve:

- Investigating the effect of metal concentration in solution on the capacity of the microalgae to the metal ion.
- Investigation of the limit of metal removal by microalgae.
- Fitting adsorption isotherms to equilibrium data to compare model parameters between the species of micoralgae.

Objective 3: to produce mathematical models that capture the adsorption kinetics of the heavy metals by the microalgae. This would involve:

- Collection of metal uptake data by each species of microalgae, and transforming it to adsorption data.
- Fit the three common adsorption kinetic models
    - Lagergren.
    - Second Order.
    - Elovich.
- Investigation of the hybrid kinetic form of the Langmuir rate equation to determine whether the Lagergren, the second order model or a hybrid model containing components of the Lagergren and second order model is most suitable to model metal uptake by microalgae.
- Investigation into whether the presence of a second metal affects the adsorption rate of the metal ions by the microalgae.

Objective 4: Investigate the practicalities of using microalgae for the removal of microalgae. This would involve:

- Preliminary studies into the immobilisation of the microalgae using paper biocomposites to investigate whether the presence of microalgae improves the metal sorption performance of the biocomposite.
- Investigate the removal of metals from industrial wastewater samples using a novel species of algae *Oocystis sp*. that was identified on the site of a wastewater treatment plant.

Chapter 2 Literature Survey

2.1 Background

2.1.1 Climate Impact of Wastewater Treatment

Wastewater treatment processes release greenhouse gasses (GHGs), such as carbon dioxide (CO_2), methane (CH_4) and nitrous oxide (N_2O) as by-products [31]. N_2O is a concern as it is 310 times more potent as a GHG than CO_2, and has an atmospheric lifespan of 120 years. Indonesia, USA, India and China accounted for 50% of global N_2O from wastewater. Furthermore, wastewater treatment in the USA in the year 2000 accounted for 9% of global CH_4 emissions. When wastewater is released without prior treatment, the overall GHG emissions are higher [31].

Globally, the number of wastewater treatment processes will grow in future years, as the pressure on fresh water resources are ever-increasing due to growing populations. Currently in sub-Saharan Africa water stress is around 70%, which means that 70% of the available freshwater water is currently utilised. With further industrialization and without better water management, there is a considerable risk of demand exceeding supply [32]. Expanding wastewater treatment plants using more sustainable technologies will be an important component to reducing the global GHG emissions.

The main source of N_2O during the wastewater treatment process is the activated sludge process [33]. Anaerobic digestion increases the production of CH_4, but this has the added advantage of being collected for fuel [33]. Nitrogen removal by *C. vulgaris* showed an increase in mitochondria production within the cells, suggesting that the cells are consuming the nitrogen from the wastewater [34], although *C. vulgaris* itself has been observed as a source of N_2O release [35]. However there is evidence that microalgae can consume large quantities of dissolve nitrogen compounds [36].

2.2 Current Wastewater Treatment Processes and Technologies

Wastewater treatment is a series of processes that sequentially remove solid particles and hazardous compounds from a variety of wastewaters. The most common wastewater is the municipal wastewater that originates from domestic dwellings, however agricultural and industrial wastewaters usually contain compounds that are more hazardous to the environment [37].

The larger wastewater treatment plants will treat wastewater from a variety of sources, and in the UK the most common treatment process involves an Activated Sludge (AS) stage. The process as a whole can be simplified into three (sometimes four), treatment stages;

1. Primary wastewater treatment
2. Secondary wastewater treatment
3. Tertiary wastewater treatment

(4) Quaternary wastewater treatment

The primary wastewater treatment stage is a phase separation stage that removes solids such as sand, grit and dense organic solids. The liquid phase then proceeds to the secondary wastewater treatment stage where dissolved nutrient compounds (mainly phosphates and nitrates), are removed by an Activated Sludge process. This is an aerobic process where the growth of respirating microorganisms is facilitated; it is these microorganisms that consume the nitrate and phosphate compounds.

The AS process causes the accumulation of organic solids within the treated water. The tertiary wastewater treatment process is a clarification process where the organic solids are settled anaerobically. A portion of the settled solids are then recycled to the AS process, while excess sludge is further processed and disposed of. In the absence of industrial pollutants and if the effluent meets regulations, the supernatant of the settled treated wastewater could then be released into the environment. In the majority of treatment processes, a further treatment process is required that incurs high operational costs and is necessary to remove metals, pharmaceuticals and other toxic materials. A theoretical process flow diagram is shown in Figure 1, with the main process as described shown as a central linear

process from "*Sewage*" to *"Treated Wastewater Release*". In reality the process is more complex, with further processing stages that process the biproducts of the wastewater treatment process.

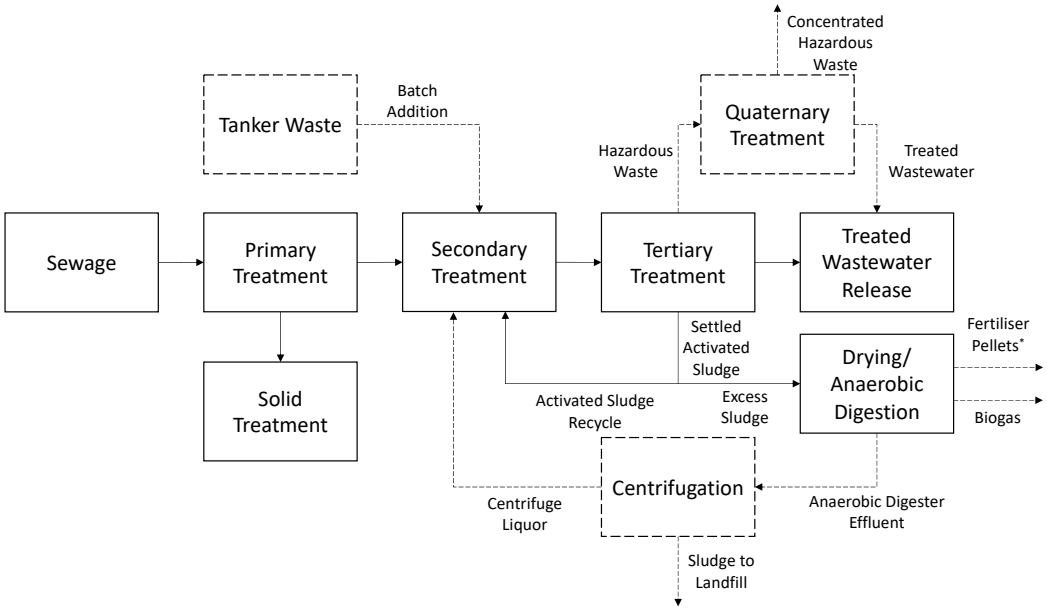

Figure 1: Flow diagram of a conventional wastewater treatment plant, with the Secondary Treatment stage facilitated by an Activated Sludge Process. Unit operations represented by dashed lines are not ubiquitous, but are present in in many processes and are becoming more prominent.

From an emissions perspective, there are GHGs released in all three of the main wastewater treatment processes displayed in Figure 1. During the primary treatment, solid waste settles to the bottom of a large tank, bringing with it bacteria that can undergo anaerobic respiration causing the release of methane (CH_4).

During the AS process, carbon dioxide (CO_2) is released by the microorganism as they proliferate and consume the eutrophication-causing compounds. One method by which nitrogenous compounds are removed from wastewaters is the oxidation to nitrous oxide gas (N_2O). This is especially problematic if the waste contains high levels of ammonia [38]. Following the AS process, the wastewater undergoes tertiary treatment where the wastewater is transferred to a clarifier and the sludge is allowed to settle anaerobically. During this process, the remaining dissolved oxygen is consumed and remaining nitrogenous compounds are also broken down. This causes the release of CO_2 and N_2O in smaller quantities compared to the AS process. As the solids settle to the base of the clarifier, the remaining bacteria begin to undergo anaerobic respiration, which leads to the further release of CH_4.

Some sites incorporate an anaerobic digestion (AD) stage to treat settled solids and spent activated sludge that would otherwise be broken down aerobically and anaerobically leading to the release of CO_2 and CH_4. The AD process anaerobically treats the solids in a controlled system to produce CH_4 that can be collected and used for fuel. The AD process also produces wastewater that has a high ammonia concentration, with a high solid content. During the colder months of winter, treating biproducts produced by AD processes via AS becomes less efficient, with a reduced rate of removal of ammonia [39, 40].

If there are toxic compounds such as pharmaceuticals or if the wastewater has a high concentration of heavy metals, the wastewater will require quaternary treatment prior to release. This process usually occurs at the end of the wastewater treatment process as the technologies used to remove these pollutants can be fouled by solids present in the wastewater.

The most common method of metal removal involves the addition of potassium hydroxide to increase the pH and cause the dissolved metal ions to precipitate out of solution in the form of metal hydroxides. Increasing the pH this way would negatively impact the AS process without pH correction [6]. Potassium hydroxide addition is effective for metal concentrations above $10mg.L^{-1}$, and produces a sludge that is rich in heavy metals and requires further processing.

Alternative technologies such as ion exchange are expensive, prone to fouling and for a $20,000m^3$ per day (i.e. large-scale) treatment process, the operating cost adjusted for inflation would be an additional £2.1 million annual operating cost for the one unit operation [6]. For comparison, a study in southern Spain analysed the cost of wastewater treatment of urban wastewater had an upper estimate of a total process cost of £5.9 million for $20,000m^3$ per day where only secondary wastewater treatment was employed [41]. Therefore ion exchange is rarely used and is often only used for purification of drinking water [10].

More cost effective alternatives for metal removal often utilise adsorption processes, with biosorbents of particular interest [37]. If an algae process can be used for wastewater treatment, it would employ a self-replenishing adsorbent that

has the potential to reduce metals to parts per billion levels and produce secondary high value products such as biofuels [5, 29, 42-45].

Industries that involve electroplating, metal surface treatment processes and oil refining intrinsically will produce harmful waste effluent, but metal wastes are also produced from more unexpected sources. The production of printed circuit boards and photographic films also cause the production of heavy metal wastes, but so do certain treatments used in the wood processing industry [37]. Many of these processes are labour intensive and part of the manufacturing industry, which for decades have been outsourced on a large scale to developing nations to reduce manufacturing costs [46]. These nations often have less stringent regulations, and as the process for reducing levels of these pollutants to acceptable levels is expensive; many developing nations are neglecting to thoroughly treat wastewater in favour of cheaper processing and more rapid economic development [10, 47].

Algae-based unit operations could be used alongside conventional systems to reduce the nitrogen and heavy metal load prior to activated sludge processes. This has the potential to reduce the CO_2 and N_2O emissions for the wastewater treatment process as well as reducing heavy metal content of the wastewater, prior to the Activated Sludge (AS) process. With the volumes of wastewater being treated, the AS process cannot be replaced using a microalgae only system. AS processes are not limited by light penetration, so they are undertaken in large vessels with considerable depth; algae cultivations need a shallow depth to facilitate optimum light penetration [40]. To process the same volume as AS systems, the microalgae system will require a considerable area to compensate the reduction in depth.

Heavy metals can generally be defined as a metal that has an atomic mass of greater than 20amu. However in an ecological sense, any metalloid can be classed as a heavy metal [4]. Some of these metals are essential (in trace quantities) for plant and algae growth [48]. These include zinc, copper, manganese and cobalt. However, others that are present in effluent waterways are toxic to biological life, including mercury, cadmium and lead [4].

The UK follows EU directives for the treatment of wastewaters, with the Urban Wastewater Treatment Directive (91/271/EEC) setting limits for nitrogen and phosphorus limits that can be released into the environment. Activated sludge processes are sufficient to remove these salts to acceptable levels, however metals such as copper and cadmium are regulated by more stringent legislation, and their removal requires more intensive processing techniques.

The Dangerous Substances Directive (76/464/EEC) classifies toxic agents into lists. Cadmium is categorised into List I, which contains substances that pose a severe and everlasting threat to the environment, whereas copper is categorised into List II. List II also contains substances of significance when it comes to toxicity, but their effects are less severe than those present in List I. For England and Wales, any effluent discharge must contain less than 10×10^{-3} mg.L^{-1} of copper, and less than 5×10^{-3} mg.L^{-1} of cadmium. To achieve this, a mixture of chemical precipitation and ion exchange is often utilised and this is an expensive process [4, 49].

From a pollution prevention standpoint, it is desirable to transform the metals to less toxic forms, but it is important to prevent the release of these stable complexes to the environment as they will be converted to more hazardous forms. Metals are conserved in the environment; they cannot be broken down, and if they enter the food chain they will be passed on from prey to predator causing irreparable damage [1-3].

Conventionally, chemical methods have been used alongside biological methods for many years in the wastewater treatment process [5]. The removal of metal from waste effluent is a difficult process and is associated with high processing costs especially when reducing concentrations of metals to parts per billion levels [4]. Conventional methods for removal metal ions from solution include precipitation and flotation, membrane filtration, adsorption and electrodialysis.

Adsorption processes are most cost effective, but they have the drawback of producing a highly contaminated adsorbent that requires further treatment. Adsorbents can be composed of synthetically produced zeolites, or industrial or agricultural bi-products. Similarly to chemical precipitation and flocculation, the

metal ions are precipitated out of solution and are separated from the bulk liquid by sedimentation or flotation, and the process is unselective in which metal ions are removed from the solution [37].

Membrane filtration and electrodialysis have better selectivity but these are more expensive to operate. Ultrafiltration has a pore size range of 5 to 20nm, and nanofiltration use membranes with a pore size between 0.5 to 2 nm. Ultrafiltration membranes are able to remove materials with a mass as low as 1000Da (1.7×10^{-21}g), and nanofiltration membranes are able to remove materials with a mass as low as 200Da (3.3×10^{-22}g). As a result these membranes are easily fouled by components present in wastewaters [37].

Electrodialysis is another membrane separation technique that separates metal ions from the bulk liquid across an ion exchange membrane. Figure 2 displays the simplified mechanism by which electrodialysis operates. The anode and cathode chambers are separated from the bulk liquid by cation exchange membranes. These membranes are semipermeable to cations, and impermeable to anions. A voltage is applied across the anode and the cathode causing the positive cations to migrate towards the anode across the cation exchange membrane. The anions migrate towards the cathode, but are unable to cross the cation exchange membrane and remain in the bulk liquid.

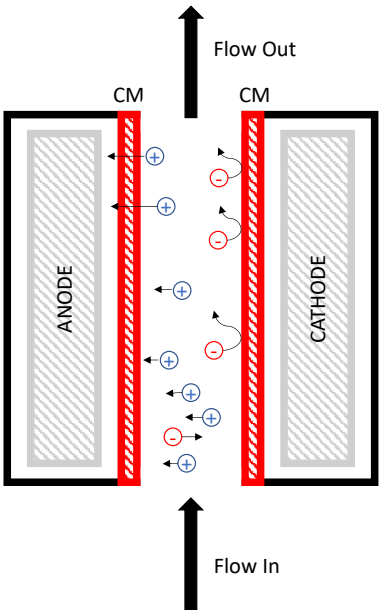

Figure 2: Mechanism of action by Electrodialysis. CM – the cation exchange membrane that separates the anode and cathode chambers from the flow of contaminated water.

Electrodialysis incurs both operating and maintenance costs due to the power usage of the system and the clearing of the membranes which are easily fouled by components within the wastewater [37]. Additionally, cation exchange membranes have a significant capital cost, with a commercially available Nafion® perflouronated membrane costing approximately £9500 per square metre [50].

Many species of microalgae have been shown to bind metals, and to remove and utilise nitrogen present in contaminated waters. Algae are able to directly absorb nitrogenous compounds, and are able to oxidise these compounds prior to uptake [10]. Biological mechanisms are more efficient at removing nitrogen when compared to removing phosphorus [11], but *Chlorella vulgaris* is still able to achieve a removal efficiency of phosphorous up to 55% [10].

Algae has been shown to be highly effective at removing nitrogen in the form of ammonia, and is also capable of removing phosphates from wastewaters. As a result algae are being more widely employed during wastewater treatment as they offer a cheaper alternative to conventional, chemical treatments [43, 51].

Treating wastewater using microalgae could offer a dual purpose of algae cultivation for biofuels, while simultaneously treating wastewater for safe release

into the environment. This could potentially reduce the cost for both biomass cultivation and the costs associated with wastewater treatment [52].

Difficulties occur however when treating industrial wastewater. Industrial wastewater can contain many toxins that could be harmful to the algae, and although algae has been shown to be effective at heavy metal sequestering, there is disagreement between sources where some studies suggest treatment using algae is not as efficient as chemical treatment [40], whereas others studies suggest treatment by microalgae is more efficient [17, 53]. Industrial wastewaters may also not contain the necessary levels of nitrogen and phosphorous required for algae growth [40].

2.3 Microalgae

Microalgae are one of the oldest living organisms on Earth. They are unicellular, aquatic organisms that have a high reproductive rate [54]. Microalgae have been studied extensively in the past for their ability to be cultivated in wastewater and for their potential for biofuel production [55]. Microalgae are able to accumulate energy compounds such as carbohydrates and lipids, and many proteins produced by microalgae are potential pre-cursors to high value compounds [43]. This property of the microalgae allows for the potential to integrate wastewater treatment to the production of biofuels, or for the production of other high value compounds such as the production of certain precursors of certain pharmaceuticals, vitamins and cosmetics [43, 44, 56, 57].

A major advantage of microalgae over terrestrial plants is that the photosynthetic rate of microalgae is higher than that of the land-based fuel crops. Microalgae cells absorb excess photons and excess CO_2: more than is required for the photosynthesis process [58]. This is a cellular defence mechanism evolved to saturate the cellular cytoplasm with CO_2 to prevent photorespiration which irreversibly consumes the enzyme, rubisco. For every gram of algal biomass produced via photosynthesis, approximately 1.8g of carbon dioxide is consumed [59, 60].

The most common form of photosynthesis that is utilised by microalgae is oxygenic photosynthesis, which produces oxygen as a by-product of the reaction [40]. It is

for this reason that microalgae saturate their cytoplasm with carbon dioxide to out compete the oxygen for Rubisco. Photosynthetic organisms primarily produce cellular precursors for their metabolic processes via the Calvin Cycle. The Rubisco-catalysed reaction involves the fixation of CO_2 to Ribulose 1,5-bisphosphate (RuBP) to produce two molecules of 3-phosphoglycerate (3-PGA). The overall reaction is three molecules of CO_2 are fixed by three molecules of RuBP and rubisco, to produce six molecules of 3-PGA (Equation 1).

$$\begin{array}{llll} CO_2 & RuBP & 3-PGA & 3-PGA \\ CO_2 + & RuBP & \rightarrow 3-PGA & 3-PGA \\ CO_2 & RuBP & 3-PGA & 3-PGA \end{array} \quad (1)$$

Five molecules of 3-PGA are used to regenerate three molecules of RUBP, and the sixth molecule of 3-PGA is used as a precursor for the production of cellular material [61]. The Calvin cycle is a complex series of enzymatic reactions, which is represented in Figure 3.

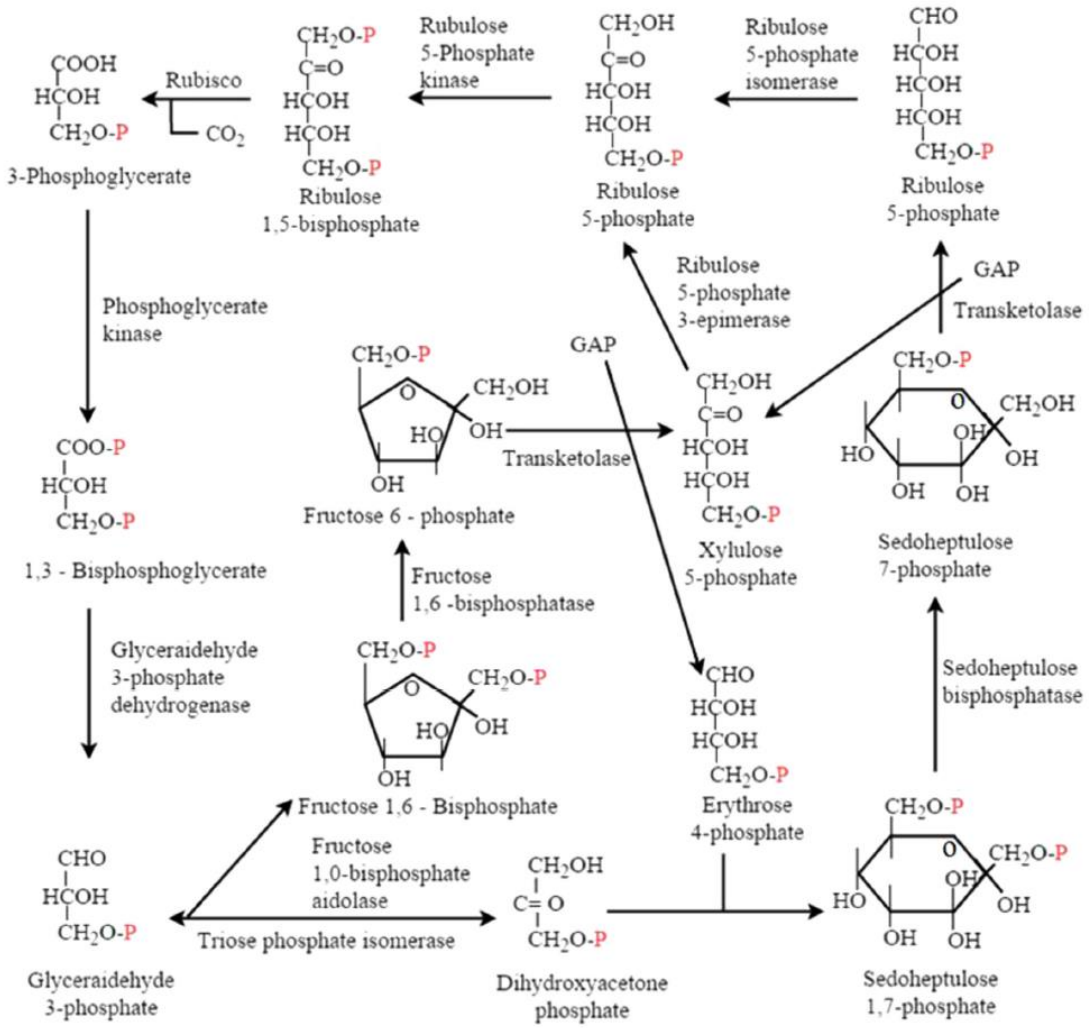

Figure 3: Calvin Cycle for the regeneration of ribulose 1,5-bisphosphate following carbon fixation by Rubisco [55]. The generation of cellular material from the excess 3-phosphoglycerate is not shown.

The Calvin Cycle is the stage of photosynthesis that is independent of light and involves the enzyme-driven synthesis of hexavalent hydrocarbons using CO_2 [62]. During the Calvin Cycle, the enzyme rubisco lyses ribulose 1,5-bisphosphate using one molecule of CO_2 to produce two molecules of 3-phosphoglycerate that undergo further enzymatic reactions that eventually regenerates 1,5-bisphosphate while producing cellular compound precursors [40, 58].

Photorespiration is an undesirable process that involves the reaction of oxygen with Rubisco to produce only one molecule of 3-phosphoglycerate, and a molecule of 2-phophoglycolate. 2-phosphglycolate is further metabolised to glycine which will condense with another glycine molecule to form serine. This process releases one molecule of CO_2 per molecule of serine produced [58].

2.3.1 Metal Uptake by Microalgae

Microalgae contain numerous functional groups on the cell wall that are involved in the natural uptake of nutrient metals. These include carboxyl, sulfonate, phosphate, amino and hydroxyl groups [1, 9]. Carboxyl groups appear to have a significant role in metal binding [9, 63]. The metal binding by these individual functional groups show little specificity, with carboxyl groups having shown a greater affinity to copper, cadmium, lead and gold (III), sulfonate groups showing more of an affinity for cadmium and lead, and phosphate groups showing an affinity to many divalent metals [9].

Algae possess these metal-binding functional groups because they require various metals for their metabolic pathways, all of which they absorb from their environment [9, 10, 64]. Copper and iron are components of photosynthetic transport proteins, and manganese is also involved in photosynthesis in that it is a component of a photosynthetic oxidising centre of the enzyme PSII [65]. Zinc has multiple roles for a number of different enzymatically controlled pathways in that it is a component of *carbonic anhydrase*, *RNA polymerase*, and *alkaline phosphatase*; the latter being involved in phosphorous uptake. Other metals involved in nutrient uptake and assimilation include molybdenum, iron and vanadium [48]. There are examples of algae utilizing unusual heavy metals in the absence of others: *Thalassiosira weissflogii* have been found to incorporate cadmium into carbonic anhydrase in the absence of zinc [66], and researchers have previously conditioned microalgae species including *Dunaliella* and *Tetraselmis* to tolerate the presence of cadmium at higher concentrations [67].

The binding of metals to the cell wall can be considered along with the secretion of metal chelating compounds as a form of "*avoidance to toxicity*", in that they prevent the metals from gaining access to the internal components of the cell and causing damage. "*Tolerance to toxicity*" is facilitated by producing internal, sacrificial proteins to bind and transport metal complexes to vacuoles [1].

The ideal uptake mechanism of metals by microalgae is depicted in Figure 4. It depicts the active uptake of metal ions via protein channels, and the exchange of

other metals along a concentration gradient across the cell wall. Ideally, toxic metals will be complexed with specialised metal chelators and transported into the cell's vacuoles to prevent damage to delicate cell structures. Unfortunately in reality, this is not always the case with toxic metals finding their way into structures such as the chloroplasts and the mitochondria [68].

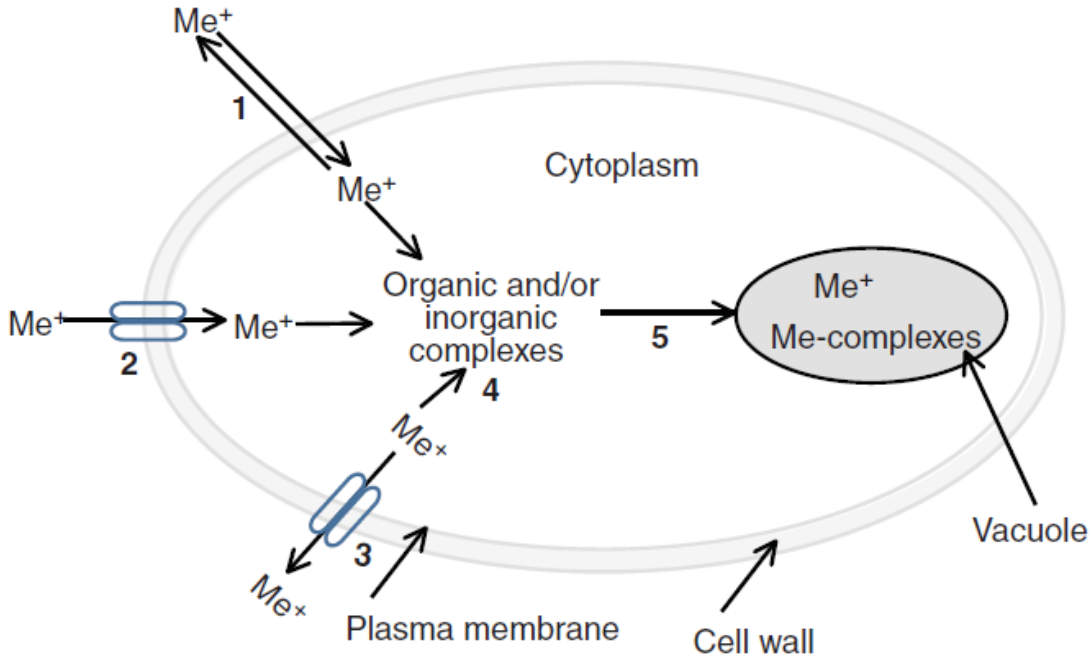

1 – Diffusion (inactive process); 2 – active uptake via ion transporters; 3 – active efflux of free metal ions; 4 – Formation of complexes of the free metal ions with various organic and/or inorganic compounds in the cytoplasm; 5 – transport to the vacuole and stored either as free metal ion or as complexes.

Figure 4: Ideal metal uptake pathway taken from Kaplan 2013[1]

Metals are present in the environment in a variety of different forms including free metal ions, metal salts, minerals in rocks, and can be bound to airborne particles. Some forms of metals are more hazardous than others with free metal ions of particular interest from a toxicological standpoint. However, there are also forms of mercury that are bound in organic complexes that are readily consumed by living organisms, and are more toxic than free mercury ions [1].

Metals from both municipal wastewater and industrial wastewater can pollute the environment and have been implicated in human illness. Metals are known to accumulate in the muscle tissue of aquatic life [69], and are thus conserved within the food chain [17]. Algae has been recognised as a route into the food chain; by first sequestering the metal pollutants and then being consumed by grazers that are

in turn consumed by predators. In aquatic systems, the metals can be passed from predator to predator and eventually consumed by humans [17].

Studies into the impact that the presence of heavy metals has on microalgae have found that although the presence of heavy metals may slow algal growth, microalgae have proven tolerant to the levels of many heavy metals that have been found in industrial wastewaters [53]. The metals of significant interest are lead, mercury and cadmium, but other metals such as copper, zinc and aluminium are also of interest [64]. Algae can sequester metals through two main processes, known as “active uptake” and “passive uptake”. Passive uptake involves the adsorption of metal ions onto the external surface of the algae cells, and this can occur if the cells are living or dead. Active uptake involves surface proteins and pores actively absorbing the metal ions into the cytoplasm via metabolic processes [9, 53]. Some strains of algae are better at sequestering metal ions than others, therefore careful selection of species is required [9, 53].

The efficiency of metal sequestering by individual algal cells is increased in lower biomass concentrations, but generally a more concentrated biomass culture will collectively sequester more metal ions [9]. For some species of microalgae, the presence of metals will promote the accumulation of energy compounds [53].

The sequestering properties of microalgae have led them to be considered as a potential cheaper and more environmentally friendly alternative to conventional ion-separation methods. Chemical and ion separation techniques are less efficient when it comes to removing metals when concentrations fall below 10mg.L^{-1}, and the presence of magnesium and calcium can interfere with membrane separation and certain adsorbent materials. Previous studies have shown that algae are able to remove heavy metals from fresh water in parts per trillion concentrations [64], but research in this field is not advanced, with only a few species of algae previously being evaluated [70].

When absorbed into algal cells, the toxicity of the metals can occur by a number of mechanisms including the blocking of enzymatic functional groups, displacement of essential metals in proteins and by the production of Reactive Oxygen Species (ROS)

[1]. For this reason, algae have had to evolve robust cellular defence mechanisms. This involves the production of defensive proteins known as *Metalothioneins*. There are two different classes of *Metalothioneins* in algae: enzyme-synthesised *Class III Metlaothioneins* (MTIII), known as *phytochellatins*, and complex gene-encoded *Class II Metalothioneins* [68]. Other defence mechanisms include the release of extracellular polysaccharides. However their link to metal defence is not fully understood as only certain polysaccharides have been shown to bind metals [63].

The defence mechanisms involving MtIII involve the binding of the metal within the cell's cytoplasm, and then transporting the MtIII-metal complex to vacuoles or externally. The presence of metals such as cadmium, lead, copper as well as other heavy metals have been shown to be promoters of Metalothionein activity [68]. The internal compartmentalisation of metal ions involves two phases; adsorption onto the cell surface, followed by transport across the cell wall and cell membrane, prior to transportation to intercellular compartments such as the vacuoles or mitochondria.

Analysis of the surface chemistry of *C. vulgaris* demonstrated that the cell surface had a net negative charge, and carboxyl groups were present on the cell surface [71]. These carboxyl groups are most likely contained within the carbohydrate molecules that make up approximately 50% of the cell wall in *C. vulgaris* [72]. *Voigt et al* (2014) discovered that the cell wall of *S. obliquus* contains glycoproteins related to those of *Chlamydomonas reinhardtii* [73]. These are proteins that contain large chains of polysaccharides that contain functional groups that are potential binding points for heavy metals.

2.4 *Chlorella* and *Scenedesmus* Lab studies

AlgaSORB® is a commercially available adsorption column that has been in use for over thirty years to facilitate the removal of metals from contaminated water [28]. This column works on the principle that both live and dead microalgae can be used to sequester metals, and uses deceased and treated microalgae and cyanobacteria as a cost effective biosorbent for multiple adsorption/desorption cycles. AlgaSORB®

has been shown to be affective using a single column for 100 adsorption, desorption cycles with minimal loss of metal binding affinity [9, 74].

In a similar concept, *Tam et al* (1998) immobilised *C. vulgaris* in alginate beads for the purpose of removing copper [21]. These columns are reusable, but their efficacy does decrease over time [11, 64]. Although dead and live algae cells can be immobilised for metal recovery purposes [10, 11, 75-80], research is limited when analysing the metal uptake by active, sessile cells.

Sessile *C. vulgaris* has been studied for the adsorption of cadmium [14, 15, 19, 20, 81], nickel [19, 22, 81-83], copper [20-22, 82] and lead [15, 20]; and sessile *S. obliquus* has been studied for the adsorption of cadmium [17, 25], copper [22, 24, 26, 84], nickel [22] and zinc [85]. Adsorption Isotherms, and in some cases adsorption kinetics were derived for these studies, with their findings summarised below.

Copper waste is prevalent in areas where there are dying, paper and petrochemical industries. Conventional treatment methods, such as precipitation, membrane exchange and solvent extraction are often insufficient when metal concentrations are too low, and are susceptible to interference by other compounds present in wastewaters [6]. *Chlorella vulgaris* has previously been shown to be effective at removing phosphate and nitrate from metal sludges, and both live and dead *C. vulgaris* biomass was able to recover metal ions from contaminated waters [21]. Furthermore, studies have shown that *Scenedesmus obliquus* was able to remove copper ions with a high binding capacity, and has been modelled using the Freundlich isotherm which indicates of a multi-layered binding process, and binding is facilitated predominantly by *van der Waals* forces, and is reversible [24].

Previous studies investigating the ability of *Scenedesmus obliquus* to remove cadmium ions from solution have found that the algae is able to recover as much as 39% of cadmium from dilute solutions [86], with the majority of metal uptake by *S. obliquus* occurring during the early stages of the investigation via adsorption [7, 25, 86].

C. vulgaris has been shown to remove up to 60% of copper ions within 45 minutes of algae contact [82]. The extent of copper removal by *C. vulgaris* has been found to be directly proportional to the initial concentration of biomass, and similarly to the previous *S.* obliquus studies, the majority of the metal removal occurred within the first stages of contact experiments [21]. The study found that the copper uptake process consisted of two main mechanisms; a rapid adsorption to the cell surface followed by a slower metabolism-dependent absorption through the cell membrane [21].

2.5 Adsorption Isotherms

2.5.1 Langmuir Isotherm

The Langmuir Isotherm was first proposed by Langmuir in 1916 and was used to describe the adsorption of gases onto platinum, glass and mica [87]. The isotherm has the following assumptions [88]:

1. There are a fixed number of binding sites on the surface of the adsorbent.
2. The binding sites all have equal energy.
3. Adsorption is reversible.
4. The binding sites can only bind one molecule of adsorbate at a time.
5. The adsorbed species do not interact once adsorbed.
6. The adsorbate condenses onto the surface of the adsorbent in a monolayer mechanism.

The impact of the assumptions is that the model predicts a homogeneous adsorption of molecules that each have identical enthalpies and activation energies. Once bound, the adsorbed species will not migrate across the surface of the adsorbent [89]. The Langmuir Isotherm is often applied to adsorption by biosorbents from aqueous solutions despite the model assumptions not being strictly followed [90]. The Langmuir Isotherm is represented by Equation 2:

$$Q_e = \frac{Q_{max} \cdot b_L \cdot C_e}{1 + b_L \cdot C_e} \quad (2)$$

Where:

- Q_e is the adsorption of metal ion per gram of algae at equilibrium (mg.g^{-1})

- C_e is the residual concentration of metal ion at equilibrium ($mg.L^{-1}$)
- Q_{max} is the maximum quantity of metal ion that can be adsorbed ($mg.g^{-1}$)
- b_L is the isotherm constant ($L.mg^{-1}$)

The Langmuir Isotherm has been used in the past to model adsorption of heavy metals onto microalgae [91-93], macroalgae [94-97], sewage sludge [98], dried fruit [99, 100] and peppermint [101]. It is assessed for its fit by how the linear model can fit to the experimental data, this method of fit is known as Linear Least Squares Regression (LSR) [102]. The model is usually linearized using the Lineweaver-Burk model [88]:

$$\frac{1}{Q_e} = \frac{1}{Q_{max}\, b_L}.\frac{1}{C_e} + \frac{1}{Q_{max}} \tag{3}$$

The reciprocal of the adsorption on the biosorbent at equilibrium, plotted against the concentration remaining in solution at equilibrium will give the y-axis intercept of the reciprocal of the maximum adsorption of the biomass, and the gradient of the reciprocal of the product of the maximum adsorption and the Langmuir constant b_L.

The Lineweaver-Burk method is just one of four techniques that can be used to linearize the Langmuir model to derive values for Q_{max} and b_L. A study using model data simulated using MATLAB R2014b determined that the most accurate method for linearization was the *Hanes-Woolf* linearization [102]:

$$\frac{C_e}{Q_e} = \frac{1}{Q_{max}}.C_e + \frac{1}{Q_{max}\, b_L} \tag{4}$$

With the gradient being the reciprocal of the maximum adsorption onto the biomass, and the y-axis intercept being the reciprocal of the product of the maximum adsorption and the Langmuir constant b_L. The Lineweaver-Burk plot also produced accurate values for Q_{max} and b_L. Furthermore, as C_e/Q_e and C_e are not completely independent variables, the linear relationship of the *Hanes-Woolf* plot can be overestimated [88].

The Langmuir constant, b_L represents the relationship between the rate of adsorption and the rate of desorption. This is often denoted as K_L and usually has the units of L.g^{-1} or L.mmol^{-1}. The Langmuir equilibrium constant has been used in the past to directly calculate the Gibbs free energy of the system using Equation 5

$$\Delta G = -RT \ln(K_c) \tag{5}$$

Where K_c is the equilibrium constant of the system, and is dimensionless. Previous studies have shown that b_L can be substituted for K_c for non-polar or ionic solutions that have a very low concentration [90, 103], however although this may be numerically correct, it is not mathematically correct. Mathematically, the natural logarithm cannot be calculated for a value that is not dimensionless [104].

There are two methods reported to convert b_L to a dimensionless K_c and each of these is according to a specific assumption. The most widely used transform is to multiply the value of b_L by the density of pure water if the units of b_L are in L.g^{-1}, or by the density of water divided by the molecular mass of pure water if the units are in L.mol^{-1} [104-107]. This assumes the mechanism of adsorption is substitutive in that the adsorbed ion displaces a molecule of water [104].

The second method of converting b_L to dimensionless K_c takes into consideration the activities of the ions in solution. The concentration reference state (usually 1 mol.L^{-1}), divided by the activity of the ions in solution (dimensionless), multiplied by b_L will return a value of K_c if the units of b_L are L.mol^{-1}. If b_L has units of L.g^{-1}, multiply by the molecular weight of the adsorbed species also [90, 104]. There are many examples in the literature that do not attempt to transform the b_L constant to its dimensionless counterpart, and incorporate it directly into Equation 5 [92, 95]. The Langmuir Isotherm has been used in the past as a comparative tool between different biosorbents, despite the biosorbents not adhering to the assumptions of a homogeneous adsorbent surface [89].

2.5.2 Freundlich Isotherm

An alternative isotherm to the Langmuir Isotherm is the Freundlich Isotherm. Unlike the Langmuir Isotherm, the Freundlich Isotherm describes non-ideal and reversible

adsorption onto a non-uniform, heterogeneous surface [89]. The Freundlich Isotherm is a purely empirical isotherm, and although attempts have been made to derive the isotherm from thermodynamic [108] and statistical theories [109, 110], the model parameters are not descriptive of the physical adsorption process [111]. The Freundlich Isotherm has the following form:

$$Q_e = K_f . C_e^{1/n} \quad (6)$$

Where:

- Q_e is the adsorption of metal ion per gram of algae at equilibrium ($mg.g^{-1}$)
- C_e is the residual concentration of metal ion at equilibrium ($mg.L^{-1}$)
- K_f is the distribution coefficient $(mg.g^{-1})(mg.L^{-1})^n$
- n is a correction factor.
- K_f and n are dependent on the adsorbate, adsorbent and the temperature.

Similarly to the Langmuir constant, b_L, the distribution coefficient K_f can be transformed to a dimensionless number (depending on the units used), and incorporated into Equation 5 . If the units are in $(mg.g^{-1})(mg.L^{-1})^n$, the equilibrium constant can be determined from K_f using Equation 7.

$$K_c = K_f \rho_{H_2O} \left(\frac{10^6}{\rho_{H_2O}}\right)^{\left(1-\frac{1}{n}\right)} \quad (7)$$

If the units of K_f are in $(mmol.g^{-1})(mmol.L^{-1})^n$, K_c can be calculated as follows:

$$K_c = \frac{K_f \rho_{H_2O}}{M_x} \left(\frac{10^3}{M_x . \rho_{H_2O}}\right)^{\left(1-\frac{1}{n}\right)} \quad (8)$$

The Freundlich Isotherm has been described as a descriptive isotherm as the values of K_f and n bear no relation to the underlying mechanisms or sorption processes involved [112], and it does not relate to thermodynamic basis, as Henry's Law does not apply at low adsorbate concentrations [89]. It has however indicated that adsorption is a function of the concentration of the adsorbate within the bulk liquid, leading to the hypothesis that the quantity of adsorbed adsorbate is equal to the sum of the all of the binding sites, with the sites with the highest bonding energy

being occupied first, and the energy of adsorption decreasing exponentially as the sites are occupied [89].

2.5.3 The Temkin Isotherm

The Temkin Isotherm has a potential advantage as it can be used to investigate thermodynamic interactions between adsorbate and adsorbent, and it assumes the energy of the binding sites is uniformly distributed across the adsorbent's surface [100, 113]. The Temkin Isotherm is shown in Equation 9.

$$Q_e = \frac{RT}{b_T}.\ln(a_T.C_e) \tag{9}$$

Where:

- Q_e is the adsorption at equilibrium as before (mmol.g^{-1}).
- C_e is the residual concentration of metal ion at equilibrium (mg.L^{-1}).
- a_T is the equilibrium binding constant (L.mg^{-1}).
- b_T is the Temkin constant related to heat of sorption (Jmol^{-1}).
- R is the universal gas constant (8.314 Jmol^{-1}K^{-1})
- T is the absolute temperature (288 K)

Some researchers substitute the term B into Equation 9:

$$B = \frac{RT}{b_T}$$

This term B has units of mmol.g^{-1}, however Edris et al incorrectly give it the units of mg.g^{-1}, which is mg of adsorbate per g of adsorbent [14, 15]. Unlike for the previous Isotherms, the adsorption data obtained for the Temkin Isotherm has to be converted to mmol.g^{-1}.

The Temkin Isotherm can be linearised as displayed in Equation 10.

$$Q_e = \frac{RT}{b_T}.\ln(a_T) + \frac{RT}{b_T}.\ln(C_e) \tag{10}$$

To determine the equilibrium binding constant, a_T and the Temkin heat constant, b_T Q_e was plotted against the natural logarithm of C_e, and b_T is calculated by dividing the product of the universal gas constant, R and the temperature, T by the gradient of the linear fit. a_T is calculated by taking the exponential of the y-axis intercept divided by the gradient.

The Temkin Isotherms both returns a value for a_T which is the Temkin Equilibrium constant that has been used to calculate the heat of adsorption [101, 113], using the expression shown in Equation 11.

$$\ln(a_T) = \frac{\Delta S^\circ}{R} - \frac{\Delta H^\circ}{RT} \tag{11}$$

Where:

- a_T is the equilibrium binding constant ($L.g^{-1}$).
- ΔS is the change in entropy (JK^{-1})
- ΔH is the change in enthalpy (J)
- R is the universal gas constant (8.314 $Jmol^{-1}K^{-1}$)
- T is the absolute temperature (K)

Equation 10 is an adaptation of the Van't Hoff Equation, and Boulaiche et al [113] claim that a_T is equivalent to the equilibrium constant. A plot of the natural logarithm of a_T against the reciprocal of its corresponding temperature will return a gradient equal to the enthalpy change divided by the universal gas constant R.

The units of a_T are the same as the units of the Langmuir constant, b_L (Lmg^{-1}). This would suggest that the Langmuir constant could be used within the Van't Hoff equation also, however this is not universally the case. Ghosal et al [90] explain that the equilibrium constant is related to the Langmuir constant but it is not directly equivalent, although at low concentrations it can be used as an accurate approximation.

The Temkin Isotherm is best suited to describe simpler adsorption systems onto uniform adsorbents, usually liquid phase adsorption processes are not well represented by the Temkin Isotherm [89]. The Temkin Isotherm cannot be used for large adsorbate or small adsorbate concentrations [114]. The Temkin constant b_T is

related to the heat of adsorption and is indicative of the adsorption intensity [115], which is explained by *Yang et al* (1993) who derived the Temkin equation using the *ensemble theory* and concluded that the b_T is related to the energy associated with the lateral interaction of bound adsorbate molecules [114].

2.5.4 Adsorption Isotherms Applied to Adsorption by Microalgae

Previous adsorption studies of metals adsorption on *C. vulgaris* and *S. obliquus* have shown that binding mechanisms can follow either the Langmuir or the Freundlich Isotherm [7, 21, 25, 86], but to the author's knowledge there have been no investigations that capture initial uptake kinetics. Nobel Prize winning chemist, Irving Langmuir proposed the Langmuir isotherm for monolayer surface adsorption of gasses in 1916 [116].

The Freundlich Isotherm is an empirical model that derived mathematically from experimentation; it does not hold the same theoretical assumptions as the Langmuir Isotherm. The Freundlich Isotherm assumes the surface is heterogeneous and binding can occur via a multi-layer process [117].

Previous studies using the Langmuir isotherm found Q_{max} for zinc by *S. obliquus* was 6.67mg.L^{-1} studying zinc concentration from 0mg.L^{-1} to 8mg.L^{-1} [85]. Copper adsorbed by both *S. obliquus* and *C.* vulgaris exhibited a higher Q_{max} for *C. vulgaris* compared to *S. obliquus* 48.2mg.g^{-1} compared to 33.3mg.g^{-1} when analysing concentrations of 25 to 250mg.L^{-1}, for nickel the finding was the same with Q_{max} found to be 59.7mg.g^{-1} and 30.2mg.g^{-1} for *C. vulgaris* and *S. obliquus* respectively [22]. The Freundlich Isotherm was also examined, but had a lower correlation coefficient (R^2) than the Langmuir isotherm. The Freundlich constant was 24.90 and 18.31 for copper and nickel respectively on *C. vulgaris*, and 2.85 and 0.27 for copper and nickel respectively adsorbed by *S. obliquus* [22] (units not stated).

Previous findings using the Langmuir and Freundlich isotherm are displayed in Table 1 and Table 2, respectively.

Table 1: Langmuir Isotherm parameters for the adsorption of heavy metals by species of microalgae obtained by previous studies.

Algae	Metal	R^2	Q_{max} ($mg.g^{-1}$)	Langmuir constant (Lmg^{-1})	Reference
C. vulgaris	Cadmium	1.00	86.6	0.042	[19]
		0.90	149.9	0.013	[15]
		0.99	6.79	0.062	[14]
		1.00	44.98	0.115	[93]
	Copper	0.78	76.71	6.77	[82]
		1.00	48.2	0.122	[22]
		0.95	25.42	0.058	[93]
	Nickel	0.99	58.4	0.035	[19]
		0.99	59.7	0.050	[22]
		0.99	21.13	0.052	[93]
	Lead	1.00	178.5	0.009	[15]
		0.99	14.93	0.018	[14]
	Zinc	0.95	31.33	0.009	[93]
S. obliquus	Cadmium	0.99	68.6	0.101	[17]
	Copper	1.00	33.3	0.019	[22]
	Nickel	0.99	30.2	0.022	[22]
Cladophora hutchinsiae	Selenium	1.00	74.9	0.009	[94]
Parachlorella sp	Cadmium	0.97	92.63	0.050	[92]
Spirulina platensis	Cadmium	0.96	69.02	0.036	[118]
	Nickel	0.95	66.48	0.045	[118]
Chlamydomonas reinhardtii	Cadmium	0.92	77.56	0.054	[16]
	Lead	0.96	141.11	0.038	
	Mercury	0.95	112.36	0.054	

There have been more investigations of adsorption of heavy metal ions by *C. vulgaris* compared to *S. obliquus*. Table 1 displays data for Cd^{2+}, Cu^{2+} and Ni^{2+} adsorption by *C. vulgaris* that were obtained by numerous authors. The Q_{max} for adsorption by *C. vulgaris* ranges from $149.9mg.g^{-1}$ to $6.8mg.g^{-1}$ for Cd^{2+}, $76.7mg.g^{-1}$ to $25.4mg.g^{-1}$ for Cu^{2+}, $59.7mg.g^{-1}$ to $21.13mg.g^{-1}$ for Ni^{2+} and $178.5mg.g^{-1}$ to $14.9mg.g^{-1}$ for Pb^{2+}. Two independent studies investigating the adsorption of the same metal by *S. obliquus* could not be found. The R^2 values for Langmuir Isotherm fitted to the adsorption of Cd^{2+} and Ni^{2+} by *C. vulgaris* are all above 0.9, but there is no agreement between the studies for the values obtained for Q_{max}.

There have been fewer studies applying the Freundlich isotherm to metal sorption data by microalgae compared to the Langmuir Isotherm. Parameters obtained from fitting the Freundlich Isotherm to metal sorption data are shown in Table 2.

However, some of the studies have fitted the Freundlich Isotherm without reporting model parameters [24, 93], or reported the parameters without supplying units [16, 94]. Others report the Freundlich parameter, K_f as having units of Lg^{-1} [14, 15], while others report the units as $mg.g^{-1}$ [17, 20], where the correct units are accepted as $(mg.g^{-1})(mg.L^{-1})^n$ [19, 88, 118].

Table 2: Freundlich Isotherm parameters for the adsorption of heavy metals by species of microalgae found in literature. The superscript [a] refers to units Lg^{-1} and the superscript [b] refers to units $mg.g^{-1}$

Algae	Metal	R^2	K_f $(mg.g^{-1})(mg.L^{-1})^n$	n	Reference
C. vulgaris	Cadmium	0.99	8.93	2.60	[19]
		0.95	0.122[a]	1.436	[15]
		0.92	4.76[b]	0.85	[20]
		0.95	0.54[a]	1.34	[14]
	Copper	0.73	9.47[b]	0.78	[20]
	Nickel	1.00	7.19	2.43	[19]
	Lead	0.95	0.233[a]	1.436	[15]
		0.95	0.43[a]	1.39	[14]
		0.87	10.96[b]	0.57	[20]
S. obliquus	Cadmium	0.94	19.79[b]	4.01	[17]
Parachlorella sp	Cadmium	0.96	12.45	2.48	[92]
Spirulina platensis	Cadmium	0.99	9.22	2.62	[118]
	Nickel	0.99	10.73	2.84	

There is great deal of variation in the values recorded for K_f and also in the units reported for this parameter. Two studies undertaken by *Edris et al* [14, 15] both reported the K_f values as having units of $L.g^{-1}$ but found very different values, 0.1 $L.g^{-1}$ [15] and 0.5 $L.g^{-1}$ [14], for cadmium adsorbed by *C. vulgaris*. These two studies used the same procedure for each experiment. The only difference is the strain of *C. vulgaris* used for each experiment. The study that returned a K_f of 0.1 Lg^{-1} obtained their culture from Carolina Biological Supply, North Carolina, US and cultivated using Bold's Basal medium [15], whereas the *C. vulgaris* used for the study that returned a K_f of 0.5 $L.g^{-1}$ was purchased from the Botany department of Alexandria University, Egypt and was cultivated using Bristol culture medium [14].

A third isotherm that researchers have used to describe adsorption by microalgae was the Temkin Isotherm. This is not as widely used as the Langmuir or the Freundlich Isotherm in the studies examined, but it has been used to investigate the uptake of metals by microalgae [14, 15, 92]. Results from these studies are displayed in Table 3.

Table 3: Temkin Isotherm parameters for the adsorption of heavy metals by species of microalgae found in literature

Algae	Metal	R^2	a_T ($L.g^{-1}$)	b_T ($Jmol^{-1}$)	Reference
C. vulgaris	Cadmium	0.77	1.02	28.42	[15]
		0.77	0.06	1687.42	[14]
	Lead	0.78	112	24.80	[15]
		0.78	1.04	1981.6	[14]
Parachlorella sp	Cadmium	0.96	0.60	132.39	[92]

There are fewer examples of the Temkin Isotherm being fitted to adsorption data of metals by microalgae. The two sets of data obtained for cadmium adsorbed onto *C. vulgaris* as shown Table 3 were both obtained by Edris et al [14, 15], but there is no agreement in the calculated model parameters obtained for each study. There were no studies found that investigated the Temkin Isotherm for metal adsorption by *S. obliquus*.

Of the three isotherms that have been previously investigated, the Langmuir Isotherm has been most applied to metal uptake by microalgae, followed by the Freundlich model, with the Temkin model being reported in only three studies investigating metal sorption by microalgae. *Dirbaz et al* (2018) [92] compared the three isotherms for cadmium uptake by *Parachlorella sp*. and determined that the Langmuir Isotherm had the best fit to the data over a range of temperatures and pH. The authors of this study calculated the average R^2 and root means square error values (RMSE) for each isotherm. For each Isotherm, the average R^2 was greater than 0.95, and the average RMSE value was less than six for each isotherm, which led to the authors concluding that all three Isotherms were able to fit the adsorption data [92].

The assumptions of the Langmuir Isotherm do not reflect the surface of the microalgae and this has been noted by previous studies, however they still report the Langmuir parameters as good approximations for adsorption capacity [90]. The Freundlich Isotherm has the limitations in that it is purely empirical and that it cannot be used to predict the maximum sorption capacity [111]. The Temkin Isotherm is related to the interaction potentials of adjacent, bound ions [114], but previous researchers have suggested that the isotherm is more suited to gas phase

systems than liquid phase systems [89]. The data shown in Table 1, Table 2 and Table 3 indicate similar but independent studies on metal sorption by microalgae do not agree. It is therefore difficult to conclude which isotherm is most applicable to metal sorption by microalgae by analysing the findings of previous studies alone.

2.6 Kinetic Models

Adsorption isotherms model the data once equilibrium has been achieved between the surface of the adsorbent and the bulk liquid. Previous studies have applied empirical models that represent the increase in adsorbate loading over time on various adsorbents, but only a few model the uptake of metals by microalgae [14, 15, 92], although there are other examples of studies of adsorption of metals by macroalgae (seaweed) [84, 119-121], and cyanobacteria [118].

All of these studies investigated the fitting of the pseudo-first order, Lagergren model that was first proposed in 1898 to model the uptake of oxalic and malonic acids onto activated carbon [122]. This model assumes that the rate of change of adsorption onto the adsorbent is directly proportional to the difference between an equilibrium value the adsorption at time t.

$$\frac{dQ_t}{dt} = k_t(Q_e - Q_t) \tag{12}$$

The expression is integrated with respect to Q_t and t to rearrange the expression in terms of Q_t:

$$\int_0^{Q_t} dQ_t = \int_0^t k_t(Q_e - Q_t)dt$$

$$\int_0^{Q_t} \frac{dQ_t}{(Q_e - Q_t)} = k_t \int_0^t dt$$

$$-[\log_e(Q_e - Q_t)]_0^{Q_t} = k_t[t]_0^t$$

$$-\log_e\left(\frac{(Q_e - Q_t)}{Q_e}\right) = k_t.t$$

$$\frac{(Q_e - Q_t)}{Q_e} = e^{-k_t.t}$$

$$Q_t = Q_e(1 - e^{-k_t.t}) \quad (13)$$

Where:

- Q_t is the adsorption at time t (mg.g^{-1}).
- Q_e is the adsorption at equilibrium (mg.g^{-1}).
- k_t is the first order rate constant (s^{-1}).
- t is the time elapsed (s).

Q_e and k_t are the model constants that can be derived by linearising the experimental data by applying the following transformation:

$$ln(Q_e{}^* - Q_t) = -k_t .t + ln(Q_e) \quad (14)$$

A plot of $ln(Q_e{}^* - Q_t)$ against t will return a gradient that is equal to $-k_t$ and an intercept that should equal $ln(Q_e)$. As Q_e is present on both sides of the equation, this is initially estimated from experimental data, and this estimate is represented by $Q_e{}^*$.

This model is considered a "pseudo-first order" because if the model was a true first order model, $ln(Q_e)$ would equal the intercept of a plot of $ln(Q_e{}^* - Q_t)$ against t [123, 124]. For the Lagergren model, this is rarely the case [124-127] and the value for $Q_e{}^*$ either has to be calculated iteratively, or the values for k_t and Q_e are obtained by fitting Equation 13 to the experimental data by non-linear regression. Another reason researchers discount the Lagergren model as a true first order model is that the expression $k_t(Q_e - Q_t)$ does not represent the number of binding sites on the adsorbent [123, 124], and the adsorption process is not driven by the concentration gradient of the adsorbate in solution [128].

The second-order model is an adaptation of the Lagergren model that has been largely attributed to Ho & McKay [129-132], although Tüzün et al attributes the earliest derivation to Ritchie in 1977 [16, 133]. Unlike the Lagergren model, the second-order model has been found to reflect adsorption kinetic data over the entire process, including when equilibrium has been achieved [124-127]. The second

order model assumes the rate of change of adsorption onto the adsorbate is directly proportional to the difference between adsorption at equilibrium and the adsorption at time, *t* squared:

$$\frac{dQ_t}{dt} = k_t(Q_e - Q_t)^2 \tag{15}$$

$$\int_0^{Q_t} dQ_t = \int_0^t k_t(Q_e - Q_t)^2 dt$$

$$\int_0^{Q_t} \frac{dQ_t}{(Q_e - Q_t)^2} = k_t \int_0^t dt$$

$$\left[\frac{1}{Q_e - Q_t}\right]_0^{Q_t} = k_t[t]_0^t$$

$$\frac{1}{Q_e - Q_t} - \frac{1}{Q_e} = k_t.t$$

$$\frac{Q_e}{Q_e(Q_e - Q_t)} - \frac{Q_e - Q_t}{Q_e(Q_e - Q_t)} = k_t.t$$

$$\frac{Q_t}{Q_e(Q_e - Q_t)} = k_t.t$$

$$Q_t = k_t.t(Q_e^2 - Q_eQ_t)$$

$$Q_t + Q_tQ_ek_t.t = Q_e^2k_t.t$$

$$Q_t = \frac{Q_e^2k_t.t}{1 + Q_ek_t.t} \tag{16}$$

Where:

- Q_t is the adsorption at time *t*, as before (mg.g^{-1}).
- Q_e is the adsorption at equilibrium, as before (mg.g^{-1}).
- k_t is the second order rate constant (g.mg^{-1}.s^{-1}).
- *t* is the time elapsed (s).

To obtain Q_e and k_t equation 16 can be rearranged to the linear form:

$$\frac{1}{Q_t} = \frac{1}{Q_e^2 k_t} \cdot \frac{1}{t} + \frac{1}{Q_e} \quad (17)$$

The reciprocal of the adsorption at each time-point can then be plotted against the reciprocal of the elapsed time. Q_e can be calculated by finding the reciprocal of the y-axis intercept, and k_t can be found by dividing the square of the y-axis intercept by the gradient.

The third model used in this study is the Elovich model, which has a different basis to the Lagergren and second-order models. It is not based on adsorption at equilibrium. Instead the Elovich model assumes that the rate of adsorption decreases with time from a maximum adsorption rate.

$$\frac{dQ_t}{dt} = \alpha e^{-\beta Q_t} \quad (18)$$

Equation 18 can be rearranged in terms of Q_t by separation of the variables and integrating:

$$\int_0^{Q_t} e^{\beta Q_t} = \alpha \int_0^t dt$$

$$\left[\frac{e^{\beta Q_t}}{\beta}\right]_0^{qQ_t} = \alpha [t]_0^t$$

$$\frac{e^{\beta Q_t} - 1}{\beta} = \alpha t$$

$$e^{\beta Q_t} = \alpha\beta t + 1$$

$$\beta Q_t = \log_e(\alpha\beta t + 1)$$

$$Q_t = \frac{1}{\beta} ln(\alpha\beta t + 1) \quad (19)$$

Where:

- Q_t is the adsorption at time t, as in the Lagergren Model and second order model (mg.g^{-1}).
- β is the desorption constant (g.mg^{-1}).

- α is the maximum adsorption rate (mg.g^{-1}.s^{-1}).
- *t* is the time elapsed (s).

The Elovich model assumes a solid surface that is energetically heterogeneous, and that there are no interactions between the adsorbed species [134]. As the algae surface contains a variety of functional groups, the assumption of heterogeneity is satisfied. Equation 19 shows the non-linear form of the Elovich model. If the adsorption process is fast, the model can be linearized by making the assumption that the value for the maximum adsorption rate multiplied by the desorption constant, multiplied by the elapsed time (greater than 0), is greater than 1:

$$\alpha\beta t \gg 1$$

This makes the term $\alpha\beta t + 1$ tend towards $\alpha\beta t$, and allows for Equation 19 to be rearranged to the form:

$$Q_t = \frac{1}{\beta} ln(t) + \frac{1}{\beta} ln(\alpha\beta) \qquad (20)$$

A plot of the Q_t against *ln(t)* would return a linear fit, with the gradient equal to the reciprocal of the desorption constant and the maximum adsorption rate is calculated from the y-axis intercept by:

$$\alpha = \frac{e^{c.\beta}}{\beta}$$

Where *c* is the y-axis intercept.

The degree of fit of the kinetic models are often attributed to the correlation of the linearised models to experimental data. As there are only few examples of studies that investigate adsorption kinetics of metals by microalgae, literature was examined that investigated the kinetic models for metal adsorption by a variety of biosorbents. The results of previous studies that have fitted the Lagergren model to metal sorption data are shown in Table 4.

Table 4: Lagergren model parameters from various adsorbents from past studies found in literature. Values are obtained from heavy metal batch experiments using microalgae, macroalgae and cyanobacteria.

Adsorbent Type	Adsorbent Used	Adsorbate	Q_e ($mg.g^{-1}$)	k_t (s^{-1})	R^2	Reference
Microalgae	*Chlorella vulgaris*	Cadmium	1.5	1.2×10^{-3}	0.99	[14]
			19.7	1.1×10^{-3}	0.99	[15]
		Lead	1.9	9×10^{-4}	1.00	[14]
			18.4	1.4×10^{-3}	1.00	[15]
	Chlamydomonas reinhardtii	Cadmium	95.5	11.5	0.95	[16]
		Lead	261.1	12.8	0.95	
		Mercury	88.3	14.0	0.92	
Macroalgae	*Cystoseira indicia*	Copper	76.1	1.9×10^{-3}	0.89	[95]
		Cobalt	54.6	2.3×10^{-3}	0.59	
	Cystoseira indica	Chromium	NA	8.6×10^{-4}	0.81	[119]
	NA	Cadmium	5.1	3.3×10^{-4}	0.96	[120]
		Lead	152.6	6.7×10^{-4}	0.97	
		Nickel	5.7	3.3×10^{-4}	0.83	
	Ulva lactuca	Cadmium	120.0	1.0×10^{-3}	0.98	[121]
		Lead	128.9	6.0×10^{-4}	0.98	
		Copper	91.0	1.2×10^{-3}	0.96	
		Nickel	60.3	6.4×10^{-4}	0.99	
Cyanobacteria	*Spirulina platensis*	Cadmium	16.5	5.7×10^{-4}	0.98	[118]
		Nickel	17.0	4.7×10^{-4}	0.98	

The R^2 values displayed in Table 4 show good linear fit for the majority of the previous adsorption studies that modelled the kinetics using the Lagergren model. Copper and cobalt adsorption by *C. indicia* [95] and chromium adsorption by *C. indica* [119], and nickel adsorption by an unspecified species of macroalgae [120] appear to be the only examples that do not show a good linear correlation to the linearised Lagergren model, with all experiments returning an R^2 value less than 0.9.

Ho & McKay have reported on the uses of the Lagergren model for the adsorption of dyes onto wood [126] and sphagnum moss [125, 127]. They compared the Lagergren models to the second order model, and in a review article [124] they concluded that the Lagergren model was unable to represent the data over the entire dataset. They recommend using the data obtained during the initial stages of the adsorption process, prior to equilibrium being reached. As a result, the Lagergren model often underestimates the value of Q_e without further model fitting [124].

The studies that produced the results represented in Table 4 also compared the Lagergren model to the second order model. The Q_e and k_t values for the second order models are presented in Table 5.

Table 5: Second order model parameters from various adsorbents from past literature. Values are obtained from heavy metal batch adsorption experiments using microalgae, macroalgae and cyanobacteria.

Adsorbent Type	Adsorbent Used	Adsorbate	Q_e ($mg.g^{-1}$)	k_t ($g.mg^{-1}s^{-1}$)	R^2	Reference
Microalgae	*Chlorella vulgaris*	Cadmium	1.9	6.6×10^{-4}	0.95	[14]
			24.3	8.4×10^{-4}	0.95	[15]
		Lead	2.4	3.4×10^{-4}	0.96	[14]
			21.8	1.3×10^{-3}	0.92	[15]
	Chlamydomonas reinhardtii	Cadmium	40.5	3.1×10^{-2}	1.00	[16]
		Lead	95.3	2.4×10^{-2}	0.95	
		Mercury	68.2	2.4×10^{-2}	0.98	
Macroalgae	*Cystoseira indicia*	Copper	80	4.9×10^{-5}	1.00	[95]
		Cobalt	59.2	5.1×10^{-5}	1.00	
	Cystoseira indica	Chromium	29.9	6.9×10^{-6}	0.99	[119]
	NA	Cadmium	4.2	63.2	0.99	[120]
		Lead	106.4	12	0.99	
		Nickel	11.7	72	0.99	
	Ulva lactuca	Cadmium	116.3	3.7×10^{-5}	1.00	[121]
		Lead	144.9	1.1×10^{-5}	1.00	
		Copper	90.1	8.2×10^{-5}	1.00	
		Nickel	58.5	3.0×10^{-5}	1.00	
Cyanobacteria	*Spirulina platensis*	Cadmium	17.3	3.7×10^{-5}	0.99	[118]
		Nickel	19.4	2.8×10^{-5}	0.99	

The R^2 values represented in Table 4 for the adsorption of cadmium and lead by *C. vulgaris* are larger than those shown in Table 5, which would indicate that the Lagergren model (R^2>0.9) has a better fit to the data than the second order model (R^2<0.96). The Q_e for the adsorption of cadmium by *C. vulgaris* was measured to be 1.4$mg.g^{-1}$, which is closer to the value predicted by the Lagergren model (1.5$mg.g^{-1}$), than the value predicted by the second order model (1.9$mg.g^{-1}$). This result was repeated for results of the lead adsorption experiments. The measured value of adsorption at equilibrium was 1.7$mg.g^{-1}$, which again was closer to the prediction made by the Lagergren model (1.9$mg.g^{-1}$), when compared to the value predicted by the second order model (2.4$mg.g^{-1}$) [14].

Edris et al (2014) [15] repeated their work using a new strain of *C. vulgaris* (strain ID unspecified), and recorded a new value of adsorption at equilibrium of cadmium by *C. vulgaris* as being 19.1$mg.g^{-1}$ (measured by atomic adsorption spectroscopy),

which was closer to the value predicted by the Lagergren model which was 19.7mg.g^{-1} [15]. The second order model predicted the adsorption at equilibrium of cadmium by *C. vulgaris* to be 24.3mg.g^{-1}. The adsorption at equilibrium of lead in this study was measured to be 18.3mg.g^{-1} and was predicted by the Lagergren model to be 18.4mg.g^{-1}, while the second order model predicted the value to be 21.8mg.g^{-1} [15]. With these results, Edris et al conclude that the Lagergren model is more applicable to their experimental data compared to the second order model.

The other example of the Lagergren model and the second order model being applied to microalgae was the analysis of the adsorption of cadmium, lead and mercury on *C. reinhardtii*. In this case, the R^2 values for cadmium and mercury were higher for the second order model (1.00 and 0.98 compared to 0.95 and 0.92 for cadmium and mercury respectively), and the value for lead remained at a value of 0.95 [16].

Tüzün et al measured the adsorption at equilibrium of cadmium by *C. reinhardtii* to be 42.7mg.g^{-1}, with the Lagergren model predicting the value to be 95.5mg.g^{-1}, and the second order model predicting the value to be 40.5mg.g^{-1}. The adsorption of lead was measured to be 97.4mg.g^{-1}, with the Lagergren model predicting the value to be 261.1mg.g^{-1}, and the second order model predicting it to be 95.3mg.g^{-1}. The improvement in predicted value was observed for the mercury experiment also; it was measured to be 72.2mg.g^{-1} and predicted to be 88.3mg.g^{-1} by the Lagergren model, and 68.2mg.g^{-1} for the second order model [16]. The findings of *Tüzün et al* suggest the second order model represents adsorption data more closely compared to the Lagergren model, which is in contrast to the findings of *Edris et al*.

With two separate studies on microalgae returning conflicting results regarding the predictions of the Lagergren model and the second order model; there is a gap in the research investigating the initial adsorption kinetics of metals by microalgae. Numerous studies and review articles have indicated that the metal uptake is by a two stage process, with an initial quick uptake driven by surface adsorption, and a slower metabolically driven absorption process, without measuring the rates of the two mechanisms [9, 10, 68, 135].

Only one study was found that investigated the Lagergren, second-order model and the Elovich model on the adsorption of chromium on the macroalgae *C. Indica* [119]. The R^2 value for the Elovich model was found to be 0.98, which was a better fit compared to for the Lagergren model (R^2 = 0.81). The R^2 for the second order model was marginally better at 0.99, but both the Elovich model and the second-order model showed a good linear fit for the *C. indica* adsorption of chromium. The study did not return the Q_e values for the Lagergren model, or the Elovich model. Without experimental data, the Q_e value for the Lagergren model cannot be calculated, but using the Elovich model parameters, the maximum adsorption rate, α and the desorption constant β, the expected Q_e was calculated to be 18.4mg.g^{-1}. The authors did not report the Q_e value measured during the experiment, however the value reported for the second-order model prediction was 29.9mg.g^{-1}. This indicates that the two models do not agree with one another. The authors did however report that the sum of square error (SSE) for the Elovich model was 2.6, and the SSE for the second order model was reported as 0.2, which indicates that the second order model represents the experimental data better than the Elovich model.

There have been four other studies identified that have fitted the Elovich model to adsorption kinetics, with three of them investigating a biosorbent. The results of these studies are displayed in Table 6.

Table 6: Results from previous studies that investigated the biosorption of heavy metals by biosorbents, comparing the predictions of the Lagergren model, second order model and the Elovich model.

Adsorbent	Adsorbate	Lagergren Q_e (mg.g^{-1})	Lagergren R^2	Second order Q_e (mg.g^{-1})	Second order R^2	Elovich Q_e (mg.g^{-1})	Elovich R^2
C. indica [119]	Cr(IV)	NA	0.81	29.9	0.99	18.4	0.98
Coconut Shell [136]	Pb(II)	NA	NA	1.7×10^3	1.00	62.2	0.64
Soil [137]	Cd(II)	0.5	0.91	0.6	0.96	0.6	0.89
	Pb(II)	0.7	0.90	0.8	0.98	0.8	0.87
Pepper-mint [101]	Pb(II)	5.3	0.97	18.1	1.00	18.5	0.84

The data presented in Table 6 suggests that the Elovich model has only been successfully applied to the data presented by Basha et al, with the R^2 value reported

as 0.98. They did not explicitly report their Q_e that they measured during the experiment, but they presented a graph of Q_t against elapsed time. This suggests that the adsorption at equilibrium Q_e was approximately 20mg.g^{-1}; which suggests that the Elovich model represents the experimental data better than the second order model, contradicting the reported SSE values as described above [119].

Okpara et al (2020) [136], investigating the adsorption of lead by activated carbon produced from coconut shells, investigated the Lagergren model, the second order model and the Elovich model. There are errors in the reporting of the data within this study. in the body of the text the authors explain that the Lagergren model shows a poor linear fit, but do not return values of Q_e or R^2 obtained by the Lagergren linear least squares analysis; however presented in *Table 2* of their study, they report the results of the second order model as results of the Lagergren model [136]. The recorded experimental value for adsorption at equilibrium of Pb(II) by the coconut shell was 1.7×10^3 mg.g^{-1}, which was reflected by the value predicted by second order model, whereas the Elovich model greatly underestimated the value to be 62.2mg.g^{-1}.

Gholami et al found that the second order model and the Elovich model could predict the adsorption at equilibrium more accurately than the Lagergren model for the adsorption of cadmium and lead by soil, but the Elovich model had a poorer linear fit of R^2 = 0.89 and 0.87 (cadmium and lead respectively), compared to R^2 = 0.91 and 0.90 for the Lagergren model, and R^2 = 0.96 and 0.98 for the second order model [137]. This suggests that the linear R^2 value alone cannot be used as an indicator of model fit.

A similar result was observed by *Ahmad et al* (2017) for the adsorption of lead using peppermint leaves. The Lagergren model was unable to predict the Q_e data obtained by experimentation, but both the second order model and the Elovich model did predict the measured value of Q_e within 2.8%. The R^2 value for the Elovich model (0.84) was lower than that obtained for the second order model (1.00). Interestingly, the R^2 value for the Lagergren model was found to be 0.97, but the Q_e value predicted by this model was 5.3mg.g^{-1}, compared to the experimental value which was 18.0mg.g^{-1} [101].

Although previous adsorption studies have fitted the Lagergren Model [122], or modified it to derive a second order adsorption rate model [124-127], few have attempted to put the models into theoretical context. Azizian is credited with deriving both the Lagergren model and the second order model directly from Langmuir kinetics [138-141], however Liu et al highlight that the assumptions made during the derivations may be dubious [140, 141].

Liu et al observed that for the assumption that allows for the Langmuir rate equation to be simplified to the Lagergren model, implies that the rates of adsorption is negligible. The assumption used to simplify the Langmuir rate equation to the second order model implies that the adsorbate concentration in solution is infinitesimal, or that the second order model would only be applicable during the initial stages of the adsorption process [140].

Leu et al (2003) [142] proposed an alternative method for the derivation of the Lagergren model used the assumption of Langmuir that the overall rate of adsorption is equal to the difference between the product of rate of adsorption and the concentration of adsorbate remaining in solution; and the product of the rate of desorption and the equivalent concentration of the adsorbate bound to the adsorbent surface. This is rearranged to the sum of the rate of adsorption and the rate of desorption multiplied by the difference between the concentration of adsorbate in solution and the concentration of adsorbate at equilibrium. Integration of this relationship returns the Lagergren model [142]. In this study, Liu et al did not linearise the first order model, instead they fitted the first order model directly to the experimental data, to obtain the adsorption rate and the adsorption at equilibrium. This method still however does not put theoretical context behind the model parameters, other than the adsorption rate is a function of both the adsorption rate and the desorption rate.

A later study by *Liu et al* returned to the Langmuir kinetic model, with the overall rate of adsorption is equal to the rate of adsorption minus the rate of desorption. For this derivation, the rate of adsorption is arranged into terms of adsorption and the initial concentration of the adsorbate. This has the form of a quadratic formula, and can be rearranged and simplified to a hybrid model that contains a first order

rate term, and a second order rate term. The rates are calculated from the Langmuir Isotherm, and the ratio of the first order rate constant to the second order rate constant determines whether the kinetics can be approximated by a first order expression, a second order expression; or whether the kinetics is represented by a hybrid kinetic model containing both terms. This model has rarely been used, but Lui et al have shown it to represent adsorption data accurately, for the adsorption of antibiotics onto activated carbon [140].

The most common method for modelling the adsorption kinetics is via the Lagergren model or the second order model [14, 15, 124-127, 143, 144]. Linearizing experimental data using the Lagergren method does not produce accurate model parameters without further regression techniques to converge the model to the data [125]. For this reason, Ho and McKay adapted the pseudo-first order Lagergren model to a second order model that has been found to fit adsorption data onto natural biosorbents such as peat, wood and moss more accurately when compared to the pseudo-first order model [125-127], although uses of a second order model has been reported by researchers prior to Ho et al [16, 133, 145].

2.7 Use of Microalgae for Experimental Processes

2.7.1 Cultivation and Nutrient Requirements

Many species of microalgae have been isolated and specifically cultivated for the production of biofuels and nutraceuticals. Modifying the cultivation conditions can have a significant impact on intracellular makeup of the microalgae which can be used in important precursors for industrial processes [40, 58]. As microalgae is able to be cultivated in brackish waters and wastewater, this negates the need for artificial fertilisers and reduces competition for farmland compared to other cash crops [42].

The initial inspiration for this research was the potential for the recovery of metal pollutants and contaminants in wastewater to enhance the lipid production by microalgae. Lipids produced by microalgae are a potential precursor for biofuel production, and previous studies have found that the presence of cadmium and copper increase the lipid content of the algae cells [29, 53].

For a stable algal culture, the biomass needs access to a source of carbon, nitrogen and phosphorus. Nitrogen is essential for all biological organisms as it is an essential component of proteins. Microalgae are able to assimilate inorganic nitrogen from nitrates, nitrites and ammonium. Nitrate is the preferred form of nitrogen for growth medium for microalgae as the proliferation of microalgae cells causes the pH to rise which will cause ammonium to be converted to ammonia. This is readily consumed by microalgae but can have toxic effects [146], whereas nitrate is the more stable nitrogenous compound in aqueous solutions [70]. Phosphorous is important for the synthesis of Adenosine Triphosphate (ATP) from Adenosine Diphosphate (ADP): this is an essential energy compound, and the reduction of this compound is essential for energy intensive, metabolic processes. Carbon is predominantly obtained from CO_2 during photosynthesis and is an essential building material for the cellular structures. Autotrophic microalgae obtain their carbon exclusively from the atmosphere, but some species exhibit mixotrophy where they are able to obtain carbon from CO_2 and from organic carbon sources in solution [70]. *Chlorella vulgaris* is able to produce high quantities of lipids when grown in mixotrophic conditions [147].

To cultivate microalgae for experimental study, it is possible to grow the algae in municipal wastewater [148], and synthetic wastewater [149]; but a reliable and widely used medium is the freshwater, BG-11 medium. This has been used to cultivate a variety of freshwater microorganisms such as *C. vulgaris* [22, 150]*, S. obliquus* [24, 26, 151], cyanobacteria [152, 153] and *Bacillus sp.* [154] and *Synechocystis sp.* [155].

The optimum cultivation temperature for cultivation of microalgae is dependent on the species [156]. The optimum cultivation temperature for *C. vulgaris* for the purposes of lipid production was found to be between 25 and 30°C [157]. Previous studies working with *C. vulgaris* have cultivated their cultures at 25°C [19, 20, 25, 71, 72, 82, 158]. CO_2 assimilation is a property of light intensity and light duration. During periods of light, photosynthesis occurs producing ATP, which is required for the synthesis of cellular structures and proteins required for cell replication and regular cell metabolism [156].

2.8 Analysis of Metal in Solution

Studies in the past that have investigated metal sorption by algal biomass have used atomic adsorption spectroscopy (AAS) [14-16, 95, 118] and inductively-coupled plasma spectroscopy (ICP) [29, 120, 159]. ICP is usually coupled with optical emission spectroscopy (OES), or with mass spectroscopy (MS). ICP is a technique that allows for the analysis of multiple elements all at once, and to a high degree of precision [160-162].

When samples are analysed by ICP, they are passed through a high energy argon plasma flame. If the analysis is conducted by ICP-OES, the elements within the sample are energised, which causes the emission of photons, the wavelength of the emitted photons identify the elemental species and the intensity of the signal indicates the concentration of the element present. ICP-OES operates in two configurations, axial and radial configuration which is shown in Figure 5. If analysis is undertaken by ICP-MS, the sample is ionised within the argon plasma flame. The ions are then fed into a mass spectrometer where the ions are separated in accordance to their mass and charge ratios.

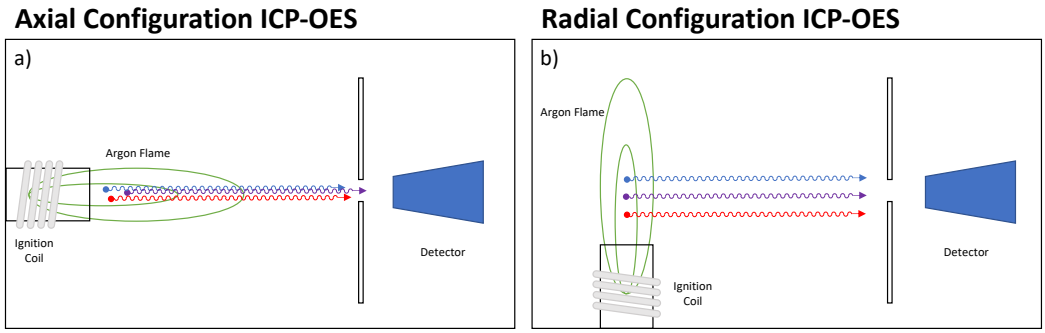

Figure 5: Plasma flame configuration for ICP-OES. a) shows the horizontal orientation for axial configuration. In this configuration signals are detected from energised elements from the whole length of the flame. b) shows the vertical orientation for radial configuration. In this configuration, the signals are detected by a detector that is perpendicular to the plasma flame. The signals are analysed from a horizontal cross-section of the vertical flame.

ICP-OES works in two configurations, *axial* and *radial*. For axial configurated ICP's, the torch is orientated horizontally, and the analyser measures the signal from the entire length of the flame. In radial configurations, the detector is perpendicular to the plasma flame. In this configuration, height of the detector is utilised as different elements become excited at different positions within the flame. As radial configurations only analyse a small component of the flame, it is usually less prone

to matrix interference, but has higher detection limits compared to those in axial orientation [163, 164].

The sample matrix refers to the composition of the sample analyte. The performance of the ICP is sensitive to the properties of the samples being analysed, and the standards used to calibrate the equipment. Flow of the samples is affected by the sample viscosity, and certain acids can degrade the tubing and nebuliser. It is recommended to avoid sulphuric acid and to acidify samples either with nitric acid or hydrochloric acid [165].

The number of analytes within the samples will increase the potential for interference in the optical emission spectrum. For this reason, axial configurations had a reputation for poor reliability for when analysing environmental samples, until improvements were made by modifying the torch. The common modification is to add a second argon line to provide shear gas [163]. This is applied tangentially to the plasma flame following the region of highest temperature in the flame, with the intention to remove elements of lower energy and those that can absorb photons themselves [164]. These improvements to remove the excess plasma tail have improved the reliability of the axial ICP-OES systems to compete with those of radial systems [163, 164, 166, 167].

Even with the performance modifications, ICP-OES is still susceptible to sample interference and measurement drift. Elements such as calcium and sodium cause signal suppression within the equipment; sodium can suppress the signal by 20% [160] which makes the analysis of saline samples difficult. Measurement drift is a phenomenon that occurs when the analyser records variation in signal measurement, this has been reported to be a function of sample temperature [162]. Both ICP-OES and ICP-MS are susceptible to equipment drift. To compensate the effect of this, an internal standard can be employed. This is where an element of known concentration is added to the blank, the standard solutions and each sample. The measured concentrations of each element are multiplied by a correction factor, which is the ratio of the known concentration of the internal standard to the measured concentration of the internal standard. This compensates for the experimental drift, and reduces the requirement for regular recalibration [168].

ICP-MS are usually more costly, and have a far lower limit of detection than ICP-OES. ICP-MS are able to measure as low as parts per trillion, compared to the ICP-OES that can go as low as part per billion [160]. However, interference can occur with ICP-MS, with the presence of chlorine, phosphorus and sulphur a source of interference with copper measurements, and argon oxide ($^{40}Ar^{16}O$) can be produced within the plasma flame and recorded as ^{56}Fe [169]. Whichever ICP is used, care needs to be taken when preparing samples for analysis.

Chapter 3 Methodology

3.1 Algae cultivation

The freshwater microalgae, *Chlorella vulgaris* and *Scenedesmus obliquus* were cultivated in freshwater Bg-11 medium. Culture cultivations for experimentation were performed on a 10L scale. The Bg-11 medium had a concentration of 1.5gL^{-1} sodium nitrate, 40mg.L^{-1} dipotassium phosphate, 65mg.L^{-1} magnesium sulphate heptahydrate, 36mg.L^{-1} calcium chloride dihydrate, 6mg.L^{-1} citric acid, 6mg.L^{-1} ammonium ferric citrate green, 1mg.L^{-1} $EDTANa_2$, 20mg.L^{-1} sodium carbonate [22, 24, 26, 150, 151].

To maintain the experimental stock cultures, they were cultivated in a growth chamber manufactured on site. The temperature was maintained at 25°C, while the cultures were constantly aerated and illuminated under an eight hour-light, sixteen-hour dark cycle by light provided by pure white LED lighting, with and intensity of 33.6 µmol.m^{-2}.s^{-1} ±0.8 µmol.m^{-2}.s^{-1} (photons per m^2 per second). The algae was cultivated in a 10L polycarbonate Nalgene® carboy, sealed with a three-port venting/aeration closure. Aeration was supplied by a Blagdon® KOY Air 25, pond pump, through a sterile 0.2µm Whatman® HEPA-VENT filter. Algae cultures were cultivated in sterile conditions, with the growth medium autoclaved within the 10L carboy, prior to aseptic inoculation of algae culture. The carboy setup is shown in Figure 6.

Figure 6: 10L Nalgene® carboy containing *Synechococcus elongatus*. The vented closure allows for air to be passed through the HEPA-VENT filter, and escape via a three-way stopcock. The Blagdon® KOY pond pump is shown in the background.

To set up a new culture, algae biomass can be harvested from a previous 10L culture, but this should not be done more than twice. Usually, the procedure for setting up a 10L culture is a stepwise process beginning with cultivation on an agar plate, and sequentially scaling the culture up in volume from 50mL, 200mL, 1L and finally 10L.

To create BG-11 agar, 15g.L^{-1} of agar is created and autoclaved separately to a double strength equal volume of BG-11 solution. Once the double strength BG-11 medium and the agar solution has cooled to below 60°C, the solutions are mixed under aseptic conditions and transferred to sterile petri dishes. The agar plates were inoculated with algae biomass using a sterile wire loop, and these plates are stored for up to two months.

The cultures grown on the agar plates are harvested using a wire loop, and transferred to 50mL BG-11 solution, and cultivated for up to two weeks. This volume is steadily scaled up to 250mL, 1L and then 10L, aseptically. This allows for the constant creation of backup cultures, and reduces the risk of bacterial contamination compared to constant inoculation from a previous 10L stock solution.

3.2 Monitoring Cell Growth

The monitoring if the growth of the cell cultures was performed using three methods; visual counting under a microscope [170], optical density using a UV-Vis spectrometer with wavelength of 680nm [171], and analysis of dry weight using gravimetric analysis [172].

3.2.1 Manual Cell Counting

For this analysis, 100µL algae culture was sampled. A *Neubauer*™ haemocytometer with a depth of 0.1mm and two counting grids was used as the counting chamber. Approximately 50µL of sample was inserted under the cover slip, over each counting grid, and the haemocytometer was set aside undisturbed for five minutes to allow the sample to settle.

The volume within the counting cells (of the grid) was 4nL (4×10^{-9}L), so the conversion factor to obtain cells.mL^{-1} was 2.5×10^{5}. The haemocytometer was placed within an Olympus BX41 microscope, connected to an Olympus UC50 digital camera. The algae cells were counted within ten of the grid squares, five from each of the innermost counting grids of each side of the haemocytometer. The cell concentration was determined by calculating the arithmetic mean of the cell count within each grid square, and multiplied by the conversion factor.

$$X_{Algae} = \frac{\sum_{i=1}^{n} x_i}{n} \times 2.5 \times 10^{5} mL^{-1}$$

Where:

- X_{Algae} is the concentration of the algae culture (cells.mL^{-1}).
- x_i is the number of cells within a grid square (cells)
- n is the number of grid squares counted.

3.2.2 Optical Density

The optical density was the fastest and least laborious method of monitoring cell growth. The absorbance was measured using UV-Vis spectroscopy at a wavelength of 680nm. This wavelength was chosen as previous studies suggest it is the

wavelength that is most absorbed by algae chlorophyll [171]. Although metal contact may affect chlorophyll a content of the algae cells [173], this was no issue for this analysis as the cells were not exposed to metal contamination during biomass cultivation, and kinetic experiments were not performed over time periods where the effects would become significant.

FisherBrand™ Polystyrene cuvettes composed of polystyrene and acrylic glass with a path length of 4.5mm and a volume of 1.5mL were used, one was filled with deionised water and used to as a blank to calibrate the spectrophotometer. In a new microcuvette each time, a 1.5mL culture sample was analysed for absorbance using a Jenway® 7305 Spectrophotometer.

3.2.3 Dry Weight

The final method of growth monitoring involved the extraction and drying of cellular biomass from a known volume of algae culture. In triplicate, Whatman® Nuclepore® Polycarbonate filters with a 0.22μm pore size were added to three labelled, oven-proof foil dishes. These were placed within an oven set to 80°C for one hour. The dried filters were transferred to a desiccator to cool for five minutes in a dry atmosphere, before being weighed using a Mettler Toledo MS105 balance, and the weights of each foil dish with the dry filter recorded.

The filters were then placed individually within a vacuum filter and 10mL of algae culture were filtered, while retaining the algae biomass on the filter. The filters were returned to their corresponding foil dish, and returned to the oven to dry at 80°C for two hours. Once dry, the foil dishes were returned to the desiccator and allowed to cool for five minutes, prior to being re-weighed with the MS105 balance.

The concentration was measured with units of $mg.L^{-1}$, by subtracting the new weight from the initial weight, and multiplied by 100.

$$X_{Algae} = \frac{\sum_{i=1}^{3}(\beta_i - \alpha_i)}{3} \times 100L^{-1}$$

Where:

- X_{Algae} is the algae concentration ($mg.L^{-1}$).

- β_i is the weight of the foil dish, filter and dried algae biomass (mg).
- α_i is the initial weight of the foil dish and filter prior to filtering the culture sample (mg).

3.2.4 Standard Curve to Determine Algae Concentration

The cell count, optical density and the dry weight were measured simultaneously so that the obtained values were comparable with each other. This allowed for the creation of standard curves that allowed for the algae concentration to be determined in $mg.L^{-1}$ and $cells.mL^{-1}$ by measuring the optical density at 680nm. This allows for the rapid measurement of algae concentration when sampling algae for experimental procedures.

The standard curve created for *C. vulgaris* showing the relationship between cell concentration ($mg.L^{-1}$) and absorbance at 680nm. Dry weight was chosen over cells per millilitre as it is a more quantitative measure that can be used to compare the algae species with each other. The standard curve for *C. vulgaris* is displayed in Figure 7.

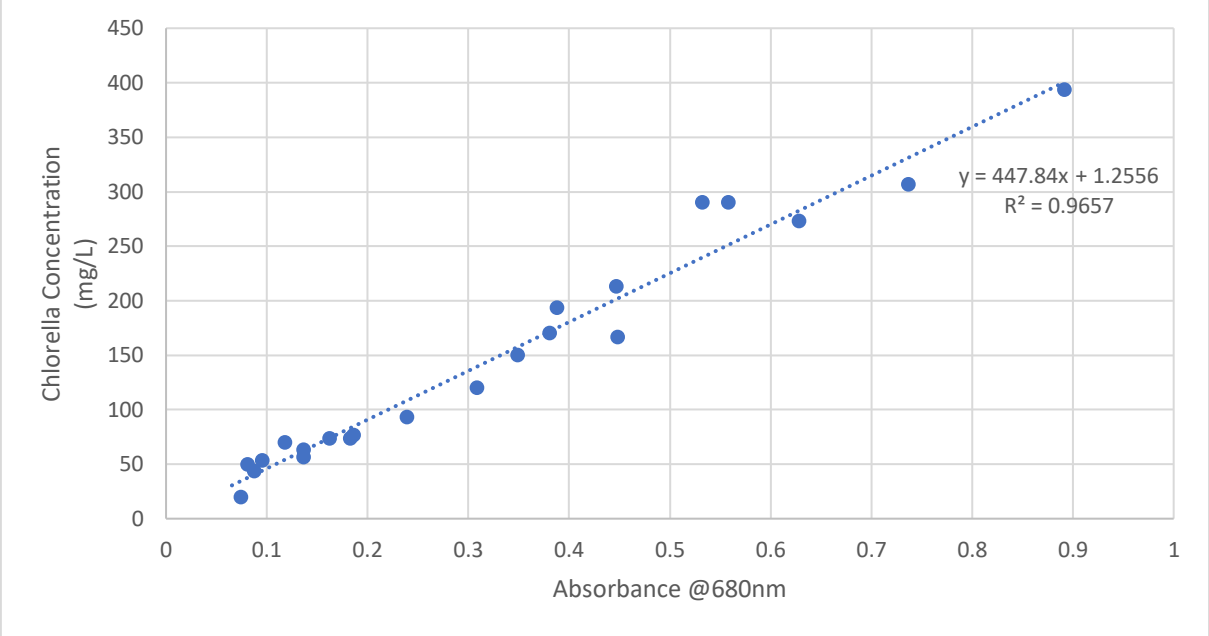

Figure 7: Standard curve of dry weight of *Chlorella vulgaris* plotted against the optical density

There is a good linear correlation between dry weight of *C. vulgaris* and absorbance at 680nm, with an R^2 value of 0.97. A linear model was derived from the data in

Figure 7 which was used to convert absorbance at 680nm to concentration of *C. vulgaris*.

$$[C.vulgaris] = 448 \times A_{680} + 1.3$$

Where:

- $[C.vulgaris]$ is the concentration of *C. vulgaris* (mg.L^{-1})
- A_{680} is the absorbance of the sample measured at 680nm

The standard curve showing the relationship between the dry weight of *S. obliquus* and the absorbance of the culture at 680nm is shown in Figure 8.

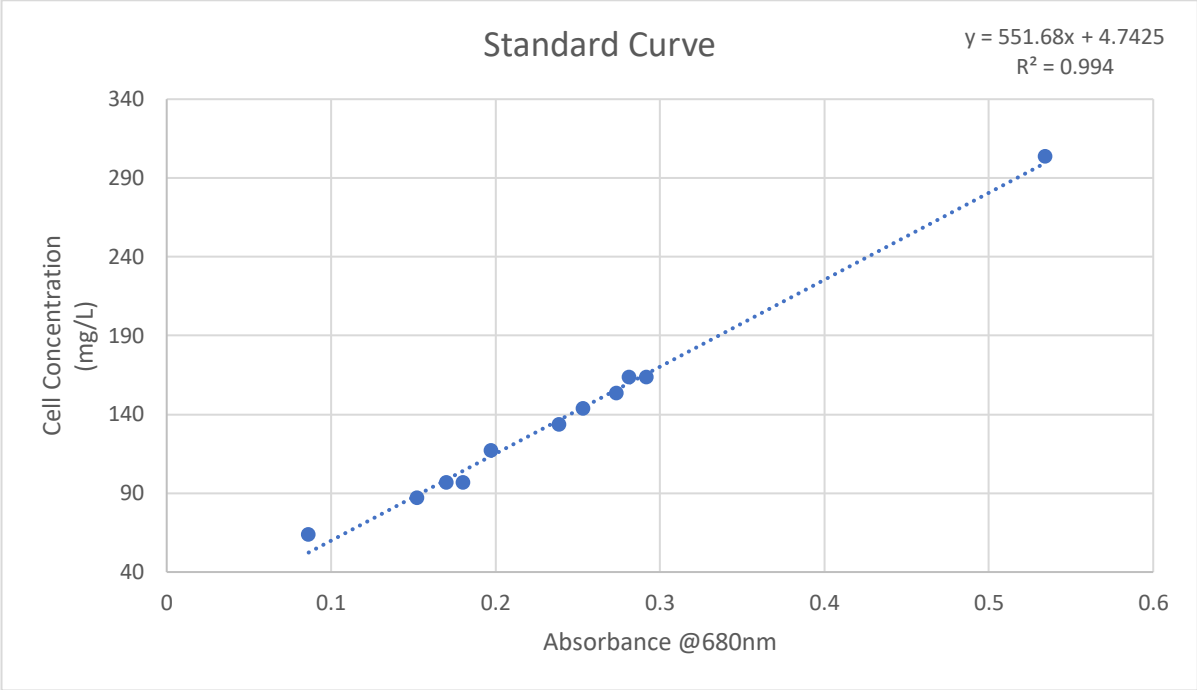

Figure 8: Standard curve of dry weight of *Scenedesmus obliquus* plotted against the optical density.

As in Figure 7, the dry weight of *S. obliquus* and absorbance at 680nm shows a good linear correlation, with an R^2 value of 0.99. The concentration of the *S. obliquus* in mg.L^{-1} is related to absorbance at 680nm by linear regression using the data displayed in Figure 8, allowing for the concentration to be determined by measuring the optical density.

$$[S.obliquus] = 552 \times A_{680} + 4.7$$

Where:

- $[S.obliquus]$ is the concentration of *C. vulgaris* (mg.L^{-1})
- A_{680} is the absorbance of the sample measured at 680nm

The concentration of the algae cultures used during the experimental procedures were all determined using the expressions derived from Figure 7 and Figure 8, by measuring the optical density of the algae cultures. If the cell cultures did not have the desired concentration, they were either diluted by addition of deionised water to attain the desired optical density, or were centrifuged at 3000rpm for three minutes using an Epindorf® 5810 centrifuge and then diluted with deionised water to attain the required optical density.

3.3 Overall Copper Uptake Experiments

This experiment was intended to capture the initial uptake kinetics of adsorption, and the slower mechanism of metal internalisation by the microalgae. *Chlorella vulgaris* was investigated for the uptake of copper from BG-11 medium that had been contaminated with copper ions.

The initial microalgae concentration for these experiments was intended to be 500mg.L^{-1}, and the initial copper concentration present within the BG-11 medium was 1.0mg.L^{-1}. To achieve these concentrations, the *C. vulgaris* stock concentration was concentrated to 1000mg.L^{-1} (determined by UV-vis measured at 680nm). 400mL of the algae solution was required for the experiment. In addition to this solution, 400mL of double strength BG-11 medium, contaminated with 2mg.L^{-1} Cu^{2+} ions was created. The composition of this solution is shown in Table 7.

Table 7: Concentration of salts required to create a double strength BG-11 medium, contaminated with 2mg.L^{-1} copper ions.

Component Salt	Concentration
$NaNO_3$	3g.L^{-1}
K_2HPO_4	80mg.L^{-1}
$MgSO_4.7H_2O$	130mg.L^{-1}
$CaCl_2.2H_2O$	72mg.L^{-1}
Citric acid	12mg.L^{-1}
Ammonium Ferric Citrate Green	12mg.L^{-1}
$EDTANa_2$	2mg.L^{-1}
Na_2CO_3	40mg.L^{-1}
H_3BO_4	5.72mg.L^{-1}
$MnCl_2.4H_2O$	3.62mg.L^{-1}
$ZnSO_4.7H_2O$	0.44mg.L^{-1}
$Na_2MoO_4.2H_2O$	0.78mg.L^{-1}
$CuSO_4.5H_2O$	0.16mg.L^{-1}
$Co(NO_3)_2.6H_2O$	0.1mg.L^{-1}
$CuCl_2.2H_2O$	5.4mg.L^{-1}

The copper chloride dihydrate was maintained in solution which was acidified by addition of 1% by volume of 70% nitric acid. When contaminated BG-11 solutions were created, pH was raised to pH 6 by the dropwise addition of 0.1M potassium hydroxide solution.

200mL of double strength BG-11 medium, containing the component salt concentrations as displayed in Table 7 but omitting the $CuCl_2.2H_2O$, was pre-prepared and autoclaved. The final component required for the experimental mixtures was 200mL deionised water that was also pre-autoclaved.

The three experimental replicates were composed of 100mL of 1000mg.L^{-1} *C. vulgaris* solution and 100mg.L^{-1} of double strength BG-11 medium contaminated with 2mg.L^{-1} copper ions. This produced an initial experimental concentration of 500mgL^{-1} *C. vulgaris* and 1mg.L^{-1} copper contaminant.

A control, referred to as *"Control 1"* was created by mixing 100mL of double strength BG-11 medium with 100mL autoclaved deionised water, *"Control 2"* was created by mixing 100mL 1000mg.L^{-1} *C. vulgaris* solution and 100mL double strength BG-11 medium, and the final control; labelled *"Control 3"* was created by mixing 100mL double strength BG-11 medium with 100mL deionised water.

The Experimental setup is shown in Figure 9. Immediately after each bottle was created, 4mL sample was taken and filtered through a 0.22µm FisherBrand® non-sterile nylon syringe filter (25mm diameter). The liquid holdup of the syringe filters were approximately 0.3mL, resulting in the sample volume being approximately 3.7mL. The samples were collected in a 5mL glass vial and were acidified by the addition of 37µL of 70% nitric acid.

Samples were taken every hour for the first three hours, and then daily for the next three days. Each sample was collected and acidified with 70% nitric acid for analysis with ICP.

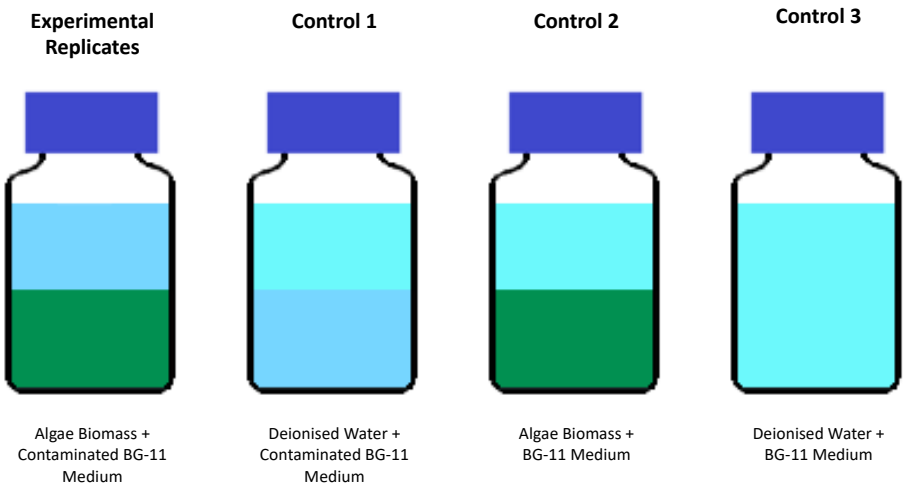

Figure 9: 200mL metal uptake by microalgae experimental setup. Composition of the experimental replicates, and the three control bottles.

3.4 Initial Uptake Kinetic Experiments

3.4.1 BG-11 Experiments

The procedure for the 200mL experiments was modified to focus in on the initial metal uptake rate by the microalgae. For this procedure, the contaminated media was mixed with microalgae biomass within a 5mL syringe, and filtered at set time intervals. Initially the microalgae biomass concentration was kept at 500mg.L^{-1}, but this needed to be reduced to 250mg.L^{-1} as the syringe filters became easily blocked.

Contaminated BG-11 medium was created following the same procedure as described in Section 3.3. 2mL of the contaminated BG-11 was drawn into a syringe, followed by 2mL of deionised water. This was filtered through a 0.22µm

FisherBrand® non-sterile nylon syringe filter (25mm diameter), into a 5mL vial and acidified by the addition of 37µL of 70% nitric acid. This was to obtain the initial metal concentration.

2mL of contaminated BG-11 was again drawn into the syringe, and this time 2mL of algae solution was drawn into the same syringe. After five seconds, this was filtered through a 0.22µm nylon syringe filter, into a 5mL collecting vial, and acidified once again by the addition of 1% by volume of 70% nitric acid. This procedure was repeated, with the time intervals increasing by five seconds up until 60 seconds, and then every thirty seconds until three minutes, and then for four and then five minutes. All time points were sampled in triplicate.

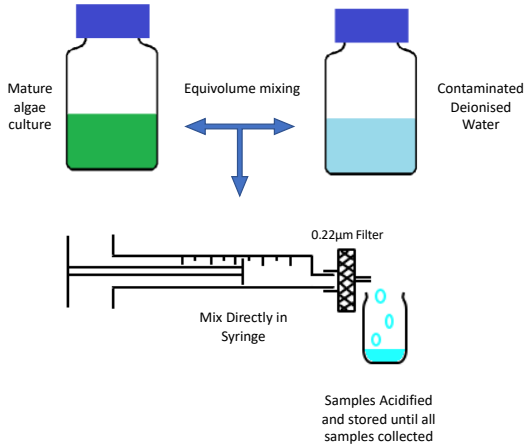

Figure 10: Procedure for performing the 4mL syringe, batch experiments to capture the initial adsorption kinetics of the microalgae. 2mL of each solution is drawn into the syringe, and at pre-determined time-points the mixture in ejected through a 0.22µm syringe filter into a collection vial.

3.4.2 Deionised Water Experiments

Following the experiments investigating the initial kinetics of the metal by the microalgae from contaminated BG-11 solution, the procedure was modified once more to measure the uptake of metals from deionised water. This would remove any interference caused by the medium salts to the adsorption process.

The microalgae stock solution was centrifuged at 3000rpm for five minutes using an Eppendorf® centrifuge 5810. The supernatant was drained off, and the algae pellet was resuspended in deionised water. This procedure was repeated twice to remove any residual BG-11 salts. The resuspended microalgae was diluted to the desired biomass concentration by the addition of deionised water.

Copper and cadmium solutions of 0.5mg.L^{-1}, 1mg.L^{-1}, 1.5 mg.L^{-1} and 5mg.L^{-1} were created to investigate the uptake rate of each metal by *Chlorella vulgaris* and *Scenedesmus obliquus* over a range of metal concentrations. These were created by dissolving copper chloride dihydrate and cadmium sulphate octahydrate in deionised water, with the concentrations shown in Table 8.

Table 8. Concentration of copper chloride dihydrate and cadmium sulphate octahydrate required to produce copper and cadmium solutions with a concentration of 0.5, 1.0, 1.5 and 5.0mg.L^{-1}.

Metal Concentration ($mg.L^{-1}$)	$CuCl_2.2H_2O$ Concentration ($mg.L^{-1}$)	$3(Cd.SO_4).8H_2O$ Concentration ($mg.L^{-1}$)
0.5	1.35	1.15
1.0	2.7	2.3
1.5	4.05	3.45
5.0	13.5	11.5

The concentrations of the copper chloride dihydrate and cadmium sulphate octahydrate shown in Table 8 produce an experimental metal concentration of 0.25, 0.5, 0.75 and 2.5 mg.L^{-1} of each metal ion. The sampling procedure followed that as described in Section 3.4.1, with the initial metal concentration determined by mixing 2mL of the metal solution with 2mL of deionised water, filtered through 0.22μm nylon syringe filter and acidified by the addition of 1% by volume of 70% nitric acid. 2mL of algae solution was then mixed with 2mL metal solution within the syringe and after five seconds, filtered and acidified. The procedure was repeated with the time increasing in increments of five seconds until the final sample was filtered after forty seconds. All samples were collected in triplicate.

3.5 Immobilised Algae Experiments

3.5.1 Biocomposite Pulp Creation

The paper biocomposites were produced as follows from a mixture of pre-prepared pulp stocks. These are:

1. Hardwood pulps
2. Softwood pulps
3. Microfibrillar Cellulose (MFC) pulp
4. Chitosan binder

Previous studies have used BG-11 media to create the pulps to embed nutrients into the structure. Preliminary experiments within this study however used deionised

water to prevent unwanted bacterial growth while the pulps were stored. Future studies shall use both BG-11 medium and deionised water.

The hardwood pulp was created by shredding 1.75g of a Georgia Pacific Hardwood sheet and suspending the particles in 516.8g of deionised water. A Mettler Toledo® precision balance was used to weigh out the components. 1.75g of the hardwood pulp was cut to approximately $1cm^2$ pieces, and added to a food processor. 129.3g deionised water was weighed in a large weighing boat and transferred to the food processor and the mixture was processed for five minutes on a high setting. 387.5g of deionised water was then added to the food processor, and mixed for a further ten minutes on the high setting. This produced a hardwood pulp that had a dry weight of approximately 0.3% by mass.

The softwood pulp was created in an identical way, but as the Georgia Pacific Softwood sheet had a lower moisture content compared to the hardwood sheet, 1.73g of the softwood was required.

Microfibrillar Cellulose pulp was purchased from Cellulose Laboratories, Canada. The moisture content of the pulp was measured by measuring 10g of the pulp into a pre-weighed foil weigh-boat. The total mass was recorded. The weigh-boat was transferred to an oven and the pulp was dried over night at a temperature between 70 and 80°C. The mass of the weigh-boat containing the dried pulp was remeasured, and the mass of the empty weigh-boat was subtracted from the new value. The dry weight was recorded by dividing the difference by 10g, and multiplied by 100. The MFC used in this study had a 2.9% by mass solid content.

The chitosan solution was created by diluting 2mL glacial acetic acid ($60.1gmol^{-1}$) by addition of 98mL deionised water within a volumetric flask. The 2% acetic acid solution was then transferred to a 100mL Duran®, and to this 1g of chitosan powder was added. A magnetic flea was added to the solution, and the bottle was agitated overnight on a magnetic stirrer. This created a $10mg.mL^{-1}$ chitosan solution.

The three pulps and chitosan solution were autoclaved and stored within a refrigerator when not in use.

3.5.2 Biocomposite paper creation

The MFC content has been found during previous experiments to be a mitigating factor in the stability of the Biocomposite structure. However, too high an MFC concentration affects the water permeability of the biocomposite [174].

The biocomposites were created with an algae biomass of 200mg per algae paper to make the microalgae biomass content equivalent to a previous sessile experiment undertaken at a 200mL scale. Paper was cut to fit scaffolds that were 3D printed to hold the paper in place within solution. The paper was cut to an area of 11.4cm^2, and required 36.5mg of biomass within this area. The paper structures were circular (shown in Figure 11), with an area of 62.2cm^2, so 200mg of algae was required for the necessary 3.2mg.cm^{-2} of algae biomass to achieve the 36.5mg of algae for the experiments.

The volume of algae solution depends on the absorbance of the solution at 680nm, path length 4.5mm.

$$[C.vulgaris] = 448 \times A_{680} + 1.3$$

$$[S.obliquus] = 552 \times A_{680} + 4.7$$

All pulps were removed from the fridge and allowed to reach room temperature prior to mixing. This was done in a 2L volume beaker, and mixed on a magnetic stirrer with a large magnetic flea. The masses of each component required to produce the biocomposite paper and the control paper are shown in Table 9. For the control paper, the mass of softwood and hardwood pulps were increased to compensate for the absence of algae biomass.

Table 9: Mass of MFC, Softwood Pulp, Hardwood Pulp, Algae biomass and volume of chitosan solution required to create the biocomposites, and comparison paper controls. Both recipes produce a paper with equivalent mass.

Paper	Mass MFC Pulp (g)	Mass Soft Wood Pulp (g)	Mass Hard Wood Pulp (g)	Mass of Algae (g)	Volume of Chitosan (mL)
Algae	29.7	87.8	87.8	0.2	7.5
Control	29.7	121.1	121.1	0	7.5

The required MFC, Softwood pulp and hardwood pulp, and volume of chitosan were added to the 2L beaker and stirred. The pH was measured using a Mettler Toledo®

FiveEasy™ FE20 pH meter. The pH was raised to pH 7 by the slow addition of 1M KOH, before the necessary volume of algae solution that contains 200mg of biomass is added.

The mixture was then filtered through a Whatman® Grade 41 filter paper placed in a Büchner funnel. A baffled mixer has been 3D printed, and should be used to agitate the mixture within the funnel. Once mixed, a vacuum was applied to draw out the liquid and settle the solids in a uniform layer.

When the liquid had been drawn through the filter, the damp paper was carefully removed from the funnel, and excess liquid was pressed out of the circular paper. The paper was dried in darkness in an ambient humidity environment.

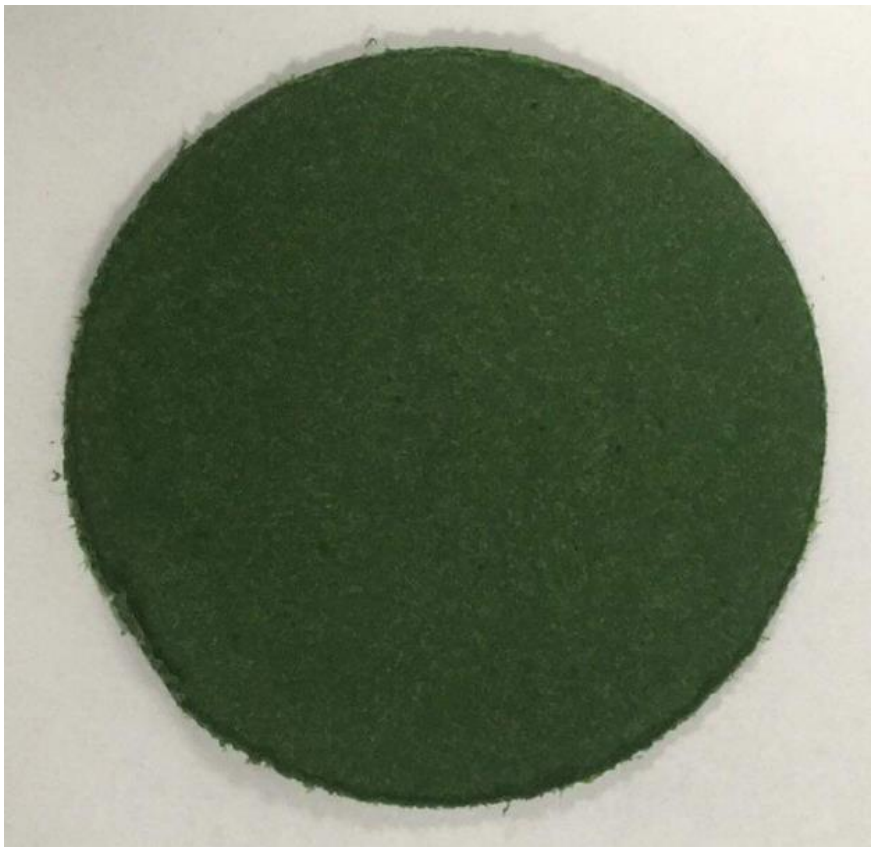

Figure 11: Algae-paper biocomposite after de-watering the pulp and algae mixture using a vacuum pump.

Following the paper creation, the Büchner funnel required washing with 1M HCl, and rinsing with boiling water to remove the chitosan from the funnel pores.

3.5.3 Cadmium Uptake by Immobilised Microalgae

To reduce the potential for bacterial contamination, prior to assembly of the apparatus, the 3D printed scaffolds were exposed to UV light for ten minutes. Eight

scaffolds were required in total. An example of an assembles scaffold is shown in Figure 12.

Figure 12: 3D printed scaffold used to secure the algae biocomposite paper for batch solutions.

Five bottles containing a concentration of 0.2 $mg.L^{-1}$ of Cu^{2+} were created and autoclaved, and two bottles of deionised water were created and autoclaved. The experimental setup showing the experimental replicates, and three sets of controls is shown in Figure 13.

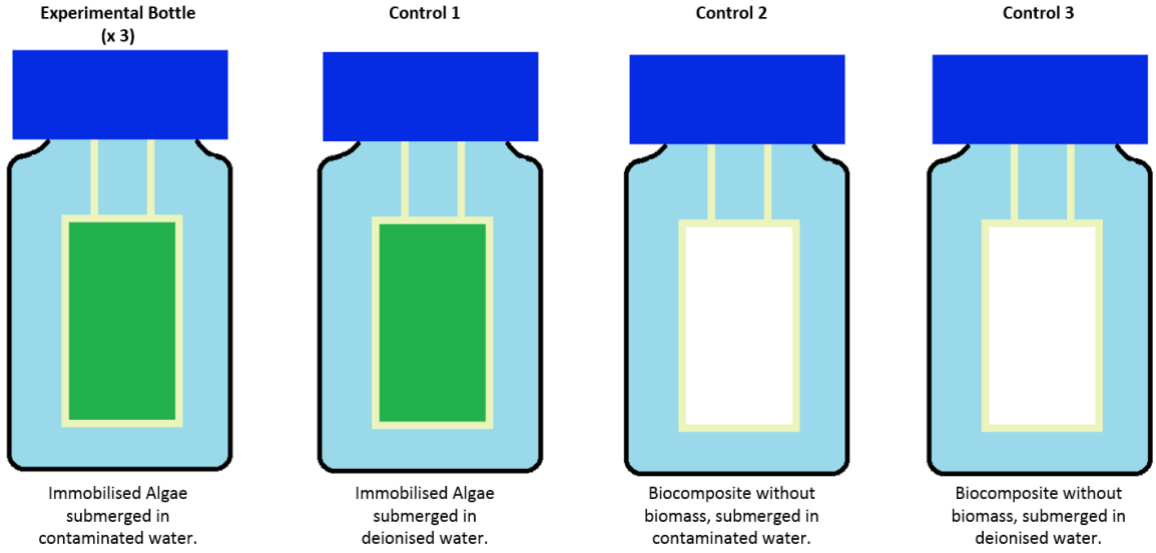

Figure 13: Experimental setup for metal ion removal from batch systems using microalgae that has been immobilised using a paper biocomposite.

For the experimental replicates, and "Control 1", four segments of 11.44cm^2 algae paper were fixed into the 3d printed scaffolds. Control 2 and 3 require two segments of 11.44cm^2 paper without embedded algae. These were also fixed inside a 3D printed scaffold. Four of the bottles containing deionised water contaminated with 0.2mgL^{-1}, were labelled "*Experiment 1*", "*Experiment 2*", "*Experiment 3*" and

"*Control 2*", and a 4mL initial sample was taken from each. These samples were collected through a 0.22μm syringe filter, and acidified with the addition of 1% by volume of HNO_3. The samples were labelled as sample 0 for each bottle.

From the fifth bottle containing deionised water contaminated with 0.2mgL^{-1} copper ions, 4mL was transferred to the bottles labelled "*Experiment 1*", "*Experiment 2*", "*Experiment 3*" and "*Control 2*". Each paper designated for the experimental replicates and the paper designated for "*Control 2*" were submerged into their respective bottle containing 0.2mgL^{-1} copper solution. Two of the remaining bottles containing deionised water were labelled "*Control 1*" and "*Control 3*". These were sampled as described in Step 5, and will be topped up with 4mL of sterile deionised water from a third sterile bottle.

The fourth 11.44cm^2 algae paper was submerged in the bottle labelled "*Control 1*", and the second 11.44cm^2 paper free from algae was submerged in the bottle labelled "*Control 4*". Samples were collected every ten seconds from each bottle for the first minute, as described in Step 5. Samples were taken every minute for five minutes, then after ten minutes, every ten minutes until an hour had passed. Further samples were taken on the second hour, third hour, first day, second day and third day.

3.6 Colourimetry Analysis Using HACH® Test Kits

To measure Ammonia and copper concentrations off sight at Bran Sands HACH® cuvette kits were used and concentrations analysed using a HACH® DR 3900 spectrophotometer. The cuvettes required were LCK329 for the copper analysis and LCK30f for the ammonium analysis. These kits came with pre-prepared reagents that were mixed in accordance to the instructions on each kit.

3.7 Inductively Coupled Plasma Spectroscopy (ICP) Analysis

3.7.1 ICP-Optical Emission Spectroscopy

Analysis of metal content was performed using a Perkin Elmer Optima 8000 ICP-OES. ICP analyses samples by energising small volumes within a plasma flame, and ICP-OES detects high energy photons released from elements present within the sample.

To quantify the elements present, ICP requires a process known as *External Calibration*, where the instrument is pre-calibrated prior to each analysis. For calibration, four standards are created:

1. Blank created with deionised water or matrix matched solution, no metal contamination.
2. A low concentration standard, that is half the expected concentration at the beginning of the experiment.
3. A middle standard that is equal to the concentration of the initial experimental metal concentration.
4. A higher concentration standard that is 1.5× the initial experimental concentration.

The standards should be matrix matched to the experimental samples; this means if the experimental samples are acidified with 1% by volume 70% nitric acid, then the standard solutions will also require acidification by the same method. If contaminated BG-11 medium was used, then the standards should be created using BG-11 media to compensate for any interaction caused by the medium salts. The standard solutions are created by diluting 1000mg.L^{-1} ICP standard solution purchased from Fisher Scientific®, with deionised water. The cadmium standard was a 1000ppm solution, dissolved in a 1M nitric acid solution. The copper standard was 1000pm copper solution, dissolved in 2% nitric acid.

The ICP was initiated and left to warm up for at least thirty minutes. The flowrate of the sample introduction pump was set to 1mL per minute, and 2% HNO_3 solution was passed through the system for five minutes to flush any residual sample from previous analyses. For the remainder of the warm up period, deionised water was passed through the equipment.

Once the equipment has warmed up, the standard curve can be created. Within the software, the order for the measurement of each standard is manually set. When the standard is analysed the equipment measures the counts per second (CPS) of the photons of interest. This CPS is then associated with the specified standard

concentration. The linear fit of the produced standard curve is checked to ensure the R^2 value is above 0.999, if it is lower the equipment is recalibrated.

Once the calibration was complete, the blank and the standard with the middle concentration was analysed to verify the curve. The samples were then analysed one by one and after ten samples were analysed, the blank and the middle concentration standard were reanalysed to check for equipment drift. If there is a greater than 5% discrepancy between this measurement of the standard, and the previous measurement of the standard, then the ICP should be recalibrated.

3.7.2 ICP- Mass Spectroscopy

Samples were sent for external analysis by Northumbria Water Scientific Services that used ICP-MS, following unforeseen performance issues with the ICP-OES. The methodology for ICP-MS and ICP-OES is largely the same.

To negate issues caused by poor sample matrix matching with the standard solutions used for calibration, the experimental procedure was modified by replacing the BG-11 medium with deionised water to create the contaminated metal solutions.

The model of ICP used in this analysis was a Thermo Scientific® iCAP RQ ICP-MS, using the KED (Kinetic Energy Discrimination) mode. The carrier gas in this analysis was helium; this removed the risk of interference by the potential presence of $ArNa^+$ that could be produced in the argon flame [175].

The analysis was undertaken at 20 times dilution, with an internal standard that contained scandium, germanium, rhodium and iridium. The standard curve was created with copper and cadmium concentrations of 0, 0.01, 0.02, 0.05, 0.1, 0.2, 1.0 and 2.0 $mg.L^{-1}$.

3.8 Data Analysis

3.8.1 Adsorption Isotherms

Three Isotherms were used in this study, the Langmuir Isotherm, the Freundlich Isotherm and the Temkin Isotherm. The Langmuir Isotherm has the form:

$$Q_e = \frac{Q_{max} \cdot b_L \cdot C_e}{1 + b_L \cdot C_e} \quad (2)$$

Where:

- Q_e is the adsorption of metal ion per gram of algae at equilibrium ($mg.g^{-1}$)
- C_e is the residual concentration of metal ion at equilibrium ($mg.L^{-1}$)
- Q_{max} is the maximum quantity of metal ion that can be adsorbed ($mg.g^{-1}$)
- b_L is the Langmuir Equilibrium constant ($L.mg^{-1}$)

The model parameters were obtained by the Lineweaver-Burke method, which involved taking the reciprocal of Equation 2, and separation of the numerator. This returns an equation of a straight line as shown in Equation 3.

$$\frac{1}{Q_e} = \frac{1}{Q_{max} \cdot b_L} \cdot \frac{1}{C_e} + \frac{1}{Q_{max}} \quad (3)$$

The model parameters are determined by plotting the reciprocal of the adsorption at equilibrium against the reciprocal of the concentration in solution at equilibrium. The y-intercept of this plot is the reciprocal of the maximum adsorption capacity of the adsorbent, and the y-intercept divided by the gradient of the plot is the Langmuir equilibrium constant.

The Freundlich Isotherm has the following form:

$$Q_e = K_f \cdot C_e^{1/n} \quad (6)$$

Where:

- Q_e is the adsorption of metal ion per gram of algae at equilibrium ($mg.g^{-1}$)
- C_e is the residual concentration of metal ion at equilibrium ($mg.L^{-1}$)
- K_f is the distribution coefficient $(mg.g^{-1})(mg.L^{-1})^n$.
- n is a correction factor.

This parameters for the Freundlich Isotherm are also determined by linearizing the model and applying it to experimental data. The natural logarithm of Equation 6 is

taken, and the right hand-side of the equation is expanded, as shown in Equation 6.1.

$$= ln(Q_e) = \frac{1}{n} . ln(C_e) + ln(K_f) \quad (6.1)$$

The natural logarithm of the adsorption at equilibrium was plotted against the natural logarithm of the concentration of the adsorbate in solution at equilibrium. The correction factor, *n* is calculated by finding the reciprocal of the gradient of the curve, and the distribution coefficient is calculated taking the exponential of the y-axis intercept.

The Temkin Isotherm has the following form:

$$Q_e = B . ln(A_T . C_e) \quad (9.1)$$

Where

- Qe is the adsorption of metal ion per gram of algae at equilibrium (mmol.g^{-1})
- Ce is the residual concentration of metal ion at equilibrium (mmol.L^{-1})
- B is a dimensionless number containing the gas constant (Jmmol^{-1}K^{-1}, temperature (K) and the Temkin constant, b_T (J.g.mmol^{-1})
- A^T is the Temkin Isotherm equilibrium binding constant (Lmmol^{-1}).

To derive the linear form of the Temkin Isotherm, the Logarithm term can be expanded as shown in Equation 10.1:

$$Q_e = B. ln(C_e) + B. ln(A_T) \quad (10.1)$$

The expression for the dimensionless number, B is shown in Equation 3.2

$$B = \frac{RT}{b_T} \quad (3.2)$$

The adsorption at equilibrium is plotted against the natural logarithm of the residual concentration. The gradient of the line corresponds to B and A_T is calculated by calculating the exponential of the y-axis intercept divided by the gradient.

3.8.2 Kinetic models

In literature, three of the most common models to be used for modelling the adsorption kinetics of biosorbents are the Lagergren Model, the second order model and the Elovich model. The Lagergren and the second order model are derived as a function of equilibrium, where the Elovich model is a function of initial rates. A fourth model that has not been seen utilised for microalgae data is the Langmuir kinetic model.

3.8.2.1 Lagergren Model

The Lagergren model is a pseudo first order model that states that the rate of change of adsorption is equal to a rate constant multiplied by the adsorption at time *t* subtracted from the equilibrium value of adsorption. This is expressed as Equation 12.

$$\frac{dQ_t}{dt} = k_1(Q_e - Q_t) \tag{12}$$

The integrated form of Equation 12 is shown by Equation 13.

$$Q_t = Q_e(1 - e^{-k_1.t}) \tag{13}$$

Where:

- Q_e is the adsorption at equilibrium (mg.s^{-1}).
- Q_t is the adsorption at time t (mg.s^{-1}).
- k_1 is the first order rate constant (s^{-1}).
- t is the elapsed time (s)

Equation 13 is the non-linear form of the Lagergren model. The model parameters are determined by linearizing the model and plotting experimental data accordingly. The linear form of the Lagergren model is shown in Equation 14.

$$\log_e(Q_e - Q_t) = -k_1.t + \log_e(Q_e) \tag{14}$$

For this model, Q_e appears on both sides of the equation. It was initially approximated from experimental data, and the logarithm of the adsorption at time

t subtracted from the approximation of the adsorption at equilibrium was plotted against time.

The adsorption at equilibrium Q_e can then be determined from the y-axis intercept, and the adsorption rate will be equal to the gradient of the fit.

These values were taken as initial estimates for the model, and the statistical software *R* was used to fit the experimental data to Equation 13 to obtain more accurate model parameters. The *nls()* function was used with the Gauss-Seidel algorithm to converge the predicted data to the experimental data.

3.8.2.2 Second Order Model

Ho and Mckay [124-127] derive the second order model from the Lagergren model by stating that the rate of change of adsorption is equal to the rate constant k_2 multiplied by the difference between the adsorption at time *t* and the adsorption at equilibrium, squared (as shown in Equation 15).

$$\frac{dQ_t}{dt} = k_2(Q_e - Q_t)^2 \tag{15}$$

Where:

- Q_e is the adsorption at equilibrium (mg.s^{-1}).
- Q_t is the adsorption at time *t* (mg.s^{-1}).
- k_2 is the second order rate constant (g.mg^{-1}.s^{-1}).
- *t* is the elapsed time (s)

The integrated form of the second order model is shown in Equation 16.

$$Q_t = \frac{Q_e^2 k_t . t}{1 + Q_e k_t . t} \tag{16}$$

As with the Lagergren model, the second order model parameters are determined by linearizing the model and plotting experimental data in accordance to this model. The linear form of the second order model is shown in Equation 17.

$$\frac{1}{Q_t} = \frac{1}{Q_e^2 k_t} . \frac{1}{t} + \frac{1}{Q_e} \tag{17}$$

By plotting the reciprocal of the adsorption against the reciprocal of the time passed, a straight line is produced from which the adsorption at equilibrium can be calculated by taking the reciprocal of the y-axis intercept, and the second order rate constant can be calculated by dividing the square of the y-axis intercept by the gradient of the slope.

The parameters obtained by linearizing the model were also fitted to Equation 16 by non-linear regression using *R*.

3.8.2.3 Elovich Model

The Elovich Model focusses adsorption rates other than equilibrium adsorption values. The Elovich Model states that the rate of change of adsorption is equal to a maximum adsorption rate multiplied by the exponential of a constant multiplied by the adsorption at time *t*. This is shown in Equation 18.

$$\frac{dQ_t}{dt} = \alpha e^{-\beta Q_t} \tag{18}$$

The integrated form of the Elovich Model is shown in Equation 19

$$Q_t = \frac{1}{\beta}\log_e(\alpha\beta t + 1) \tag{19}$$

Where:

- Q_t is the adsorption at time t (mg.s^{-1}).
- β is the desorption constant (g.mg^{-1}).
- α the maximum adsorption rate (mg.g^{-1}s^{-1}).

The assumption that $\alpha\beta t >> 0$ allows for Equation 19 to be rearranged and linearized to Equation 20.

$$Q_t = \frac{1}{\beta}\log_e(t) + \frac{1}{\beta}\log_e(\alpha\beta) \tag{20}$$

Plotting Q_t against *ln(t)*, the desorption constant is equal to the reciprocal of the gradient, and the maximum adsorption rate can be calculated by Equation 21.

$$\alpha = \frac{e^{c/m}}{\beta} \tag{21}$$

Where:

- c is the y-axis intercept.
- m is the gradient.

3.8.2.4 The Langmuir Kinetic Model

The Langmuir kinetic model states that the rate of change of adsorption is equal to the rate of adsorption minus the rate of desorption. The Langmuir model can be transformed to the form of a hybrid kinetic model containing a first order rate term and a second order rate term, as shown in Equation 22.

$$\frac{dQ_t}{dt} = k_1(Q_e - Q_t) + k_2'(Q_e - Q_t)^2 \tag{22}$$

Where:

- Q_e is the adsorption at equilibrium (mg.s^{-1}).
- Q_t is the adsorption at time t (mg.s^{-1}).
- k_1 is the first order rate constant (s^{-1}).
- k_2' is the second order rate constant (g.mg^{-1}.s^{-1}).

Equation 7 can be simplified and approximated to either a first order model, or a second order model depending on the values of Q_e, k_1 and k_2'. If $Q_e \leq k_1/k_2'$ then Equation 7 can be approximated as a first order model (Equation 22.1).

$$\frac{dQ_t}{dt} \approx k_1(Q_e - Q_t) \tag{22.1}$$

Integrating Equation 22.1, the non-linear form of the Lagergren model is obtained (Equation 12).

If $Q_e >> k_1/k_2'$, Equation 22 can be approximated to the second order model (shown in Equation 22.2).

$$\frac{dQ_t}{dt} \approx k_2{}'(Q_e - Q_t)^2 \tag{22.2}$$

Integration of Equation 22.2 will produce the non-linear form of the second order model as shown in Equation 16. If neither of the conditions are met, then the hybrid form of the Langmuir kinetics equation (Equation 22) is used. This is integrated to Equation 23.

$$Q_t = Q_e\left(1 - \frac{k_1}{(Q_e k_2{}' + k_1)e^{k_1 t} - Q_e k_2{}'}\right) \tag{23}$$

The values of Q_e, k_1, k_2 and k_2' are found by Equation 24, 25, 26 and 11 respectively.

$$Q_e = \frac{C_0 - C_e}{X_{Algae}} \tag{27}$$

Where:

- C_0 is the initial adsorbate concentration (mg.L^{-1}).
- C_e is the concentration of adsorbate once equilibrium had been reached (mg.L^{-1}).
- X_{Algae} is the adsorbent concentration (g.L^{-1}).

$$k_1 = \sqrt{b_L{}^2\left(\frac{C_0}{Q_{max}} - X_{Algae}\right)^2 + 2b_L\left(\frac{C_0}{Q_{max}{}^2} + \frac{X_{Algae}}{Q_{max}}\right) + \frac{1}{Q_{max}{}^2}} \tag{25}$$

$$k_2 = b_L X_{Algae} \tag{26}$$

The maximum adsorption capacity (Q_{max}) and Langmuir equilibrium constant (b_L) are determined from the Langmuir Isotherm (Equation 2). The Langmuir second order rate constant k_2' is found by dividing k_2 by the maximum adsorption capacity.

$$k_2{}' = \frac{k_2}{Q_{max}} \tag{27}$$

3.8.3 Goodness of Fit

For linear correlations, the data obtained from the optical density, cell count and the dry weight can be compared by using the Pearson Product-Moment correlation as follows:

$$r = \frac{\sum(x_i - \bar{x})(y_i - \bar{y})}{\sqrt{\sum(x_i - \bar{x})^2 \sum(y_i - \bar{y})^2}} \tag{28}$$

Where:

- r is the Pearson Product-Moment *coefficient*.
- x_i is values of the x-data in sample length *i*.
- $\bar{x}$ is the mean of the x-values.
- y_i is the values of the y-data in sample length *i*.
- $\bar{y}$ is the mean of the y-values.

The value for *r* represents how well a straight line can represent the experimental data. The minimum value for *r* is -1, and the maximum is 1. A value of -1 indicates perfect negative correlation, and a value of 1 indicates perfect positive correlation. If a value of zero is returned, then there is no correlation between the two datasets.

The coefficient of determination R^2 is the square of the Pearson Product-moment coefficient. R^2 ranges from 0 to 1 and indicates how well the linear model represents the relationship between the datasets, without indicating of whether the correlation is positive or negative.

The coefficient of determination can also be determined by Equation 29.

$$R^2 = \frac{\sum(y_i - \hat{y})^2}{\sum(y_i - \bar{y})^2} \tag{29}$$

Where R^2 is the Coefficient of Determination.

To analyse the goodness of fit by non-linear relationships for the kinetic data, the Root Mean Square Error (RMSE) and the Nash and Sutcliffe coefficient of Efficiency (NSE) were employed. The RMSE is calculated by Equation 30.

$$RMSE = \sqrt{\frac{\sum_{i=1}^{n}(\hat{y}_i - y_i)}{n}} \tag{30}$$

Where:

- $\hat{y}_i$ is the non-linear model prediction for the i^{th} y-value.
- y_i is the i^{th} y-value.
- n is the number of data points.

RMSE values can range from 0 to infinity. The lower the value of the RMSE, the better the fit of the model, however the presence of outliers significantly impact on this analysis.

The NSE is calculated by Equation 34.

$$NSE = 1 - \frac{RMSE^2}{\sigma^2} \tag{34}$$

The NSE analyses the ratio of the square of the RMSE and the square of the standard deviation (σ) of the dataset. The standard deviation is calculated by Equation 35.

$$\sigma = \sqrt{\frac{\sum_{i=1}^{n}(y_i - \bar{y})^2}{n}} \tag{35}$$

Where $\bar{y}$ is the mean of the independent variables.

The Chi-square test is another test that was used to test the goodness of fit for the Langmuir kinetics. Similar to the RMSE, a smaller Chi-Square Statistic indicates a better fit of the model to the experimental data. The Chi-Square statistic (χ^2) is calculated by Equation 36.

$$\chi^2 = \sum_{i=1}^{n} \frac{(y_i - \hat{y}_i)^2}{y_i} \tag{36}$$

Where:

- $\hat{y}_i$ is the non-linear model prediction for the i^{th} y-value.

- y_i is the i^{th} y-value.
- n is the number of data points.

3.8.4 Independent t-test

The Independent t-test was used to compare the adsorption at equilibrium for the metal uptake experiments. This compares the adsorption by the two microalgae species and compares the adsorption of the metal ions. The Independent t-test was performed using R software, which produced a t-statistic, and a p-value for a 95% confidence interval. If the p-value was less than the numbers of degrees of freedom, then it can be concluded that there is a statistical difference between the two datasets.

$$t = \frac{\bar{x}_1 - \bar{x}_2}{\sqrt{s^2\left(\frac{1}{n_1} + \frac{1}{n_2}\right)}} \tag{37}$$

Where:

- $\bar{x}_1$ is the mean of the first dataset.
- $\bar{x}_2$ is the mean of the second dataset.
- s^2 is the pooled sample variance of both datasets.
- n_1 is the sample size for the first dataset.
- n_2 is the sample size for the second dataset.

The pooled sample variance is calculated by Equation 38.

$$s^2 = \frac{\sum_{i=1}^{n_1}(x_i - \bar{x}_1)^2 + \sum_{j=1}^{n_2}\left(x_j - \bar{x}_2\right)^2}{n_1 + n_2 - 2} \tag{38}$$

Where:

- x_i is the i^{th} value from the first dataset.
- $\bar{x}_1$ is the mean of the second dataset.
- x_j is the j^{th} value from the second dataset.
- $\bar{x}_2$ is the mean of the second dataset.

Chapter 4 Method Development

4.1 Introduction

The complexities associated with working with biological systems are greater than that of working with most chemical systems due to the need of maintaining a healthy stock of biomass, in addition to the preparation and planning of chemical analysis.

The following section summarises the development of the experimental methods used for investigating copper and cadmium uptake by *Chlorella vulgaris* and *Scenedesmus obliquus*. The sorption experiments were undertaken in batch conditions at two scales; a 200mL scale and a 4mL scale. The aim was to capture both the initial, rapid metal uptake mechanism, and the secondary slower uptake mechanism as described previously in literature.

Five experiments were conducted using *C. vulgaris* and one was conducted using *S. obliquus* by a masters student. The experiments focussed on the uptake of copper from contaminated BG-11 growth medium.

Metal analysis was initially undertaken using ICP-OES. The effect of pH and analytical drift were analysed, and strategies devised to overcome issues encountered. The final experimental procedure was decided upon, and future experiments were devised to measure the initial fast uptake kinetics of the microalgae biomass from contaminated, deionised water, and the metal analysis was undertaken ICP-MS.

4.2 ICP-OES Investigation

4.2.1 Effect of pH on ICP-OES Measurement

This section investigates the effect of pH on analysis by ICP-OES. Due to the experimental procedure for creating stable metal stock solutions, when the contaminated media or deionised water is created it has a pH of approximately three. This was pH corrected by the addition of potassium hydroxide for the algae experiments. For this study copper solutions of 0.3mg.L^{-1}, 0.4mg.L^{-1} and 0.5mg.L^{-1}

were created in two batches. The first batch was not pH corrected and the second batch was pH corrected to a pH value of 7 by addition of 0.1M potassium hydroxide. The analysis was undertaken at three different wavelengths, 327.393nm, 324.752nm and 224.700nm.

The copper concentration of the solutions with pH 3 is shown in Figure 14. The samples were measured without further acidification to matrix match with the standard solutions used to create the standard curve.

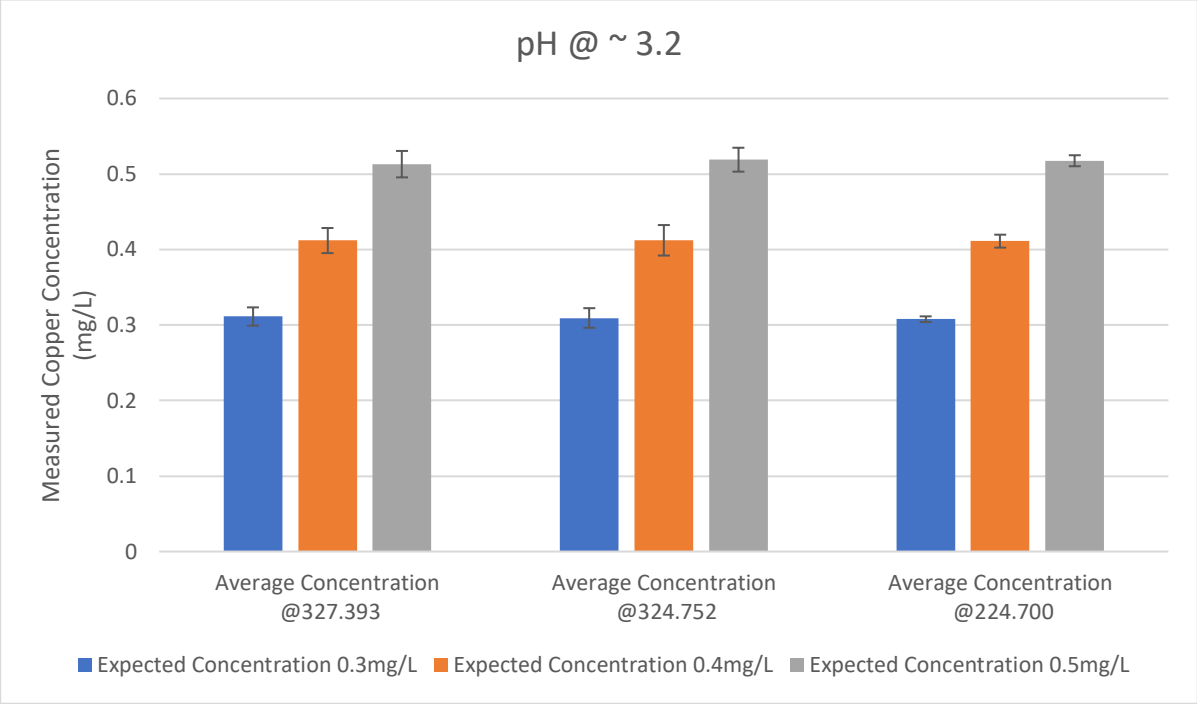

Figure 14: Copper concentrations of 0.3, 0.4 and 0.5mg.L^{-1} Cu^{2+} solutions, at pH 3.2. Concentrations measured using ICP-OES at three different wavelengths, 327.393nm, 324.752nm and 224.700nm.

Figure 14 shows that the analysis of the solutions with a pH of 3.2. These solutions were not pH corrected by addition of potassium hydroxide, and the samples taken were not matrix matched to the standard solutions by addition of 1% by volume of 70% nitric acid. The results returned copper concentrations values close to expected for all three concentrations analysed, by all three wavelengths.

The 0.3mg.L^{-1} and the 0.5mgL^{-1} solution analysed at a wavelength of 224.7 were the only result where the expected concentration is out of the margin for error, with the concentration returned as 0.31mg.L^{-1} ±0.00mg.L^{-1} and 0.52 mg.L^{-1} ±0.01mg.L^{-1} respectively. However, performing an ANOVA the critical *f-value* for all cases is 5.14; the *f-value* for the 0.3mg.L^{-1} analysis at pH3 was 1.23, the *f-value* for the 0.4mg.L^{-1}

analysis at pH3 was 0.07 and the *f-value* for the 0.5mg.L^{-1} at pH3 was 0.99. In all cases the null-hypothesis can be retained that there is no difference in the means, so the average concentration measured at all wavelengths statistically correspond to the expected concentrations in solution.

The solutions that had their pH modified to pH 7, were analysed against the same standard curves as the previous analysis. The samples taken were not matrix matched by addition of 1% by volume of 70% nitric acid. The results of this analysis is shown in Figure 15.

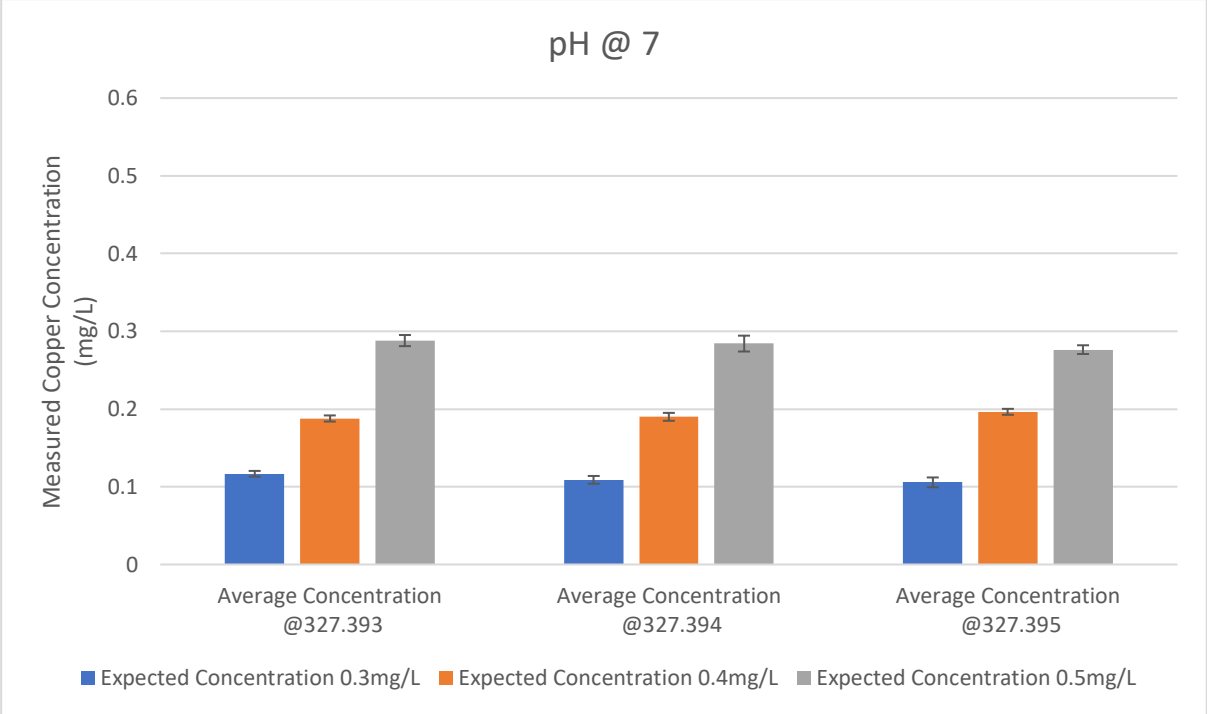

Figure 15: Copper concentrations of 0.3, 0.4 and 0.5mg.L^{-1} Cu^{2+} solutions, at pH 7. Concentrations measured using ICP-OES at three different wavelengths, 327.393nm, 324.752nm and 224.700nm.

The data shown in Figure 15 shows a clear discrepancy in concentration measured for all solutions. Analysis of the 0.3mg.L^{-1} copper solution returned a concentration on average 63% lower than expected, the 0.4mg.L^{-1} copper solution returned a concentration 52% lower than expected and 0.5mg.L^{-1} returned a concentration 43% lower than expected. Performing an ANOVA, the critical *f-value* in all cases is 5.14. The *f-value* for the 0.3mg.L^{-1} analysis at pH7 was 0.16, the *f-value* for the 0.4mg.L^{-1} analysis at pH7 was 0.03 and the *f-value* for the 0.5mg.L^{-1} at pH7 was 0.02. As with the data presented in Figure 14, the null-hypothesis is retained stating that there is no difference in the means for each concentration measured at the three wavelengths. It can therefore be concluded for all wavelengths analysed, the

analysis of the 0.3mg.L^{-1} samples at pH7 returned a concentration 63% lower than present, the analysis of the 0.4mg.L^{-1} samples at pH7 returned a concentration 52% lower than present and the analysis of the 0.5mg.L^{-1} samples at pH7 returned a concentration 43% lower than present.

The results displayed in Figure 14 and Figure 15 suggest that the pH of the solutions determine the accuracy of the analysis by ICP-OES. As the experimental samples were not matrix matched to the standard solutions, it cannot be determined from this data whether the discrepancy in the measured copper concentration is a consequence of the stability of the copper ions in solution, or a discrepancy in photons emitted from the experimental samples and the standard solutions.

To investigate the effect that solution pH has on the stability of the copper ions in solution, four solutions of BG-11 medium were created with 5mg.L^{-1} copper contamination. Each bottle had a different pH, pH 3, 5, 7 and 9. Samples were taken daily from each bottle over a four-day period, and the samples were acidified by the addition of 1% by volume of 70% nitric acid. The standard solutions to create the standard curves were created by using 1% by volume of 70% nitric acid, and copper ICP standard. The copper concentration of each solution was recorded over the four-day period and the data is shown in Figure 16.

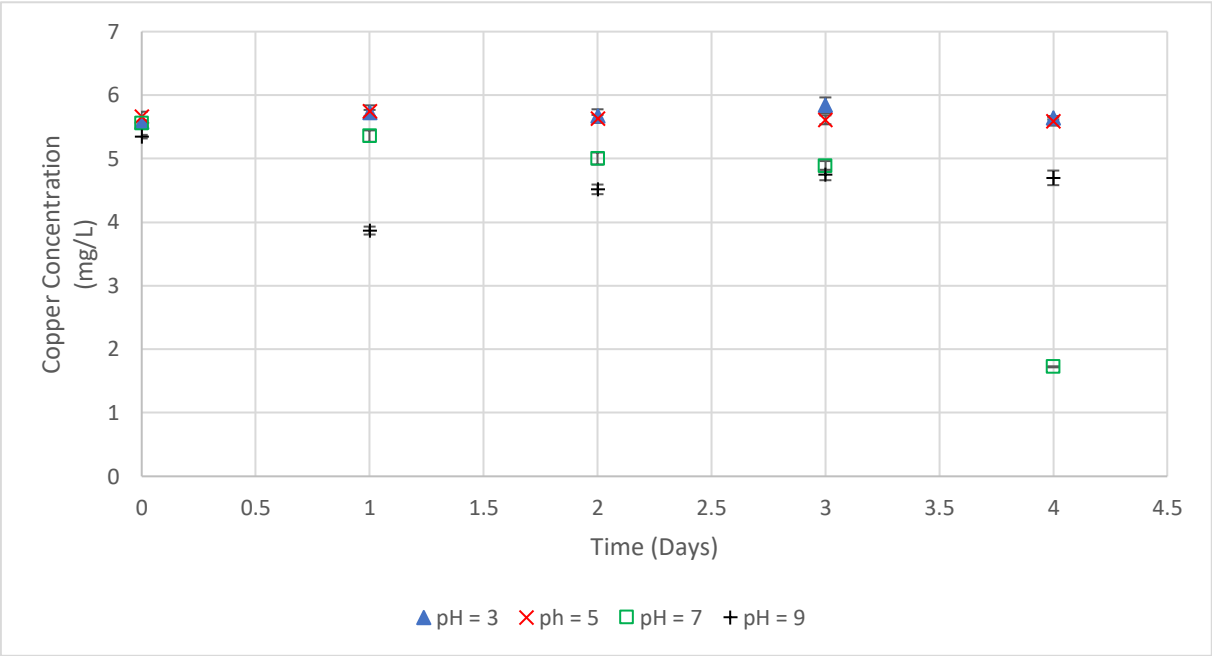

Figure 16: Four solutions of BG-11 growth medium contaminated with 5mg.L^{-1} copper ions. Comparison of how copper concentration varies within solution at pH 3, pH 5, pH 7 and pH 9 monitored over a four-day period.

The data displayed in Figure 16 shows that over the four day period the solutions containing BG-11 at an acidic pH were more stable than those maintained at pH 7 or pH 9. The errors associated with each datapoint were low, indicating reliability of the analytical equipment. Statistically there is no difference between concentration of the copper within the BG-11 medium maintained at pH 3 and pH 5, with an independent t-test returning a P-value of 0.4 with a 95% confidence interval. This indicates that the null hypothesis that there was no difference between the mean of the two datasets could be retained. On the fourth day, the copper concentration within the BG-11 medium maintained at pH 9 had dropped by 12%, and the copper concentration of the BG-11 medium maintained at pH 7 dropped by 69%.

However, performing an ANOVA on the whole dataset, the critical *f-value* is 3.24, and the *f-value* obtained from the analysis was calculated to be 2.92. the calculated *f-value* is lower than the critical *f-value*, therefore the null hypothesis can be retained that there is no difference in the means between the datasets, and therefore pH does not have a significant effect on copper stability in solution, although extended the experimental time period would be necessary to rule out the data point for pH 7 on day 4 as an outlier (Figure 16).

The data presented in Figure 14 and Figure 15 each indicate that pH has to be considered when undertaking metal experiments. The data in Figure 15 indicates that the pH of the analytical samples prior to analysis can significantly affect the analysis by ICP-OES, with the concentrations recorded in all cases lower than expected when the pH of the sample differs from the pH of the analytical standard. A previous study that investigated the uptake of copper and cadmium by a selection of microalgae isolated from freshwater, brackish water and seawater maintained the metal solutions at a pH of 6 in their experimental method to prevent sedimentation of the metal ions [159]. For the kinetics experiments in this study this method was therefore adopted. The kinetics experiment ran for a maximum time of five minutes, so the effect that pH had on growth did not need to be taken into consideration as it was assumed there was no significant growth in this timeframe. For the longer experiments that investigated uptake over a number of days, the pH was not controlled.

4.2.2 ICP-OES Analytical Drift

Both ICP-OES and ICP-MS are susceptible to drift. This occurs when the equipment records variation in counts per second values corresponding to the sample concentrations. To test for this, during the ICP-OES analysis the consistency of the equipment was monitored by analysing a standard with a known concentration periodically throughout the analysis. The discrepancy is calculated by finding the percentage difference between the expected concentration and the recorded concentration.

Displayed in this section is the data obtained by analysing a copper analytical standard with a concentration of 0.4mg.L^{-1}. This standard was labelled as "Mid" and was analysed for copper concentration thirteen times at a wavelength of at 327.4, 325.8 and 224.7nm. The copper concentration data is displayed in Figure 17.

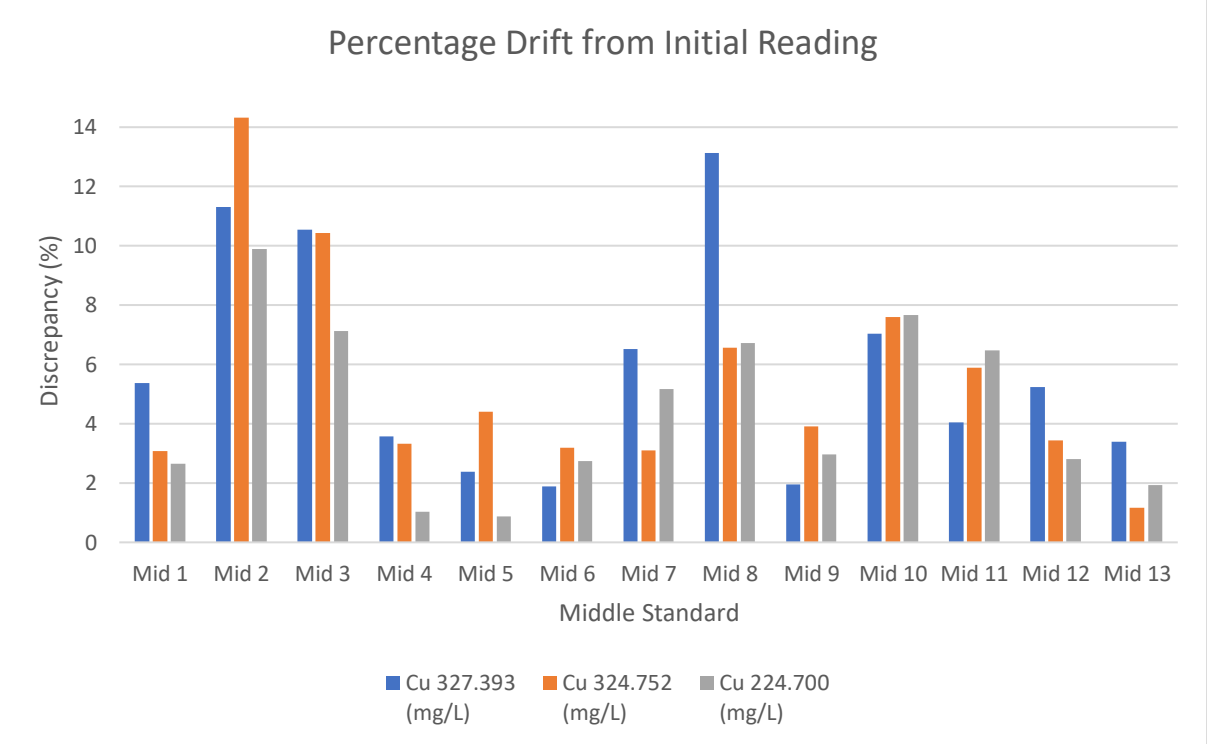

Figure 17: The variation in analysis of the 0.4mg.L^{-1} standard used to create the standard curve for ICP-OES analysis. The standard analysed was the middle standard used to calibrate the ICP-OES for sample analysis.

If the discrepancy in the measured copper concentration exceeded 5% for any of the wavelengths, the equipment was recalibrated. Figure 17 shows that the equipment required recalibration after the first reading. During this analysis, the

equipment required recalibration six times, which considerably added to the time taken for sample analysis.

Equipment drift is caused by variations in the sample introduction to the equipment. This is most likely caused by variations in the ambient temperature, but can also be caused a build-up of residue within the tubing, restricting the flow of analyte. To avoid sample contamination, the ICP torch should be soaked weekly in 2% nitric acid, and the tubing should be replaced weekly.

The procedure that produced the data displayed in Figure 17 was undertaken on the 16th of July 2019. Five of the standard curves that related counts per second (CPS) of photons with the wavelength 327.4nm, to copper concentration are displayed in Figure 18, along with standard curves produced on four previous dates over the preceding month. All curves were produced using an identical copper standard solution.

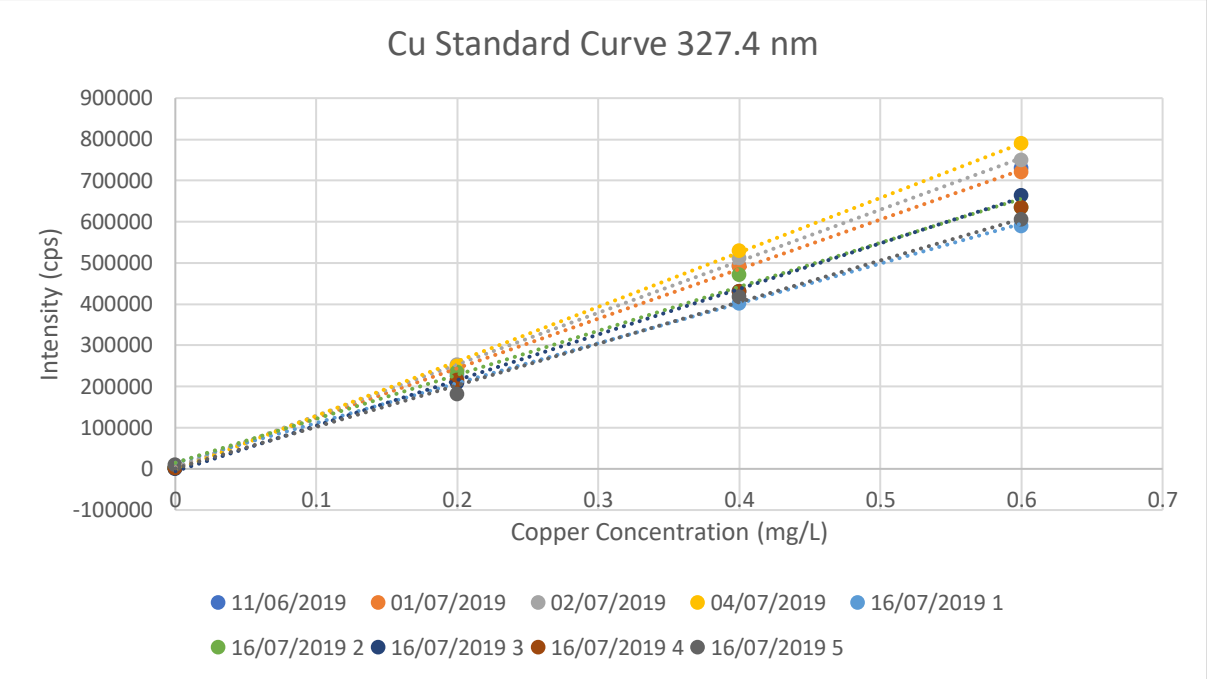

Figure 18: ICP-OES standard curves for copper measured at 327.4nm, Intensity in counts per second plotted against known concentrations of standard solutions. The standard curve was produced on five separate days, and on the fifth day the curve was redrawn a further five times.

The standard curves displayed in Figure 18 show that there is a variation in CPS over time. This indicates that the quantity of standard solution reaching the plasma flame varies with each curve. The charts produced on the 11th June, 1st, 2nd and 4th of July show a higher intensity (CPS) recorded for the 0.6mg.L^{-1} standard compared to the

curves produced on the 16th of July. This indicates that over the month period, the sample introduction system had become less efficient by the 16th. This further emphasised the importance of a regular maintenance regime of the ICP-OES equipment.

4.2.3 Preliminary Results for Copper Uptake by Chlorella Vulgaris

The following subsection details the results of the initial copper sorption experiments by microalgae. The initial experiments were intended to capture both the initial rapid uptake kinetics, and the long term slower secondary uptake mechanism. The experiment was undertaken at a 200mL scale, with samples initially taken over the first three hours. Samples were then taken daily over the following three days. Samples were filtered through a 1μm syringe filter, and acidified by addition of 1% by volume of 70% nitric acid.

As well as data for copper concentration, the biomass concentration was monitored over the three days by UV-Vis. The bottles were agitated at 80rpm on a SciTech LabAPP® SLA-OS-200 orbital shaker over the experimental period. The copper concentration in solution is plotted for the experimental triplicates, the contaminated medium control (Control 1), the algae control containing no metal contaminant (Control 3), and the biomass concentration present within the experimental bottles is plotted on a secondary axis. This data is displayed in Figure 19.

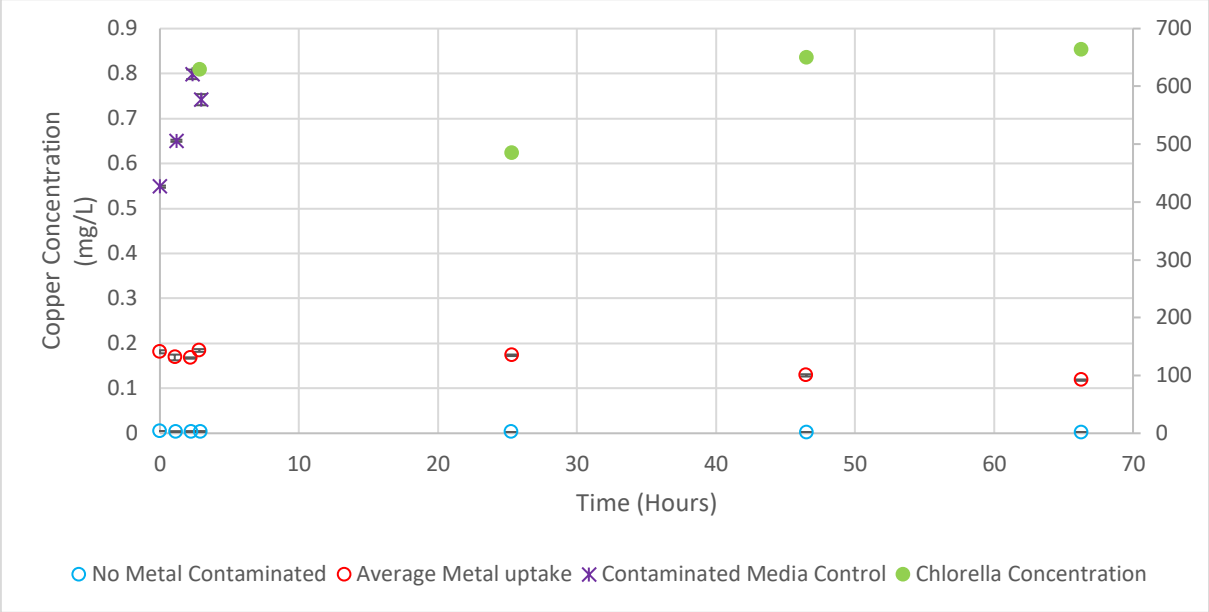

Figure 19: Copper uptake by *Chlorella vulgaris* over a three-day period. Primary axis shows the copper concentration over time for the experimental replicates, the control containing algae but no metal contaminant and the control containing contaminated medium and no algae. The secondary axis records the biomass concentration within the experimental replicate bottles.

The data representing the contaminated media control (purple stars) was collected for the initial three hours of the experimental period. It was not possible to obtain further samples from this control following the fourth sample. The data collected from this control did not return a consistent copper concentration within the first three hours, whereas the data collected from the other control (BG-11 medium without metal contamination, as represented by blue circles), and the data collected from the experimental replicates (represented by the red circles), did return consistent readings for copper concentration.

This could be indicative that the ICP may not have concluded its warm up procedure in time prior to analysis, or that this BG-11 control was not a well-mixed solution.

The residual copper concentration data collected for the experimental replicates are consistent, but there is a big difference between the concentration of the control bottle and the concentration of the experimental replicates. Over the first twenty-four hours the copper concentration within the experiment replicates were recorded to being slightly lower than 0.2mg.L^{-1}. By day two and day three the copper concentration had dropped again to 0.13mg.L^{-1} and 0.12mg.L^{-1} respectively.

This further reduction in copper concentration coincided with a recovery of the *C. vulgaris* concentration as represented by the solid green circles in Figure 19. This *C.*

vulgaris concentration data could be representing the lag phase caused by the *C. vulgaris* biomass adapting to new environmental conditions. After twenty-four hours the cells had settled, but after 48 hours the Biomass appears to have recovered and re-suspended.

The main conclusion taken from this experiment is that the primary uptake mechanisms of the algae was too quick for the current experimental procedure to capture, but the slower, secondary copper uptake mechanism was observed which coincided with a recovery of biomass culture.

4.2.4 Measurement of secondary uptake kinetics

The experimental time period was extended to capture more data associated with the slower secondary uptake mechanism. The results displayed in this section were obtained from experiments undertaken over a two-week period for copper uptake by *Chlorella vulgaris*, and over eleven days for copper uptake by *Scenedesmus obliquus*. The latter data collected for adsorption by *S. obliquus* was obtained by Alex Hunt, a master's student who's project was linked to the current study.

The experiments were undertaken at a 200mL scale, with an experimental replicate containing algae biomass exposed to BG-11 medium contaminated with 2.5mg.L^{-1} copper ions. The concentration of copper was increased from the previous experiment with the intention of having a higher concentration in solution following the initial fast uptake mechanism. Every two days over a two-week period, samples were taken from a set of experimental triplicates, along with samples obtained from a control containing BG-11 contaminated with 2.5mg.L^{-1} copper ions, without the presence of *C. vulgaris* biomass. The data was recorded and displayed in Figure 20.

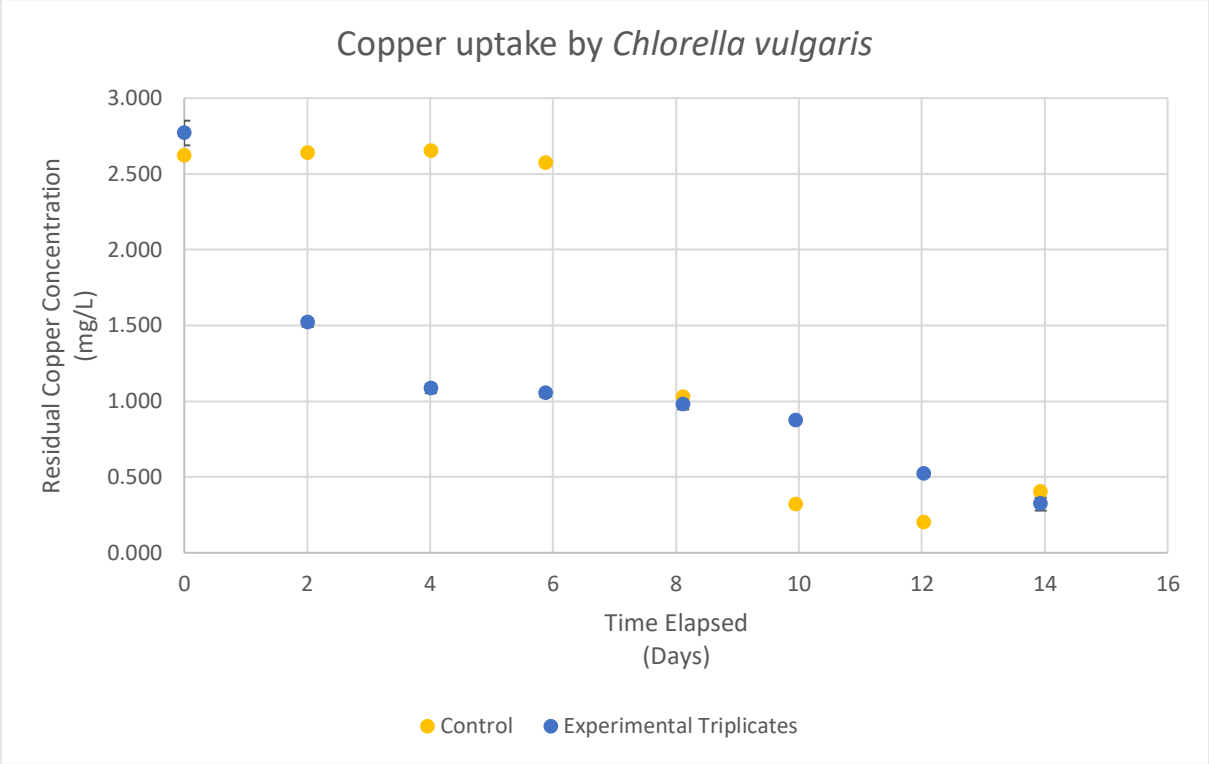

Figure 20: Monitoring of copper uptake by *Chlorella vulgaris* over a two week period, by recording the residual concentration of copper in solution.

The data presented in Figure 20 that represents the residual copper concentration within the experimental triplicates (represented by the blue circles), shows a more gradual metal removal mechanism compared to that shown in Figure 19. In this case there does not appear to be a rapid uptake mechanism, or the uptake mechanism is not as fast as it was in Figure 19.

During the first six days, there is a clear difference in concentration between the control (represented by the yellow circles), and the experimental triplicates. It appears that when the fifth sample taken from the control an issue occurred with the sample introduction mechanism to the ICP. This could be caused by a drop in carrier gas pressure, or a blockage caused by sample crystallisation within the tubing.

This data was compared to the copper concentration data obtained from the *S. obliquus* experiment undertaken by the master's student. In this experiment, the initial copper concentration of the BG-11 medium was $1mg.L^{-1}$. This makes these experimental conditions more comparable to those used to create Figure 19, than Figure 20. The data for the variation in copper concentration for the *S. obliquus* experiment is shown in Figure 21.

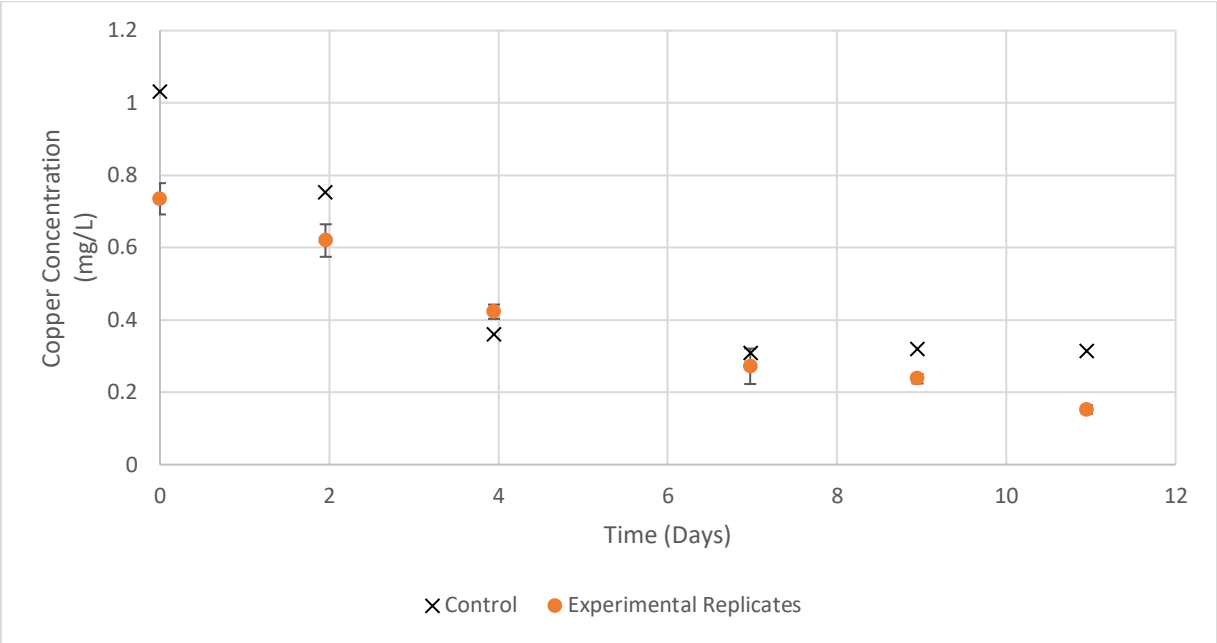

Figure 21: Data obtained from the 200mL *S. obliquus* experiment. The copper concentration, time profiles for the experimental control (grey crosses), and the experimental replicates (orange circles).

The copper concentration within the experimental control (grey crosses) in Figure 21 suggests that over time there is a decline in copper concentration in BG-11 solution when the *S. obliquus* is absent. This data was collected by another researcher, so it is difficult to ascertain what issues there may have been. The decline in concentration appears to be gradual so could be an issue with carrier gas running low and a declining plasma flame.

All three datasets produced from the 200mL batch experiments return unique characteristics. The data shown in Figure 19 is the only dataset that represents what is expected from literature regarding the two uptake mechanisms previously observed for metal uptake by microalgae; an initial rapid uptake mechanism followed by a slower uptake mechanism [9, 53].

In all three figures, when examining the copper concentration recorded within the experimental controls containing copper contaminant; there is an unexpected behaviour noticed. In Figure 19, the concentration appears to increase over the first three hours, in Figure 20 the copper concentration is stable for the first six days before dropping suddenly on the eighth day, and in Figure 21 the copper concentration of the control decreases at a similar rate to the copper concentration within the experimental replicates. For the latter data, the Pearson Product-Moment correlation was calculated between the copper concentration of the BG-11

control and the copper concentration within the experimental replicates. This returned an *r* value of 0.94 which indicates a strong positive correlation between the two concentration datasets, indicating there is little difference between the copper removal rate recorded in the control and the experimental replicates.

4.2.5 Initial Copper Uptake Experiments

To capture the initial metal uptake kinetics that was not captured by the 200mL procedure shown in Figure 19, the experimental procedure was modified so the experiment was performed at a 4mL volume within a 5mL syringe. The algae solution was ejected and filtered through a syringe filter at set time intervals to obtain the samples for ICP analysis.

2mL of double strength BG-11 medium contaminated with 2mgL^{-1} copper ions was drawn into a syringe, followed by 2mL of deionised water. This was filtered through a 0.22µm syringe filter, and the sample retained as time-point zero. The procedure was repeated, but with 2mL of *C. vulgaris* solution in place of deionised water. These latter samples were filtered in increments of five seconds for the first minute, and every thirty seconds for the first two minutes and then every minute for the first five minutes. This produced eighteen data points, as shown in Figure 22.

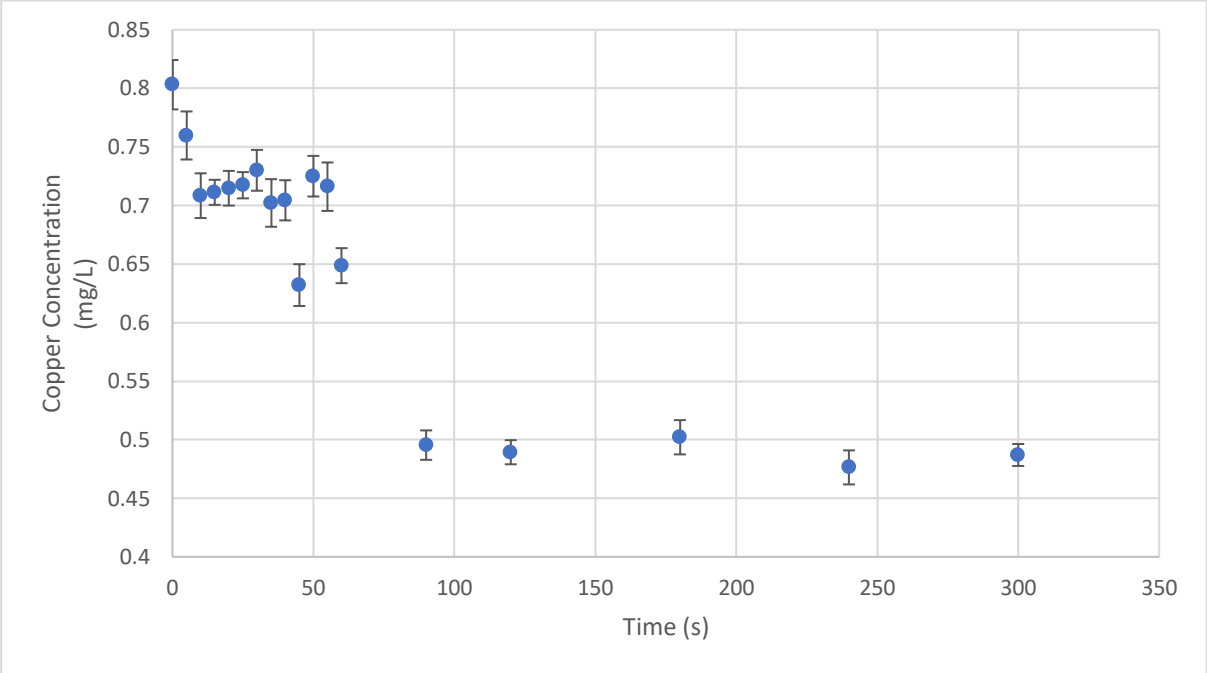

Figure 22: Residual copper concentration within contaminated BG-11 medium that was exposed to 140mg.L^{-1} *C. vulgaris*, over a five minute time period. Initial experiment to record metal adsorption onto the surface of the microalgae biomass. Analysis done using ICP-OES.

The data shown in Figure 22 shows a clear metal removal mechanism over the initial 90 second time period, however the kinetics between the 10s sample and the 60s sample do not show a clear trend to model the initial kinetics. Following this analysis, ICP-MS was adopted as the ICP-OES equipment was taken out of service for an extended period. The algae solution used for this experiment was obtained from a dilute culture leading to an experimental concentration of *C. vulgaris* of 140mg.L^{-1}.

The final metal uptake was calculated by dividing the difference in copper concentration by the concentration of *C. vulgaris* biomass. This was calculated to be 2.16 mg of copper per gram of algae with an extent of copper removed calculated to be 37%.

4.3 ICP-MS Analysis

The experiment used to produce Figure 22 was repeated using a higher *C. vulgaris* concentration to make the experiment equivalent to the 200mL experiment undertaken to produce the data presented in Figure 19. This next experiment had a *C. vulgaris* concentration of 630mgL^{-1} and a copper concentration of 0.8mg.L^{-1}. The samples in this experiment were collected over a three-minute period as opposed to five minutes. For the first minute samples were collected every five seconds, and for the second minute samples were taken every ten seconds and for the third minute samples were taken every thirty seconds.

These samples were acidified by the addition of 1% by volume of 70% nitric acid, and sent to Northumbrian Water Scientific Services for analysis by ICP-MS. The results of this analysis are displayed in Figure 23.

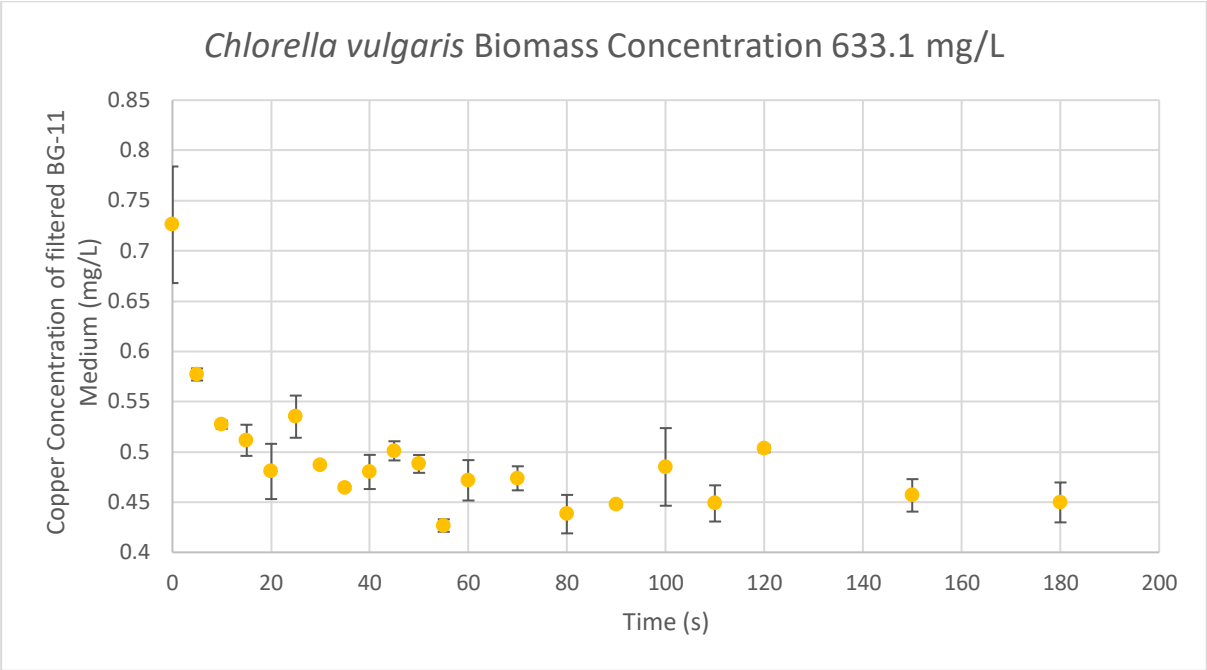

Figure 23: Residual copper concentration within contaminated BG-11 medium that was exposed to 633mg.L^{-1} *C. vulgaris*, over a three minute period. Experiment to capture the initial metal removal kinetics facilitated by the adsorption of the metal ions onto the *C. vulgaris* cell surface. Analysis undertaken by ICP-MS.

The data presented in Figure 23 shows more of a clear, undisturbed trend for copper removal compared to the data presented in Figure 22. Equilibrium appears to have been achieved after forty seconds, and the data appears to show an exponential decay towards an equilibrium value. The final copper uptake by the *C. vulgaris* in this case calculated to be 0.44mg of copper per gram of *C. vulgaris*, and the extent of copper removal was 40%. With the algae concentration increased from 140mg.L^{-1} to 640mg.L^{-1} there was not a significant effect on extent of metal removal; which is indicative that the extent of copper removal is not a function of algae biomass concentration.

A third experiment was undertaken using a higher concentration of *C. vulgaris* biomass to test whether an algae concentration of 1000mgL^{-1} could be analysed using the syringe method without causing blockages to the syringe filters. To maintain consistency in the initial experimental conditions, the copper concentration was raised to 1.15mg.L^{-1} to keep the ratio of biomass concentration to metal concentration consistent with that of the previous experiment used to produce Figure 23. The experimental period was intended to be maintained at three minutes, however due to syringe filter blockages it was not possible to collect all

samples over the three-minute period. The data for this experiment is displayed in Figure 24.

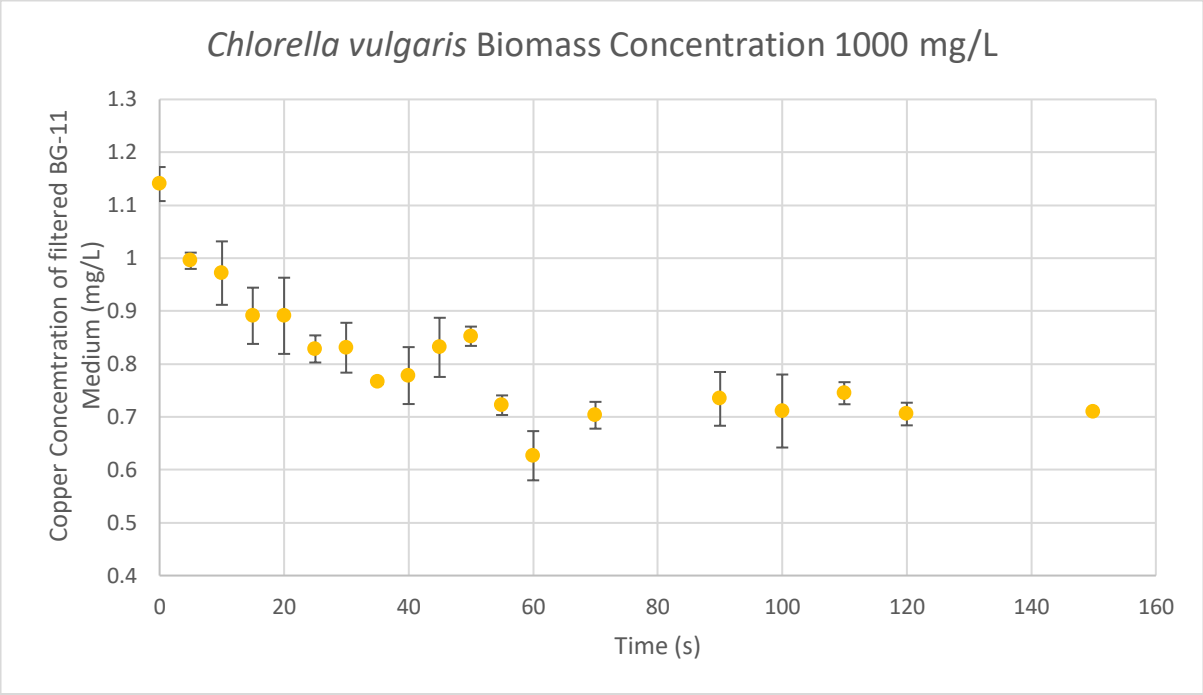

Figure 24: Residual copper concentration within contaminated BG-11 medium that was exposed to 1000mg.L^{-1} *C. vulgaris*, over a two and a half minute period. Experiment to capture the initial metal removal kinetics facilitated by the adsorption of the metal ions onto the *C. vulgaris* cell surface. Analysis undertaken by ICP-MS.

The data returned for the final experiment as shown in Figure 24 shows a more gradual reduction in copper concentration compared to the trend as shown in Figure 23. The uptake process appears to take 55s, and the final copper uptake was calculated to be 0.45mg of copper per gram of algae, and the extent of removal was 40%. These values are equivalent to those obtained from Figure 23, indicating that the uptake capacity of the microalgae is dependent on the concentration of the metal in solution, and the extent of removal is common for all three experiments.

In the three cases where the metal removal was measured from the BG-11 medium solution, the extent of removal did not exceed 40%. The future experiments would focus on copper and cadmium removal from deionised water to determine whether the concentration can be reduced to near 0mg.g^{-1} copper. Removal rates were calculated by fitting mathematical models to model the removal kinetics.

4.3.1 Conclusions obtained from preliminary experiments

The previous section summarises the results obtained by analysis of copper solutions, undertaken by ICP-OES and ICP-MS. The initial experiments investigated the effect that pH has on the analysis of copper ions present within BG-11 growth medium. This analysis was conducted using ICP-OES, and demonstrated that samples with a pH of 7 returned a copper concentration that was considerably lower than the concentration present within the sample. Samples with a pH of 3 were analysed more accurately by ICP-OES, signifying the importance of sample acidification prior to analysis using ICP-OES.

The second investigation involved measuring the copper concentration of four BG-11 solutions with a known copper concentration of 5mg.L^{-1}. These had a pH of 3, 5, 7 and 9, and were sampled over a four-day period. The samples obtained from the bottles kept at pH 3 and 5 appeared to show that at this pH the copper solutions were stable over the four-day period. This was corroborated by an independent t-test returned a p-value of 0.4, indicating that there was no difference in copper concentrations between the two solutions. A further ANOVA of all of the datasets (pH 3, pH 5, pH 7 and pH 9), returned an *f-value* of 2.92 which was less than the critical *f-value* of 3.24. This indicates that pH has no significant effect on the stability of the copper ions in solution. From literature however, previous researchers have indicated pH 6 is an optimal pH to maintain metal solutions for metal sorption experiments [159], so this technique was adopted for future kinetic experiments.

The operational procedure of the ICP-OES was also investigated for analytical drift. A set of copper standards were analysed over the course of a day and during this analysis, the reported copper concentration varied frequently. The ICP-OES required frequent recalibration on the day, and six different standard curves were created. Five of these standard curves were plotted alongside a selection of other standard curves created using the same standard solutions, but created on previous dates. There was a variation in gradient in each curve produced which indicated a reduction in quantity of solution reaching the plasma flame. This emphasised the importance of equipment recalibration with each analysis undertaken, and indicated that analytical drift was an issue over short time periods.

Metal uptake experiments by microalgae involved a batch adsorption procedure, investigated at two different scales. Copper adsorption by *Chlorella vulgaris* was conducted at a scale of 200mL and 4mL, and adsorption of copper ions by *S. obliquus* was conducted at a scale of 200mL only.

The 200mL experiments, analysis by ICP-OES produced inconsistent results. An initial experiment involving the adsorption of 0.8mg.L^{-1} copper ions by 640mg.L^{-1} *C. vulgaris* returned results that were consistent with previous studies showing a clear, immediate difference in concentration between the experimental control and the experimental replicates; and a further gradual decrease in concentration over time within the experimental replicates. However, analysis of the experimental control which consisted of 0.8mg.L^{-1} copper ions dissolved in BG-11, returned inconsistent results. Furthermore only four samples of this control were able to be obtained.

The experiment was repeated, but modified with a 2.5mg.L^{-1} copper concentration and an experimental period of two weeks. The initial algae concentration was 640mg.L^{-1}. The results of this experiment indicated no rapid uptake mechanism, but a gradual decrease towards an equilibrium value over a six-day period. During this same period, the copper concentration in the control was consistently measured at 2.5mg.L^{-1}. On day eight however, the copper concentration within the control dropped to 1mg.L^{-1}, and then to less than 0.5mg.L^{-1} on the tenth day. Between day eight and day fourteen, there was no significant difference between the copper concentration within the experimental replicates and the experimental control.

A third experiment undertaken at a 200mL scale used the microalgae *S. obliquus* and a copper concentration of 1mg.L^{-1}. This was undertaken over an eleven-day period, and the copper concentration present within the experimental control and within the experimental replicates decreased at a similar rate.

The 4mL batch experiments were designed to capture the initial rapid uptake of metal ions from initial contact with microalgae biomass. The first 4mL experiment had a low concentration of algae biomass of 140mg.L^{-1} and an initial copper concentration of 0.8mg.L^{-1}. The samples from this experiment were analysed using

ICP-OES, and the data did show a gradual decrease towards an equilibrium concentration.

Two further 4mL experiments were undertaken with an algae concentration of 640mg.L^{-1} and a copper concentration of 0.8mg.L^{-1}; and an algae concentration of 1000mg.L^{-1} with a copper concentration of 1.15mg.L^{-1}. These concentrations were chosen to maintain a common ratio of biomass to metal concentration between the two experiments.

The analysis of the last two experiments were undertaken externally using ICP-MS, and although there was a difference in initial concentrations the results were identical for these two experiments. Both had a final binding capacity of approximately 0.45mg.g^{-1}, and an extent of removal of copper of 40%. The first 4mL experiment had an extent of removal of 37%, but a copper capacity of 2.16mg.g^{-1}. This suggests that the extent of copper removal is independent of biomass concentration, but the biomass capacity for copper increases as biomass concentration decreases.

A biomass concentration of 1000mg.L^{-1} caused the syringe filters used for sampling to become blocked very quickly. This made sampling inefficient and utilised many more syringe filters compared to experiments with lower biomass concentrations. For this reason, all future experiments were capped at 500mg.L^{-1} of algae.

It was not possible to continue analyses with ICP-OES, so all future analyses was undertaken externally using ICP-MS by Northumbria Water Scientific Services. This increased analysis cost, and as they created their own standard curves; future analyses were done using contaminated deionised water in place of contaminated BG-11 medium. This would reduce the work requirement for matrix matching the standards to the samples.

Chapter 5 Quantitative Metal Uptake by Microalgae

In Section 3.4, the methodology was selected where the adsorption kinetics was measured by contacting 2mL of microalgae culture to 2mL metal solutions within a syringe, which was filtered at set time intervals. As well as measuring the metal removal kinetics, this methodology was also able to analyse the effect of algae and metal concentration on the adsorption process.

The following section summarises the investigation into how initial concentration of adsorbent (algae biomass), and adsorbate (metal ion) concentration affects the final accumulation of copper and cadmium by *C. vulgaris* and *S. obliquus*. The section outlines how initial concentration can be used to predict the final binding capacity of the biomass, and the percentage removal of the dissolved metal ions. The adsorption from a solution containing a single metal ion is compared to adsorption from a binary metal solution, and adsorption from a complex solution containing a variety of dissolved salts.

C. vulgaris concentrations ranging from 240mg.L^{-1} to 1000mg.L^{-1} were contacted with copper and cadmium solutions with concentrations ranging from 0.25mg.L^{-1} and 2.5mg.L^{-1}. The *S. obliquus* concentration was varied from 190mg.L^{-1} to 460mg.l^{-1} and the copper and cadmium concentrations were varied from 0.25mg.L^{-1} to 2.5mg.L^{-1}.

Three common isotherms that were identified in literature were applied to the equilibrium data, to determine which isotherm is most suited to representing adsorption of metal ions by microalgae.

5.1 The effect of initial adsorbate and adsorbent concentration

The adsorbent used in this investigation was either *C. vulgaris* or *S. obliquus*, and the adsorbate was either copper or cadmium. The following subsection compares the effect that the initial concentration of adsorbate and adsorbent in solution, has on the adsorption of copper and cadmium by *C. vulgaris* and *S. obliquus*.

5.1.1 Single Metal solution

Researchers have previously reported that for metal adsorption studies by microalgae, the value for adsorption at equilibrium is affected by the initial concentration of the algae biomass and the initial metal concentration in solution [91, 93, 97]. The higher the concentration of the adsorbate, the higher the binding capacity of the adsorbate at equilibrium. However few studies appear to relate the ratio of initial metal concentration to biomass concentration and the adsorption rate, although *Lee et al* (2011) did vary microalgae concentration and graph the relationship between adsorption at equilibrium, and mass of biomass [97].

In this current study, both the microalgae concentration and the concentration of the metal were varied. The ratios of the initial dissolved metal ions to microalgae concentration are displayed in Table 10.

Table 10: Comparison of initial experimental conditions, represented by the ratio of biomass concentration ($mg.L^{-1}$) to the initial concentration of the metal ions ($mg.L^{-1}$). Each figure represents the mg of algae per mg of metal at the beginning of each experiment.

Initial Metal Concentration	Copper Chlorella vulgaris	Cadmium Chlorella vulgaris	Copper Scenedesmus obliquus	Cadmium Scenedesmus obliquus
0.25	2083	962	1772	718
0.50	1111	479	954	447
0.75	667	325	246	308
2.5	89	97	102	94

There were sixteen experiments; four concentrations of copper and cadmium were adsorbed by *C. vulgaris* and *S. obliquus*. Each data point presented in the charts displayed in Figure 25 refer to each experiment grouped by the initial copper or cadmium concentration. These were 0.25, 0.5, 0.75 and $2.5 mgL^{-1}$. The concentration of the adsorbent and adsorbate for each experiment are displayed in Table 11. The reason the concentration of the microalgae varied was that at higher biomass concentrations, some of the syringe filters used to collect each sample quickly became blocked. This led to the algae concentration being reduced from $500mg.L^{-1}$ to $250mg.L^{-1}$.

Table 11: The measured *C. vulgaris* and *S. obliquus* concentration, and metal concentration in solution at the beginning of each adsorption experiment.

Copper experiments				
Desired Metal Concentration ($mg.L^{-1}$)	**Chlorella Vulgaris**		**Scenedesmus obliquus**	
	Measured Concentration (mgL^{-1})	**Algae Concentration (mgL^{-1})**	**Measured Concentration (mgL^{-1})**	**Algae Concentration (mgL^{-1})**
0.25	0.24	500	0.26	460
0.5	0.45	500	0.49	460
0.75	0.75	500	0.79	195
2.5	2.68	240	2.4	245
Cadmium Experiments				
Desired Metal Concentration ($mg.L^{-1}$)	**Chlorella Vulgaris**		**Scenedesmus Obliquus**	
	Measured Concentration (mgL^{-1})	**Algae Concentration (mgL^{-1})**	**Measured Concentration (mgL^{-1})**	**Algae Concentration (mgL^{-1})**
0.25	0.26	250	0.33	240
0.50	0.52	250	0.53	240
0.75	0.77	250	0.77	240
2.5	2.59	250	2.61	245

The values of the adsorption at equilibrium for each experiment were plotted against their corresponding ratios in Table 10. These charts are displayed in Figure 25.

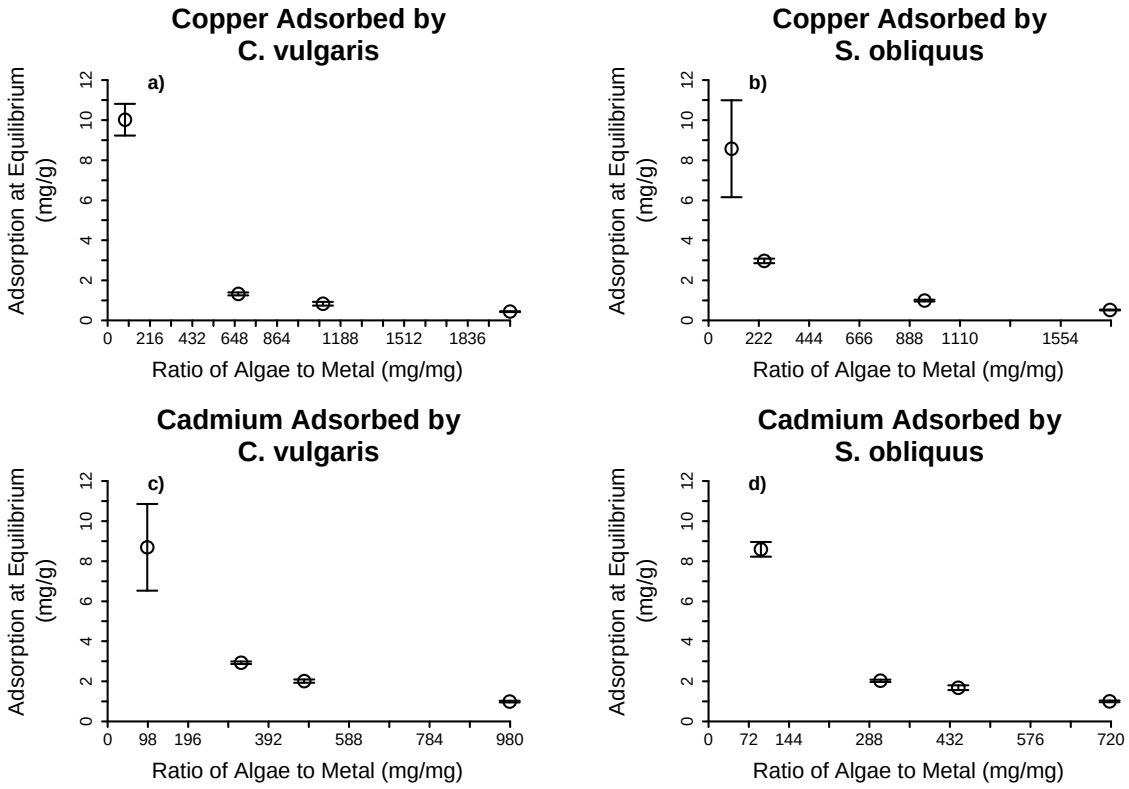

Figure 25: Adsorption at equilibrium plotted against the ratio algae biomass concentration to the initial concentration of the copper and cadmium in solution, at the beginning of each experiment.

Figure 25 shows that there is a common trend shared between all experiments. This indicates that there is a relationship between the adsorption at equilibrium and the initial concentrations of the algae biomass and the metal in solution. *Lee et al* (2011) [97] concluded that the adsorption at equilibrium was inversely proportional to the microalgae concentration when investigating the adsorption of lead and copper by the microalgae *Spirogyra sp* and *Cladophora sp*. If the relationship observed by Lee et al can apply copper and cadmium adsorbed by *C. vulgaris* and *S. obliquus*, an inverse expression of the form shown by Equation 1 will be able to be fitted to each chart in Figure 25.

$$Q_e = \frac{\alpha_{eq}}{ratio} \tag{1}$$

Where

- Q_e is the adsorption at equilibrium ($mg.g^{-1}$)
- α_{eq} is an empirical constant ($mg.g^{-1}$)
- *ratio* is the initial algae concentration ($mg.L^{-1}$) divided by the metal concentration ($mg.L^{-1}$).

To test this relationship, the adsorption at equilibrium was plotted against the reciprocal of the ratio of algae concentration to initial metal ion concentration. These charts are displayed in Figure 26.

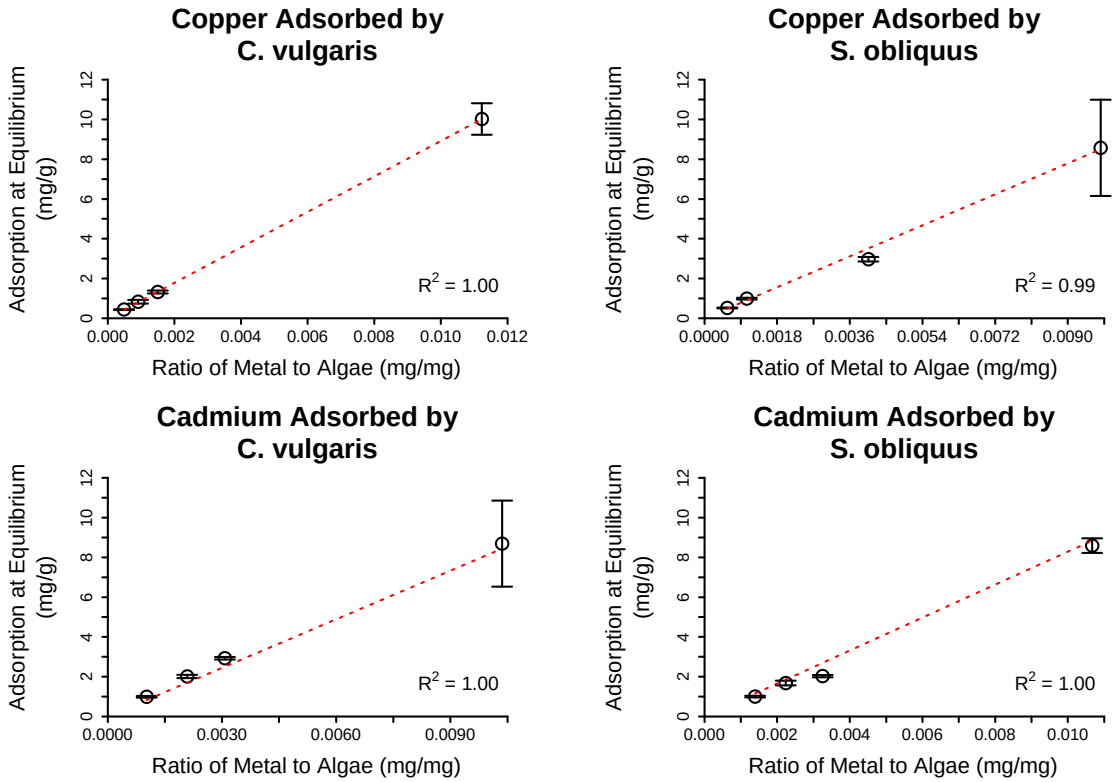

Figure 26: Charts of the adsorption at equilibrium (Q_e) plotted against the ratio of initial metal concentration to initial biomass concentration. Charts a to d, copper adsorbed by *C. vulgaris*, cadmium adsorbed by *C. vulgaris*, copper adsorbed by *S. obliquus* and cadmium adsorbed by *S. obliquus*.

In all charts displayed in Figure 26, the R^2 values were greater than 0.99, indicating a strong linear relationship between the Q_e and the ratio of dissolved metal ions to microalgae concentration at the beginning of the process.

The coefficient, α in Equation 1 is equal to the gradient of the linear models that are displayed in Figure 26a to *d*. Values of α_{eq} are displayed in Table 12 for each metal adsorbed by *C. vulgaris* and *S. obliquus*.

Table 12: Empirical constants (α_{eq}) relating sorption capacity of the microalgae to the ratio of the initial concentration of algae biomass to the initial concentration of the metal ions.

Metal	C. vulgaris	S. obliquus
Copper	892	866
Cadmium	814	829

The α_{eq} values for each metal adsorbed by each algae species were applied to Equation 1 and plotted alongside their corresponding experimental data. These models shown in Figure 27.

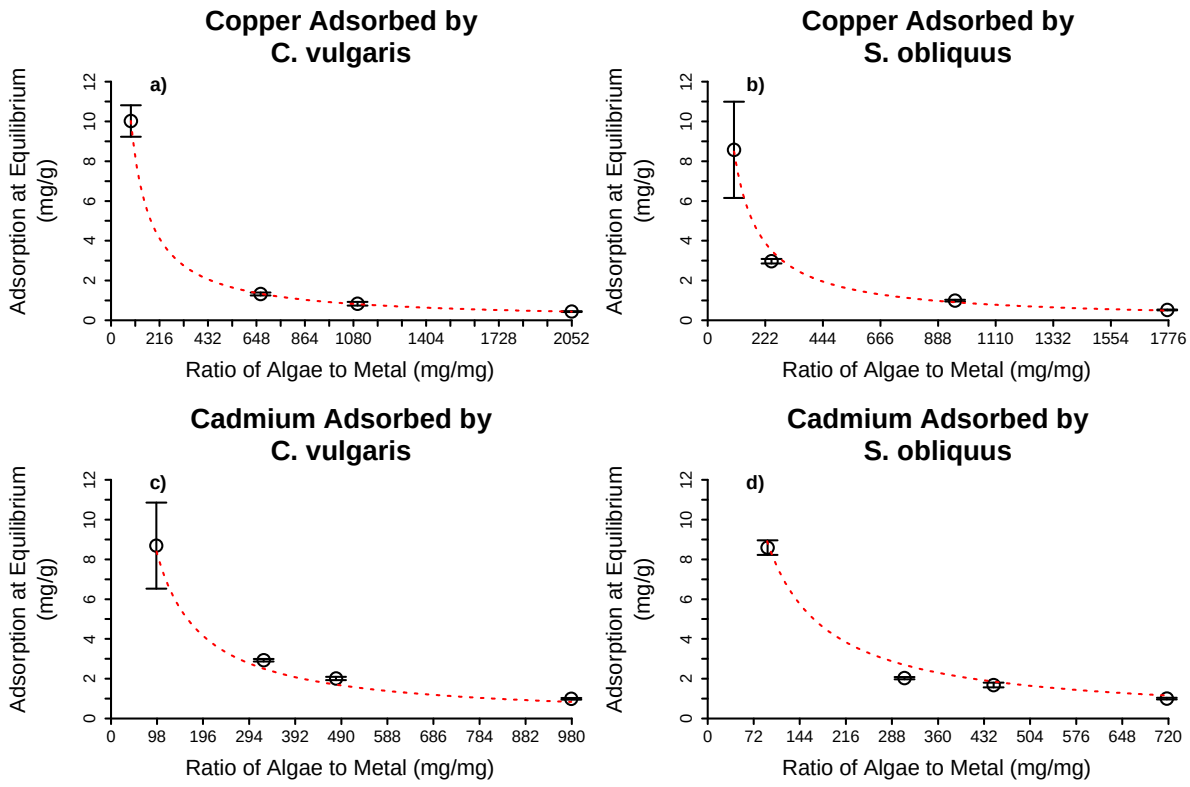

Figure 27: Profiles of how adsorption at equilibrium relates to the ratio of the initial, algae biomass concentration to the initial metal concentration vs predictions of the inverse model.

Examining the empirical constants (α_{eq}), in Table 12 it can be concluded that *C. vulgaris* has a higher binding capacity for copper when compared to *S. obliquus*, and *S. obliquus* has a higher binding capacity for cadmium compared to the *C. vulgaris* biomass. Both species have a higher capacity for copper compared to cadmium.

Lee et al (2011) [97] in their study maintained the copper and lead concentration, and varied the microalgae concentration. In the current study, the copper and cadmium concentration was varied, and the aim was to maintain the algae concentration at a constant value. The conclusions by *Lee et al* were that the Q_e varied inversely with the microalgae concentration, whereas the data displayed in Figure 26 in this study indicates that Q_e varies linearly with the initial metal concentration. This was analysed by plotting Q_e vs the initial metal concentration to determine whether Q_e is determined by the metal concentration alone, or whether the algae concentration also has an effect. These plots are displayed in Figure 28.

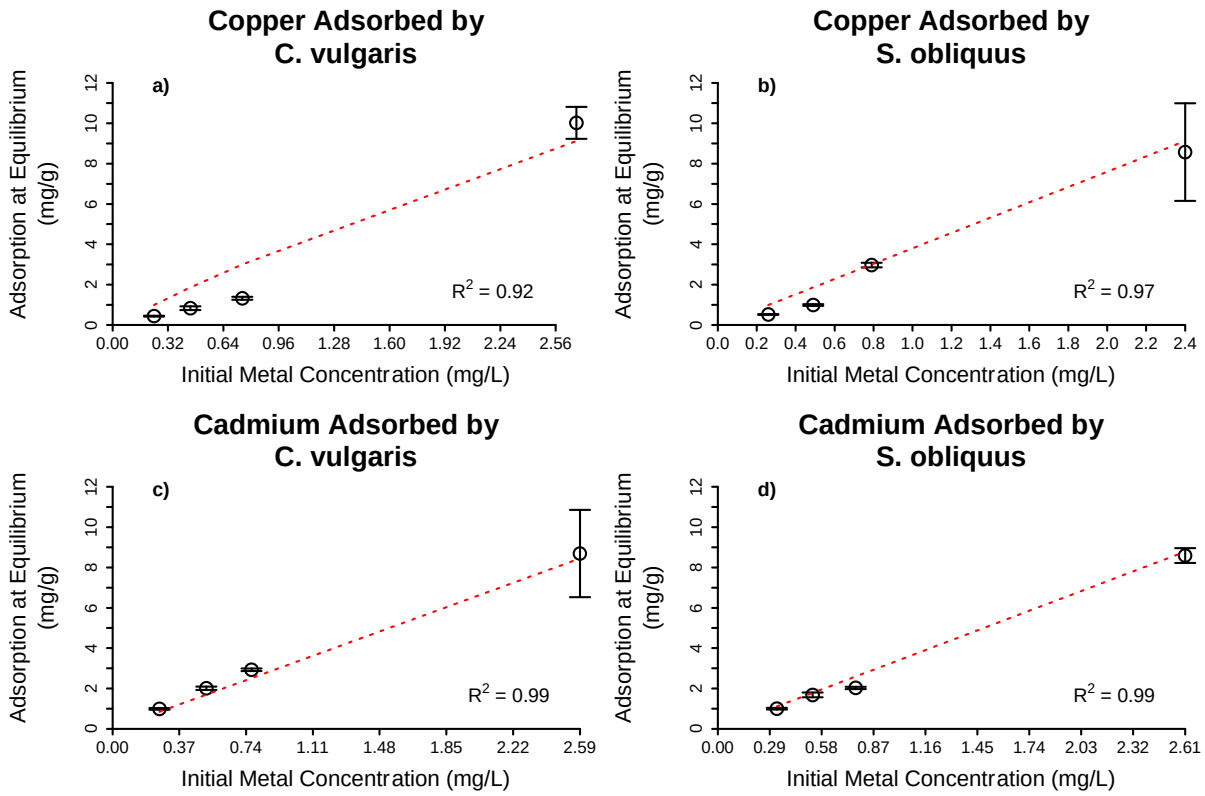

Figure 28: Charts of the adsorption at equilibrium (Q_e) plotted against the initial metal concentration. Charts a to d, copper adsorbed by *C. vulgaris*, cadmium adsorbed by *C. vulgaris*, copper adsorbed by *S. obliquus* and cadmium adsorbed by *S. obliquus*.

Examining the charts in Figure 28, the R^2 values are all greater than 0.92, suggesting a good linear relationship for all experiments. However, analysing individual charts, Figure 28c and d had the best R^2 values, and examining the algae concentrations in Table 11, it is these two charts where the variation in microalgae biomass concentration was minimum. The outlier data point in Figure 28*a* correspond to the algae concentration being lowered from 500mg.L^{-1} to 240mg.L^{-1}. In Figure 28*b* there was less consistency in algae concentration (460 mg.L^{-1}, 195 mg.L^{-1} and 245mg.L^{-1}), however the R^2 value was 0.97 so there was a better linear fit for this relationship compared to that shown in Figure 28*a*.

When the algae concentration varies with the initial metal concentration, it is necessary to normalise the data by dividing the initial metal concentration by the initial algae biomass concentration. The linear relationships displayed in Figure 26*a* to *d* all have an R^2 greater than 0.99, compared to the correlations displayed in Figure 28 where only Figure 28*c* and *d* had an R^2 that was greater than 0.99. In these two experiments there was less variation in the *C. vulgaris* and *S. obliquus* concentration respectively.

5.1.2 Multi Component Solution

5.1.2.1 Presence of a secondary metal

In the previous section, single metal solutions of copper and cadmium were mixed with solutions of *S. obliquus* and *C. vulgaris* to investigate a relationship between initial metal concentration, initial algae concentration and adsorption at equilibrium. This led to the derivation of Equation 1:

$$Q_e = \frac{a_{eq}}{ratio} \quad (1)$$

Equation 1 can be rearranged to the following form:

$$Q_e = \alpha_{eq}.ratio^* \quad (2)$$

Where ratio* is the ratio of metal concentration to algae biomass concentration at the beginning of the experiment. For the single metal experiments, the α_{eq} values for copper and cadmium adsorption by C. vulgaris and copper and cadmium adsorption by S. obliquus, as derived in Section 5.1.1 are displayed in Table 13.

Table 13: Reminder of the values for the empirical constant, a_{eq} that relate the final sorption capacity of *C. vulgaris* and *S. obliquus* to copper and cadmium, derived by investigating metal sorption by the microalgae from a single metal solution.

Metal	C. vulgaris	S. obliquus
Copper	892	866
Cadmium	814	829

Further sorption experiments were undertaken using a mixture of copper and cadmium, each with a concentration of 2.5mg.L^{-1}. The adsorption over time was measured for each metal and the results are displayed in Figure 29.

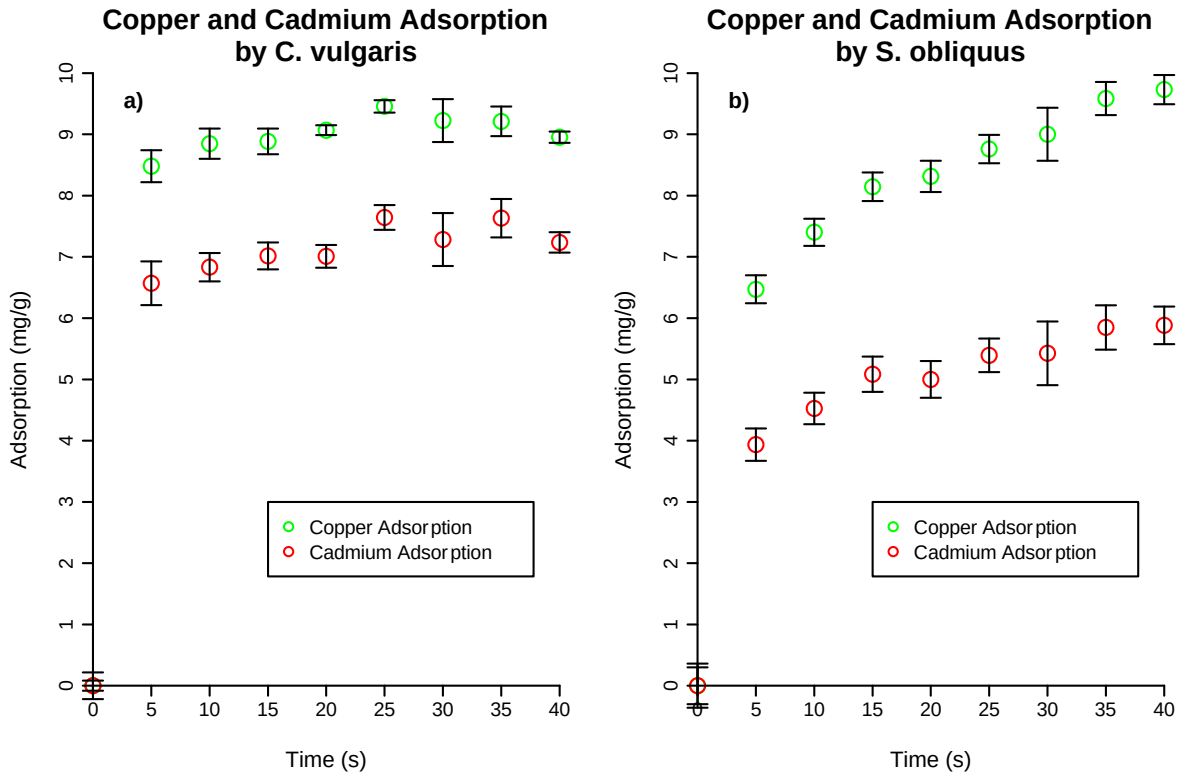

Figure 29: Adsorption, time profiles for the adsorption of copper and cadmium from mixed metal solutions by *Scenedesmus obliquus* and *Chlorella vulgaris*.

In Figure 29a, the *C.* vulgaris concentration was 250mg.L^{-1}, the copper concentration was 2.7mg.L^{-1}, and the cadmium concentration was 2.6mg.L^{-1}. In Figure 29b, the *S. obliquus* concentration was 204mg.L^{-1}, the copper concentration was 2.6mg.L^{-1} and the cadmium concentration was 2.6mg.L^{-1}. To investigate whether the presence of a second metal ion had an effect on adsorption, the expected Q_e was calculated in accordance to Equation 2 and the α_{eq} values present in Table 13. These values are compared to the measured values of adsorption at equilibrium and presented in Table 14.

Table 14: Values of adsorption at equilibrium for the adsorption experiments of copper and cadmium from a binary-metal solution. Analysis undertaken using ICP-MS, and estimated values calculated using Equation 2.

	C. vulgaris		S. obliquus	
Metal	**Q_e Estimated (mg.g^{-1})**	**Q_e Measured (mg.g^{-1})**	**Q_e Estimated (mg.g^{-1})**	**Q_e Measured (mg.g^{-1})**
Copper	9.51	9.13	11.15	9.73
Cadmium	8.46	7.30	10.40	5.88

The values calculated for Q_e when copper is adsorbed by *C. vulgaris* was found to be 9.51mg.g^{-1}, which was slightly higher than that for the measured value of Q_e

which was 9.13mg.g^{-1}. Q_e for the adsorption of cadmium was calculated to be 8.46mg.g^{-1}, which is over 1mg.g^{-1} lower than the Q_e value measured as 7.30mg.g^{-1}.

It is more difficult to analyse the values calculated and measured for *S. obliquus* as the data in Figure 29*a* does not appear to have reached equilibrium within the experimental time period. For this reason the maximum adsorption values for copper and cadmium adsorbed by *S. obliquus* were taken as the Q_e value. These are still lower than the estimated values being 11.15mg.g^{-1} compared to 9.73mg.g^{-1} for copper, and 10.40mg.g^{-1} compared to 5.88mg.g^{-1} for the cadmium adsorption.

For both *C. vulgaris* and *S. obliquus*, the inhibition of cadmium adsorption by the presence of copper is greater than the inhibition of the adsorption of copper caused by the presence of cadmium. The Q_e for cadmium adsorption by *C. vulgaris* is 14% less than the calculated Q_e value obtained from Equation 2, and the Q_e value for the adsorption of cadmium by *S. obliquus* is 43% lower than the estimated value. For copper, the Q_e value was measured to be 4% lower than expected for adsorption by *C. vulgaris*, and Q_e was found to be 13% lower than predicted for copper adsorption by *S. obliquus*.

5.1.2.2 Presence of BG-11 medium ions

The *C. vulgaris* and *S. obliquus* were cultivated using BG-11 growth medium. This is a robust, freshwater cultivation medium that was prepared in accordance to the *Culture Collection of Algae and Protozoa* (CCAP) recipe for the cultivation of freshwater microorganisms as previously used for the cultivation of freshwater cyanobacteria [152], *Chlorella emersonii* and *Chlorella salina* [176], *Scenedesmus obliquus* [24] and *Chlorella vulgaris* [177]. The composition of BG-11 is displayed in Table 15.

Table 15: Nutrient and buffer salts required for freshwater, BG-11 growth medium for the cultivation of *S. obliquus* and *C. vulgaris*.

Nutrient	Medium Concentration (mg/L)
K_2HPO_4	40
$MgSO_4.7H_2O$	65
$CaCl_2.2H_2O$	36
Citric Acid	6
Ammonium ferric citrate green	6
Na_2EDTA	1
Na_2CO_3	20
H_3BO_3	2.86
$MnCl_2.4H_2O$	1.81
$ZnSO_4.7H_2O$	0.22
$Na_2MoO_4.2H_2O$	0.39
$CuSO_4.5H_2O$	0.08
$Co(NO_3)_2.6H_2O$	0.05

Preliminary experiments investigated the copper uptake from BG-11 contaminated with copper by *C. vulgaris*. This was made up of three experiments; the first had a *C. vulgaris* concentration of 140mg.L^{-1}, a copper concentration of 0.8 mg.L^{-1}, and the analysis was undertaken using ICP-OES. The second and third experiments were analysed with ICP-MS, and were devised so that the initial copper concentration to algae concentration were kept constant. The adsorption time profiles for copper removal from BG-11 solution by *C. vulgaris* are displayed in Figure 30. Table 16 contains the initial concentration of copper, and *C. vulgaris* for each of the BG-11 experiments, along with their corresponding, calculated ratio of the concentration of aqueous copper ions to the *C. vulgaris* concentration.

Table 16: Initial Copper and *C. vulgaris* concentrations used in the experiment that investigated copper adsorption from BG-11 growth medium.

Experiment	Initial Algae Concentration (mgL^{-1})	Initial Copper Concentration (mgL^{-1})	Ratio of Copper concentration to C. vulgaris concentration ($mg_{Cu}.mg_{algae}^{-1}$)
ICP-OES	140	0.8	5.8×10^{-3}
ICP-MS 1	630	0.73	1.1×10^{-3}
ICP-MS 2	1000	1.14	1.1×10^{-3}

As the two investigations analysed by ICP-MS had the same initial copper to biomass ratio of 1. $1\times10^{-3}mg_{Cu}.mg_{algae}^{-1}$, Equation 2 would predict that their Q_e values would be identical.

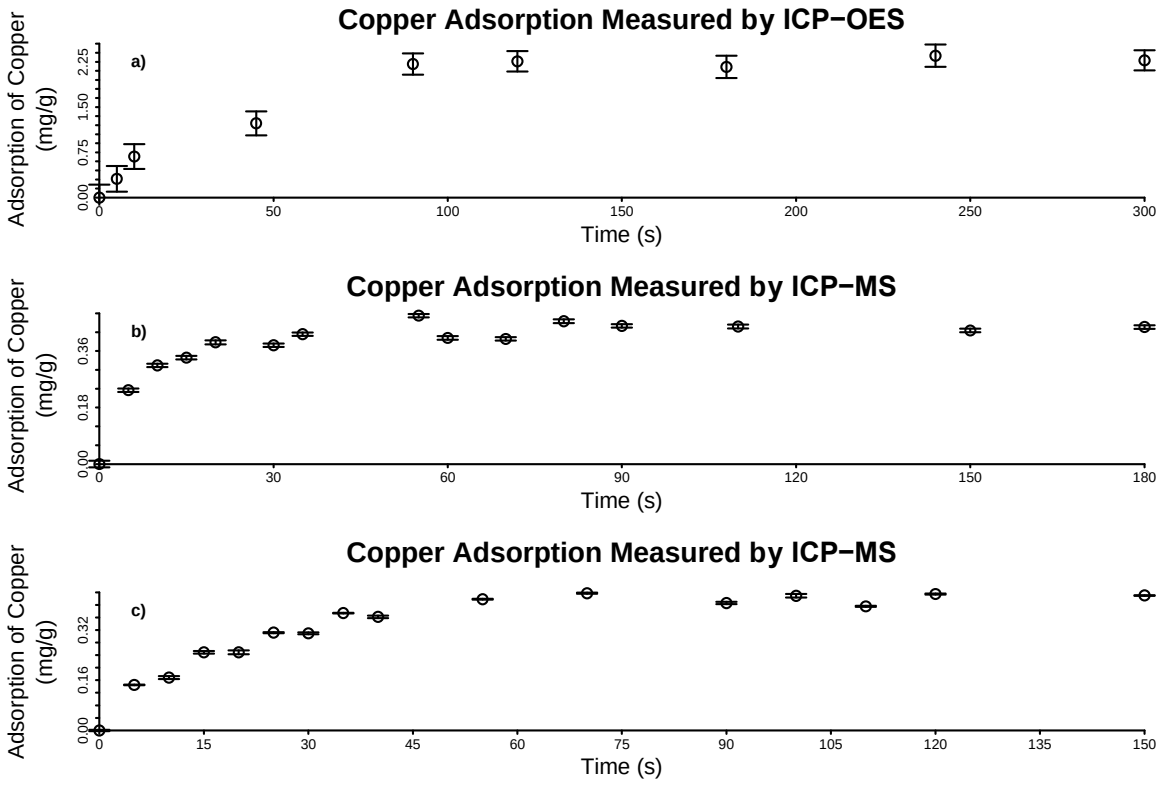

Figure 30: Adsorption time profiles for the adsorption of copper ions by *Chlorella vulgaris* from BG-11 culture medium that had been contaminated with copper.

The Q_e for each experiment was calculated by finding the average Q_e from Figure 30a, b and c, once Q_e had reached the equilibrium value. Figure 30*a* displays the data for the analysis undertaken by ICP-OES, and had a Q_e of 2.1mg.g^{-1}. The Q_e for experiments analysed by ICP-MS were calculated in the same way from Figure 30*b* and *c*, and these values were calculated to be 0.43mg.g^{-1} and 0.42mg.g^{-1} respectively. These values are displayed along with their corresponding expected values that were calculated using Equation 2, in Table 17.

Table 17: Expected values of adsorption at equilibrium according to Equation 2, compared to values measured for adsorption at equilibrium by ICP-OES and ICP-MS, for copper adsorption by *C. vulgaris*.

Experiment	Expected Q_e	Measured Q_e
ICP-OES	5.15	2.1
ICP-MS 1	1.02	0.43
ICP-MS 2	1.02	0.42

The expected values of Q_e displayed in Table 17, as observed in Table 14 overestimated the Q_e values for the copper adsorption when adsorbed from *BG-11* solution. The ICP-OES experiment the expected Q_e was 5.15 mg.g^{-1}, but it was measured to be 2.1mg.g^{-1}. The ICP-MS experiments returned an expected Q_e value to be 1.02mg.L^{-1}. With the ratio of initial copper concentration to initial algae

concentration the same for both experiments; their expected Q_e values were identical. Although the measured Q_e values were lower than the estimated value, they were measured to be 0.43 and 0.42mg.g^{-1}. This reinforces that the Q_e values are a function of the ratio of initial copper concentration to microalgae concentration.

Examining the concentrations of the salts present within BG-11 medium (as shown in Table 15), there are seven salts of significant concentration. The experiment with results analysed using the ICP-OES had an initial copper concentration of 0.8mg.L^{-1}, and the first experiment that used the ICP-MS had a copper concentration of 0.73mgL^{-1}. These copper concentrations are considerably lower than nine of the nutrient salts present in solution. For example, the concentration of potassium diphosphate and the concentration of magnesium sulphate heptahydrate are 40mg.L^{-1} and 65mg.L^{-1}. The concentration of competing ions within the BG-11 medium is considerably greater than that of the copper ions.

However, as the measured Q_e values for the two ICP-MS experiments are equivalent, it can be concluded that the adsorption at equilibrium of the metal ions is a function of the initial biomass concentration and the initial metal concentration. This is true whether the adsorption is from a single component solution or whether there are other ions present in solution.

5.1.3 Extent of removal

The following section analyses the effect that initial adsorbate and adsorbent concentrations in the extent of metal ion removal from deionised water. Each combination of metal and algae had four metal concentrations. The data is split into four groups, *C. vulgaris* adsorbing copper at concentrations of 0.25mg.L^{-1}, 0.5mg.L^{-1}, 0.75mg.L^{-1} and 2.5mg.L^{-1}; *C. vulgaris* adsorbing cadmium at concentrations of 0.25mg.L^{-1}, 0.5mg.L^{-1}, 0.75mg.L^{-1} and 2.5mg.L^{-1}; *S. obliquus* adsorbing copper at concentrations of 0.25mg.L^{-1}, 0.5mg.L^{-1}, 0.75mg.L^{-1} and 2.5mg.L^{-1}; and *S. obliquus* adsorbing cadmium at concentrations of 0.25mg.L^{-1}, 0.5mg.L^{-1}, 0.75mg.L^{-1} and 2.5mg.L^{-1}. Figure 31 displays extent of removal by each algae species for each metal species investigated.

The extent of removal was calculated by finding the difference between the concentration of copper or cadmium in solution at the beginning, and the concentration at equilibrium, divided by the initial metal ion concentration.

$$\%E = \frac{C_0 - C_e}{C_0} \times 100\%$$

Where:

- C_0 is the initial copper or cadmium concentration (mg.L^{-1}).
- C_e is the copper or cadmium concentration at equilibrium (mg.L^{-1}).
- $\%E$ is the extent of removal (%)

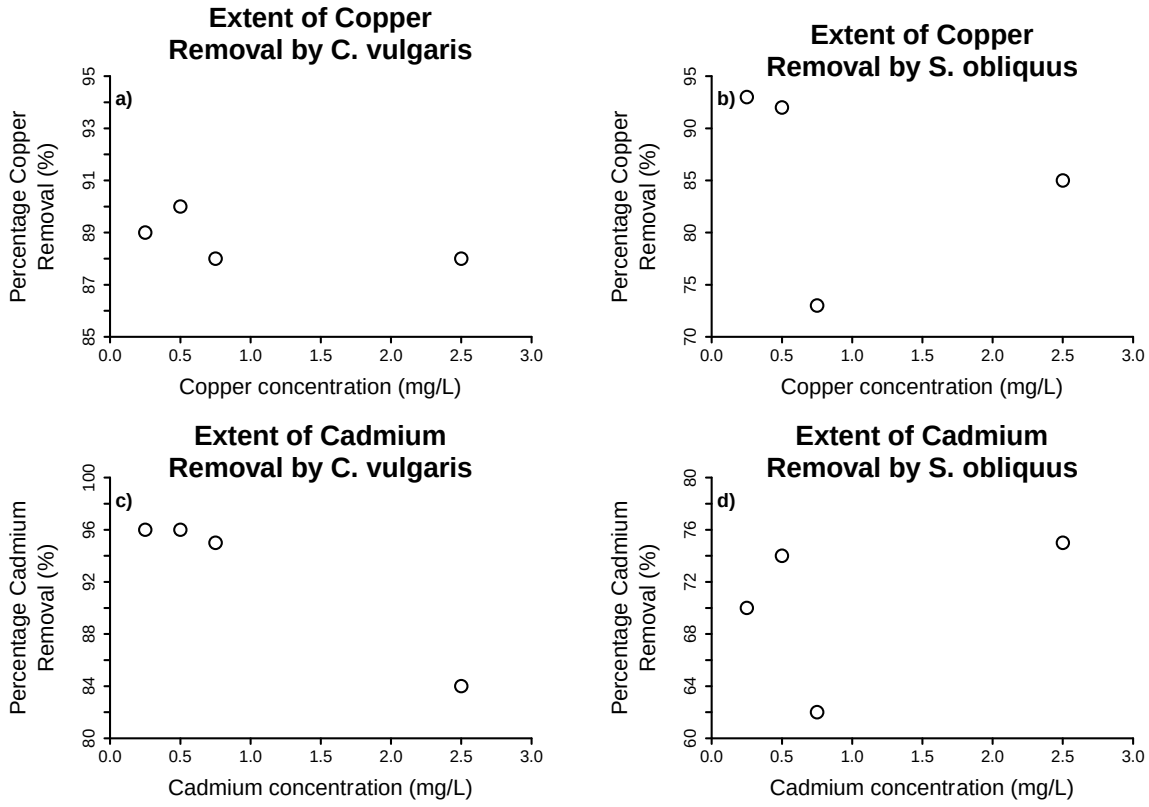

Figure 31: Extent of removal of copper and cadmium adsorbed by *C. vulgaris* and *S. obliquus*, expressed by percentage of metal removed, plotted against initial metal concentration.

Examining Figure 31*a*, the average extent of removal of copper by *C. vulgaris* for all four copper concentrations investigated was 88.75% with a standard deviation of 0.96 and a coefficient of variance as ±1.08%. In comparison, Figure 31*c* displays data for the extent of cadmium removal by *C. vulgaris* from solutions of 0.25mgL^{-1}, 0.5mg.L^{-1} and 0.75mg.L^{-1} remained around 95% (average 95.8% and coefficient of variance of 0.57%). The extent of removal then dropped to 83.8% for the initial cadmium concentration of 2.5mg.L^{-1}. This could indicate that the adsorption limit

of *C. vulgaris* for cadmium, is between 0.75mg.L and 2.5mg.L^{-1} in solution. The *C. vulgaris* concentrations used to obtain all four data points in Figure 31*c* were all consistent at 250mg.L^{-1}.

The data for *S. obliquus* has a more complex relationship compared to that of *C. vulgaris*. In both Figure 31*b* and *d* the percentage removal of copper and cadmium (respectively), drop from 92% to 75% when the copper concentration increases from 0.5mg.L^{-1} to 0.75mg.L^{-1}, and drop from 74% to 63% when the cadmium concentration rose to 0.75mg.L^{-1} for 0.5mg.L^{-1}. When the copper concentration increased to 2.5mg.L^{-1}, the percentage removal increased to 85%, and when the cadmium concentration increased to 2.5mg.L^{-1}, the extent of removal rose to 75%. The *S. obliquus* concentration for the data points in Figure 31*d* representing the initial cadmium concentration of 0.25mg.L^{-1}, 0.5mg.L^{-1} and 0.75mg.L^{-1} were all consistent at 240mg.L^{-1}, and the concentration of the *S. obliquus* was slightly higher at 245mgL^{-1} for the data point representing the cadmium concentration of 2.5mg.L^{-1}. As the concertation of *C. vulgaris* and *S. obliquus* used to obtain the data in Figure 31*c* and *d* (respectively), were kept consistent, It does not appear that the extent of removal is a function of the biomass concentration in the present study.

A possible explanation for the varying extent of removal of copper and cadmium by *S. obliquus* may be a result of a cellular defence mechanism. At lower metal concentrations, functional groups on the cell wall may be able to repel metal ions, but the increase in concentration of the metals in solution may cause a larger concentration gradient able to overcome these defence mechanisms leading to greater adsorption. Scenedesmus are a species of algae chosen for research due to their tolerance to the presence of heavy metals, various species are able to produce extracellular polymers to bind toxic metals externally [178]. A previous study into copper removal by *S. obliquus* (over a longer time period), found that *S. obliquus* has a complex profile for the percentage removal from solution. This study investigated the contact over a number of days and fund the copper removal by *S. obliquus* gradually accelerated to a maximum removal extent or around 90%. When the copper concentration exceeded 0.5mg.L^{-1}, the rate of removal significantly decreased but the overall extent of removal did not change, reaching 80-90% [26].

Tuzen et al (2010) investigated meta removal by the algae *Cladophora hutchinsiae* while varying the biomass concentration and observed a rapid increase in metal removal as biomass concentration increased until the optimum biomass concentration was reached, resulting in no further metal removal [94]. The results of this current study indicate that the effect of metal concentration on the extent of removal my microalgae is complex, and in need of further study.

5.2 Adsorption Isotherms

5.2.1 Langmuir Isotherm

In this section the equilibrium data of the adsorption processes are investigated, with the fitting of commonly used Isotherms to the experimental data. A commonly used isotherm is the Langmuir Isotherm, which assumes that the adsorption occurs within a monolayer on the surface of the adsorbent, where adsorbate binds to a finite number of binding sites, with a homogeneous energy profile.

The Langmuir isotherm has the following form:

$$Q_e = \frac{Q_{max} b_L C_e}{1 + b_L C_e} \tag{3}$$

Where:

- Q_e is the adsorption of metal ion per gram of algae at equilibrium (mg.g^{-1}).
- Q_{max} is the maximum surface adsorption of the adsorbent (mg.g^{-1}).
- b_L is the Langmuir Constant (L.mg^{-1})
- C_e is the concentration of adsorbate remaining in solution (mg.L^{-1})

The maximum adsorption (Q_{max}) and Langmuir Constant (b_L) are derived by linearizing Equation 3 and applying it to experimental data. The linear form of the Langmuir Isotherm is shown in Equation 4.

$$\frac{1}{Q_e} = \frac{1}{Q_{max}} + \frac{1}{b_L Q_{max}} . \frac{1}{C_e} \tag{4}$$

A plot of the reciprocal of the adsorption at equilibrium (Q_e^{-1}) against the reciprocal of the concentration of the adsorbate remaining in solution (C_e^{-1}) will return a y-

axis intercept equal to the reciprocal of Q_{max}, and a gradient that is equal to the product of b_L and Q_{max}. The linear Langmuir Isotherms for each metal adsorbed by each species of microalgae is shown in Figure 32.

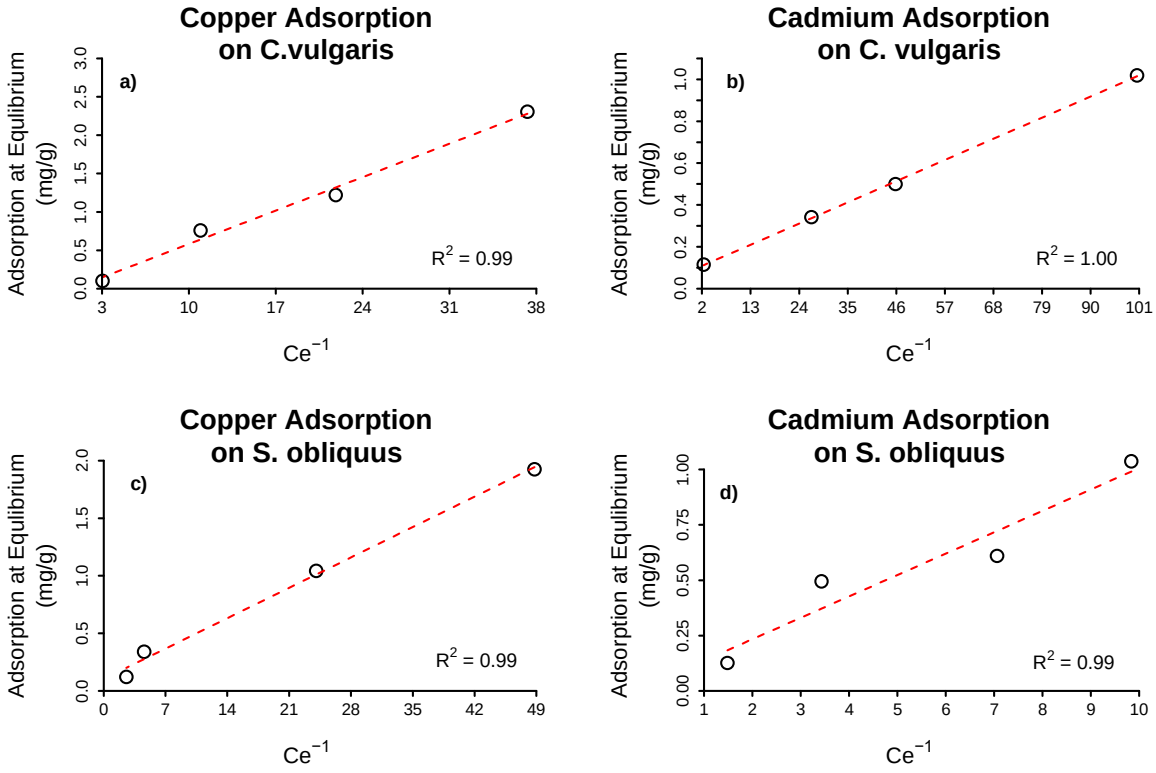

Figure 32: Linear Langmuir Isotherms for a) copper adsorbed by *C. vulgaris*, b) cadmium adsorbed by *C. vulgaris*, c) copper adsorbed by *S. obliquus* and d) cadmium adsorbed by *S. obliquus*.

In all charts, Figure 32*a* to *d* show a strong linear relationship; the R^2 for all charts is greater than 0.99. The Q_{max} and b_L are displayed in Table 18.

Table 18: Langmuir Isotherm parameters derived for the adsorption of copper and cadmium by *C. vulgaris* and *S. obliquus* from single metal solutions.

Algae	Metal	Q_{max} (mg.g^{-1})	b_L (L.mg^{-1})	R^2
Chlorella vulgaris	Copper	-25.43	-0.66	0.98
Chlorella vulgaris	Cadmium	11.06	9.83	1.00
Scenedesmus obliquus	Copper	9.70	2.73	0.99
Scenedesmus obliquus	Cadmium	24.72	0.42	0.88

The Langmuir constant, b_L (L.mg^{-1}) indicates the binding affinity of the adsorbate to the adsorbent. A higher value indicates that there is a greater binding affinity. The values for b_L in Table 18 indicate that cadmium has a higher binding affinity to *C. vulgaris* (9.83 Lmg^{-1}), and copper has a higher binding affinity to *S. obliquus* (2.73 Lmg^{-1}). It is important to notice that a higher value of b_L does not necessarily

indicate a higher binding capacity, Q_{max} of the adsorbent. *S. obliquus* has a higher binding capacity for cadmium compared to copper (24.72mg.g^{-1} to 9.70mg.g^{-1}, respectively), but *S. obliquus* has a higher affinity to copper. This is an observation that has been observed in studies investigating adsorption of zinc, nickel and cadmium by sewage sludge [98].

The Langmuir Isotherm did not represent the adsorption of copper by *C. vulgaris* as the values for Q_{max} and b_L were both negative. This error could be a result of the low concentrations of adsorbate used in the study, and a limited number of datapoints used to produce the isotherms. The adsorption Isotherms were produce using four data points, with concentration range of 0.25mg.L^{-1} to 2.5mg.L^{-1}. To create more accurate isotherms, a larger concentration range for copper cadmium ions should be investigated.

5.2.2 Freundlich Isotherm

The Freundlich Isotherm is an empirical model that assumes adsorption occurs via a multi-layer binding mechanism, on an adsorbate with a surface with heterogeneous energy profile. The Freundlich Isotherm is shown by Equation 5.

$$Q_e = k_F C_e^{1/n} \tag{5}$$

Where:

- Q_e is the adsorption at equilibrium as before (mg.g^{-1}).
- C_e is the residual concentration of metal ion at equilibrium (mg.L^{-1}).
- k_F is the Freundlich constant (mg.g^{-1})(Lg^{-1})^n.
- n is a correction factor.
- k_F and n are dependent on the adsorbate, adsorbent and the temperature.

The Freundlich constant (also known as the distribution coefficient), k_F and the correction factor, n are found by linearising Equation 5, and applying it to experimental data as before. The linear form of the Freundlich isotherm is given by Equation 6.

$$\ln(Q_e) = \frac{1}{n}\ln(C_e) + \ln(k_F) \tag{6}$$

The Freundlich constant and the correction factor (also known as the biosorbent intensity [95]), *n* are found by plotting the natural logarithm of the adsorption at equilibrium against the natural logarithm of the concentration of adsorbate remaining in solution, at equilibrium. The correction factor, *n* is calculated by finding the reciprocal of the gradient, and k_F is calculated by taking the exponential of the y-axis intercept. The linear Freundlich Isotherms are displayed in Figure 33.

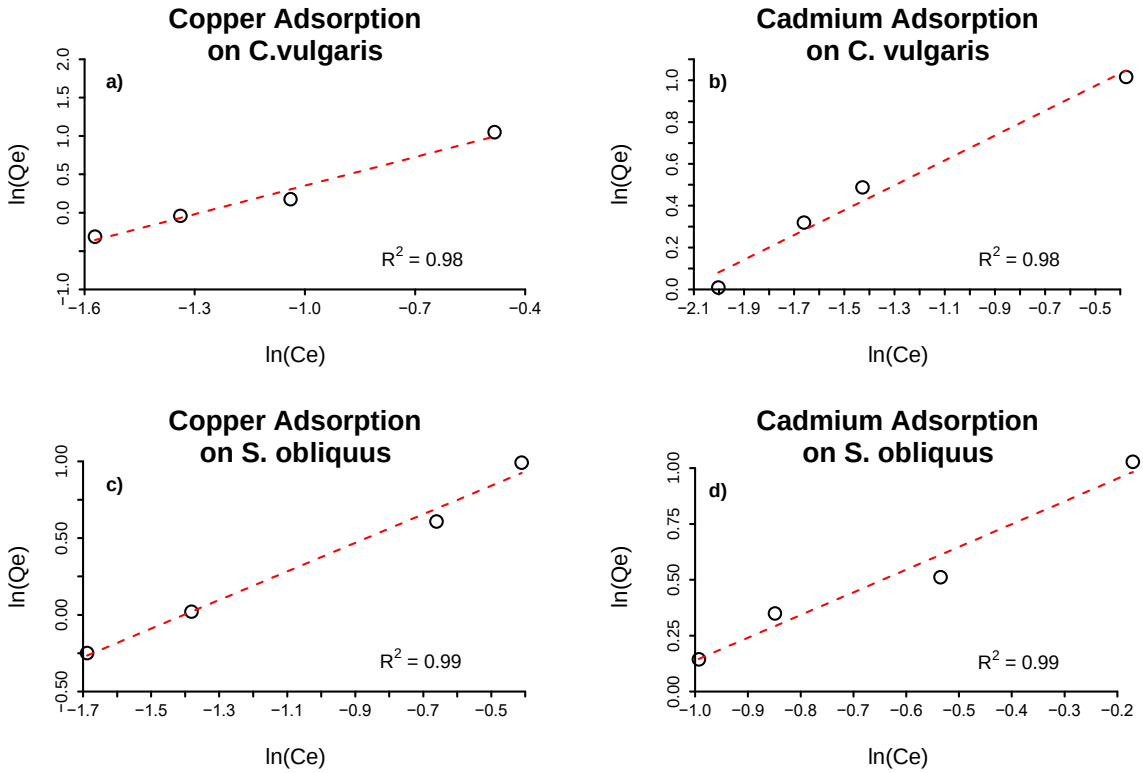

Figure 33: Linear Freundlich Isotherms for a) copper adsorbed by *C. vulgaris*, b) cadmium adsorbed by *C. vulgaris*, c) copper adsorbed by *S. obliquus* and d) cadmium adsorbed by *S. obliquus*.

Similarly to the linear Langmuir charts as displayed in Figure 32, all linear Freundlich charts showed a good linear correlation, with all R^2 values calculated to be greater than 0.98. The values for k_F and *n* are displayed in Table 19.

Table 19: Freundlich Isotherm parameters derived for the adsorption of copper and cadmium by *C. vulgaris* and *S. obliquus* from single metal solutions.

Algae	Metal	k_F $(mg.g^{-1})(Lg^{-1})^{1/n}$	n	R^2
Chlorella vulgaris	Copper	39.23	0.81	0.98
Chlorella vulgaris	Cadmium	18.63	1.68	0.98
Scenedesmus obliquus	Copper	20.30	1.07	0.99
Scenedesmus obliquus	Cadmium	14.32	0.98	0.99

The Freundlich constant k_f is related to the binding capacity for the biosorbent. In all but one case, K_f is greater than Q_{max} obtained from the Langmuir isotherm, the k_F for cadmium adsorbed by *S. obliquus* was calculated to be 14.32(mg.g^{-1})(Lg^{-1})$^{1/n}$, and Q_{max} for cadmium adsorbed by *S. obliquus* was calculated to be 24.72mg.g^{-1}. In previous studies of copper and cobalt being adsorbed by macroalgae, it was found that in all cases Q_{max} to be greater than k_F [95]. The sorption intensity constant, n is related to the concentration of the adsorbate [99]. If $n > 1$, this suggests that the conditions are favourable to adsorption. The data presented in Table 19 suggests that adsorption was favourable for cadmium adsorbed *C. vulgaris* and copper on *S. obliquus* (n is 1.68, and 1.08 respectively), but not for copper adsorbed by *C. vulgaris* (n=0.81) or cadmium adsorbed by *S. obliquus* (n=0.98).

The Freundlich Isotherm predicts that an increase in adsorbate concentration in solution leads to an increase in adsorption of the adsorbate [99], which is a characteristic of metal sorption by microalgae as described earlier in Section 5.1.1. where it was observed that Q_e increased linearly with an increase in the adsorbate to adsorbent concentration ratio.

The Freundlich Isotherm also implies that the heat of adsorption decreases logarithmically with adsorbate coverage [96]. The Temkin Isotherm has previously been applied to metal sorption studies [96, 101, 113], and implies that the reduction in heat of adsorption decreases linearly with surface coverage [96].

5.2.3 Temkin Isotherm

The Temkin Isotherm has an advantage as it can be used to investigate thermodynamic interactions between adsorbate and adsorbent, and it assumes the energy of the binding sites is uniformly distributed across the adsorbent's surface [100, 113]. The Temkin Isotherm is shown in Equation 7.

$$Q_e = \frac{RT}{b_T}.\ln(a_T.C_e) \tag{7}$$

Where

- Q_e is the adsorption at equilibrium as before (mmol.g^{-1}).
- C_e is the residual concentration of metal ion at equilibrium (mg.L^{-1}).

- a_T is the equilibrium binding constant (L.g^{-1}).
- b_T is the Temkin constant related to heat of sorption (J.g.mol^{-1}).
- R is the universal gas constant (8.314 Jmol^{-1}K^{-1})
- T is the absolute temperature (288 K)

The Temkin Isotherm can be linearised as displayed in Equation 8.

$$Q_e = \frac{RT}{b_T}.\ln(a_T) + \frac{RT}{b_T}.\ln(C_e) \quad (8)$$

To determine the equilibrium binding constant, a_T and the Temkin heat constant, b_T Q_e was plotted against the natural logarithm of C_e, and b_T is calculated by dividing the product of the universal gas constant, R and the temperature, T by the gradient of the linear fit. a_T is calculated by taking the exponential of the y-axis intercept divided by the gradient. The linear Temkin Isotherms are displayed in Figure 34.

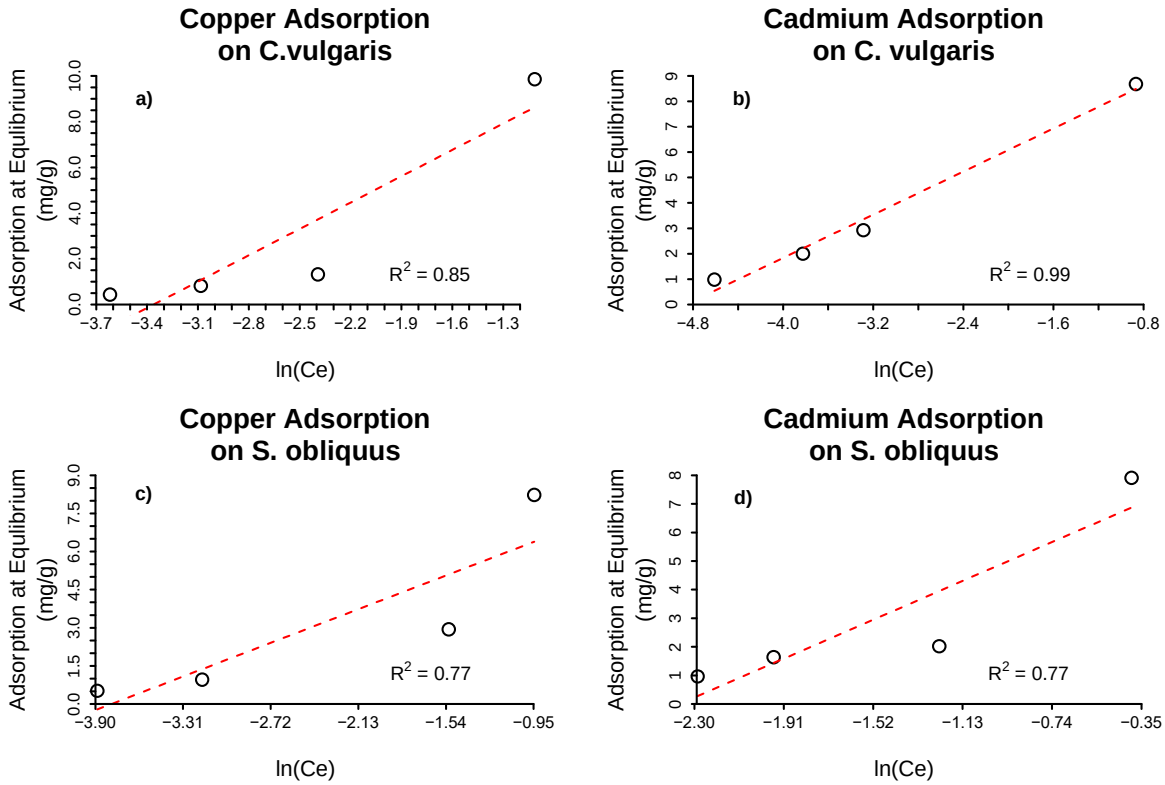

Figure 34: Linear Temkin Isotherms for a) copper adsorbed by *C. vulgaris*, b) cadmium adsorbed by *C. vulgaris*, c) copper adsorbed by *S. obliquus* and d) cadmium adsorbed by *S. obliquus*.

The Temkin Isotherm does not have a good a linear fit compared to the Langmuir or Freundlich Isotherms, with only cadmium adsorbed by *C. vulgaris* (Figure 34*b*) showing a good linear correlation with an R^2 value of 0.99.

Table 20: Temkin Isotherm parameters derived for the adsorption of copper and cadmium by *C. vulgaris* and *S. obliquus* from single metal solutions.

Algae	Metal	b_T (Jmmol^{-1})	a_T (*L.mg^{-1}*)	R^2
Chlorella vulgaris	*Copper*	*624*	*29*	*0.85*
Chlorella vulgaris	*Cadmium*	*1128*	*130*	*0.99*
Scenedesmus obliquus	*Copper*	*1066*	*44*	*0.77*
Scenedesmus obliquus	*Cadmium*	*687*	*11*	*0.77*

The Temkin model does not fit the experimental data as well as the other two Isotherms. As all b_T values are positive, it can be concluded that the adsorption process is endothermic [100]. A previous study investigating the Langmuir Isotherm, Freundlich Isotherm and the Temkin Isotherm when modelling the adsorption of cadmium by *Parachlorella sp.* found the Temkin Isotherm had the worst linear fit with an R^2 of 0.955. The Langmuir had am R^2 of 0.97 and the Freundlich had an R^2 of 0.96 [92]. This study found that all three Isotherm models had a good fit for when cadmium is adsorbed by *C. vulgaris*. The Langmuir Isotherm returned an R^2 of 1.00, the Freundlich and R^2 of 0.98 and the Temkin an R^2 of 0.99. For this combination of algae and metal, the correct Isotherm cannot be determined by linear fit alone.

The Temkin Isotherms both returns a value for a_T which is the Temkin Equilibrium constant that can be used to calculate the heat of adsorption [101, 113], using the expression shown in Equation 9.

$$\ln(a_T) = \frac{\Delta S^\circ}{R} - \frac{\Delta H^\circ}{RT} \tag{9}$$

Where:

- a_T is the equilibrium binding constant (L.g^{-1}).
- ΔS is the change in entropy (JK^{-1})
- ΔH is the change in enthalpy (J)
- R is the universal gas constant (8.314 Jmol^{-1}K^{-1})
- T is the absolute temperature (K)

Equation 9 is an adaption of the Van't Hoff Equation, and Boulaiche et al [113] claim that a_T is equivalent to the equilibrium constant. A plot of the natural logarithm of a_T against the reciprocal of its corresponding temperature will return a gradient equal to the enthalpy change divided by the universal gas constant R. To undertake

this analysis, further investigation would be required to gather data for a_T with varying temperature.

The units of a_T are the same as the units of the Langmuir constant, b_L (Lmg^{-1}). This would suggest that the Langmuir constant could be used within the Van't Hoff equation also, however this is not universally the case. In the present study, the adsorbate is ionic, and is present in a low concentration, so it may be applicable. However Ghosal et al [90] explain that the equilibrium constant is related to the Langmuir constant, but is not directly equivalent, although at low concentrations it can be used as an accurate approximation.

Many previous studies have focused on the adsorption isotherms relating adsorption capacity to the initial concentrations and the metal ions using the Langmuir, Freundlich and Temkin Isotherms [15, 19, 20, 82, 91-93, 95]. Many of the findings are inconsistent with some favouring Langmuir [15, 92, 121, 131, 179], and others favouring Freundlich [19, 20, 82, 120], while Tüzün *et al* (2005) [16] found the Langmuir Isotherm entirely unsuitable for their data for cadmium adsorption by the microalgae, *Chlamydomonas reinhardtii* due to R^2 values of a "semi-reciprocal Langmuir model", returning an R^2 value of 0.92. The R^2 value for the adsorption of cadmium was calculated to be 0.98, but both values would suggest good correlation [16].

In this study, the linear Langmuir charts returned an R^2 value of 0.99 for copper adsorbed by *C. vulgaris*, 1.00 for cadmium adsorbed by *C. vulgaris*, 0.99 for copper adsorbed by *S. obliquus* and 0.99 for cadmium adsorbed by *S. obliquus*. In all cases the fit of the model suggests that the Langmuir Isotherm is suitable for the adsorption process. However assumptions of the Langmuir Isotherm require the metals to be bound by a mono-layer mechanism, no interaction between adsorbed species and the surface of the adsorbent to be energetically homogeneous [16, 101, 113]. Microalgae does not satisfy the homogeneous surface condition of the Langmuir Isotherm [92], so could therefore on this basis it could be discounted. The Langmuir parameters produced from the Lineweaver-Burk plot for copper adsorption by *C. vulgaris* (Figure 32*a*), returned negative values for Q_{max} and the Langmuir constant. Previous studies have acknowledged that biosorbents do not

follow the assumptions of the Langmuir Isotherm and did not discount it [90], but findings in this current study conclude that the Freundlich Isotherm is the model that best represents the adsorption process for copper and cadmium adsorption by the microalgae *C. vulgaris* and *S.obliquus*.

5.3 Chapter Summary

This chapter focussed on the conditions of the adsorption process after the adsorption equilibrium had been reached. The extent of removal, adsorption at equilibrium and the adsorption isotherms for the adsorption of copper and cadmium by *C. vulgaris* and *S. obliquus* were investigated.

A relationship between the adsorption at equilibrium and the initial concentrations of adsorbent and adsorbate was derived. By plotting the values of Q_e against the ratio of algae concentration to metal concentration at the beginning of the experiment, a linear relationship with an R^2 greater than 0.99 was produced for all experiments. From these charts, a mathematical expression was derived and is shown by Equation 2:

$$Q_e = \alpha.ratio^* \quad (2)$$

Where:

- Q_e is the adsorption at equilibrium ($mg.g^{-1}$)
- α is an empirical constant ($mg.g^{-1}$)
- $ratio^*$ is the initial metal concentration ($mg.L^{-1}$) divided by the algae concentration ($mg.L^{-1}$).

The values for α derived for copper adsorbed by *C. vulgaris* was found to be 892, 866 for cadmium adsorbed by *C. vulgaris*, 814 for copper adsorbed by *S. obliquus* and 829 for cadmium adsorbed by *S. obliquus*. These values would suggest that if the algae and metal concentrations wear all kept constant, *C. vulgaris* would have a higher capacity for copper compared to cadmium, and *S. obliquus* has a higher capacity to cadmium compared to copper.

These values for α were applicable to adsorption from a single metal solution only. When adsorption of copper and cadmium was investigated from a mixture of the

two ions, Equation 2 predicted Q_e values that were higher than those measured by ICP-MS. This effect was also observed for the adsorption of copper by *C. vulgaris* from contaminated BG-11 solution. The presence of the BG-11 salts also reduced the Q_e values compared to those predicted by Equation 2. In the presence of competing ions, the Q_e of copper was still a function of the ratio of copper ions to the concentration of *C. vulgaris* at the beginning of the experiment.

The extent of metal removal by each species of microalgae was investigated by measuring the concentration of the metal ion remaining in solution after adsorption equilibrium had been reached. The extent of removal does not appear to be related to biomass concentration. When copper was adsorbed by *C. vulgaris*, the percentage copper removal was 89% for all copper concentrations investigated, and this was the case for when the copper concentration rose to 2.5mgL^{-1} and the *C. vulgaris* concentration dropped from 500mg.L^{-1} to 240mg.L^{-1}. When analysing the cadmium adsorption by *C. vulgaris*, the biomass concentration was consistent for all four experiments, but when the cadmium concentration rose from 0.75mg.L^{-1} to 2.5mg.L^{-1}, the percentage removal decreased from 95% to 84%.

The Relationship between extent of removal and the metal concentration for *S. obliquus* appears to be more complex. When investigating copper adsorption, the extent of copper removal dropped from 92% to 73% when the copper concentration increased from 0.5mg.L^{-1} to 0.75mg.L^{-1}; and then increased again to 85% when the copper concentration increased to 2.5mg.L^{-1}. The effect was also observed when cadmium was adsorbed by *S. obliquus*. The extent of cadmium removal dropped from 74% to 62% when the cadmium concentration increased from 0.5mg.L^{-1} to 0.75mg.L^{-1}; and then removal increased to 75% when the cadmium concentration increased to 2.5mg.L^{-1}. This effect appears to be independent of algae concentration.

Finally, adsorption Isotherms were fitted to each equilibrium profile for the copper and cadmium adsorption by *C. vulgaris* and *S. obliquus* from a single metal solution. The Langmuir Isotherm had the best fit, returning an R^2 higher than 0.99 for all experiments. The Freundlich Isotherm also had a good fit, returning an R^2 value of 0.98 for the *C. vulgaris* isotherms, 0.99 for the *S. obliquus* isotherms. As algae cells

are not likely to have homogeneous binding sites, and as the Freundlich Isotherm predicts the increase in adsorbate binding with an increase of concentration of adsorbate in solution; the Freundlich isotherm will most likely represent the adsorption process compared to the Langmuir Isotherm. The Temkin Isotherm only returned an R^2 value greater than 0.99 for the cadmium adsorption by *C. vulgaris*, all other adsorption experiments returned an R^2 below 0.86.

Chapter 6 Uptake kinetics of heavy metals by microalgae

The aim of this chapter is to investigate the fit of three models of onto microalgae. In the case of the Lagergren Model and the second-order model, these have in the past been used for metal uptake by various species of macroalgae [95, 119] and microalgae [16, 17, 118, 180], and are widely used to describe adsorption process from aqueous solutions [129]. The Elovich Model is less well reported with a single paper found for its use with macroalgae [119], but previous studies have found the model representative of batch adsorption by other bio-sorbents [124, 132, 181]. The outcomes of this chapter will be the comparison and analysis of the use of the three kinetic models when they are applied to batch adsorption processes of copper and cadmium by *Chlorella vulgaris* and *Scenedesmus obliquus*.

6.1 Adsorption from a Single Metal Solution

6.1.1 Lagergren Model

The Lagergren Model, first proposed in 1898 [122], is a pseudo first-order model that was derived to model the uptake of oxalic and malonic acids on to activated carbon. In this model Q_t, the adsorption at time t, is a function of the adsorption at equilibrium, and has the non-linear form:

$$Q_t = Q_e(1 - e^{-k_t.t}) \quad (1)$$

Where:

- Q_t is the adsorption at time t (mg.g^{-1}).
- Q_e is the adsorption at equilibrium (mg.g^{-1}).
- k_t is the first order rate constant (s^{-1}).
- t is the time elapsed (s).

Q_e and k_t are constants that can be derived by linearising the experimental data as follows:

$$ln(Q_e - Q_t) = -k_t . t + ln(Q_e) \quad (2)$$

A plot of $ln(Q_e\text{-}Q_t)$ against t will return a gradient that is equal to $-k_t$ and an intercept that should equal $ln(Q_e)$. As Q_e is present on both sides of the equation, this is value is initially estimated from experimental data. Previous studies have found that these model parameters rarely correspond well with the experimental data [124-127], so to test the parameters obtained from Equation 2, Equation 1 is modified to produce Equation 1.1 which represents represent an *initial model*:

$$Q_t = Q_{e0}(1 - e^{-k_{t0}.t}) \quad (1.1)$$

Where:

- Q_{e0} is the adsorption at equilibrium obtained from Equation 2 ($mg.g^{-1}$).
- k_{t0} is the first order rate constant obtained from Equation 2 (s^{-1}).

The reason the model is considered a "pseudo-first order" model is that if the model was a true first order model, $ln(Q_e)$ would equal the intercept of a plot of $ln(Q_e\text{-}Q_t)$ against t; and $k_t(Q_e\text{-}Q_t)$ does not represent the number of binding sites on the adsorbent [123, 124]. For the Lagergran model, this is rarely the case [124-127].

Using the statistical software package "R", Equation 1 was fitted to the experimental data using a non-linear regression function. This function uses the Gauss-Seidel method, with the model parameters obtained from Equation 2 as the initial parameter approximations for the model. This methodology produces two models, and allows for the comparison of the first-order model parameters obtained by linearising the Lagergren model, and the model parameters produced by fitting the Lagergren model directly to the experimental data.

The adsorption time profiles for the adsorption of copper and cadmium by *C. vulgaris* and *S. obliquus*, at varying metal ion concentrations are shown in Figure 35 to Figure 38.

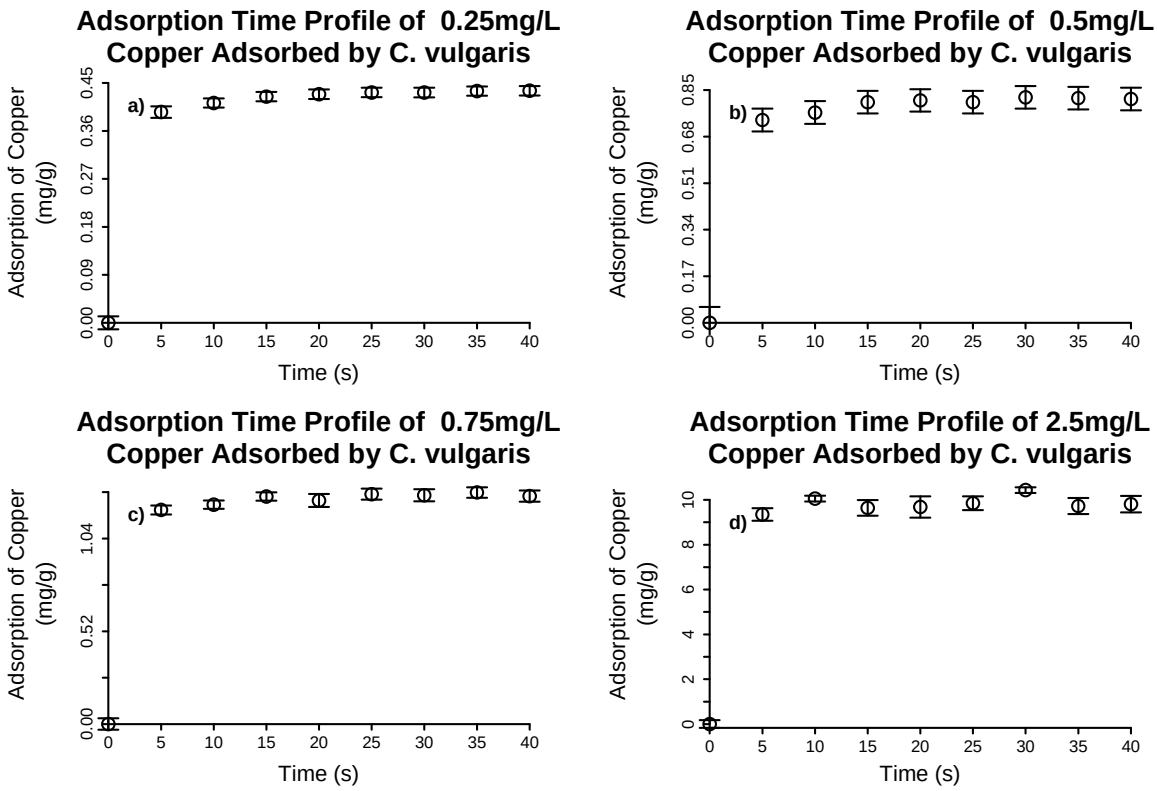

Figure 35: Copper uptake data by *C. vulgaris*. Top left to bottom right, *C. vulgaris* concentration 500mg/L, 500mg/L, 500mg/L, 240mg/L.

Figure 35 shows the adsorption time profile of the adsorption of copper by *C. vulgaris*. For all concentrations analysed, the adsorption profile shows a very rapid uptake with equilibrium reached by the five second time point for all concentrations.

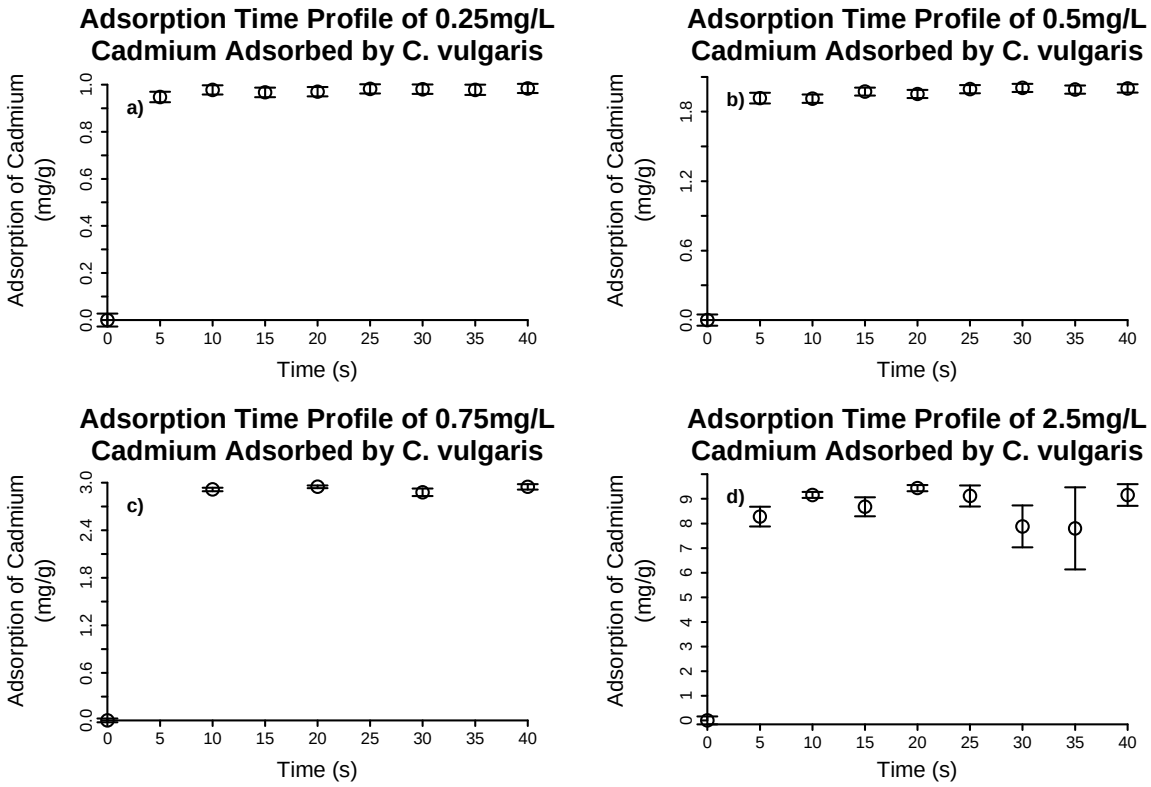

Figure 36: Cadmium uptake data by *C. vulgaris*. Top left to bottom right, *C. vulgaris* concentration 250mg/L, 250mg/L, 250mg/L, 250mg/L.

Figure 36 shows the adsorption time profile of the adsorption of cadmium by *C. vulgaris*. For all concentrations analysed, the adsorption profile shows a very rapid uptake with equilibrium again reached by the five second time point for all concentrations. Figure 36*c* has fewer datapoints compared to the other charts in Figure 36. The reason for this was that the batch of syringe filters used in this experiment became blocked, which reduced the number of samples able to be collected.

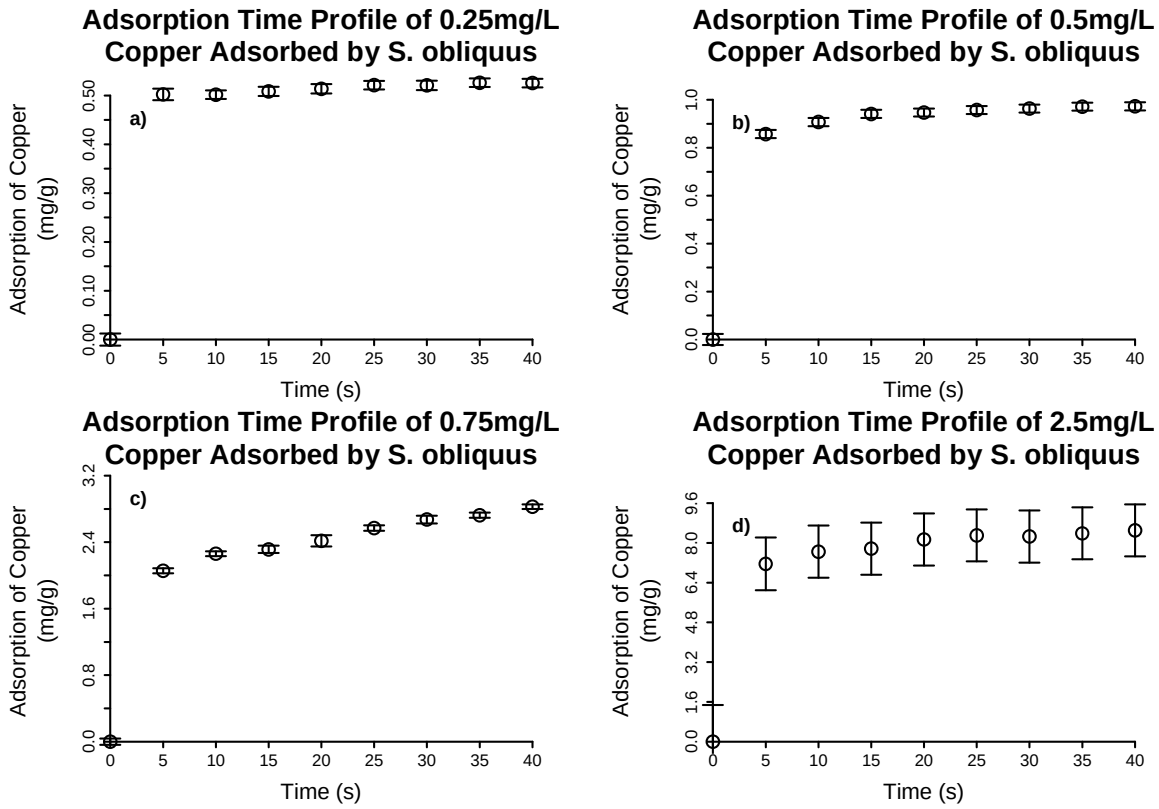

Figure 37: Copper uptake data by *S. obliquus*. Top left to bottom right, *S. obliquus* concentration 460mg/L, 460mg/L, 190mg/L, 240mg/L.

Figure 37 shows the copper uptake by *S. obliquus* at varying copper and algae concentrations. The adsorption, time profiles displayed in Figure 37 show a more gradual kinetic profile for the copper removal from solution compared to the removal of copper by *C. vulgaris* as displayed in Figure 35. Figure 37a showing the uptake of 0.25mg.L^{-1} copper ions by 460mg.L^{-1} *S. obliquus* reaches equilibrium by the 5s timepoint. With the increase in copper ion concentration, the time taken for adsorption equilibrium to be achieved increases.

Table 21: Copper and *S. obliquus* concentration, and the time for the biosorption to reach equilibrium.

Copper Concentration (mg.L^{-1})	***S. obliquus* Concentration (mg.L^{-1})**	**Time to reach Equilibrium (s)**
0.25	460	<5
0.50	460	15
0.75	190	>40
2.5	240	20

The data presented in Table 21 suggests that the as the ratio of the concentration of copper ions to the concentration of the *S. obliquus* biomass increases, the time taken for the system to reach equilibrium increases. The greatest time taken to

reach equilibrium appears to be shown in Figure 37*c*; equilibrium does not appear to have been met during the experimental period.

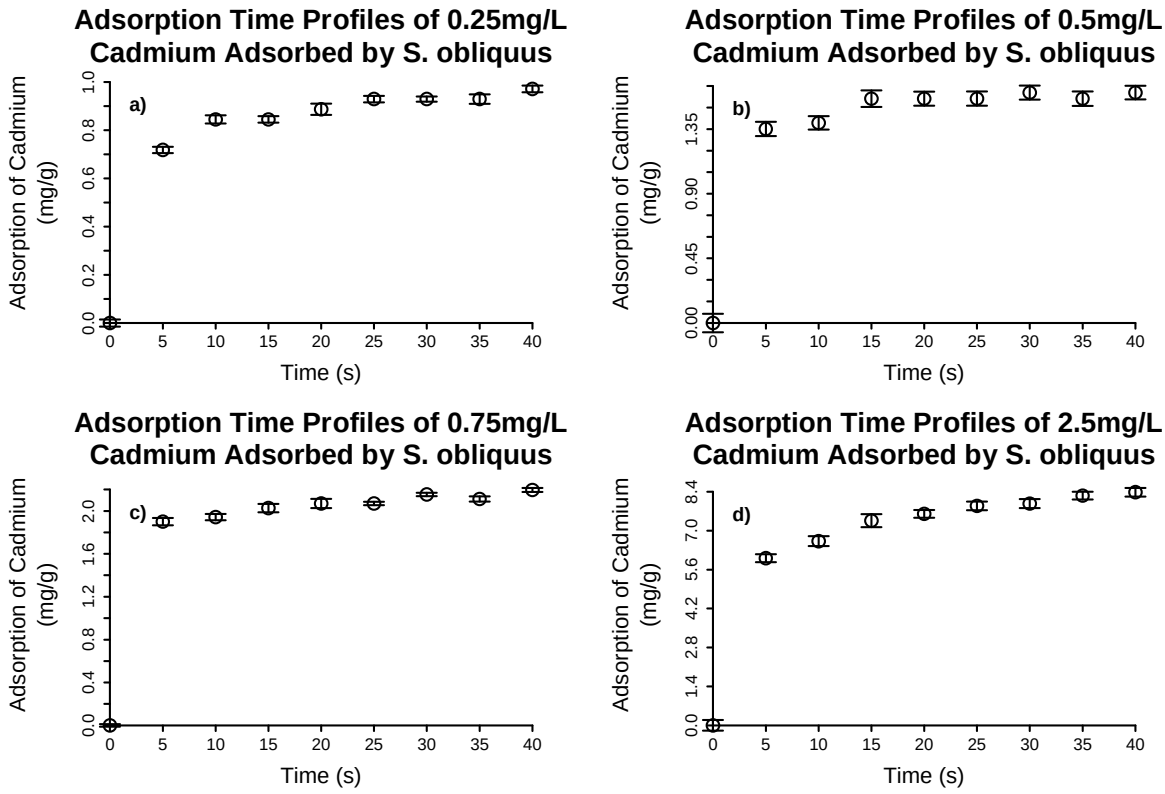

Figure 38: Cadmium uptake data by *S. obliquus*. Charts a) to C) *S. obliquus* concentration 240mg.L^{-1}, chart d) *S. obliquus* concentration 245mg.L^{-1}.

Figure 38 shows the cadmium uptake by *S. obliquus* at four different concentrations. In all cases, the time taken to reach equilibrium for the adsorption of cadmium appears to be greater than 5s. The data presented in Figure 35, Figure 36, Figure 37 and Figure 38 indicate that the copper and cadmium uptake by *C. vulgaris* is faster than that of *S. obliquus*.

As many of the experiments depicted in the charts above were conducted on different days, there was a high variation in the biomass concentrations utilised, ranging from 500mg.L^{-1} to as low as 190mg.L^{-1}. Table 22 compares each experiment's starting concentrations by taking the ratios of biomass to metal concentration at the beginning of the experiment.

Table 22: Comparison of initial experimental conditions, represented by the ratio of biomass concentration (mg.L^{-1}) to the initial concentration of the metal ions (mg.L^{-1}). Each figure represents the mg of algae per mg of metal at the beginning of each experiment.

Initial Metal Concentration (mg.L^{-1})	Copper *C. vulgaris*	Cadmium *C. vulgaris*	Copper *S. obliquus*	Cadmium *S. obliquus*	Mean	St Dev	Coefficient of variance (%)
0.25	2083	962	1772	718	1384	648	47
0.5	1111	479	954	447	748	335	45
0.75	667	325	246	308	386	190	49
2.5	89	97	102	94	95	5	6

The coefficient of variance in the starting conditions are between 45% and 49% for all experimental sets with the exception of the 2.5mg.L^{-1} experiment. Here the difference is 6%, so the initial parameters are more comparable for the experiments analysing the 2.5mg.L^{-1} metal solutions when compared to the other analyses.

The data for each experiment (2.5mgL^{-1} copper adsorbed by *C. vulgaris*, 2.5mgL^{-1} cadmium adsorbed by *C. vulgaris*, 2.5mgL^{-1} copper adsorbed by *S. obliquus* and 2.5mgL^{-1} cadmium adsorbed by *S. obliquus*), were transformed to fit Equation 2, as shown in Figure 39.

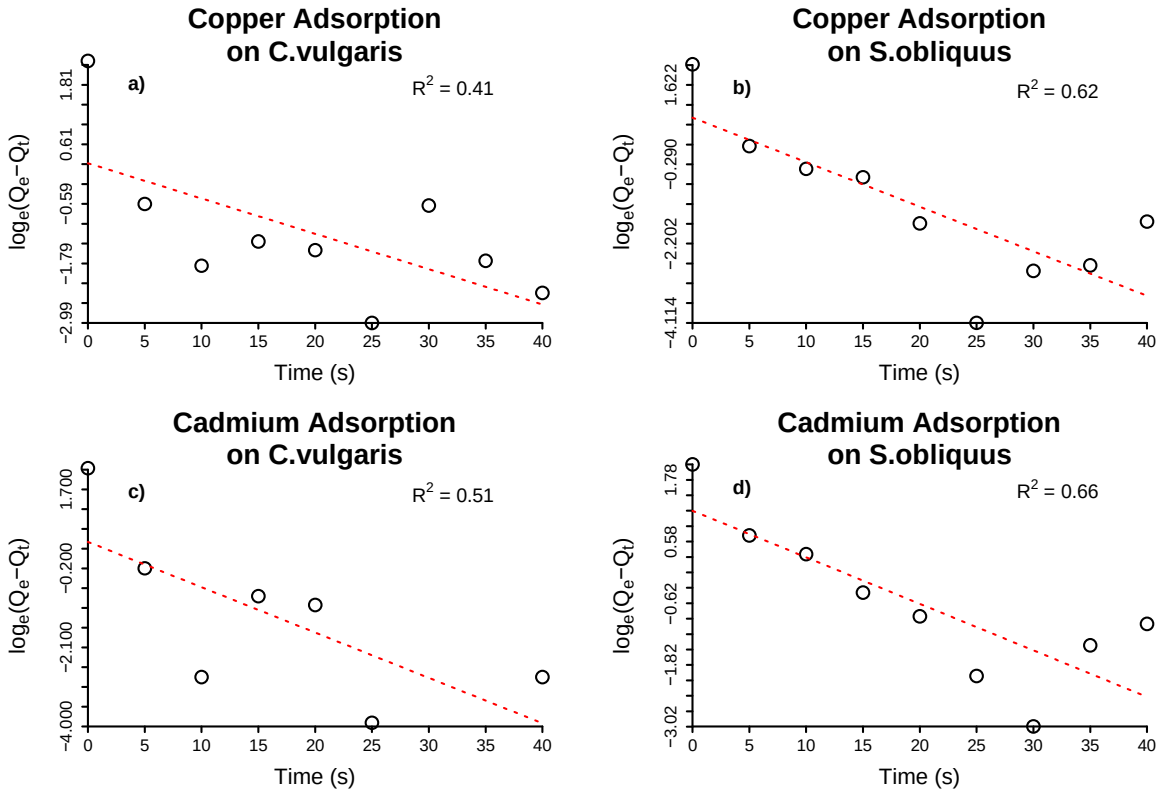

Figure 39: Linearised Lagergren models to derive the initial estimates for the rate constants (k_{t0}) and adsorption at equilibrium (Q_{e0}) for the 2.5mgL^{-1} copper and cadmium uptake experiments by *C. vulgaris* and *S. obliquus*, single metal analysis.

In all four experiments, the data presented in Figure 39 does not show a good linear correlation. This has been observed in previous studies that show mixed results when it comes to the R^2 values for the Lagergren model [17], and Ho & McKay suggesting that the Lagergren model is only appropriate for the initial stages of the process, which they concluded as being the first twenty to thirty minutes. The authors do not elaborate on this, but this is the time period before equilibrium is met [124]. This suggests that the model may not be valid for the experimental data as equilibrium is met very quickly.

The initial values for Q_e obtained by linearising the data for the 2.5mg.L^{-1} of copper and cadmium adsorbed by *C. vulgaris* and *S. obliquus* are displayed in Table 23. To obtain these values, the adsorption at equilibrium was estimated from experimental data displayed in graph *d* in Figure 35 to Figure 38. These values were estimated to be 10 mg.g^{-1} for copper adsorbed by *C. vulgaris*, 8 mg.g^{-1} for copper adsorbed by *S. obliquus*, 9 mg.g^{-1} for cadmium adsorbed by *C. vulgaris* and 8 mg.g^{-1} for cadmium adsorbed by *S. obliquus*.

Table 23: First order parameters (adsorption at equilibrium, Q_{e0} and first order rate constant, k_{t0}), derived by linearising the Lagergren model. Displayed are initial estimates for the adsorption at equilibrium and first order rate constants for the adsorption of copper and cadmium from single metal solutions with a concentration of 2.5mg.L^{-1}.

	Chlorella vulgaris			Scenedesmus obliquus		
Metal	**Qe_0 (mg.g-1)**	**kt_0 (s^{-1})**	**R^2**	**Qe_0 ($mg.g^{-1}$)**	**kt_0 (s^{-1})**	**R^2**
Copper	1.26	0.07	0.41	2.3	0.11	0.62
Cadmium	1.55	0.11	0.51	3.25	0.09	0.66

The values for the adsorption at equilibrium are lower than those estimated from Figure 35d (9.9mg.g^{-1}), Figure 36d (8.3mg.g^{-1}), Figure 37d (9.1mg.g^{-1}) and Figure 38d (8.0mg.g^{-1}). Although it has been previously stated that studies have found the Lagergren models showed poor linear correlation; Tüzün *et al* used the Lagergren model and found the correlation coefficient for cadmium adsorbed by *Chlamydomonas reinhardtii* to be 0.95 [16]. However if the intercept of $ln(Q_e - Q_t)$ vs *t* was not equal to $ln(Q_e)$, but the R^2 is above 0.9; this indicates that the process may not follow a first order mechanism [127].

Ho et al [124-127] fitted their values for the first order rate constant and adsorption at equilibrium to their experimental data but found that this was only applicable to

the data obtained at the beginning of the adsorption process prior to equilibrium being achieved. *Chen et al* [17] discounted the Lagergren model for the adsorption of cadmium by *S. obliquus*, as the model showed poor linear correlation and values that they obtained for Q_e from this model did not reflect their measured values.

The values obtained for Q_{e0} and k_{t0} in this study (Table 23), were fitted to their corresponding experimental data, as shown in Figure 35 to Figure 38. The fitted values for Q_e and k_t are displayed for each metal and their corresponding microalgae in Table 24:

Table 24: Fitted values for adsorption at equilibrium (Q_e) and first order rate constants (k_t) for the Lagergren model, describing the adsorption of 2.5mg.L^{-1} of copper and cadmium from single metal solutions, by *C. vulgaris* and *S. obliquus*.

	Chlorella vulgaris		***Scenedesmus obliquus***	
Metal	**Q_e (mg.g^{-1})**	**k_t (s^{-1})**	**Q_e (mg.g^{-1})**	**k_t (s^{-1})**
Copper	9.89 (± 0.1)	0.59 (± 0.11)	8.19 (± 0.10)	0.39 (± 0.05)
Cadmium	8.75 (± 0.24)	0.61 (± 0.31)	7.93 (± 0.17)	0.24 (± 0.03)

The Q_e values displayed in Table 24 are more representative of the data displayed in Figure 35 to Figure 38, compared to the Q_{e0} values displayed in Table 23. These values represent the adsorption at equilibrium. The values of Q_e in Table 24 are close to those that were estimated for linearizing the data in accordance to Equation 2. The first order rate constants (k_{t0} in Table 23 and k_t in Table 24) also differ considerably in all experiments. As the R^2 values for the linear Lagergran plots are all low (≤0.66), and as the recorded values for $ln(Q_e)$ do not reflect the intercept of the plot of $ln(Q_e - Q_t)$, previous studies would conclude that the experimental data does not fit the Lagergran model [127]. This is a contentious conclusion as more accurate values for Q_e and k_t (as displayed in Table 24), were obtained by fitting the model using non-linear regression.

To demonstrate this, the model parameters (k_{t0} and Q_{e0}) from Table 23 were inserted into equation 1.1 and the model parameters (k and Q_e) from Table 24 were inserted into equation 1 and plotted alongside their corresponding experimental data in Figure 40.

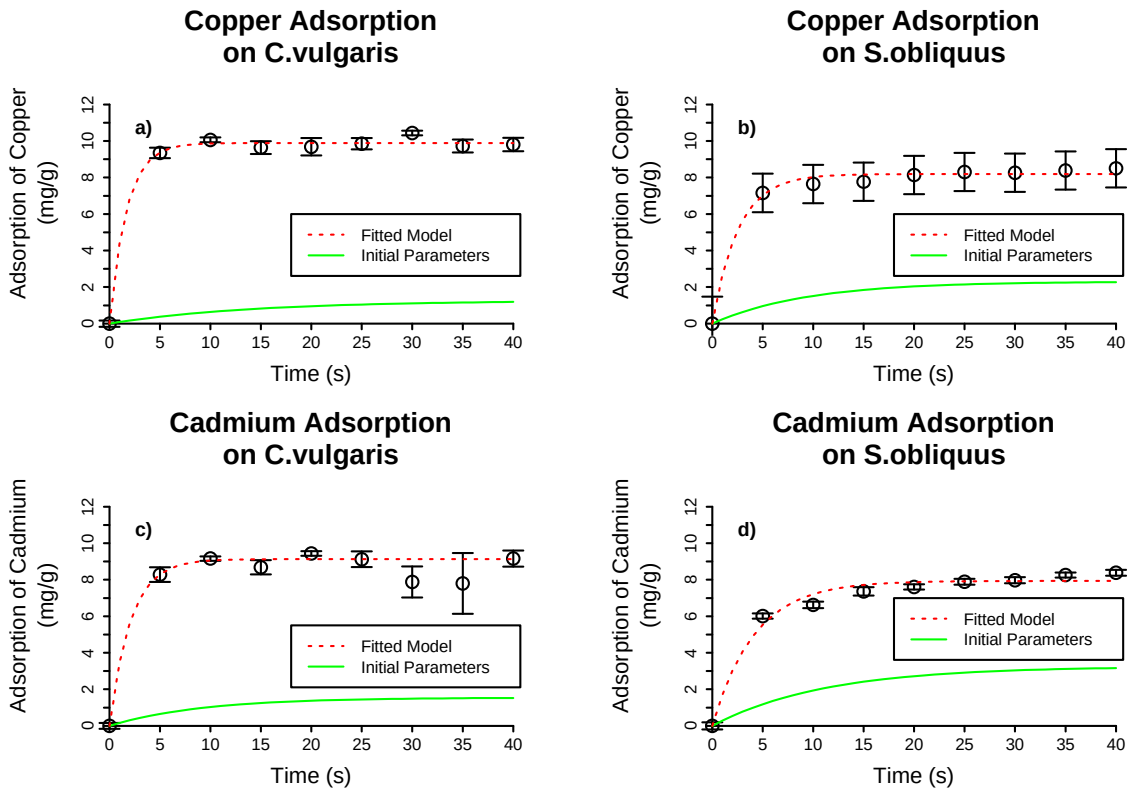

Figure 40: Adsorption-time profiles for copper and cadmium on *C. vulgaris* and *S. obliquus* (open circles) vs Lagergren predictions using parameters obtained from linearized data (solid green line), and Lagergren predictions using model parameters obtained by fitting the Lagergren model using non-linear least squares (red dotted line).

Figure 40 shows that the Lagergren model does appear to represent the experimental data when Q_e and k_t are obtained by fitting Equation 1 directly to the experimental data using a non-linear least squares algorithm. The model produced by linearizing the data using Equation 2 does not represent the experimental data in any of the experiments conducted. This, along with the low R^2 values shown in Table 23 suggest that although the Lagergren model as shown in Equation 1 is of a form that can represent the experimental data. Obtaining the values for the rate constant and the adsorption at equilibrium by linearising the model will not produce parameters that reflect the adsorption process.

To determine how well the Lagergren model fitted by non-linear least squares represents the experimental data, the root-mean square error and the Nash-Sutcliffe Efficiency (NSE) coefficient was calculated for how the predictions by this Lagergren model (Equation 1 with parameters from Table 24) represent the experimental data. These values are displayed in Table 25, along with the R^2 values for the linearized data (Figure 38).

Table 25: R^2 values for the linearized Lagergren model, and the RMSE and NSE values to determine the accuracy of the Lagergren model derived by fitting it directly to experimental data.

	Copper on Chlorella vulgaris	Copper on Scenedesmus obliquus	Cadmium on Chlorella vulgaris	Cadmium on Scenedesmus obliquus
Linear R^2	0.41	0.62	0.51	0.66
Root Mean Square Error (RMSE)	0.23	0.23	0.38	0.35
Coefficient of efficiency (NSE)	0.91	0.88	0.81	0.71

An R^2 value close to 1 indicates a good linear fit, and a low RMSE value represents a good non-linear fit. However a low RMSE is dependent on the data. RMSE values can range from 0 to infinity and can be skewed by the presence of outliers [52]. Similar to R^2, the NSE values range between 0 and 1, and NSE values greater than 0.65 are said to be acceptable; greater than 0.8 are said to be "good" and greater than 0.9 are said to be "very good" fits [52].

Overall, the R^2 values in Table 25 show that the fit to the Lagergren model is mainly unsatisfactory: only the data for copper adsorbed by *C. vulgaris exhibits* an NSE value above 0.9. Copper adsorbed by *S. obliquus* and cadmium adsorbed by *C. vulgaris* have NSE values that indicate a good fit, and the NSE value of 0.71 for cadmium adsorbed by *S. obliquus* indicates that the model has only an "acceptable" fit to the experimental data.

6.1.2 Second Order Model

The second order model is an adaptation of the Lagergren model that has been largely attributed to Ho & McKay [129-132], although Tüzün et al attributes the earliest derivation to Ritchie in 1977 [16, 133]. Unlike the Lagergran model, the second model has been found to reflect adsorption kinetic data accurately even after equilibrium has been reached [124-127]. This model has the non-linear form:

$$Q_t = \frac{Q_e^2 k_t . t}{1 + Q_e k_t . t} \tag{3}$$

Where:

- Q_t is the adsorption at time t, as before (mg.g^{-1}).

- Q_e is the adsorption at equilibrium, as before (mg.g^{-1}).
- k_t is the second order rate constant (g.mg^{-1}.s^{-1}).
- t is the time elapsed (s).

To obtain Q_e and k_t equation 3 can be rearranged to the linear form:

$$\frac{1}{Q_t} = \frac{1}{Q_e^2 k_t} \cdot \frac{1}{t} + \frac{1}{Q_e} \qquad (4)$$

The reciprocal of the adsorption at each time-point can then be plotted against the reciprocal of the elapsed time. Q_e can be calculated by finding the reciprocal of the y-axis intercept, and k_t can be found by dividing the square of the y-axis intercept by the gradient.

The linearized data for each metal, adsorbed by each species of microalgae as before and the charts are displayed in Figure 41:

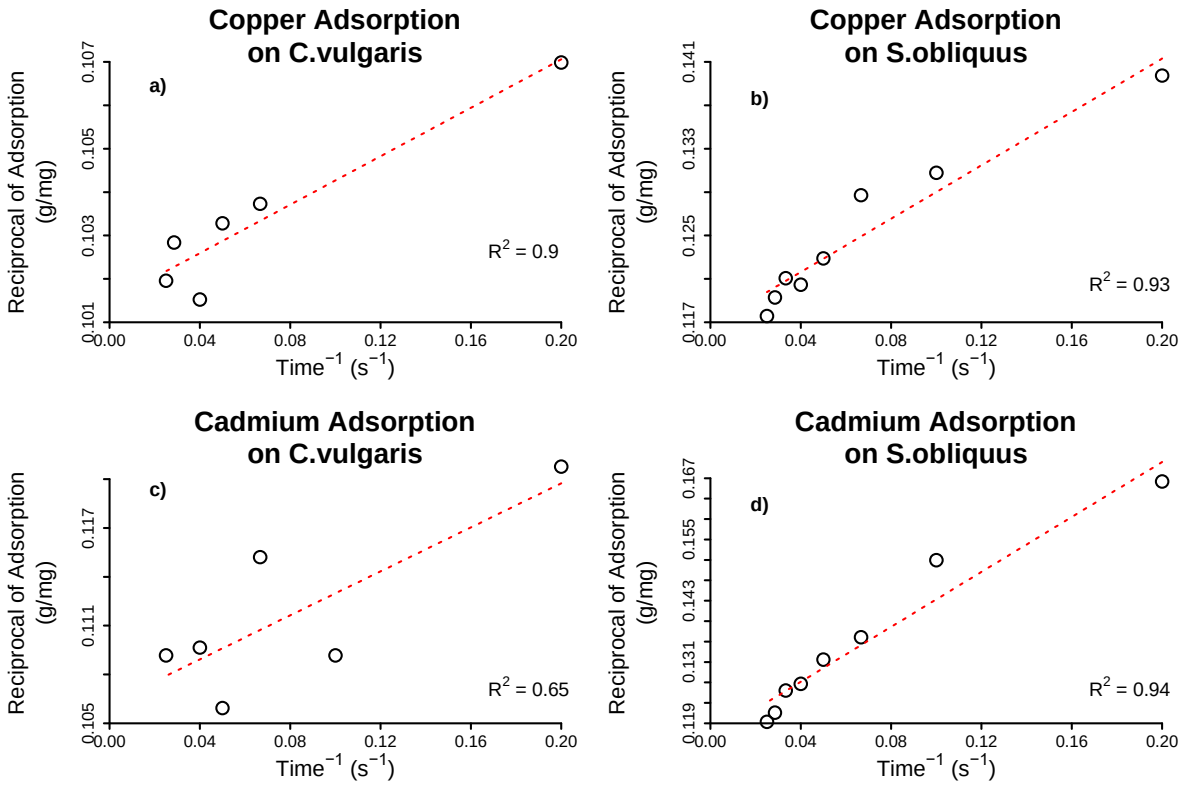

Figure 41: Linearised Second Order models to derive the initial estimates for the rate constants (k_{t0}) and adsorption at equilibrium (Q_{e0}) for the 2.5mgL^{-1} copper and cadmium uptake experiments by *C. vulgaris* and *S. obliquus*, single metal analysis.

All the data in Figure 41 show higher correlation than their counterparts for the Lagergren model (Figure 39), with only the cadmium adsorption by *C. vulgaris*

(Figure 41c) showing poor correlation. The improvement in correlation coefficients for the second order linear plots compared to the plots of the linear Lagergren plots (Figure 39) was also observed by Tüzün et al [16], who studied the adsorption of mercury, cadmium and lead by the microalgae, *Chlamydomonas reinhardtii*.

The initial model parameters and the correlation coefficients for the linear charts used to derive them are displayed in Table 26 below. The adsorption at equilibrium Q_{e0}, having the same units; should be equivalent to their Lagergren counterparts.

Table 26: Second order parameters (adsorption at equilibrium Q_{e0}, and second order rate constants k_t), derived by linearising the second order model. Displayed are initial estimates for the adsorption at equilibrium and first order rate constants for the adsorption of copper and cadmium from single metal solutions with a concentration of 2.5mg.L^{-1}.

	Chlorella vulgaris			Scenedesmus obliquus		
Metal	Qe_0 (mg.g^{-1})	k_{t0} (g.mg^{-1}.s^{-1})	R^2	Qe_0 (mg.g^{-1})	k_{t0} (g.mg^{-1}.s^{-1})	R^2
Copper	9.85	0.37	0.90	8.57	0.11	0.93
Cadmium	9.41	0.17	0.65	8.59	0.05	0.94

Together with the improved R^2 values in Table 26, the values obtained for Q_{e0} have a significant improvement compared to their counterparts in Table 23. The Q_{e0} values in Table 26 and those present in Table 24 are compared in Table 27.

Table 27: Comparison of values for adsorption at equilibrium for each experiment when derived by linearizing the second order model, and the values of the adsorption at equilibrium obtained by fitting the Lagergren model to the experimental data by non-linear regression. Q_{e0} refer to the values obtained by linearizing the second order model, Q_e refer to the values obtained by fitting the Lagergren model to the experimental data.

Metal	Chlorella vulgaris		Scenedesmus obliquus	
	Q_{e0} (mg.g-1)	Q_e (mg.g-1)	Q_{e0} (mg.g-1)	Q_e (mg.g-1)
Copper	9.85	9.89 (±0.10)	8.57	8.19 (±0.10)
Cadmium	9.41	8.75 (±0.24)	8.59	7.93 (±0.17)

The values for Q_{e0} are not within the standared error for the Q_e values error for all but the Q_{e0} value obtained for the adsorption of copper by *C. vulgaris*, so the Q_{e0} and k_0 values displayed in Table 26 were fitted to equation 3 by non-linear least squares, with the fitted values for the second order Q_e and k_t displayed in Table 28.

Table 28: Fitted values for adsorption at equilibrium and second order rate constants for the Second Order Model, describing adsorption of 2.5mg.L^{-1} copper and 2.5mg.L^{-1} cadmium adsorbed by *C. vulgaris* and *S. obliquus* from single metal solutions.

	Chlorella vulgaris		Scenedesmus obliquus	
Metal	Q_e (mg.g^{-1})	k_t (g.mg^{-1}.s^{-1})	Q_e (mg.g^{-1})	k_t (g.mg^{-1}.s^{-1})
Copper	10.02 (± 0.16)	0.33 (± 0.21)	8.6 (± 0.08)	0.11 (± 0.01)
Cadmium	9.12 (± 0.12)	0.17 (± 0.07)	8.72 (± 0.14)	0.04 (± 0.01)

The parameters in Table 28 are within experimental error of the values displayed in Table 26, however they are not within the range of their corresponding Lagergren Q_e values for *S. obliquus* as displayed in Table 24. This may indicate that the adsorption process for the *S. obliquus* has not yet reached equilibrium, and the second order model reflects this, while the Lagergren model assumes equilibrium has already been reached (Figure 40b and d). The values of Q_e obtained by the Lagergran model fitted by non-linear regression, and the values obtained by the second order model fitted by non-linear regression are displayed in Table 29.

Table 29: Comparison between the adsorption at equilibrium values obtained by fitting the Lagergran model to the experimental data by non-linear regression (Qe_L), and the adsorption at equilibrium values obtained by fitting the second order model to the same experimental data by non-linear regression (Qe_s).

	Chlorella vulgaris		Scenedesmus obliquus	
Metal	Qe_L (mg.g-1)	Qe_s (mg.g-1)	Qe_L (mg.g-1)	Qe_s (mg.g-1)
Copper	9.89 (±0.1)	10.02 (± 0.16)	8.19 (± 0.10)	8.6 (± 0.08)
Cadmium	8.74 (± 0.24)	9.12 (± 0.12)	7.93 (±0.17)	8.72 (± 0.14)

As with the Lagergren model, the Q_{e0} and the k_{t0} values from Table 26 and the Q_e and k_t values were used in equation 3, and the resultant models were plotted alongside their corresponding experimental data and displayed in Figure 42.

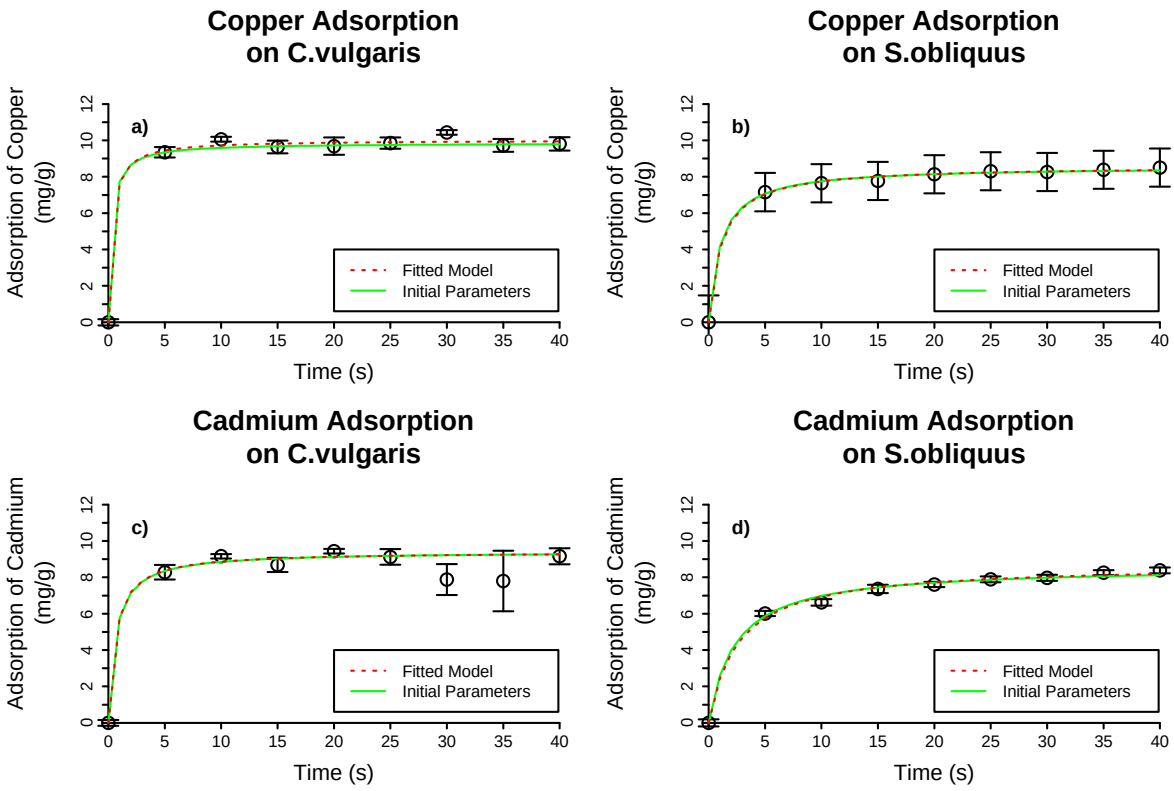

Figure 42: Adsorption-time profiles for copper and cadmium on *C. vulgaris* and *S. obliquus* (open circles) vs second-order predictions using parameters obtained from linearized data (solid green line), and second-order predictions using model parameters obtained by fitting the Lagergren model using non-linear least squares (red dotted line).

Examining the second order models as displayed in Figure 42, it is difficult to distinguish between the models created using the parameters obtained by linearizing the second-order model (Qe_0 and k_{t0} from Table 26), and the model created using the parameters obtained by fitting the second order model to the experimental data (Q_e and k_t from Table 28). The values of the parameters (Q_{e0} and k_0) are within the margin of error depicted by the standard error of the parameters obtained by fitting the second order model to the data. For clarity, these are displayed in Table 30.

Table 30: The comparison between second-order parameters obtained by linearizing the second-order model, and the parameters obtained by fitting the second order model directly to the experimental data. The subscript *0* represents the parameters that were obtained from linearizing the model, the parameters without a subscript were obtained by fitting the second order model to the data.

Chlorella vulgaris				
Metal	**Qe_0 ($mg.g^{-1}$)**	**Qe ($mg.g^{-1}$)**	**k_{t0} ($g.mg^{-1}.s^{-1}$)**	**k_t ($g.mg^{-1}.s^{-1}$)**
Copper	9.85	10.02 (± 0.16)	0.37	0.33 (± 0.21)
Cadmium	9.41	9.41 (± 0.20)	0.17	0.17 (± 0.07)
Scenedesmus obliquus				
Metal	**Qe_0 ($mg.g^{-1}$)**	**Qe ($mg.g^{-1}$)**	**k_{t0} ($g.mg^{-1}.s^{-1}$)**	**k_t ($g.mg^{-1}.s^{-1}$)**
Copper	8.57	8.6 (± 0.08)	0.11	0.11 (± 0.01)
Cadmium	8.59	8.72 (± 0.14)	0.05	0.04 (± 0.01)

The R^2 values for the linear relationship between the reciprocal of the adsorption and the reciprocal were ≥ 0.9 for all charts except for cadmium adsorption by C. vulgaris (Figure 41c). All linear models produced second-order uptake rates and adsorption at equilibrium values that were representative of the experimental data as shown in Figure 42. Table 31 compares the R^2 values of the linear relationships, root mean square error of the non-linear models and the coefficient of efficiency for the non-linear models for the four experiments.

Table 31: R^2 values for the linearised second order models, and the RMSE and NSE values to determine accuracy of the non-linear second order model using parameters Q_{e0} and k_{t0} obtained by linearising the second order model (shown in Table 26).

	Copper on Chlorella vulgaris	**Copper on Scenedesmus obliquus**	**Cadmium on Chlorella vulgaris**	**Cadmium on Scenedesmus obliquus**
Linear R^2	0.90	0.93	0.65	0.94
Root Mean Square Error	0.24	0.11	0.22	0.16
Coefficient of efficiency	0.91	0.97	0.91	0.93

In all cases, as the models returned NSE values of greater than 0.9, the second order models can be said to have a good fit to the current experimental data [52]. The models also showed good fits in terms of the NSE values and the RMSE values. The poorer R^2 value for cadmium adsorption by the *C. vulgaris* did not prevent the derivation of accurate values for k_t and Q_e for the adsorption kinetics.

6.1.3 Elovich Model

The Elovich model has a different basis then the Lagergren and second-order models. It is not based on adsorption at equilibrium. Instead, the Elovich model assumes a solid surface that is energetically heterogeneous, and that there is no interaction between the species being adsorbed [134]. The algae surface contains a variety of functional groups which will satisfy the first assumption. The Elovich model has the non-linear form:

$$Q_t = \frac{1}{\beta} ln(\alpha\beta t + 1) \quad (5)$$

Where:

- Q_t is the adsorption at time t, as in the Lagergran Model and second order model (mg.g^{-1}).
- β is the desorption constant (mg.g^{-1}).
- α is the maximum adsorption rate (mg.g^{-1}.s^{-1}).
- t is the time elapsed (s).

Equation 5 was linearized by making the assumption that the value for the maximum adsorption rate multiplied by the desorption constant is greater than 1:

$$\alpha\beta t \gg 1$$

The adsorption rates for these experiments are high, so it can be assumed α is considerably larger than 1mg.g^{-1}s^{-1}, so for every time point other than 0s, this assumption is likely valid. This allows for equation 5 to be rearranged to the form:

$$Q_t = \frac{1}{\beta} ln(t) + \frac{1}{\beta} ln(\alpha\beta) \quad (6)$$

If this assumption cannot be made, then the exponential of product of β multiplied by the adsorption at time t can be plotted against t, with β being determined iteratively. However for this experiment, the desorption constant and maximum uptake rate were able to be determined by plotting the adsorption at time t against

the natural logarithm of the elapsed time. The desorption constant, β, is found by finding the reciprocal of the gradient; and the maximum adsorption rate is found by:

$$\alpha = \frac{e^{c.\beta}}{\beta}$$

Where *c* is the y-axis intercept. The linear plots are displayed in Figure 43.

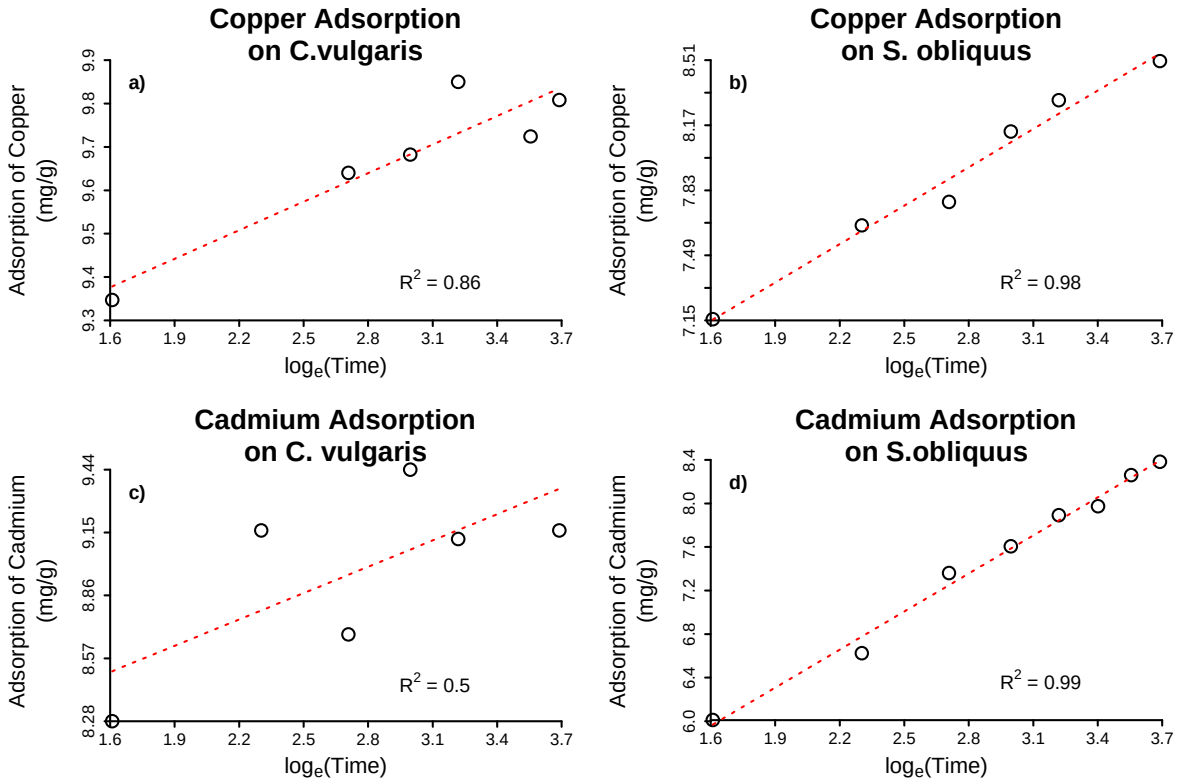

Figure 43: Linearised Elovich models to derive the initial estimates for the desorption constants (β_0) and the maximum adsorption rates (α_0) for the 2.5mgL^{-1} copper and cadmium uptake experiments by *C. vulgaris* and *S. obliquus*, single metal analysis.

Figure 43 (*b)* and (*d)* exhibit a strong correlation between Q_e and *ln(t)* for the uptake of both metals by *S. obliquus*. They have a better correlation than the linear second order fits shown in Figure 41 *b* and *d* (0.98, compared with 0.93 and 0.99 compared with 0.94 for the copper data and the cadmium data respectively). The R^2 values for the *C. vulgaris* experiments (Figure 43 *a* and *c*), are not only lower than the R^2 values for the linear Elovich models for *S. obliquus*, they are lower than the R^2 values for second-order linear models shown in Figure 41 *a* and *c*. Previous studies for adsorption of metals modelled using the Elovich model had correlation coefficients no lower than 0.996, although the adsorbent was a macroporous resin [182].

The values for the maximum adsorption rate, α, and the desorption constant, β, are shown in Figure 43. The derivation of α and β is highly sensitive to experimental outliers, with the data for cadmium adsorbed by *C. vulgaris* not able to produce suitable parameters without the removal of the seventh and eighth datapoint. The correlation between the Q_e and *ln(t)* of the remaining data has an R^2 value of 0.5, up from less than 0.01 and sufficient for the derivation of model parameters.

The values for α and β obtained by linearising the Elovich model are displayed in Table 32.

Table 32: Elovich model parameters (maximum adsorption rate, α, and desorption constant, β), derived by linearizing the Elovich Model. Model parameter estimates for 2.5mg.L^{-1} copper and 2.5mg.L^{-1} cadmium adsorbed by *C. vulgaris* and *S. obliquus* from single metal solutions.

	Chlorella vulgaris			***Scenedesmus obliquus***		
	Maximum adsorption rate, α_0 (mg.g^{-1}.s^{-1})	**Desorption constant, β_0 (mg.g^{-1})**	**R^2**	**Maximum adsorption rate, α_0 (mg.g^{-1}.s^{-1})**	**Desorption constant, β_0 (mg.g^{-1})**	**R^2**
Copper	1.59×10^{17}	4.56	0.86	5.92×10^{3}	1.50	0.98
Cadmium	1.10×10^{8}	2.47	0.50	39.15	0.86	0.99

The Maximum Adsorption rate, α, is a constant that indicates the maximum initial adsorption rate. The desorption constant, β, determines the propensity for desorption. If $\alpha >> \beta$ it is indicative that the process has a higher propensity to adsorption [183] and therefore indicates that the adsorption process is fast. The Elovich parameter β is interpreted to be related to the activation energy for chemisorption and is indicative of the total surface coverage of the adsorbate, and with a higher value of β leading to the greater driving force for desorption [132]. As with the Lagergran model, and the second order model, the Elovich model was also fitted to the experimental data using non-linear regression.

The parameters displayed in Table 32 were inserted into the Elovich model (Equation 5) and plotted along with their corresponding experimental data, as shown in Figure 44.

Table 33: Elovich model parameters (maximum adsorption rate, α, and desorption constant, β), derived by fitting the Elovich Model directly to experimental data using non-linear least squares. Model parameter estimates for 2.5mg.L^{-1} copper and 2.5mg.L^{-1} cadmium adsorbed by *C. vulgaris* and *S. obliquus* from single metal solutions.

	Chlorella vulgaris			*Scenedesmus obliquus*		
	Maximum adsorption rate, α (mg.g^{-1}.s^{-1})	**Desorption constant, β (mg.g^{-1})**	**R^2**	**Maximum adsorption rate, α (mg.g^{-1}.s^{-1})**	**Desorption constant, β (mg.g^{-1})**	**R^2**
Copper	1.35×10^{18} ($\pm4.4\times10^{19}$)	4.71 (± 0.03)	0.86	8.87×10^{3} ($\pm5.83\times10^{3}$)	1.55 (± 0.09)	0.98
Cadmium	6.87×10^{7} (± 7.28×10^{8}	2.41 (± 1.24)	0.50	38.55 (± 8.17)	0.86 (± 0.03)	0.99

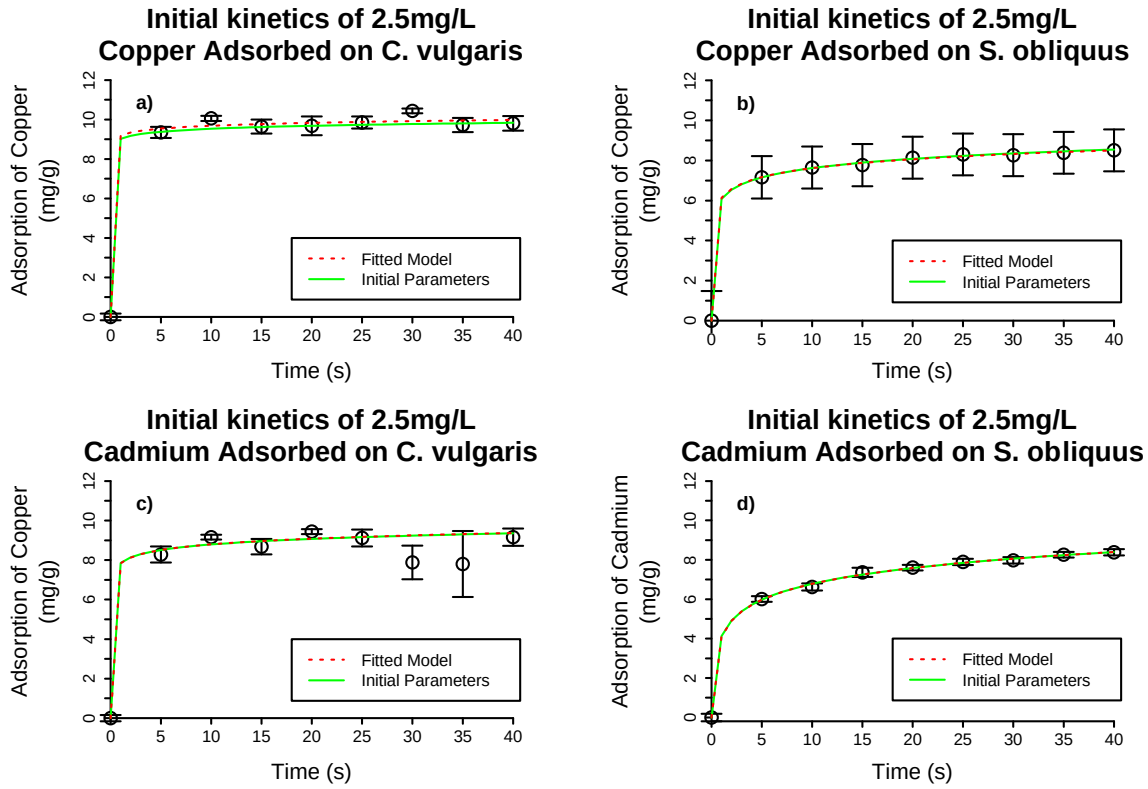

Figure 44: Adsorption-time profiles for copper and cadmium on *C. vulgaris* and *S. obliquus* (open circles) vs Elovich model predictions using parameters obtained from linearized data (red dashed line).

Despite the linear model of Q_e vs *ln(t)* having an R^2 value of 0.5 for cadmium adsorbed by *C. vulgaris*, the values obtained for the maximum adsorption rate (1.10×10^{8} mg.g.s^{-1}), and the value for the desorption constant (2.47mg.g^{-1}) do appear to follow the experimental data. However, in Figure 44a,b,c the Elovich model predicts kinetics between 0 and 5s that are not reflective within the experimental data. The linear models presented for the linear models (Q_e vs *ln(t)*) had an R^2 value of 0.86, 0.98 and 0.99 for copper adsorbed by *C. vulgaris*, copper adsorbed by *S. obliquus* and cadmium adsorbed by *S. obliquus* respectively. Of these

models, only the cadmium adsorption by *S. obliquus* does not show a trend that is not representative of the data (Figure 44d).

The model parameters were also further fitted using non-linear regression, but the models produced from fitting the data to Equation 6 (represented by the solid green line in Figure 44) were near identical to the fitted models (represented by the red dashed line). This is consistent with previous studies that have stated that the Elovich kinetics are able to model adsorption kinetics more accurately than the Lagergren model [181]. However others have found that the model falls short when compared to the second order model when measuring metal uptake [124]. A main assumption of the Elovich model is that the binding surface is energetically heterogeneous, which reflects the surface of the microalgae and the variety of functional groups present on the cell's surface [184].

The analysis of the fits of each model were determined by analysing the R^2 value for the linear plots (Figure 43), and the RMSE and NSE values for predictions of the Elovich models compared to their corresponding experimental data. These values are displayed in Table 34.

Table 34: R^2 values for the linearized Elovich models, and the RMSE and NSE values to determine accuracy of the non-linear Elovich model using parameters (α and β) obtained from the linear model.

	Copper on Chlorella vulgaris	Copper on Scenedesmus obliquus	Cadmium on Chlorella vulgaris	Cadmium on Scenedesmus obliquus
Linear R^2	0.86	0.98	0.50	0.99
Root Mean Square Error	0.29	0.06	0.25	0.07
Coefficient of efficiency	0.87	0.99	0.91	0.99

In the case of the Elovich model, the RMSE, NSE and the R^2 values for the *S. obliquus* experiments are very low compared to those displayed in Table 25 and Table 31 which indicates that the Elovich model has the best fit of all the models tested. However when visually analysing Figure 44, only the adsorption of cadmium by *S. obliquus* (Figure 44b) shows the model predictions that flow the datapoints without a major inflection between 0s and 5s. The Elovich models produced for the *C. vulgaris* experiments were not as successful. The R^2 value for cadmium adsorbed by *C. vulgaris* was found to be 0.5 which shows a poor linear fit and the NSE value for

the copper adsorption on *C. vulgaris* was found to be 0.87 indicating it only had a "good" fit. NSE values greater than 0.9 for all other adsorption profiles suggest that the Elovich models fit very well, but in Figure 44b and c for copper adsorption by *S. obliquus* and cadmium adsorption by *C. vulgaris* respectively, there are kinetics reflected by the Elovich models between 0s and 5s that have no relation to the experimental data.

6.1.4 The Langmuir Model

The Langmuir model is a hybrid order model containing both a first order term and second order term. It states that the rate of change of adsorption is equal to the sum of the first order expression and the second order expression (Equation 7).

$$\frac{dQ_t}{dt} = k_1(Q_e - Q_t) + k_2'(Q_e - Q_t)^2 \quad (7)$$

Where:

- Q_t is the adsorption at time, t ($mg.g^{-1}$).
- Q_e is the adsorption at equilibrium ($mg.g^{-1}$).
- k_1 is the first order rate constant (s^{-1}).
- k_2' is the second order rate constant ($g.mg^{-1}.s^{-1}$).

Langmuir kinetics can be assumed to follow the first order model if $k_1 >> k_2(Q_e - Q_t)$. To test whether this condition is satisfied, define a term Q_t^* which is the adsorption at time, t^* which represents any time point during the adsorption process.

$$Q_t^* = Q_e - \frac{k_1}{k_2}$$

For the assumption of the first order kinetics to be valid, $Q_t >> Q_t^*$, which will be achieved if either:

$$Q_e \ll \frac{k_1}{k_2}$$

This would make the assumption valid over the entire adsorption process, or if

$$Q_e \approx \frac{k_1}{k_2}$$

This would make the assumption valid for all but the initial time period. If either of these conditions are met, then Equation 7 can be approximated as Equation 7.1.

$$\frac{dQ_t}{dt} \approx k_1(Q_e - Q_t) \tag{7.1}$$

Similarly, Langmuir kinetics can be assumed to follow second order kinetics if $k_1 << k_2(Q_e - Q_t)$ and this assumption is met when:

$$Q_e \gg \frac{k_1}{k_2}$$

This would imply that $Q_e \approx Q_t^*$ and the assumption of second order kinetics is valid over the entire time period. Equation 7 can be approximated to Equation 7.2.

$$\frac{dQ_t}{dt} \approx k_2'(Q_e - Q_t)^2 \tag{7.2}$$

If the conditions above are not met, and k_1 is not significantly larger or smaller than $k_2'(Q_e - Q_t)$ then the hybrid form of the Langmuir Equation is required (Equation 7).

To determine which model to use, Q_e, k_1 and k_2' need to be calculated. This is done by using Equation 8, 9 and 10.

$$Q_e = \frac{C_0 - C_e}{X_{Algae}} \tag{8}$$

$$k_1 = \sqrt{b_L{}^2\left(\frac{C_0}{Q_{max}} - X_{Algae}\right)^2 + 2b_L\left(\frac{C_0}{Q_{max}{}^2} + \frac{X_{Algae}}{Q_{max}}\right) + \frac{1}{Q_{max}{}^2}} \tag{9}$$

$$k_2' = \frac{b_L X_{Algae}}{Q_{max}} \tag{10}$$

Where:

- C_0 is the initial metal ion concentration (mg.L^{-1}).
- C_e is the metal ion concentration at equilibrium (mg.L^{-1}).

- X_{Algae} is the concentration of microalgae (g.L^{-1}).
- Q_{max} is the maximum adsorption capacity of the microalgae (mg.g^{-1}).
- b_L is the Langmuir Equilibrium constant (L.g^{-1}).

The parameters Q_{max} and b_L are calculated using the Langmuir Isotherm (Section 5.2.1). If Equation 7 cannot be approximated to either the first order approximation or the second order approximation, then the integrated form of Equation 7 should be fitted to the data. This is shown as Equation 7.3.

$$Q_t = Q_e\left(1 - \frac{k_1}{(k_1 + k_2' Q_e)e^{k_1 t} - k_2' Q_e}\right) \tag{7.3}$$

The Langmuir Equilibrium parameters, concentration of the *C. vulgaris*, *S. obliquus*, initial concentration of the copper and cadmium, equilibrium concentration of the copper and cadmium, Langmuir Equilibrium constant, maximum adsorption capacity and the ratio to k_1 to k_2' are displayed in Table 35.

Table 35: Langmuir model parameters for the 2.5mg.L^{-1} copper and cadmium uptake experiments. These values are required for the determination of whether to use the first order, second order or hybrid Langmuir model.

Algae	Metal	X_{Algae} (g.L^{-1})	C_0 (mg.L^{-1})	C_e (mg.L^{-1})	Q_{max} (mg.g^{-1})	b_L (L.g^{-1})	Q_e (mg.g^{-1})	k_1/k_2'
C. vulgaris	Cu^{2+}	0.24	2.68	0.33	-24.57	-0.66	9.86	38.64
C. vulgaris	Cd^{2+}	0.25	2.59	0.42	11.06	9.83	8.68	4.3
S. obliquus	Cu^{2+}	0.24	2.40	0.39	9.70	2.73	8.23	7.8
S. obliquus	Cd^{2+}	0.24	2.61	0.68	24.72	0.42	7.91	31.4

Examining the data present in Table 35, the Langmuir Kinetic model cannot be used for the data obtained for the copper adsorption by *C. vulgaris*, as the Langmuir Equilibrium parameters do not make physical sense; Q_{max} cannot be negative. The data obtained for the cadmium adsorption by the *C. vulgaris* returns a value for Q_e was calculated to be 8.68mg.g^{-1} which was twice the value calculated for k_1/k_2' which was calculated as 4.3. This implies that the adsorption of cadmium by *C. vulgaris* should be modelled by the hybrid kinetic model (Equation 7.3).

For both of the *S. obliquus* experiments the Langmuir kinetic model can be simplified to the first order model. The adsorption of copper by *S. obliquus* returned a $Q_e \approx k_1/k_2'$ (8.23 mg.g^{-1} and 7.8 respectively), and the cadmium adsorption returned a $Q_e < k_1/k_2'$ (7.91mg.g^{-1} and 31.4 respectively).

The hybrid Langmuir rate equation was applied to the experimental data for the cadmium adsorption by *C. vulgaris*, and the first order approximation of the Langmuir kinetic model was applied to the experimental data for the adsorption of both copper and cadmium by the *S. obliquus*. These models are displayed with experimental data as shown in Figure 45.

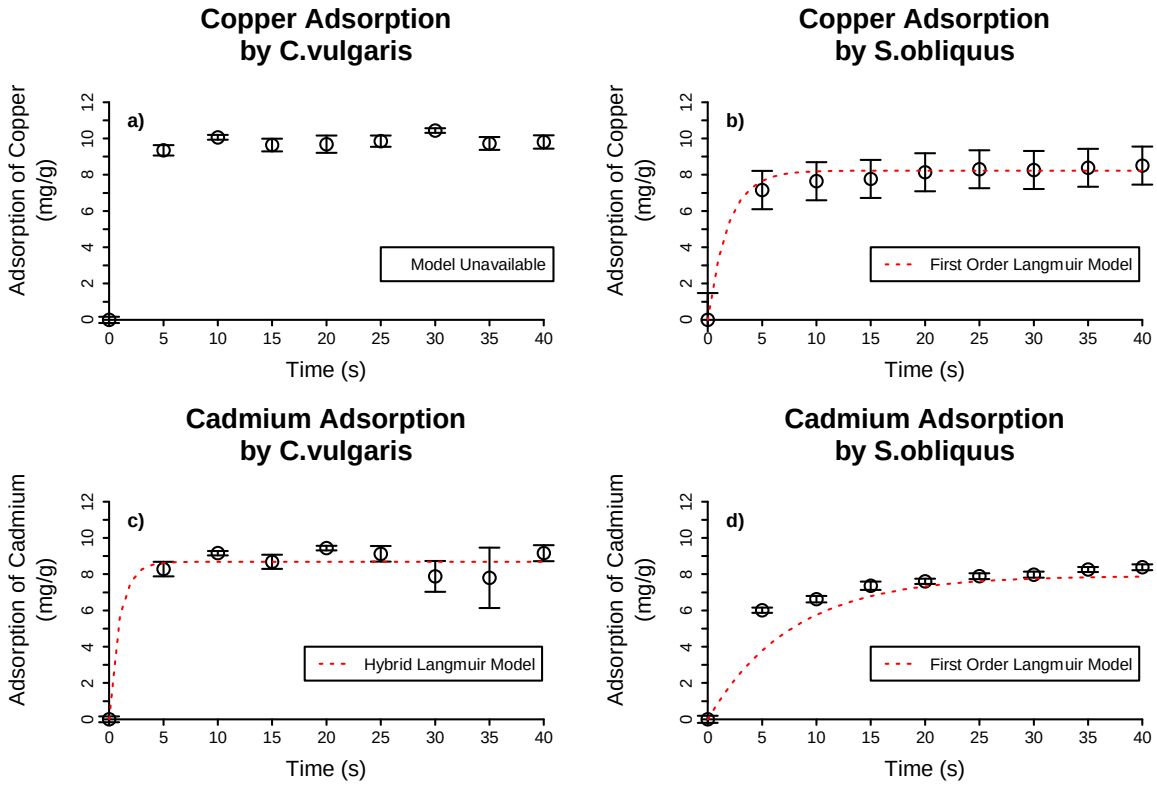

Figure 45: Adsorption-time profiles for copper and cadmium on *C. vulgaris* and *S. obliquus* (open circles) vs Langmuir model predictions using parameters obtained from the Langmuir Isotherm (red dashed line). b) and d) represent Langmuir models approximated as a first-order model, c) represents the hybrid form of the Langmuir model.

Figure 45 show the Langmuir models for copper and cadmium adsorbed by *S. obliquus* and cadmium adsorbed by *C. vulgaris*. All three models reach the equilibrium value, which was to be expected as the calculated value for the adsorption at equilibrium was used to derive Langmuir models. The first order Langmuir model (shown in Figure 45b) derived for the adsorption of copper by *S. obliquus* appears to follow the experimental data closely; as does the hybrid

Langmuir model (Figure 45c) derived for the adsorption of cadmium by *C. vulgaris*. The first order Langmuir model for the adsorption of cadmium by *S. obliquus* reaches equilibrium at a slower rate when compared to the experimental data.

The fit of each Langmuir model was determined by RMSE, NSE and Chi-Square test. These values are displayed in Table 36.

Table 36: RMSE, NSE and Non-linear Chi-Square test values calculated to determine the accuracy of the first-order Langmuir model for the adsorption of copper and cadmium by *s. obliquus*, and the hybrid form of the Langmuir kinetic model for the adsorption of cadmium by *C. vulgaris*.

	Copper on Scenedesmus obliquus	Cadmium on Chlorella vulgaris	Cadmium on Scenedesmus obliquus
Root Mean Square Error	1.56	1.15	4.01
Coefficient of efficiency	0.68	0.85	-1.34
Chi-Square Test	5.44	1.79	66.68

The values presented in Figure 49 were used to determine the statistical fit of the Langmuir models to the experimental data. The lower the value of the RMSE and the result of the non-linear Chi-Square test, the closer the model fits to the experimental data and the closer the NSE value is to 1, the closer the model prediction conforms with experimental data.

If the NSE > 0.8, this indicates that the model is a good fit to the data, and if it is greater than 0.65 the model can be considered acceptable [52]. The NSE values alone indicate that the hybrid form of the Langmuir kinetic model has a good fit to the kinetic data for the adsorption of cadmium by *C. vulgaris* (NSE = 0.85), and the first order Langmuir model has an acceptable fit to the kinetic data for the adsorption of copper by *S. obliquus*. The RMSE values shown in Table 36 are larger than their corresponding values presented in Table 25, Table 31 and Table 34 for the RMSE values for the Lagergren model, second order model and the Elovich model respectively.

The Chi-Square test returned a $\mathcal{X}^2$ value for the hybrid Langmuir model that was lower than that of the $\mathcal{X}^2$ value returned for the first order Langmuir model for the copper adsorption by *S. obliquus*; this with the corresponding lower RMSE value calculated for the hybrid Langmuir model compared to the first-order Langmuir

model indicates the best fitting model presented in Figure 45 is the hybrid Langmuir model for the adsorption kinetics of cadmium by *Chlorella vulgaris*.

The RMSE, NSE and $\mathcal{X}^2$ values for the adsorption of cadmium by *S. obliquus* indicate how sensitive these analyses are to outliers. The data points at 5 and 10 seconds (Figure 45d) are the two points that deviate from the model, but these return a RMSE of 4, a negative NSE value and a $\mathcal{X}^2$ of 66.7. It can be seen from the chart in Figure 45d that the rate of the uptake of cadmium by *S. obliquus* is underestimated by the first-order Langmuir kinetic model, but seven out of the nine datapoints are captured by the model.

The Langmuir models are all derived from the Langmuir Isotherm as detailed in Section 5.2.1. The fitting of the Isotherm was performed with only four datapoints, and a narrow metal ion concentration between 0.25mg.L^{-1} and 2.5mg.L^{-1}. The accuracy of the values for b_L and Q_{max} could be confirmed with a more rigorous adsorption investigation over a larger metal ion concentration range, which could improve the accuracy of the rate constants of the models in Figure 45, and provide kinetic rate constants for the copper adsorption by *C. vulgaris*.

Khamizov et al (2018) [128] investigated the model derived by *Liu et al* (2008) [140], and were able to derive the same model from the BET Isotherm. In their analysis of the model they observe that although the kinetics can be derived from adsorption isotherms, adsorption mechanisms cannot be determined from the first order or second order models. The authors recommend investigating other properties such as the activation energies and particle sizes when investigating the adsorption mechanism [128].

6.1.5 Summary: Single Metal Sorption Modelling

Four models, the Lagergren model, a second order model (sometimes referred to as a “pseudo second order” model), Elovich Model and the kinetic form of the Langmuir model were fitted to the adsorption time profile for the uptake of copper and cadmium by *C. vulgaris* and *S. obliquus*; all from a single metal solution.

In all cases, the linearised Lagergren model did not show a good linear correlation with all R^2 values returned as less than 0.67. Furthermore, none of the parameters produced from the linear charts produced models that reflected the experimental data. This is a characteristic of the Lagergren model that has previously been observed by Ho et al [124] leading them to conclude that their data did not follow a first order process.

This claim is not necessarily correct. Liu et al derived a rate expression for the rate of adsorption from Langmuir kinetics, which is a hybrid model and contains both a first-order term and a second-order term. When examining the equilibrium values for the adsorption of copper and cadmium by *S. obliquus,* they were found to be 8.23mg.g^{-1} and 7.91mg.g^{-1} respectively. The ratio of the first order Langmuir rate constant to the second order Langmuir rate constant (calculated using the Langmuir Isotherm), returned k_1/k_2' of 7.8 for the copper adsorption, and 31.4 for the cadmium adsorption. As $k_1/k_2' \approx Q_e$ for the copper adsorption, and $k_1/k_2' > Q_e$ for the cadmium adsorption, the Langmuir rate equation can be approximated to a first order rate equation. The first-order Langmuir model for copper adsorbed by *S. obliquus* produced a model with an acceptable fit (NSE>0.65), but the best fitting model was the hybrid Langmuir model, which contained both the first-order and the second order rate terms, derived for the modelling of the cadmium adsorption by *C. vulgaris* (NSE>0.8). The models could be potentially improved by undertaking more robust isotherm studies; only four datapoints were used to create the Langmuir Isotherms, with the isotherm for copper adsorbed by *C. vulgaris* returning negative values for Q_{max} and b_L, and the derived first order rate constant for the adsorption of cadmium by *S. obliquus* too low to reflect experimental data.

The second order linear models exhibited high levels of correlation ($R^2 > 0.9$) for all experiments with the exception of the cadmium adsorption by the *C. vulgaris* which returned an R^2 value of 0.65. However, even this was sufficient to produce Q_e and k_t values that reflected the experimental data. The model parameters produced by fitting experimental data to the linear second order model appeared to represent experimental data closely with all models showing a good fit to experimental data, with root mean square values <0.24, and an NSE greater than 0.91 for all experiments.

The linear Elovich model also showed good correlation for all experiments, but the cadmium adsorption by *C. vulgaris* (R^2 > 0.86, and R^2 = 0.5, respectively). The equation constants derived by linearizing the Elovich model all produced models with an NSE ≥ 0.87, and a RMSE ≤ 0.29 which indicated the Elovich models predicted the experimental data well. However on analysis of Figure 44, only the model for the cadmium adsorption by *S. obliquus* appeared to follow the trend of the dataset accurately. The Elovich predictions for the adsorption of copper and cadmium by *C. vulgaris* and copper by *S. obliquus*, predict that equilibrium is reached between the first and the second datapoint, which could be the case for the *C. vulgaris* but this is not recorded by experimental data. The cadmium adsorption by *S. obliquus* was the only adsorption process that was slow enough to be captured by *Elovich* kinetics.

As the Langmuir kinetics could not be fitted to the data for the copper adsorption by *C. vulgaris*, this model is deemed to have be least representative for the experimental data; although this could be improved by further Isotherm studies. To compare the three other models, the R^2, RMSE and NSE Values are all compared. The R^2 values are displayed in Table 37.

Table 37: A comparison of the R^2 values obtained from the linear Lagergren model, linear second order model and the linear Elovich model for the adsorption of copper and cadmium by *C. vulgaris* and *S. obliquus*.

Microalgae	Metal Ion	Lagergren Model	Second Order Model	Elovich Model
C. vulgaris	Cu^{2+}	0.41	0.90	0.86
C. vulgaris	Cd^{2+}	0.62	0.93	0.98
S. obliquus	Cu^{2+}	0.51	0.65	0.50
S. obliquus	Cd^{2+}	0.66	0.94	0.99

Analysing the R^2 values displayed in Table 37, the R^2 values for the Lagergren model show the worst fit compared to the other two models. The Elovich model has the better R^2 for the cadmium adsorption by *C. vulgaris* and *S. obliquus* (0.98 and 0.99 respectively), whereas the second order model has the better fit for the copper adsorption by the *C. vulgaris* and *S. obliquus* (0.90 and 0.65 respectively). The RMSE values for the Lagergren, Second order and Elovich models are displayed in Table 38.

Table 38: A comparison of the RMSE values obtained from the fitted Lagergren model, second order model and the Elovich model for the adsorption of copper and cadmium by *C. vulgaris* and *S. obliquus*.

Microalgae	Metal Ion	Lagergren Model	Second Order Model	Elovich Model
C. vulgaris	Cu^{2+}	0.23	0.24	0.29
C. vulgaris	Cd^{2+}	0.23	0.11	0.06
S. obliquus	Cu^{2+}	0.38	0.22	0.25
S. obliquus	Cd^{2+}	0.35	0.16	0.07

The RMSE values displayed in Table 38 again indicate that the Elovich model best represents the cadmium adsorption by both species of microalgae, and the second-order model better represents the copper adsorption. The NSE values are displayed in Table 39.

Table 39: A comparison of the NSE values obtained from the fitted Lagergren model, second order model and the Elovich model for the adsorption of copper and cadmium by *C. vulgaris* and *S. obliquus*.

Microalgae	Metal Ion	Lagergren Model	Second Order Model	Elovich Model
C. vulgaris	Cu2+	0.91	0.91	0.87
C. vulgaris	Cd2+	0.88	0.97	0.99
S. obliquus	Cu2+	0.81	0.91	0.91
S. obliquus	Cd2+	0.71	0.93	0.99

The NSE values displayed in Table 39 indicate that the second order model is statistically the best fitting model for the copper adsorption by *C. vulgaris* only. The copper adsorption by *S. obliquus* has an equal NSE value for both the second order model and the Elovich model, and the NSE values for the cadmium adsorption by *C. vulgaris* and *S. obliquus* shows a better fit for the Elovich model compared to the second order model.

These results would imply that the Elovich model is the model that is most representative of the adsorption kinetics, which has been observed previously for cadmium sorption onto orange peel [184]. However this is in contradiction to previous studies that compare the Lagergren, second order and Elovich models for metal sorption by biosorbents (not microalgae), which concludes the second order model best represents adsorption kinetics [185-187].

Previous studies investigating the adsorption of dyes onto biosorbents have also observed that the Elovich model is superior to the Lagergren model, but the adsorption kinetics were best represented by the second order model [124, 181]. When the predictions of the Elovich model is plotted together with the experimental

data, the adsorption equilibrium is predicted to be achieved between the first and second datapoint. The model that visually best fits the data is the Lagergren model that has been fitted to experimental data by non-linear regression.

Each model gives an indication of the adsorption rate of each metal, by each species of microalgae. The Lagergren returns a first order rate k_1, that has units per second (s^{-1}); the second order model returns a more complex rate k_2, that has units of gram per milligram per second ($g.mg^{-1}s^{-1}$), and the Elovich model returns a maximum uptake, α rate with units of milligram per gram per second ($mg.g^{-1}s^{-1}$). All models are in agreement that the uptake rate for both copper and cadmium is higher for *C. vulgaris*, than it is for *S. obliquus.* A comparison of these rates for the adsorption of each metal by each species of microalgae are displayed in Table 40.

Table 40: A comparison of adsorption rates between *C. vulgaris* and *S. obliquus* obtained by modelling copper and cadmium uptake from a single metal solution, using the Lagergren model, the second order model and the Elovich model.

Copper Adsorption Rates			
	k_1 (s^{-1})	**k_2 ($g.mg^{-1}s^{-1}$)**	**α ($mg.g^{-1}s^{-1}$)**
Chlorella vulgaris	0.59	0.37	1.59×10^{17}
Scenedesmus obliquus	0.39	0.17	5.92×10^{3}
Cadmium Adsorption Rates			
	k_1 (s^{-1})	**k_2 ($g.mg^{-1}s^{-1}$)**	**α ($mg.g^{-1}s^{-1}$)**
Chlorella vulgaris	0.61	0.17	1.10×10^{8}
Scenedesmus obliquus	0.24	0.05	39.15

The uptake rates displayed in Table 40 show that according to all models derived, that *C. vulgaris* has a faster adsorption rate than *S. obliquus* for both metals tested. The difference is largest for the cadmium uptake between *C. vulgaris* and *S. obliquus*, with the second order rate constant falling from 0.17 to 0.05 $g.mg^{-1}s^{-1}$, and the maximum adsorption rate falling from 1.10×10^{8} to 39.15 $mg.g^{-1}s^{-1}$. It would appear that the majority of the metal uptake process had occurred within the first five seconds of contact for the *C. vulgaris*, with the kinetics not being recorded with the current experimental procedure.

6.2 Adsorption from a binary metal solution

The experimental procedure was modified so that the metal solution now contained 2.5mg.L^{-1} of copper and 2.5mg.L^{-1} cadmium. This was exposed to the algae as before, to investigate whether the presence of a competing metal ion affects the adsorption of each metal by the microalgae.

When the two metal ions are present together in solution, there is a slight effect on the adsorption of copper by each microalgae species, and a more significant effect on the adsorption of cadmium by both *C. vulgaris* and *S. obliquus*. The effect is shown in Figure 46.

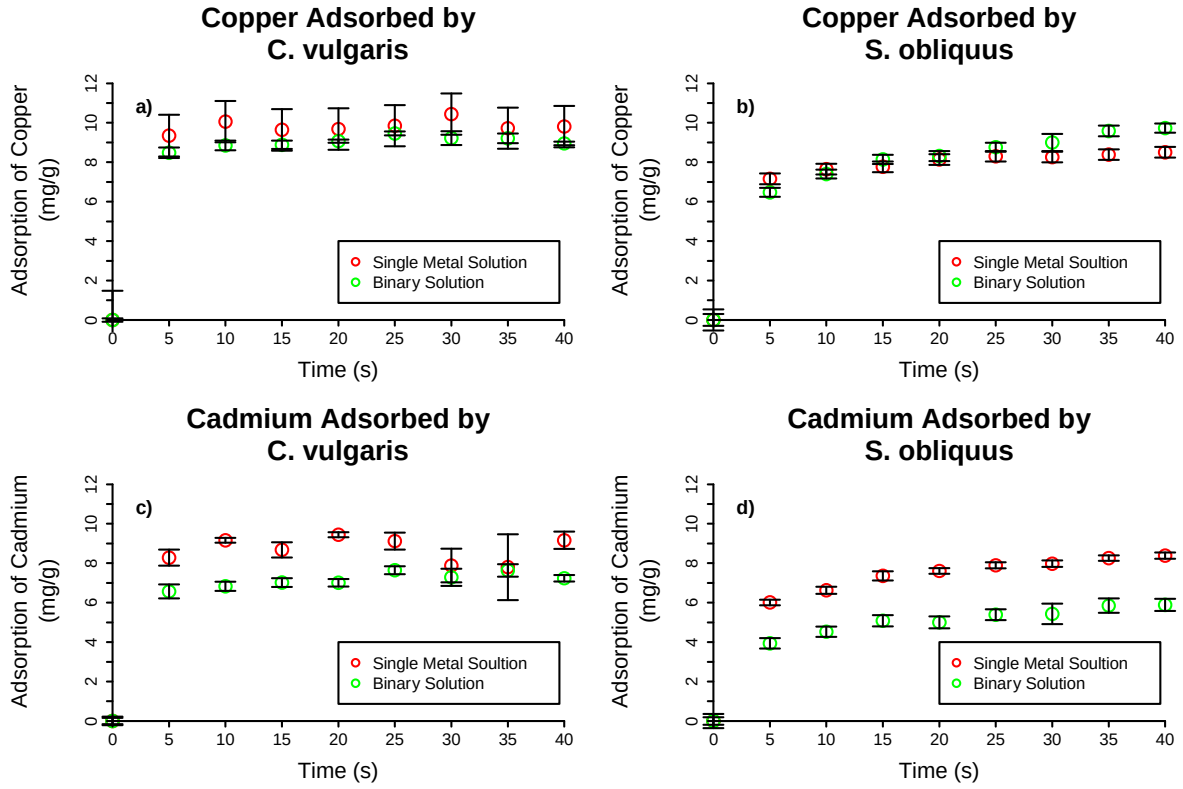

Figure 46: Charts comparing the adsorption of cadmium and copper by *C. vulgaris* and *S. obliquus*, comparing the data for metal uptake from a single metal solution and a binary metal solution for each species of microalgae. Red open circles represent the data for metal uptake from a single metal solution, green open circles contain the date for metal uptake from a binary metal solution.

There is a clear effect on the adsorption of cadmium in both species of microalgae when copper is also present. The effect of the presence of cadmium on the adsorption of copper is negligible. The data shown in Figure 46*b* shows a curious effect. The copper adsorption can increase by a small but significant amount by the time the process reaches equilibrium. However when analysing the data here it must be taken into account that the *S. obliquus* biomass concentration for the single

metal experiments was 240mg.L^{-1}, and the *S. obliquus* concentration for the binary metal experiments was 200mg.L^{-1}. Previous studies have found that the binding capacity of the algal biomass to metals (mg of metal per mg of algae), increases with decreasing concentration of the algae biomass [91, 93, 97].

The following section details the models produced for predicting adsorption of each metal from a binary solution and compares them to those that were derived in Section 6.1.

6.2.1 Lagergren Model

In this section, the Lagergren model as represented by Equation 1 in Section 6.1.1, is applied to the adsorption data of copper and cadmium, by *C. vulgaris* and *S. obliquus* from a mixed metal solution. The model parameters (the adsorption at equilibrium, Q_e and the first order adsorption rate, k_t) were obtained by linearizing the data by plotting $ln(Q_e - Q_t)$ against t, and also by fitting Equitation 1 directly to the experimental data by non-linear regression.

6.2.1.1 Chlorella vulgaris

To linearise the Lagergren model, $ln(Q_e - Q_t)$ is plotted vs time, t. As Q_e is a model constant that is obtained from the intercept of the linear plot, an initial estimate of this value is required. The initial estimates for Q_e for each of the *Chlorella* experiments are shown in Table 41.

Table 41: Estimates for the Q_e values for the linear Lagergren models to derive Q_{e0} and k_0 for the adsorption of copper and cadmium, from single and mixed solutions by *C. vulgaris*.

Metal	Q_e Estimate from a single metal solution (mg.g^{-1})	Q_e Estimate from the binary solution (mg.g^{-1})
Copper	10	9
Cadmium	8	7

The presence of a second metal reduced the adsorption of copper and cadmium by 1mg.g^{-1}. The values of Q_t were subtracted from their corresponding estimates, and the logarithm of the absolute value was calculated and plotted against time, as shown in Figure 47.

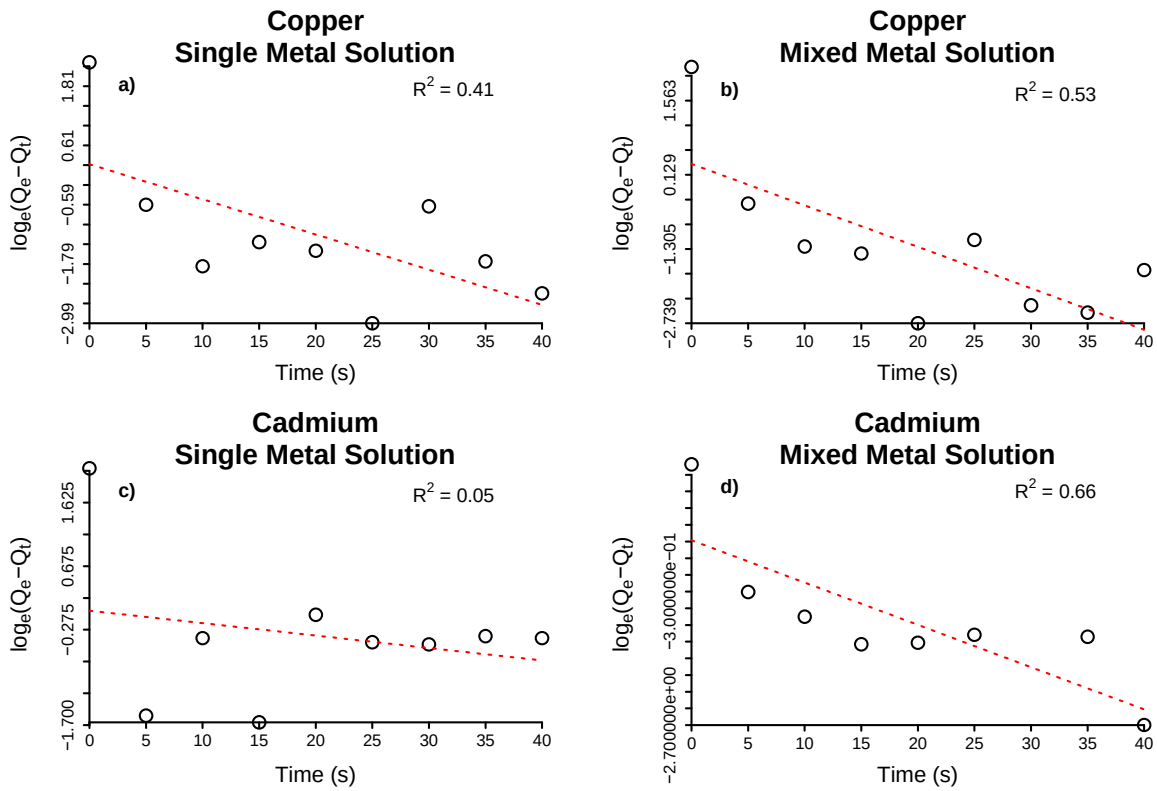

Figure 47: Linearised Lagergren models to derive the initial estimates for the rate constants (k_{t0}) and adsorption at equilibrium (Q_{e0}) for the 2.5mgL^{-1} copper and cadmium uptake experiments by *C. vulgaris*, comparison between single and binary metal analysis.

It can be observed in Figure 47b and d that the linear plots for the mixed metal solutions have a slightly higher R^2 value when compared to their single metal counterparts in Figure 47a and c, but even for the mixed metal experiments the linear Lagergren model did not exhibit a high degree of correlation to the *C.* vulgaris data.

When the Lagergren parameters, Q_t and k_t were obtained by linearizing the data for single metal adsorption (section 6.1.1), the model parameters obtained from the plots of $ln(Q_e - Q_t)$ vs t (Figure 47a and c) did not produce accurate values for Q_e and k_t.

Table 42 contains the values for Q_{e0} and k_{t0} (obtained from the linearised Lagergren model), for the copper and cadmium adsorption by *C. vulgaris* from a single and mixed metal solution. These model parameters were fitted to the experimental data using R software as before, using a non-linear least squares algorithm. Both models are plotted alongside the experimental data in Figure 48.

Table 42: First order parameters (adsorption at equilibrium and first order rate constants), derived by linearizing the Lagergren Model. Initial estimates for the first order rate constant, k_{t0} and the adsorption at equilibrium, Q_{e0} for 2.5mg.L^{-1} copper and 2.5mg.L^{-1} cadmium adsorbed by *C. vulgaris* from single and mixed metal solutions.

	Single Metal Solution		Binary Solution	
	Qe_0 (mg.g^{-1})	k_{t0} (s^{-1})	Qe_0 (mg.g^{-1})	k_{t0} (s^{-1})
Copper	1.26	0.07	1.40	0.08
Cadmium	1.55	0.11	1.96	0.09

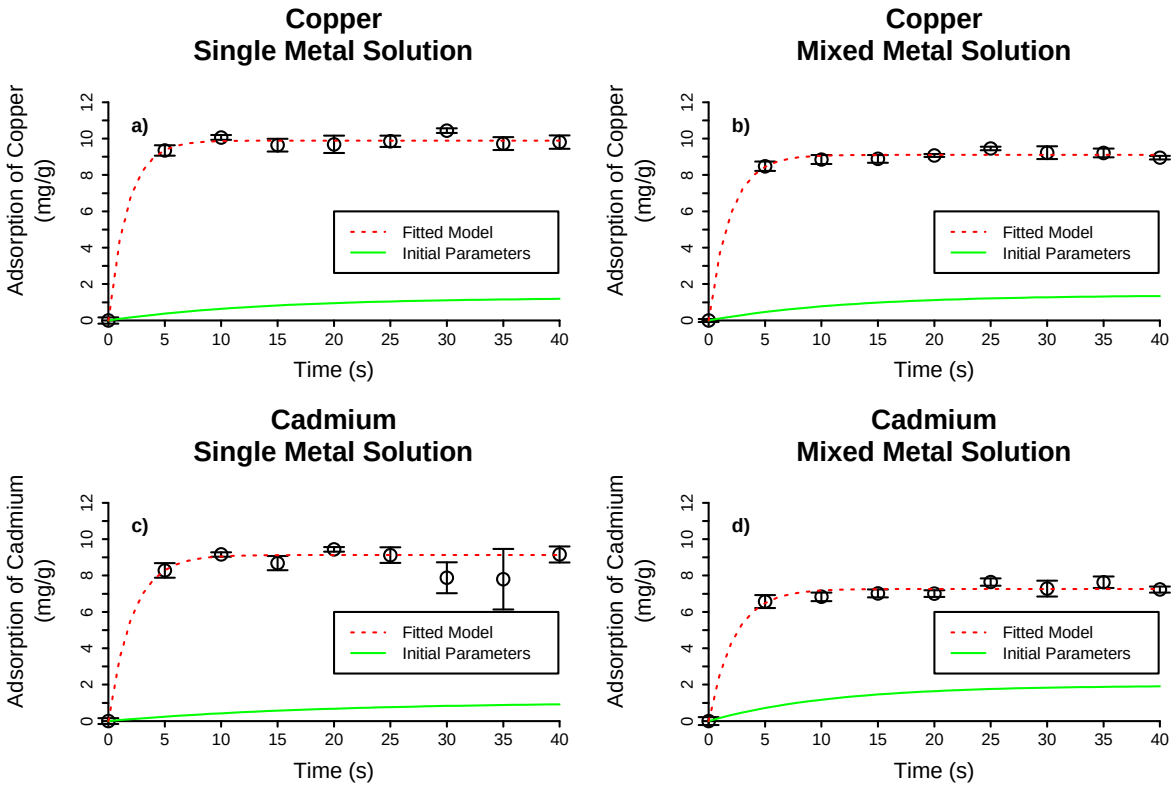

Figure 48: Adsorption-time profiles for copper and cadmium on *C. vulgaris* from a single metal solution, and a binary metal solution (open circles), vs Lagergren predictions using parameters obtained from linearized data (solid green line), and Lagergren predictions using model parameters obtained by fitting the Lagergren model using non-linear least squares (red dotted line).

The parameters derived from the linearized data (solid green line, Figure 48) once again do not represent the data obtained by experimentation for the metal uptake from a binary solution. The parameters (Q_e and k_t) obtained by fitting the non-linear Lagergren model to the experimental data did produce a model (red dashed line, Figure 48), that appeared to represent the experimental data well. The values for Q_e and k_t are shown for each experiment in Table 43.

Table 43: Fitted values for adsorption at equilibrium (Q_{e0}) and first order rate constants (k_t) for the Lagergren model, comparing the values of copper and cadmium adsorption by *C. vulgaris* adsorbed from a single metal solution and a binary metal solution with a concentration of 2.5mg.L^{-1} of each metal ion.

	Single Metal Solution		Binary Solution	
	Q_e (mg.g^{-1})	k (s^{-1})	Q_e (mg.g^{-1})	k (s^{-1})
Copper	9.89 (±0.10)	0.59 (±0.11)	9.10 (±0.08)	0.53 (±0.06)
Cadmium	8.75 (±0.24)	0.61 (±0.31)	7.26 (±0.11)	0.45 (±0.08)

The effect cadmium had on the adsorption of copper reduced the Q_e value from 9.9 to 9.1 mg.g^{-1}, and the effect that the presence of copper had on the adsorption of cadmium reduced Q_e from 8.8 to 7.3mg.g^{-1}. The first order rate constants k_t do not appear to be affected.

The fit of the Lagergren models that were created by fitting the models directly to the experimental data were determined by R^2 of the linear models, RMSE and NSE of non-linear model predictions compared to the experimental data. These values are displayed in Table 44.

Table 44: R^2 values for the linearized Lagergren model, and the RMSE and NSE values to determine accuracy of the Lagergren model derived by fitting it directly to experimental data, for copper and cadmium uptake by *C. vulgaris*, from a single metal solution and a binary solution.

	Single Metal Solution			Binary Solution		
	R^2	RMSE	NSE	R^2	RMSE	NSE
Copper	0.41	0.23	0.91	0.53	0.17	0.95
Cadmium	0.51	0.38	0.81	0.60	0.24	0.84

The root mean square error for each of the copper uptake experiments were low, and with the NSE values greater than 0.9. This indicates that the fitted model represents the current experimental data very well. However in all cases the R^2 values for the linear models are poor for metal uptake by *C. vulgaris*, indicating that in order to fit the Lagergren model to the experimental data; it is necessary to use non-linear least squares to fit the non-linear Lagergran model directly to the experimental data.

6.2.1.2 Scenedesmus obliquus

The initial estimates of Q_e required for linearising the experimental data in accordance to the Lagergren model are displayed in Table 45.

Table 45: Estimates for the Q_e values for the linear Lagergren models to derive Q_{e0} and k_0 for the adsorption of copper and cadmium, from single and mixed solutions by *S. obliquus*.

Metal	Qe Estimate from a single metal solution ($mg.g^{-1}$)	Qe Estimate from the binary solution ($mg.g^{-1}$)
Copper	8	7
Cadmium	8	5

The estimates for Q_e were found by taking the mean of the adsorption data presented in Figure 46, *b* and *d*. Single metal data represented by the red data points and binary metal data represented by the green data points. As with the *C. vulgaris*, the copper adsorbed by *S. obliquus* is reduced by $1mg.g^{-1}$ by the presence of cadmium; however with the change in biomass concentration between the *S. obliquus* experiments ($240mg.L^{-1}$ for the single metal data, and $200mg.L^{-1}$ for the binary metal data), a direct comparison between the two datasets cannot be made. Furthermore, the mixed metal data in Figure 46b does not appear to have reached equilibrium within the experimental timeframe.

The values of Q_t were subtracted from their corresponding estimates, and the logarithm of the absolute value was calculated and plotted against time. The charts are shown in Figure 49.

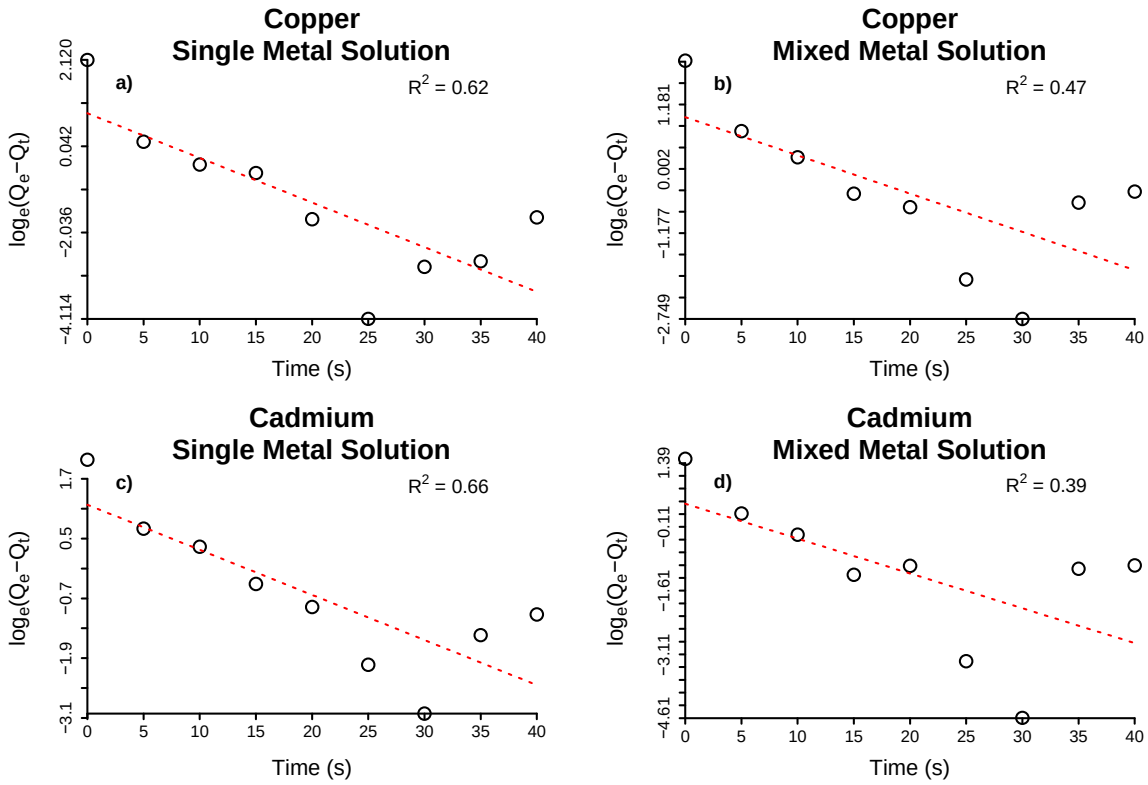

Figure 49: Linearised Lagergren models to derive the initial estimates for the rate constants (k_{t0}) and adsorption at equilibrium (Q_{e0}) for the 2.5mgL^{-1} copper and cadmium uptake experiments by *S. obliquus*, comparison between single and binary metal analysis.

The charts displayed in Figure 49a and b show a marginally better R^2 value compared to their mixed metal counterparts in Figure 49c and d. The parameters from each chart are displayed in Table 46. These are the derived values for Q_e and k_t.

Table 46: First order parameters (adsorption at equilibrium and first order rate constants), derived by linearizing the Lagergren Model. Initial estimates for the first order rate constant, k_{t0} and the adsorption at equilibrium, Q_{e0} for 2.5mg.L^{-1} copper and 2.5mg.L^{-1} cadmium adsorbed by *S. obliquus* from single and mixed metal solutions.

	Single Metal Solution		Binary Solution	
	Q_{e0} (mg.g^{-1})	k_0 (s^{-1})	Q_{e0} (mg.g^{-1})	k_0 (s^{-1})
Copper	2.30	0.11	2.59	0.07
Cadmium	3.95	0.09	1.54	0.08

As for the parameters (Q_{e0} and k_{t0} derived from Figure 49a and b), the Q_{e0} and k_{t0} obtained for the mixed metal data did not represent the experimental data well. These values were used as starting values for Q_e and k_t for fitting the Lagergren model (equation 1) to the experimental data. The fitted parameters are displayed in Table 47, and predictions using both sets of parameters are displayed in Figure 50, along with their corresponding experimental data.

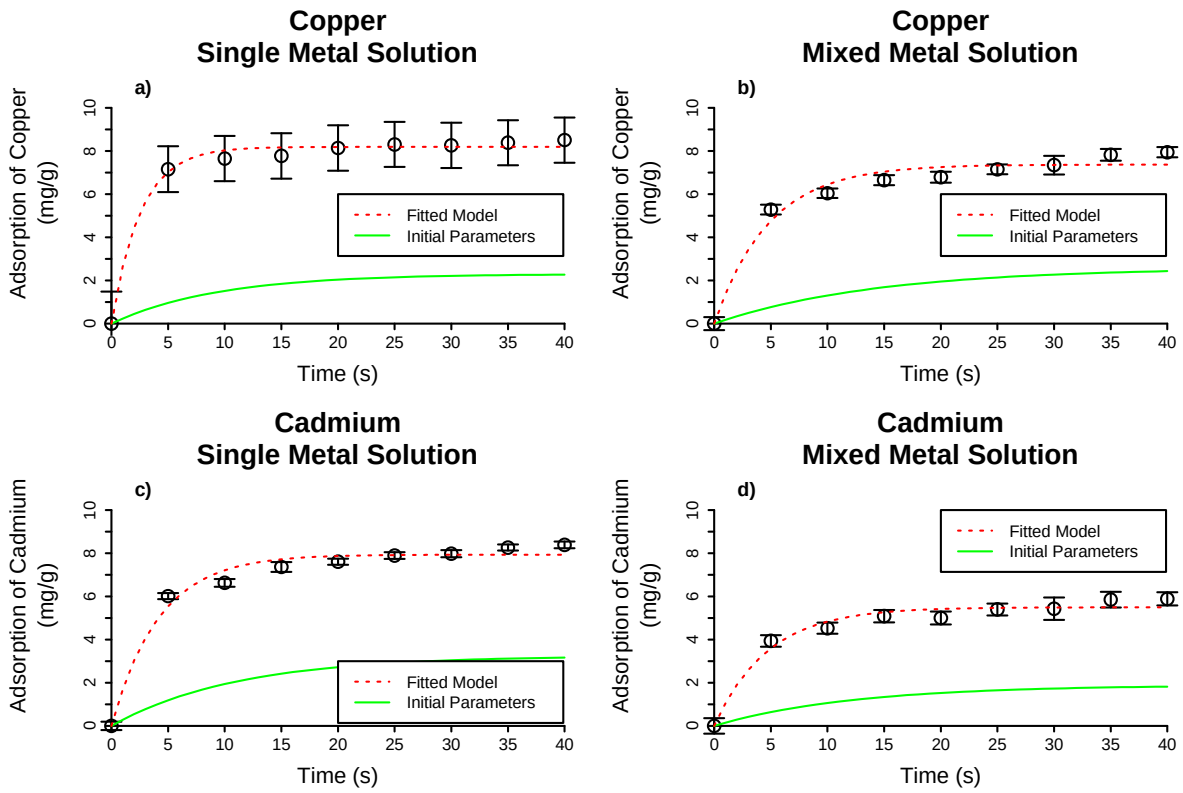

Figure 50: Adsorption-time profiles for copper and cadmium on *S. obliquus* from a single metal solution, and a binary metal solution (open circles), vs Lagergren predictions using parameters obtained from linearized data (solid green line), and Lagergren predictions using model parameters obtained by fitting the Lagergren model using non-linear least squares (red dotted line).

The model using Q_e and k_t values obtained from linearizing the experimental data (solid green line in Figure 50), do not represent the experimental data. The model using values of Q_e and k_t obtained by fitting equation 1 directly to the experimental data (red dashed line), do appear represent the data well. These parameters are displayed in Table 47.

Table 47: Fitted values for adsorption at equilibrium and first order rate constants for the Lagergren Model, describing adsorption of 2.5mg.L^{-1} copper and 2.5mg.L^{-1} cadmium adsorbed by *S. obliquus* from single metal solution, and a binary metal solution.

	Single Metal Solution		Binary Solution	
	Q_e (mg.g^{-1})	k (s^{-1})	Q_e (mg.g^{-1})	k (s^{-1})
Copper	8.19 (±0.10)	0.39 (±0.05)	7.37 (±0.20)	0.21 (±0.03)
Cadmium	7.93 (±0.17)	0.24 (±0.03)	5.49 (±0.14)	0.21 (±0.03)

As previously stated, the difference in biomass concentration between the single metal experiments (240mg.L^{-1}), and the binary metal experiments (200mg.L^{-1}), means that direct comparison between the two sets of experiments is not possible. Although Figure 46b appears to not have reached equilibrium within the timeframe, the Lagergren model for the uptake of copper from a binary mixture predicts that

the equilibrium value is 7.37mg.g^{-1}. This is approximately a 1mg.g^{-1} difference between that of the equilibrium value for copper adsorption from a single metal solution. The effect on cadmium adsorption is even greater, with adsorption at equilibrium dropping from almost 8mg.g^{-1} for the single metal data, to 5.5mg.g^{-1} for the binary metal data. This difference would have been greater if the two biomass concentrations were the same, as the link between a decrease in algae biomass and an increase in metal loading per gram of algae biomass has been widely reported [15, 19, 20].

As with the fit of the Lagergren models for the *C. vulgaris*, the models created by fitting the Lagergren model (equation 1) directly to the experimental data were determined by R^2 of the linear models, RMSE and NSE of non-linear model predictions compared to the experimental data with these values are displayed in Table 48.

Table 48: R^2 values for the linearized Lagergren model, and the RMSE and NSE values to determine accuracy of the Lagergren model derived by fitting it directly to experimental data, for copper and cadmium uptake by *S. obliquus*, from a single metal solution and a binary solution.

	Single Metal Solution			Binary Solution		
	R^2	RMSE	NSE	R^2	RMSE	NSE
Copper	0.62	0.23	0.88	0.47	0.39	0.59
Cadmium	0.66	0.34	0.71	0.39	0.23	0.62

When analysing the fit of the model in Table 48, none of the fitted first order models have an NSE greater than 0.9. The models for both metal species when adsorbed from a binary solution have a worse fit compared to their counterparts from a single metal solution. When analysing the fit with an NSE of less than 0.65, it can be concluded that both metals are inadequate to represent the experimental data[52]. Concluding from these findings, the Lagergren model (after the parameters were fitted to experimental data), is more applicable to the *C. vulgaris* data compared to the *S. obliquus* data. However, as the parameters require fitting via non-linear least squares to represent the experimental data; with the R^2 values for all linear plots showing poor correlation.

The Lagergren model can therefore be discounted as a reliable method for developing a mathematical model to predict the uptake kinetics.

6.2.2 Second Order Model

6.2.2.1 Chlorella vulgaris

The second order model previously applied to the uptake of copper by *C. vulgaris* uptake data did show a linear relationship, with the copper data correlating well (Figure 51a). The cadmium uptake by the *C. vulgaris* did not show good correlation when the data was linearized (Figure 51*c*). For the mixed metal uptake experiments, the reciprocal of the adsorption at time, t; Q_t^{-1} was plotted against the reciprocal of the time, t^{-1}. These charts are shown in Figure 51*b* and *d*.

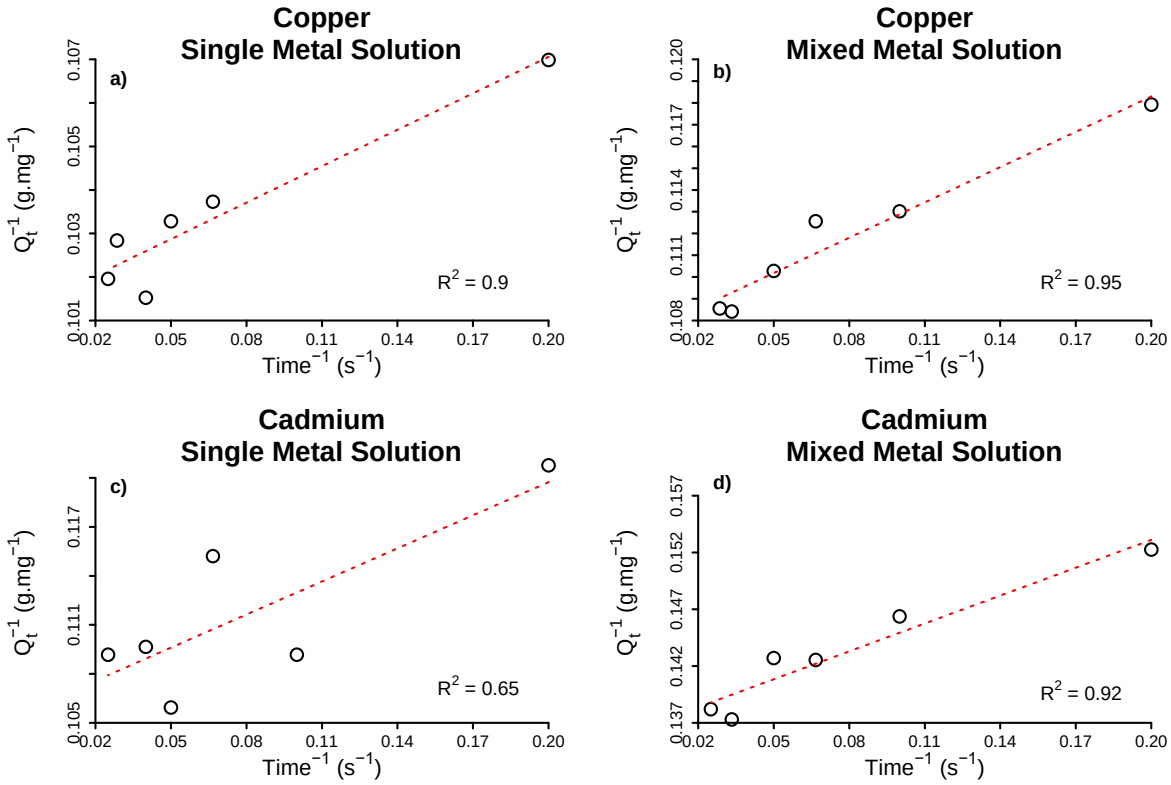

Figure 51: Linearised second order models to derive the initial estimates for the second order rate constants (k_{t0}) and adsorption at equilibrium (Q_{e0}) for the 2.5mgL^{-1} copper and cadmium uptake experiments by *C. vulgaris*, comparison between single and binary metal analysis.

Examining Figure 51b and d, the linear correlation in both cases are better than those of their single metal counterparts (Figure 51*a* and *c*). Previously, the values of Q_{e0} and k_{t0} produced by from linearizing the second order model were able to represent the experimental data for the single metal uptake. These are shown alongside the model parameters obtained by linearizing the second order model for the mixed metal uptake in Table 49.

Table 49: Second order parameters (adsorption at equilibrium and first order rate constants), derived by linearizing the second-order Model. Initial estimates for the first order rate constant, k_{t0} and the adsorption at equilibrium, Q_{e0} for 2.5mg.L^{-1} copper and 2.5mg.L^{-1} cadmium adsorbed by *C. vulgaris* from single and mixed metal solutions.

	Single Metal Solution		Binary Solution	
	Q_{e0} (mg.g^{-1})	k_0 (g.mg^{-1}.s^{-1})	Q_{e0} (mg.g^{-1})	k_0 (g.mg^{-1}.s^{-1})
Copper	9.85	0.37	9.31	0.22
Cadmium	9.41	0.17	7.52	0.17

As with the values obtained by the Lagergren model, the model parameters (Q_{e0} and k_{t0}) were used as initial estimates to fir the non-linear form of the second order model (equation 3), to the experimental data. The two models created with each set of model parameters were plotted with their corresponding experimental data and is shown in Figure 52.

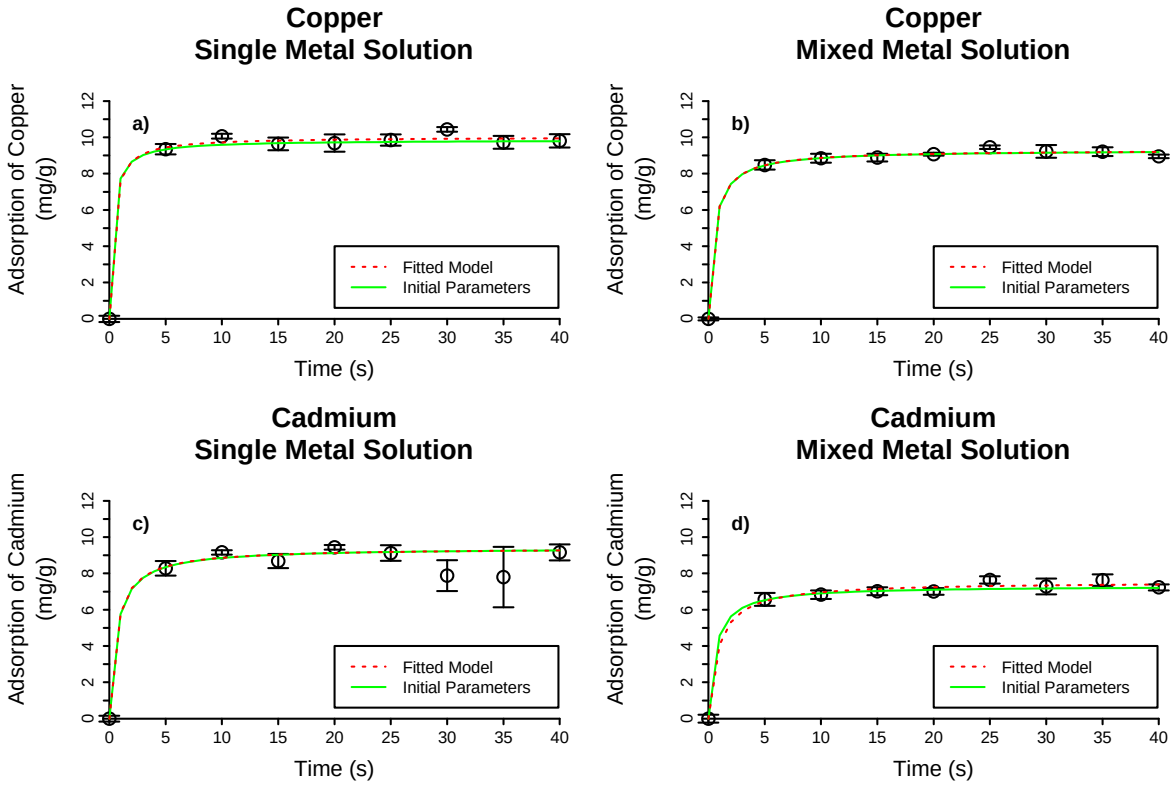

Figure 52: Adsorption-time profiles for copper and cadmium on *C. vulgaris* from a single metal solution, and a binary metal solution (open circles), vs second-order predictions using parameters obtained from linearized data (solid green line), and second-order predictions using model parameters obtained by fitting the Lagergren model using non-linear least squares (red dotted line).

The models created using parameters obtained by linearizing the data to fit equation 4 (Figure 52 green dashed line), were indistinguishable to the models created by fitting equation 3 directly to the experimental data (Figure 52, red dashed line). The model parameters (Q_e and k_t) obtained by fitting equation 3 to the experimental data are shown in Table 50.

Table 50: Fitted values for adsorption at equilibrium and second order rate constants for the Second Order Model, describing adsorption of 2.5mg.L^{-1} copper and 2.5mg.L^{-1} cadmium adsorbed by *C. vulgaris* from single metal solutions and a binary metal solution.

	Single Metal Solution		Binary Solution	
	Q_e (mg.g^{-1})	k (g.mg^{-1}.s^{-1})	Q_e (mg.g^{-1})	k (g.mg^{-1}.s^{-1})
Copper	10.02 (±0.16)	0.33 (±0.21)	9.31 (±0.10)	0.21 (±0.06)
Cadmium	9.41 (±0.20)	0.17 (±0.07)	7.55 (±0.13)	0.16 (±0.05)

The values for Q_e and k_t for copper adsorbed from a binary mixture (Table 50), are identical to those of the values for Q_{e0} and k_{t0} for copper adsorbed from a single metal mixture (Table 49). The values of Q_{e0} and k_{t0} for cadmium adsorbed from a binary mixture are within the margin for error of the Q_e and the k_t values displayed in Table 50.

When comparing the difference in Q_e values between adsorption from a single metal solution and a binary metal solution, the adsorption at equilibrium for copper drops from 10 mg.g^{-1} to 7.3mg.g^{-1}, and from 9.4mg.g^{-1} to 7.6mg.g^{-1} for cadmium when copper is present as a co-adsorbate. The values of k_t are all within the standard error of each other.

The values for Q_e and k_t that were derived by linearizing the data in the form of equation 4, were analysed for their RMSE and NSE values, alongside the R^2 values of the correlation used to produce them. These are displayed in Table 51.

Table 51: R^2 values for the linearized Lagergren model, and the RMSE and NSE values to determine accuracy of the Lagergren model derived by fitting it directly to experimental data, for copper and cadmium uptake by *C. vulgaris*, from a single metal solution and a binary solution.

	Single Metal Solution			Binary Solution		
	R^2	RMSE	NSE	R^2	RMSE	NSE
Copper	0.9	0.24	0.91	0.95	0.14	0.96
Cadmium	0.65	0.22	0.91	0.92	0.19	0.90

The R^2 value for the cadmium adsorbed from a single metal solution is the only example where the linear fit does not show a good correlation. All other datasets have an $R^2 \geq 0.9$ (Table 51). Despite the poor correlation returned for the cadmium experiment, all models show a low RMSE value and return an NSE of greater than 0.9; indicating all second order models have a very good fit for the experimental data [52].

6.2.2.2 *Scenedesmus obliquus*

The reciprocal of the adsorption at time *t* and the reciprocal of the elapsed time produced a good linear relationship for the adsorption of each metal from a single metal solution by *S. obliquus*. The same analysis was done for the metal uptake data for the metal removal from a binary solution by *S. obliquus* and the data is displayed in Figure 53.

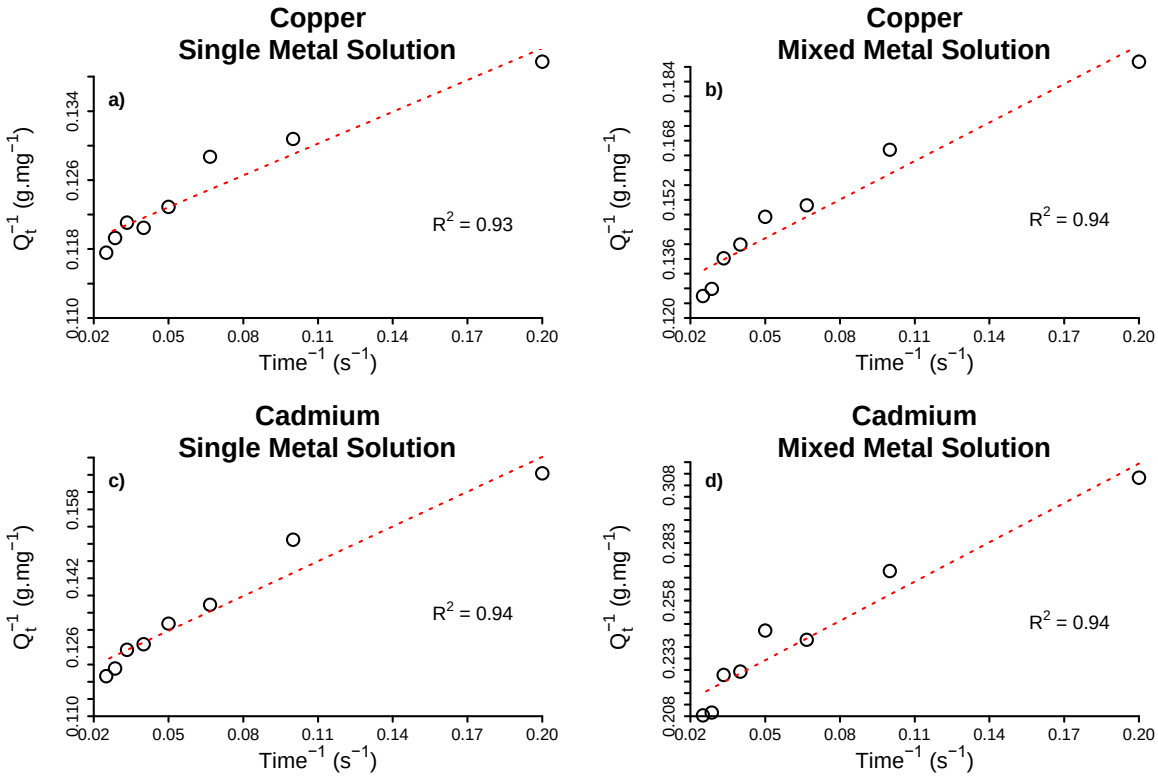

Figure 53: Linearised second order models to derive the initial estimates for the second order rate constants (k_{t0}) and adsorption at equilibrium (Q_{e0}) for the 2.5mgL^{-1} copper and cadmium uptake experiments by *S. obliquus*, comparison between single and binary metal analysis.

All correlations shown in Figure 53 are greater than 0.9. This is suggestive that the data shown in Figure 51c for cadmium adsorbed from a single metal solution by *C. vulgaris* could be an anomaly all other experimental data produced good linear fits to the second order model, which is consistent with other studies investigating metal removal using biosorbents [124]. The values of Q_{e0} and k_0 obtained from Figure 53 are displayed in Table 52.

Table 52: Second order parameters (adsorption at equilibrium and first order rate constants), derived by linearizing the second-order Model. Initial estimates for the first order rate constant, k_{t0} and the adsorption at equilibrium, Q_{e0} for 2.5mg.L^{-1} copper and 2.5mg.L^{-1} cadmium adsorbed by *S. obliquus* from single and mixed metal solutions.

	Single Metal Solution		Binary Solution	
	Q_{e0} (mg.g^{-1})	k_0 (s^{-1})	Q_{e0} (mg.g^{-1})	k_0 (s^{-1})
Copper	8.57	0.11	8.05	0.04
Cadmium	8.59	0.05	6.01	0.06

The Q_{e0} and the k_{t0} parameters displayed in Table 53 were used as initial estimates for a non-linear least squares algorithm, and values for Q_e and k_t for the second order model were derived and are shown in Table 53. Both sets of model parameters were inserted into equation 3 and plotted alongside their experimental data as displayed in Figure 54.

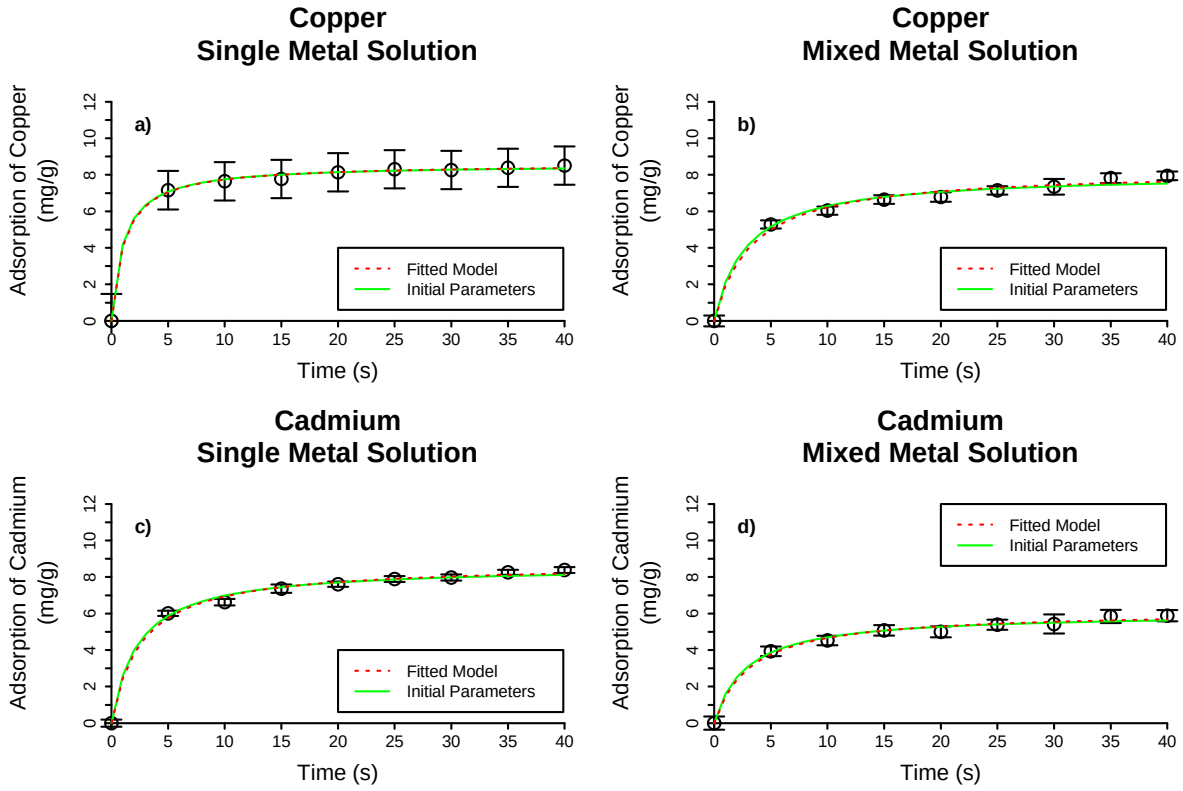

Figure 54: Adsorption-time profiles for copper and cadmium on *S. obliquus* from a single metal solution, and a binary metal solution (open circles), vs Second order predictions using parameters obtained from linearized data (solid green line), and second order predictions using model parameters obtained by fitting the Lagergren model using non-linear least squares (red dotted line).

Examining the charts in Figure 54, the models created using parameters obtained by linearizing the data (Q_{e0} and k_{t0}, as represented by the solid green line in Figure 54), appear identical to the models created from the parameters obtained by fitting equation 3 to the experimental data (Q_e and k_t, displayed in Table 53 and represented by the red, dashed line in Figure 54).

Table 53: Fitted values for adsorption at equilibrium and second order rate constants for the Second Order Model, describing adsorption of 2.5mg.L^{-1} copper and 2.5mg.L^{-1} cadmium adsorbed by *S. obliquus* from single metal solutions and a binary metal solution.

	Single Metal Solution		Binary Solution	
	Q_e (mg.g^{-1})	k (s^{-1})	Q_e (mg.g^{-1})	k (s^{-1})
Copper	8.60 (±0.08)	0.11 (±0.01)	8.25 (±0.21)	0.04 (±0.01)
Cadmium	8.72 (±0.14)	0.04 (±0.01)	6.13 (±0.16)	0.05 (±0.01)

Although visually it is difficult to tell which model has the best fit, fitting Equation 3 to the experimental data did produce slight difference in Q_e and k_t values compared to the Q_{e0} and k_{t0} values displayed in Table 52. These differences are displayed in Table 54.

Table 54: A comparison between values for adsorption at equilibrium and second order adsorption rate obtained for *S. obliquus* by 1. Linearizing copper and cadmium removal data from single metal solutions and binary metal solutions, and 2. Fitting equation 3 (non-linear form of the second-order model), directly to the experimental data.

Single metal solution				
Metal	Q_{e0} (mg.g^{-1})	k_0 (s^{-1})	Q_e (mg.g^{-1})	k (s^{-1})
Copper	8.57	0.11	8.60 (±0.08)	0.11 (±0.01)
Cadmium	8.59	0.05	8.72 (±0.14)	0.04 (±0.01)
Binary Solution				
Metal	Q_{e0} (mg.g^{-1})	k_0 (s^{-1})	Q_e (mg.g^{-1})	k (s^{-1})
Copper	8.05	0.04	8.25 (±0.21)	0.04 (±0.01)
Cadmium	6.01	0.06	6.13 (±0.16)	0.05 (±0.01)

With the model parameters (Q_{e0} and k_{t0} and Q_e and k_t) displayed in Table 54, it can clearly be seen that although there are minor changes between the Q_{e0} and their corresponding fitted Q_e values; they lie within the standard error calculated for the fitted Q_e values.

As the concentration of the *S. obliquus* in the mixed metal experiments was 200mg.L^{-1}, and the concentration of the *S. obliquus* in the single metal experiments was 240mg.L^{-1}, a direct comparison between the Q_e values cannot be accurately made. The presence of the second metal does reduce the Q_e for copper from 8.6 to 8.3 mg.g^{-1}, and the Q_e for cadmium from 8.7 to 6.1 mg.g^{-1}; the difference would have been greater if the two experiments had the same biomass concentration, as

the lower the biomass concentration, the greater the metal binding per gram of biomass [15, 19, 20].

The models created using parameters from the linear second order model were evaluated for their RMSE and NSE values when the predictions from the models were compared to experimental data. The R^2, RMSE and NSE values are all displayed in Table 55.

Table 55: R^2 values for the linearized second order model, and the RMSE and NSE values to determine accuracy of the second order model derived by linearizing the second order model, for copper and cadmium uptake by *S. obliquus*, from a single metal solution and a binary solution.

	Single Metal Solution			Binary Solution		
	R^2	RMSE	NSE	R^2	RMSE	NSE
Copper	0.93	0.11	0.97	0.94	0.22	0.87
Cadmium	0.94	0.16	0.93	0.94	0.13	0.87

In all cases, the R^2 values obtained for the data indicate a good linear trend. For the uptake of both the cadmium and the copper from the mixed metal solutions, the NSE values are poorer compared to their counterparts for coper and cadmium adsorbed from single metal solutions. NSE is a function of RMSE, and as such both measures are prone to be affected by the presence of outliers. From this analysis, although the NSE values for the copper and cadmium uptake from a binary solution indicate that the model has a "good" fit to the data, in this instance the conclusions from the R^2 values have the greater bearing. All models can be concluded to represent the experimental data with high accuracy.

6.2.3 Elovich Model

6.2.3.1 Chlorella vulgaris

Figure 55 below shows the linearised sorption kinetics for copper and cadmium adsorption by *C. vulgaris* from a single metal solution and a binary metals solution.

Figure 55*a* and *c* contain data for the copper and cadmium adsorption experiments (respectively) by *C. vulgaris* from a single metal solution, as previously displayed in Figure 43*a* and *c*. Figure 55*c* and d show the linearised data for copper and cadmium uptake by *C. vulgaris* from a binary metal solution, respectively.

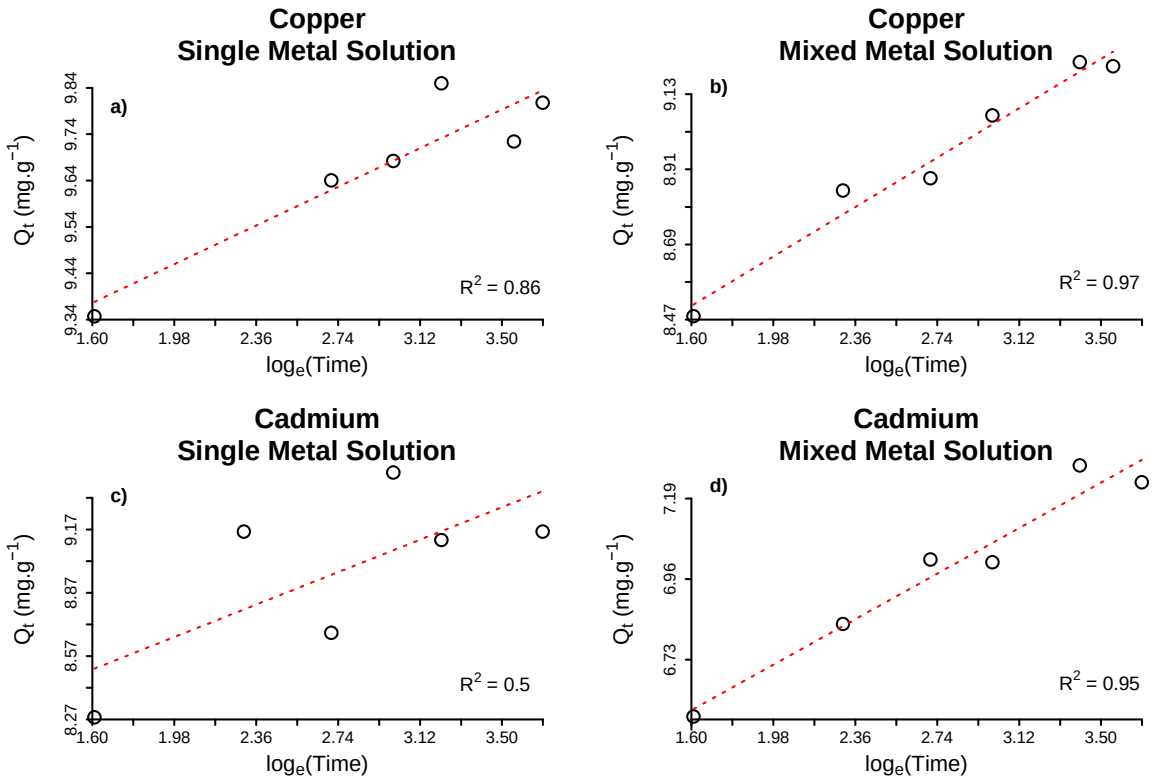

Figure 55: Linearised Elovich models to derive the initial estimates for the desorption constants (β_0) and the maximum adsorption rates (α_0) for the 2.5mgL^{-1} copper and cadmium uptake experiments by *C. vulgaris* from a single metal and a binary solution.

Figure 55*b* and *d*, show a good linear relationship between adsorption at time t, and the natural logarithm of the elapsed time. The R^2 value for copper adsorbed from a binary solution is 0.97; up from 0.86 for the R^2 value for copper adsorbed from a single metal solution. For cadmium the R^2 value is 0.96 for adsorption from a binary solution compared to 0.5 for cadmium adsorbed from a single metal solution.

The model constants; maximum adsorption rate, α and desorption constant, β obtained from Figure 55 are displayed in Table 56. These were inserted into the non-linear form of the Elovich model, given by Equation 5, and were plotted with experimental data in Table 56.

Table 56: Elovich model parameters (maximum adsorption rate, α and desorption constant, β), derived by linearising the Elovich model, comparing the values of copper and cadmium adsorption by *C. vulgaris* adsorbed from a single metal solution and a binary metal solution with a concentration of 2.5mg.L^{-1} of each metal ion.

	Single Metal Solution		Binary Solution	
	α (mg.g^{-1}.s^{-1})	β (g.mg^{-1})	α (mg.g^{-1}.s^{-1})	β (g.mg^{-1})
Copper	1.59×10^{17}	4.56	3.93×10^{7}	2.35
Cadmium	1.10×10^{8}	2.47	1.63×10^{7}	2.93

When t is greater than 0, all values of α multiplied by β, multiplied by t are substantially larger than 1; the lowest value for α is that obtained for cadmium adsorption by *C. vulgaris* from a binary solution, which is 1.63×10^{7} mg.g^{-1}s^{-1}, and the lowest value for β is 2.35g.mg^{-1} which was for copper adsorbed by *C. vulgaris* from a binary solution. This affirms the assumption made earlier that $\alpha\beta t >> 1$. In all cases the maximum adsorption rate is orders of magnitude larger than the desorption constant, β. This suggests that the propensity for adsorption is greater than the propensity for desorption [132].

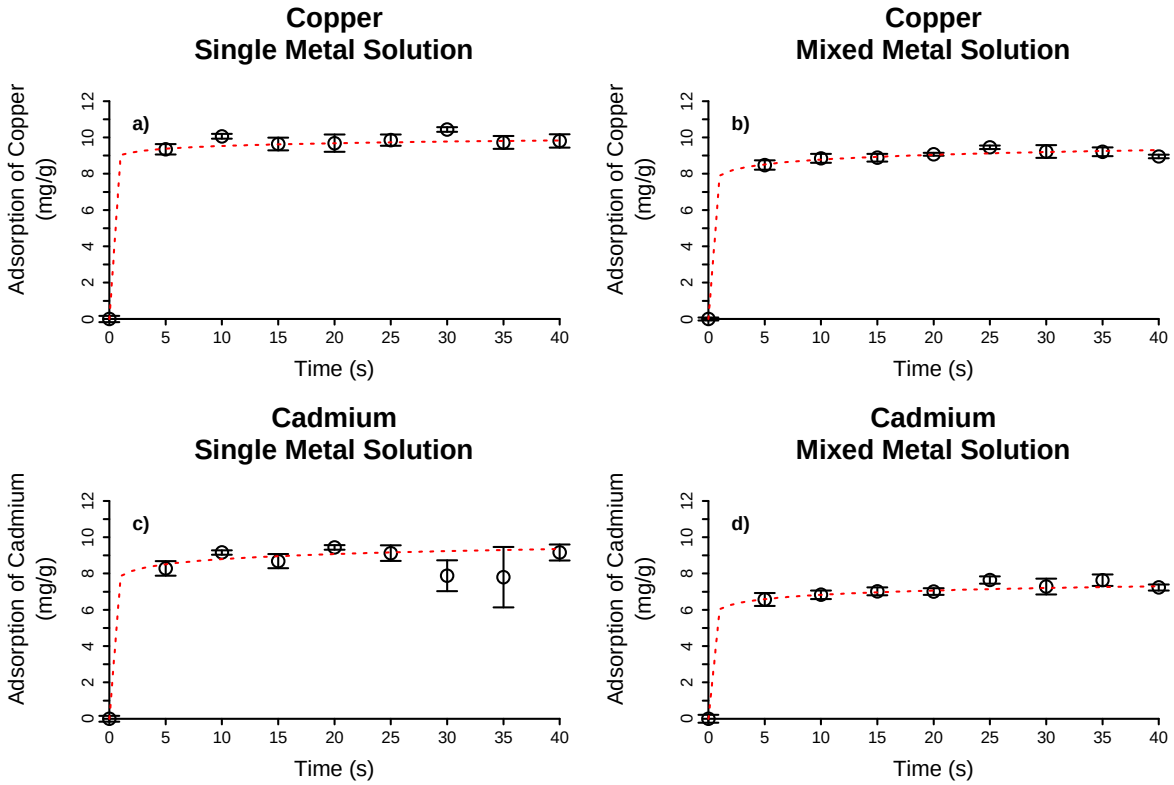

Figure 56: Adsorption-time profiles for copper and cadmium on *C. vulgaris* (open circles) vs Elovich model predictions using parameters obtained from linearized data (red dashed line), for copper and cadmium adsorption from single metal solutions and binary solutions.

The models represented in Figure 56 appear to follow the experimental data very accurately. The fit of the Elovich model is analysed by comparing the R^2 of the linear

charts Figure 55, and the RMSE and NSE values for the fit of the Elovich model to experimental data. These values are displayed in Table 57.

Table 57: R^2 values for the linearized Elovich model, and the RMSE and NSE values to determine accuracy of the Elovich model derived by linearizing the experimental data, for copper and cadmium uptake by *C. vulgaris*, from a single metal solution and a binary solution.

	Single Metal Solution			Binary Solution		
	R^2	RMSE	NSE	R^2	RMSE	NSE
Copper	0.86	0.29	0.87	0.97	0.17	0.95
Cadmium	0.5	0.25	0.91	0.95	0.21	0.87

The R^2 value for cadmium adsorbed from a single metal solution again shows poor linear correlation. To achieve the R^2 value of 0.5, outliers were removed. The Elovich model is susceptible to the presence of outliers as without their removal, the plot of Q_e against *ln(t)* was unable to produce values of α and β that was representative of the experimental data. All other models showed returned R^2 values greater than 0.85 for the linear plots indicating good correlation for the model. In all cases, analysis of fit for the non-linear Elovich model returned NSE values greater than 0.86 and RMSE values less than 0.3, which indicates that the Elovich models reflect the experimental data well. However, the profiles as represented by the Elovich models displayed in all charts in Figure 56 show that the equilibrium adsorption is reached prior to the 5s datapoint. No experimental data was obtained to confirm this, so in this case the Elovich model cannot be verified.

6.2.3.2 Scenedesmus obliquus

The final analysis for the modelling of the adsorption kinetics from a binary solution examined the uptake kinetics of *S. obliquus*. The *S. obliquus* concentration for the copper and cadmium adsorption experiments from a single metal solution had a concentration of 240mgL^{-1}, whereas the *S. obliquus* concentration for the mixed metal experiments had a lower concentration of 200mgL^{-1}.

The adsorption at time, *t,* was plotted against the natural logarithm of the elapsed time, and the data is presented in Figure 57. Figure 57a and c show the data for copper and cadmium adsorbed by *S. obliquus* from a single metal mixture respectively. Figure 57b and d show the data for copper and cadmium adsorbed from a binary mixture.

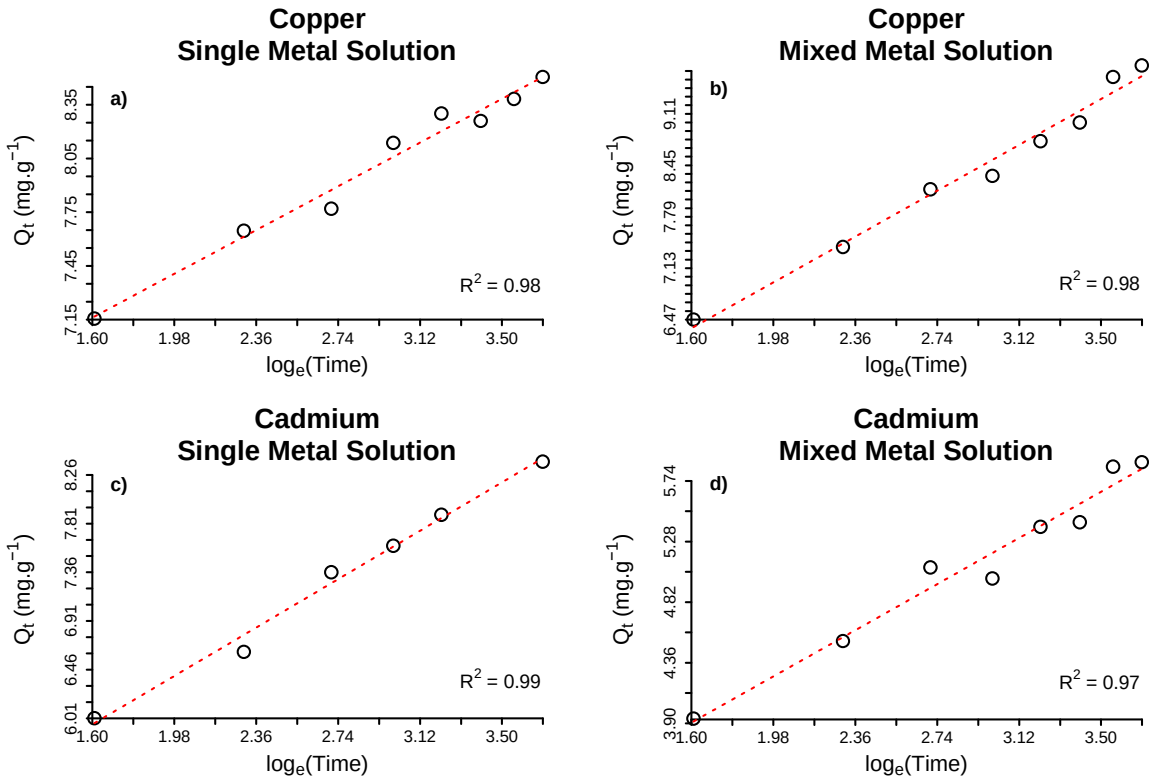

Figure 57: Linearised Elovich models to derive the initial estimates for the desorption constants (β_0) and the maximum adsorption rates (α_0) for the 2.5mgL^{-1} copper and cadmium uptake experiments by *S. obliquus* from a single metal solution and from a binary solution.

In all cases, the correlation coefficients show a strong linear relationship. The model parameters obtained from Figure 57 are displayed in Table 58.

Table 58: Elovich model parameters (maximum adsorption rate, α and desorption constant constants, β), derived by linearizing the Elovich Model. Model parameter estimates for 2.5mg.L^{-1} copper and 2.5mg.L^{-1} cadmium adsorbed by *S. obliquus* from single and binary metal solutions.

	Single Metal Solution		Binary Solution	
	α (mg.g^{-1}.s^{-1})	β (g.mg^{-1})	α (mg.g^{-1}.s^{-1})	β (g.mg^{-1})
Copper	8.87×10^{3}	1.55	19.01	0.65
Cadmium	37.24	0.85	12.87	1.08

The maximum adsorption rate (α), and desorption constant (β) vary significantly for *S. obliquus* when the metal ions are adsorbed from a single metal solution compared to a binary metal solution. The drop in the value of α from 8.87×10^{3}mg.g^{-1}s^{-1} for copper when adsorbed from a single metal solution to a value of 19.01mg.g^{-1}s^{-1} when copper is adsorbed from a binary solution, indicates that the presence of the cadmium slows the copper uptake considerably. Analysis of the α values for the cadmium, when adsorbed from a binary solution compared to a single metals solution (decreased from 37.24 mg.g^{-1}s^{-1} to 12.87 mg.g^{-1}s^{-1}), it appears that the presence of cadmium on the copper adsorption was not as significant compared the

effect that the presence of copper had on the cadmium adsorption. The desorption constant β however, indicates that the presence of copper has had a significant impact on the adsorption of cadmium. The value of β increases for the adsorption of cadmium from 0.85g.m^{-1} to 1.08g.mg^{-1}, together with the lower α value, indicating that the conditions for cadmium adsorption are less favourable compared to when copper was absent [183].

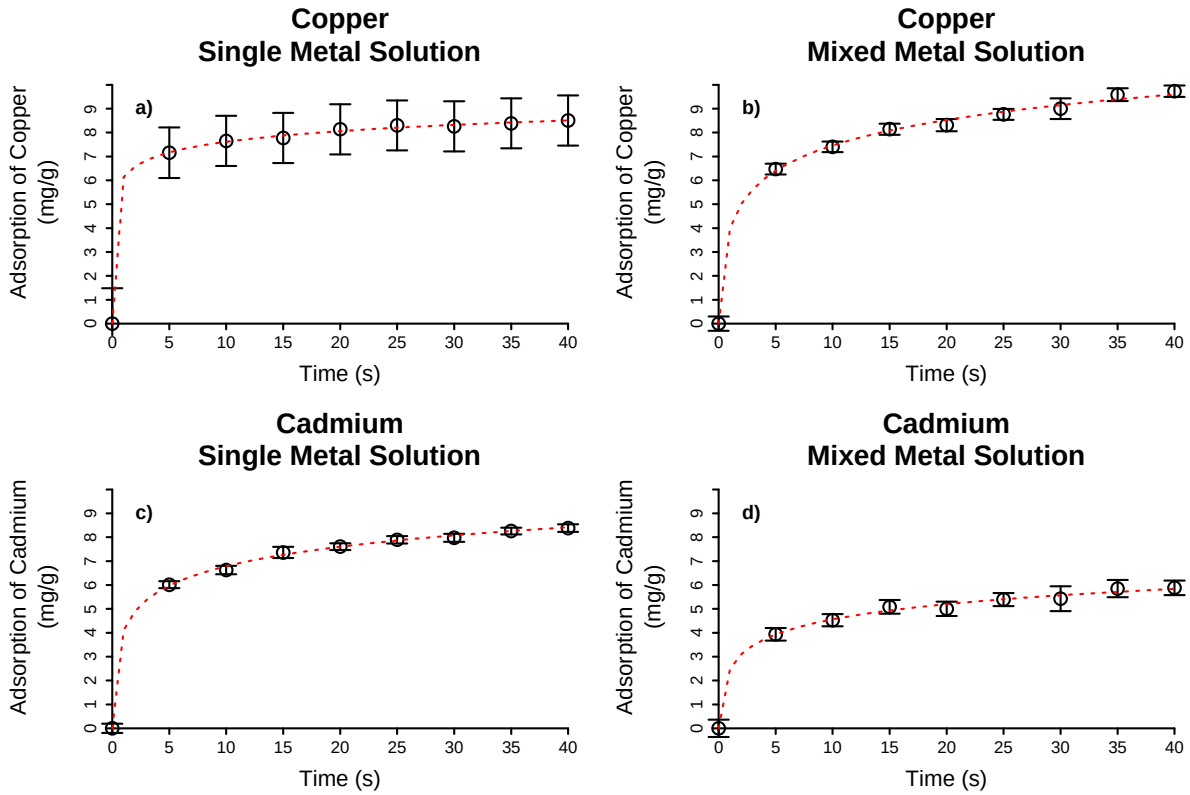

Figure 58: Adsorption-time profiles for copper and cadmium on *Si. obliquus* (open circles) vs Elovich model predictions using parameters obtained from linearized data (red dashed line), for copper and cadmium adsorption from single metal solutions and binary solutions.

The models displayed in Figure 58 both appear to fit the experimental data well. Figure 58a and d appear to show a sharper decrease in adsorption rate between 0s and 5s, compared to those charts shown in *b* and c. The effect of the smaller α value is apparent in the fact that equilibrium is not reached within the experimental timeframe. This would suggest the adsorption rate is indeed slower for adsorption in the presence of another metal. Comparing the data represented in Figure 58*c* to Figure 58*d*, it is difficult to discern a noticeable difference in the adsorption rate between the two datasets, as both datasets show Q_e increasing towards an equilibrium value which is not achieved within the experimental time period.

A comparison of the maximum adsorption rate of copper and cadmium by *S. obliquus* their corresponding values for *C. vulgaris* are shown in Table 59.

Table 59: Comparison of the Elovich maxim adsorption rates between *C. vulgaris* and *S. obliquus* for copper and cadmium when adsorbed from single metal solutions and binary metal solutions. The superscript * indicates values that were obtained after removing outlying datapoints. All units are of the form $mg.g^{-1}.s^{-1}$.

Single Metal Solution		
Metal	**C. vulgaris**	**S. obliquus**
Copper	1.59×10^{17}	8.87×10^{3}
Cadmium	1.10×10^{8}	37.24
Binary Metal solution		
Metal	***C. vulgaris***	***S. obliquus***
Copper	3.93×10^{7}	19.01
Cadmium	1.63×10^{7}	12.87

The values of α as displayed in Table 59 do indicate that the rate of adsorption for both metals is magnitudes higher for *C. vulgaris* compared to *S. obliquus* in all cases.

In the Elovich model parameters (α and β) for the *S. obliquus* experiments, the R^2 values for all charts displayed in Figure 57 indicated a strong linear correlation for the experimental data. The fit of the non-linear Elovich models using the parameters in Table 58 were evaluated by calculating the RMSE and NSE values for the models compared to the corresponding experimental datasets. These values are shown in Table 60.

Table 60: R^2 values for the linearized Elovich model, and the RMSE and NSE values to determine accuracy of the Elovich model derived by linearizing the experimental data, for copper and cadmium uptake by *S. obliquus*, from a single metal solution and a binary solution.

	Single Metal Solution			Binary Solution		
	R^2	RMSE	NSE	R^2	RMSE	NSE
Copper	0.96	0.06	0.99	0.98	0.13	0.96
Cadmium	0.99	0.07	0.99	0.97	0.11	0.92

In all cases, the results shown in Table 60 offer the highest R^2 and lowest RMSE and NSE values for any of the datasets. A clear comparison between the two algae species can be made with this model showing that the adsorption by *C. vulgaris* is far quicker than that of *S. obliquus* for copper and cadmium ions in solution.

The curves displayed in Figure 56 and Figure 58 must also be taken into account when judging the fit of the models. In all cases, in Figure 56 the adsorption has reached equilibrium before the second datapoint; this behaviour was not captured

by the experimental data and therefore cannot be verified. In Figure 58, equilibrium has not yet been reached, so the model appears to follow the experimental data well. However between the first and second data points in Figure 58a and d (and arguably c), the adsorption rate shows a significant decrease prior to the second datapoint. Without further experimental data for the behaviour between these two datapoints, the Elovich model cannot be verified.

6.2.4 Combined model for metal uptake

It has previously been established that *C. vulgaris* has a higher capacity than *S. obliquus* to both metals when adsorbed from a single metal solution. The sorption experiments investigating *S. obliquus* did not have comparable starting conditions. The single metal adsorption experiments used a higher algae concentration compared to the mixed metal experiments. As previously observed, the adsorption capacity of the algae is inversely proportional to the concentration of the adsorbent, therefore the mixed metal experiments will have a higher Q_e value compared to the single metal experiments [91, 93, 97]. For this reason, conclusions from the mixed metal sorption experiments for the *S. obliquus* compared to the single metal sorption experiments could not be definitively made. Figure 59 shows the co-adsorption of a mixture of copper and cadmium onto both algae species, with their second order models as derived in section 6.1.2.

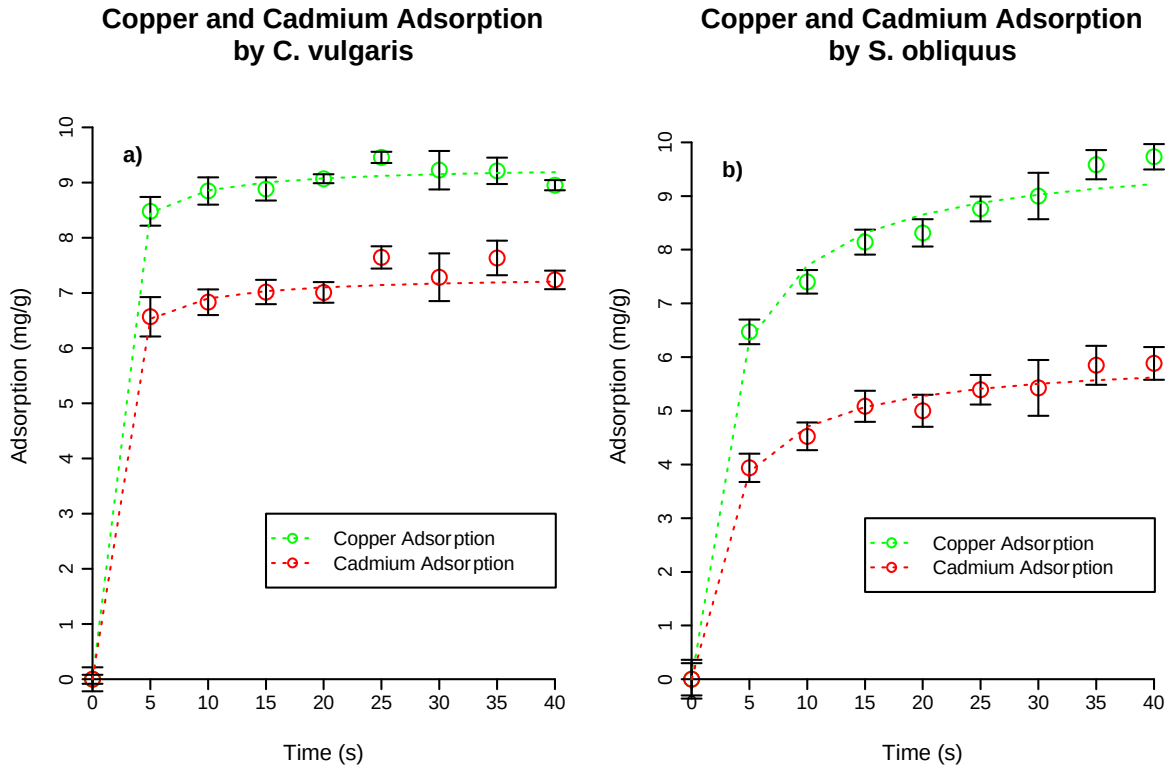

Figure 59: Adsorption-time profiles for copper and cadmium on *C. vulgaris* (open circles) vs Second order predictions for each metal. Red dashed line refers to the second order prediction for the cadmium uptake, the green dashed line refers to the second order predictions for the copper uptake.

Comparing Figure 59*a* to Figure 59*b*, the *S. obliquus* appears to have a higher capacity for copper than *C. vulgaris*. This is a demonstration of the effect of biomass concentration. The concentration of *C. vulgaris* was 250mg.L^{-1}, and the concentration of *S. obliquus* was 200mg.L^{-1}. Previous findings in this study and elsewhere [15, 19, 20] have found that, by decreasing the biomass concentration, the capacity of the biomass increases to the adsorbed metal. The driving force for adsorption appears to be a property of the solution, other than a property of the algae. The same quantity of metal ions are removed by fewer algae cells, with the capacity of the biomass to the adsorbed metal increasing with a decreasing biomass concentration.

The comparison between copper and cadmium uptake from a binary and single mixture by *C. vulgaris* are displayed in Figure 60, along with their second order models as derived in sections 6.1.2 and 6.2.2.1. The second order model parameters (Q_e and k_t) for these datasets are shown in Table 62. Figure 60 displays two charts, Figure 60*a* shows the uptake of copper by *C. vulgaris* from a single and a binary

mixture, and Figure 60*b* shows the uptake of cadmium by *C. vulgaris* from a single and binary mixture.

Table 61: Comparison between the second order model parameters derived by linearising the second order model, for copper and cadmium uptake by *C. vulgaris*, from a single metal solution, and a binary metal solution.

Metal	Single Metal Solution		Multi Metal Solution	
	Q_e (mg.g^{-1})	k (g.mg^{-1}.s^{-1})	Q_e (mg.g^{-1})	k (g.mg^{-1}.s^{-1})
Copper	9.85	0.37	9.31	0.22
Cadmium	9.41	0.17	7.52	0.17

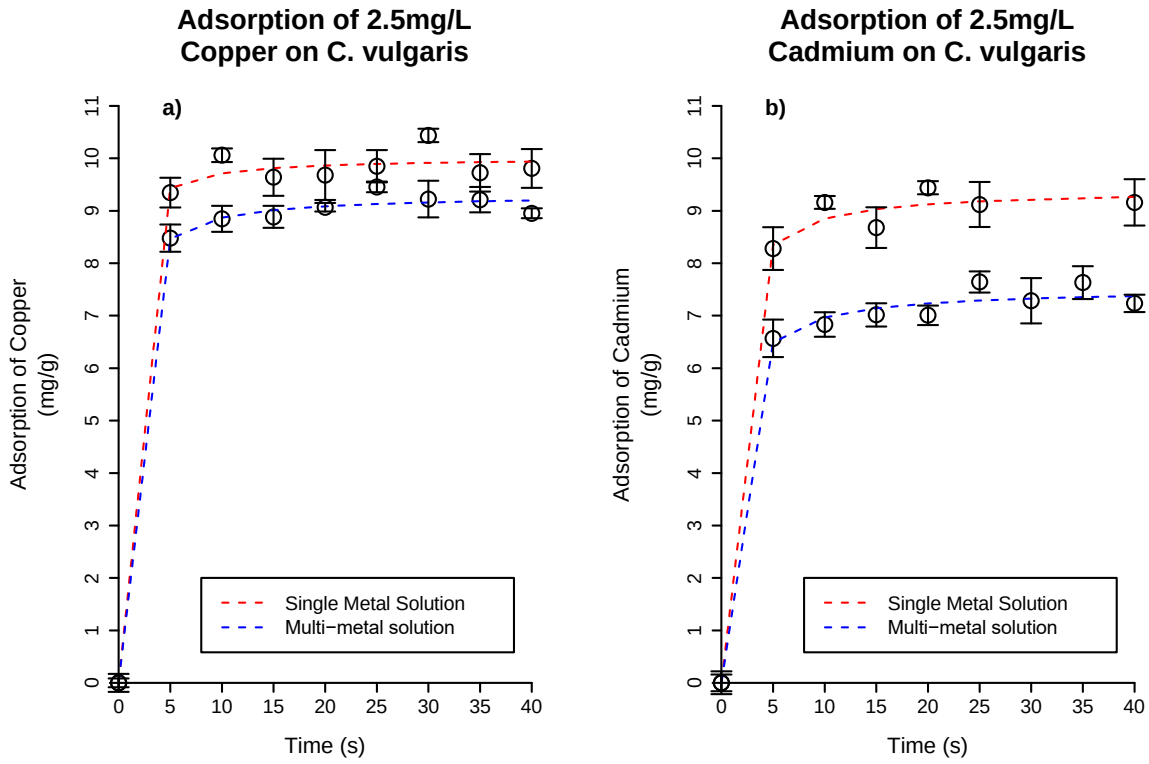

Figure 60: Adsorption-time profiles for copper and cadmium on *C. vulgaris* (open circles) vs Second order model predictions using parameters obtained from linearized data. Red dashed line refers to the predictions of the metal uptake from a single metal solution, blue dashed line refers to the uptake predictions from a binary metal solution.

Here the impact on each metal caused by the presence of the other is clearly demonstrated. The impact on cadmium adsorption is impacted to a greater extent by the presence of copper, than copper is affected by the presence of cadmium. Additive models were derived using all three of the models, but with the Lagergren, and the Elovich models being exponential models, the second order model was the only model out of the three that could be fitted this way.

The additive model for the second order model has the following structure:

$$Q_t = \frac{k_1 \,.\, {Qe_1}^2 \,.\, t}{1 + k_1 \,.\, Qe_1 \,.\, t} - \frac{k_{-1} \,.\, {Qe_{-1}}^2 \,.\, t}{1 + k_{-1} \,.\, Qe_{-1} \,.\, t} \quad (7)$$

Where:

- k_1 is the second order uptake rate of the metal species from a single metal solution ($g.mg^{-1}.s^{-1}$).
- Q_{e1} is the adsorption at equilibrium of the metal species when adsorbed from a single metal solution ($mg.g^{-1}$).
- k_{-1} is the inhibitory second order adsorption rate constant caused by the presence of the other metal species.
- Q_{e-1} is the inhibitory adsorption at equilibrium value caused by the presence of the other metal species.

The model was fitted using non-linear regression with R software, as equation 7 cannot be linearized. The model parameters are displayed in Table 62. These contain fitted parameters for k_1, Q_{e1}, k_{-1} and Q_{e-1}.

Table 62: Second order model parameters for the additive model to describe metal uptake from a mixed metal solution. RMSE and NSE values determine accuracy of the additive model to the current experimental data. These parameters are for the copper and cadmium uptake by *C. vulgaris*, from a binary meta solution.

	k ($g.mg^{-1}s^{-1}$)	**Qe ($mg.g^{-1}$)**	**k_{-1} ($g.mg^{-1}s^{-1}$)**	**Qe_{-1} ($mg.g^{-1}$)**	**RMSE**	**NSE**
Copper	0.33 (±0.21)	10.02 (±0.16)	-1.07 (±0.61)	0.72 (±0.08)	0.15	0.96
Cadmium	0.17 (±0.07)	9.41 (±0.20)	-12.45 (±208)	1.88 (± 0.18)	0.19	0.90

The additive models fit well to the experimental data with low RMSE values and NSE values greater than 0.9. However there are large errors associated with the fitted values for k_{-1} for both metals, but the standard error for k_{-1} for the cadmium uptake is an order of magnitude greater than the fitted value. Models using the parameters displayed in Table 62 are plotted alongside the corresponding experimental data in Figure 61.

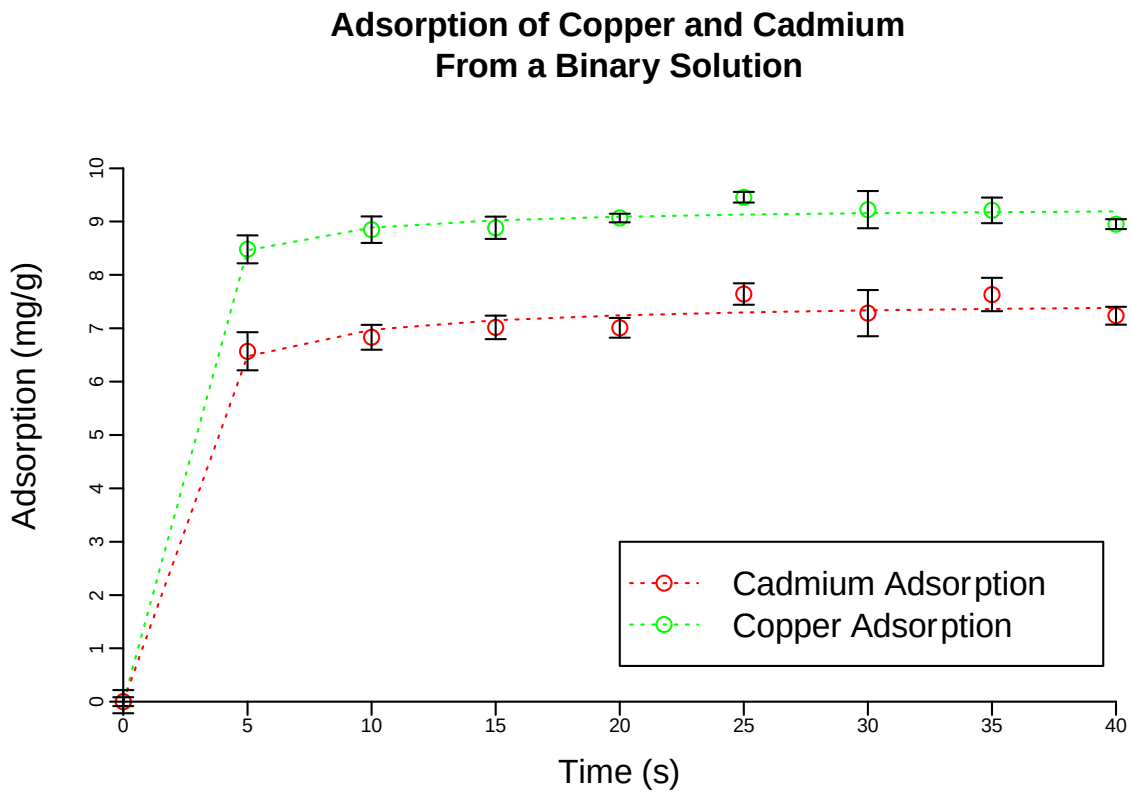

Figure 61: Adsorption-time profiles for copper and cadmium uptake by *C. vulgaris* from a binary metal solution (green open circles – copper, red open circles - cadmium), vs additive, Second order predictions using parameters fitted to the experimental data (dashed green line – copper predictions; dashed red line – cadmium uptake predictions).

The models show a good fit, however the information obtained from models focussing on the adsorption of each metal individually may be more useful. Without the additive model for the *S. obliquus* experiments for comparison, it is difficult to see the value in combining the models in this way; the adsorption by *C. vulgaris* is very fast, so the difference in adsorption at equilibrium (Q_{e-1}) is the only information that can be extracted. The adsorption by *S. obliquus* is more gradual in comparison, and it would be interesting to investigate any change in uptake rates caused by the presence of a co-adsorbent.

Without performing mixed metal isotherm studies, the Langmuir kinetics could not be derived for the mixed metal uptake data. Further work could be done in this area to derive kinetics from the Langmuir rate equation for mixed metal adsorption systems.

6.3 Adsorption Kinetics Chapter Summary

This chapter investigated four rate models used to measure adsorption kinetics of copper and cadmium by *C. vulgaris* and *S. obliquus* from single metal solutions.

These models were the Lagergren model (also known as the pseudo first order model), the second order model that was adapted from the Lagergren model, the Elovich model, and the Langmuir rate model.

Two species of microalgae, *C. vulgaris* and *S. obliquus* were exposed to solutions containing 2.5mgL^{-1} of copper, 2.5mgL^{-1} of cadmium and a solution containing a mixture of 2.5mgL^{-1} of copper and 2.5mgL^{-1} of cadmium.

All Lagergren, second order and Elovich models could be rearranged to a linearized form, to obtain the model parameters. This process worked well for the second order model and the Elovich model, in that the parameters obtained from both models were able to represent the experimental data well, when the models were reverted to their non-linear arrangement. The only issue with this method for deriving parameter values for the Elovich model arose when there were outliers in the experimental data; these needed to be removed before accurate model parameters could be derived.

There were no cases where the utilisation of the linear form of the Lagergren model was able to produce accurate model parameters to fit the experimental data. In all cases the models underestimated adsorption at equilibrium. The model parameters were used as initial estimates to successfully fit the non-linear form of the Lagergren model to the experimental data, by applying the non-linear least squares algorithm using the statistical software, *R*.

The second order model was found to be the most effective and robust model to derive adsorption kinetic parameters from the experimental data. Even when the linear form of the second order model did not show a strong correlation for the experimental data, it was still able to produce model parameters that could represent the experimental data without further model fitting using R. The second order model was not affected by the presence of outliers in the dataset, and the uptake rate, and adsorption at equilibrium could be obtained from the models.

The Langmuir kinetics can be utilised as a first order model, second order model or a hybrid model containing both a first order term and a second order term. Adsorption of cadmium by *C. vulgaris* could be modelled by the hybrid form of the

Langmuir Equation, whereas the adsorption of copper and cadmium by *S. obliquus* was best represented by the first order form of the Langmuir kinetics, although the rate constant of the Langmuir model was too small to represent the experimental data. The Langmuir Isotherm could not be produced for the copper adsorption by *C. vulgaris*, so the Langmuir kinetics could not be fitted to this experiment.

C. vulgaris had a very rapid adsorption profile for both metals tested; when adsorbed from a single metal solution and a binary solution. This made it more difficult to fit a curve as in all cases the process was complete within the first five seconds and so the kinetics of the process were not captured. The *S. obliquus* on the other hand had a more gradual adsorption profile, which allowed determination of such data to be determined more accurately.

The presence of a second adsorbent reduced the capacity of the *C. vulgaris* to each metal, but the rate did not appear to be affected. An additive model was created for the adsorption of copper and cadmium by *C. vulgaris*, but further work is needed to derive the kinetics for mixed metal systems.

Chapter 7 Immobilised Algae Biocomposites

Algae was immobilised in paper biocomposites using the technique described in *Ekins-Coward et al* [170]. This technique had previously been used to immobilise the photosynthetic bacterium *Rhodopseudomonas palustris*, and sustained it for the purposes of biohydrogen production for more than a month [174].

The idea was to create a synthetic *"leaf"* [188] that would be able to photosynthesise while removing metals from contaminated waters. Metals would then be recovered from the biocomposite using dilute EDTA solution [25]. This would be an immobilised system, similar AlgaSorb® [28], but having the advantage of using live microalgae.

7.1 Preliminary Results for Cadmium Adsorption by Immobile Algae

Paper biocomposites were created with an algae biomass content of 3.2mg.cm^{-2}. A separate biocomposite was created for each algae species. A control biocomposite was created without algae biomass but containing a greater mass of softwood and hardwood pulp. The compositions by mass of the algae biocomposites and the control biocomposites are shown in Table 63.

Table 63: Mass of MFC, Softwood Pulp, Hardwood Pulp, Algae biomass and volume of chitosan solution required to create the biocomposites, and comparison paper controls. Both recipes produce a paper with equivalent mass.

Paper	Mass MFC Pulp (g)	Mass Soft Wood Pulp (g)	Mass Hard Wood Pulp (g)	Mass of Algae (g)	Volume of Chitosan (mL)
Algae	29.7	87.8	87.8	0.2	7.5
Control	29.7	121.1	121.1	0	7.5

One set of experiments were undertaken to test whether the biocomposites offered any advantage over paper for the removal of cadmium ions from contaminated deionised water. The algae biocomposite paper, and a control paper were exposed to 0.2mg.L^{-1} cadmium solution in deionised water, pH 6.

The concentration of cadmium remaining in solution is plotted against time, and data for the control, *C. vulgaris* and *S. obliquus* are displayed in Figure 62.

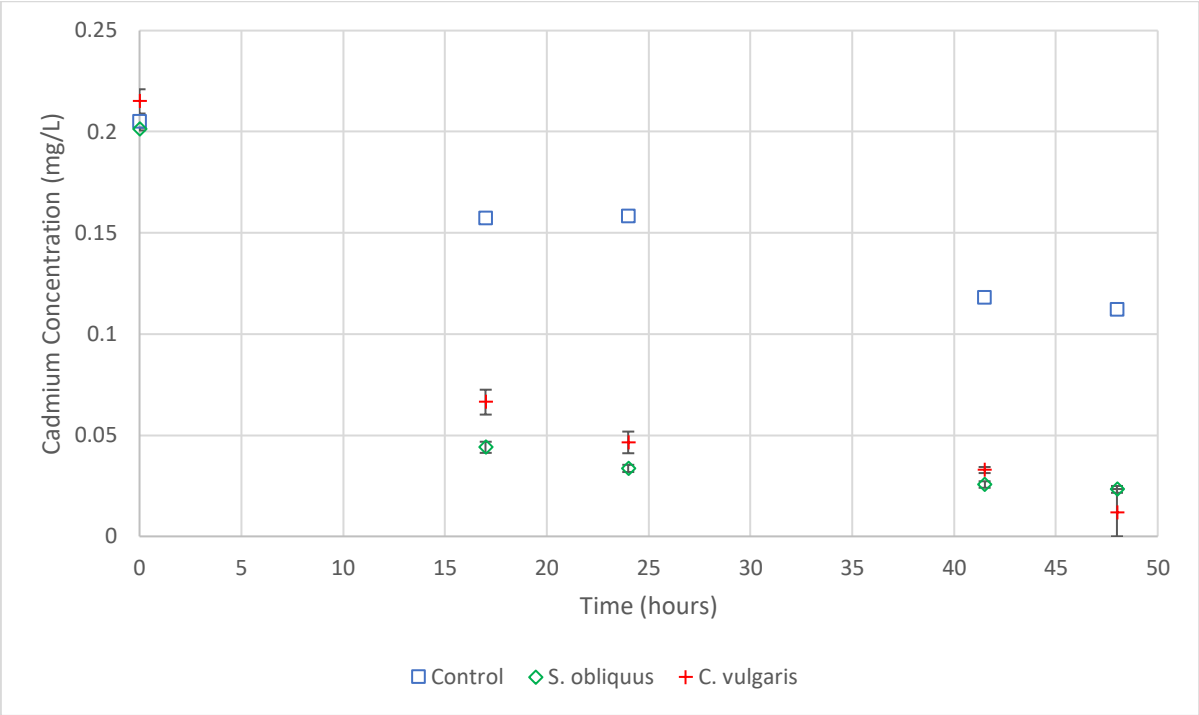

Figure 62: Cadmium removal by 1) paper biocomposite (blue squares), containing no algae biomass; 2) *S. obliquus* paper biocomposite (green diamonds) and 3) *C. vulgaris* paper biocomposite (red crosses).

The data presented in Figure 62 show a reduction in cadmium concentration from 0.2mg.L^{-1} to 0.11mg.L^{-1} for the control experiment with no algae biomass present within the biocomposite. The paper containing embedded *C. vulgaris* reduced the cadmium concentration within the bottle from 0.2mg.L^{-1} to 0.01mg.L^{-1}, and the paper with embedded *S. obliquus* reduced the cadmium concentration from 0.2mg.L^{-1} to 0.02mg.L^{-1}.

The presence of algae within the biocomposite has a clear positive effect on the cadmium removal when compared to the paper biocomposite without embedded algae biomass. The results presented in this section were preliminary results and they indicate a proof of concept that the presence of algae biomass improves the cadmium binding performance of the biocomposites. Further studies would be necessary to further investigate the potential of the technology.

Chapter 8 Study Using Industrial Wastewater

Bran Sans have operated an anaerobic digestion plant since 2010 for biogas production to power unit operations on site. The biproduct of this process is a sludge with a high suspended solids content, and also a high ammonia concentration. During the winter months, the high ammonium concentration is problematic for the activated sludge process, so a pilot study was set up to investigate the potential of a precursory algae-based unit operation for the treatment process.

Following the anaerobic digestion, the digestate was centrifuged to remove the larger solids, and the centrate was transferred to a settling tank. This centrate had a copper concentration that ranged from 2.5mg.L^{-1} to 5mg.L^{-1} of dissolved copper. The cadmium concentration was negligible.

A species of *Oocystis* sp. was isolated on site, and two bioreactors were selected for the pilot scale study, a high-rate algae pond and a tubular photobioreactor. In addition, three lab-based studies were undertaken at 1L, 5L and 10L batch volumes.

8.1.1 Bench Scale Analysis

The experiment was conducted in three different volumes in a batch setup. The centrate was passed through a sequential water filter system to remove any solids that had not settled. The algae cultivations were undertaken at a temperature of approximately 23°C, under an eight-hour light, sixteen-hour dark cycle. These experiments were undertaken within a new lab, and resources weren't available to monitor algae growth until the final stages of the project.

Biomass concentration and proliferation was therefore not recorded during the bench scale experiments. The ammonia and copper concentrations were recorded in Figure 63, Figure 64 and Figure 65, for the cultivation at 1L, 5L and 10L respectively. The cultivations were undertaken over a longer time period compared with previous metal experiments, to capture the ammonium removal. The intended purpose of the algae unit operation is to reduce the ammonia concentration by up to 80%.

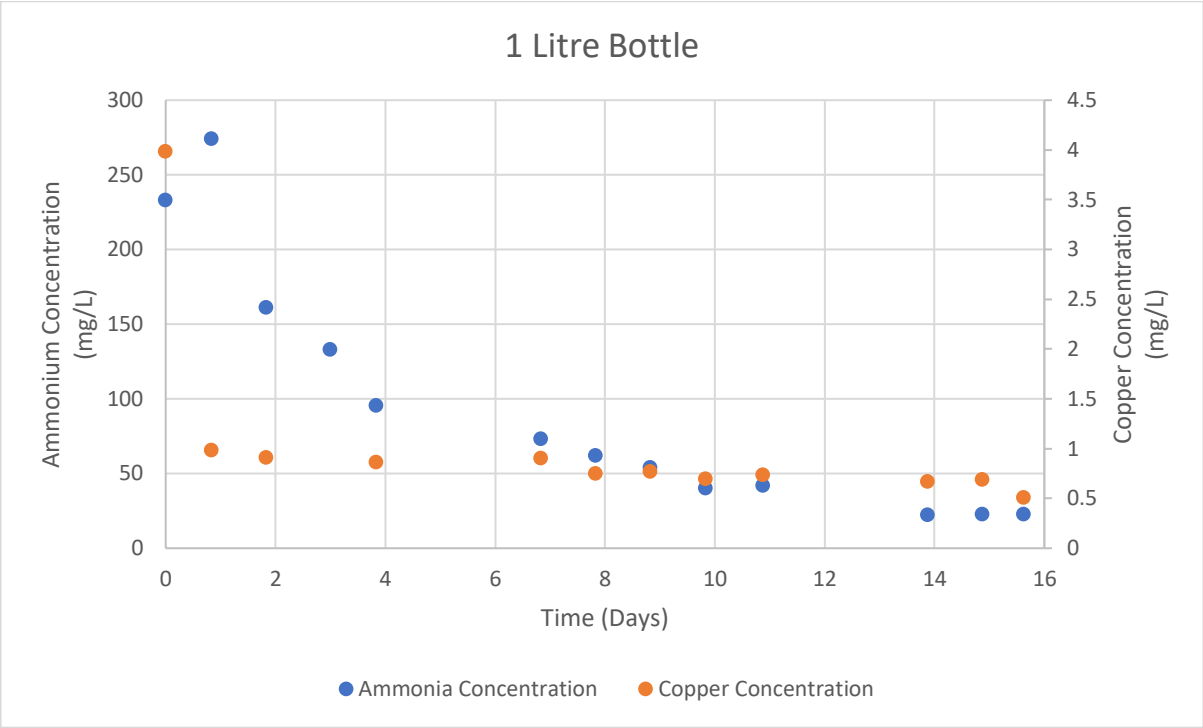

Figure 63: The concentration, time profiles of copper ions and ammonia being consumed by *Oocystis sp.* by a cultivation undertaken in a 1L bottle.

The data presented in Figure 63 shows the initial concentration of ammonia for the 1L experiment was between 250 and 300mg.L^{-1}. There was a slight increase in concentration between the first and the second data point which can be attributed to the mixing within the bottle. The copper concentration reduced very rapidly, within the first day whereas the ammonium concentration took approximately eight days to be reduced by 80%.

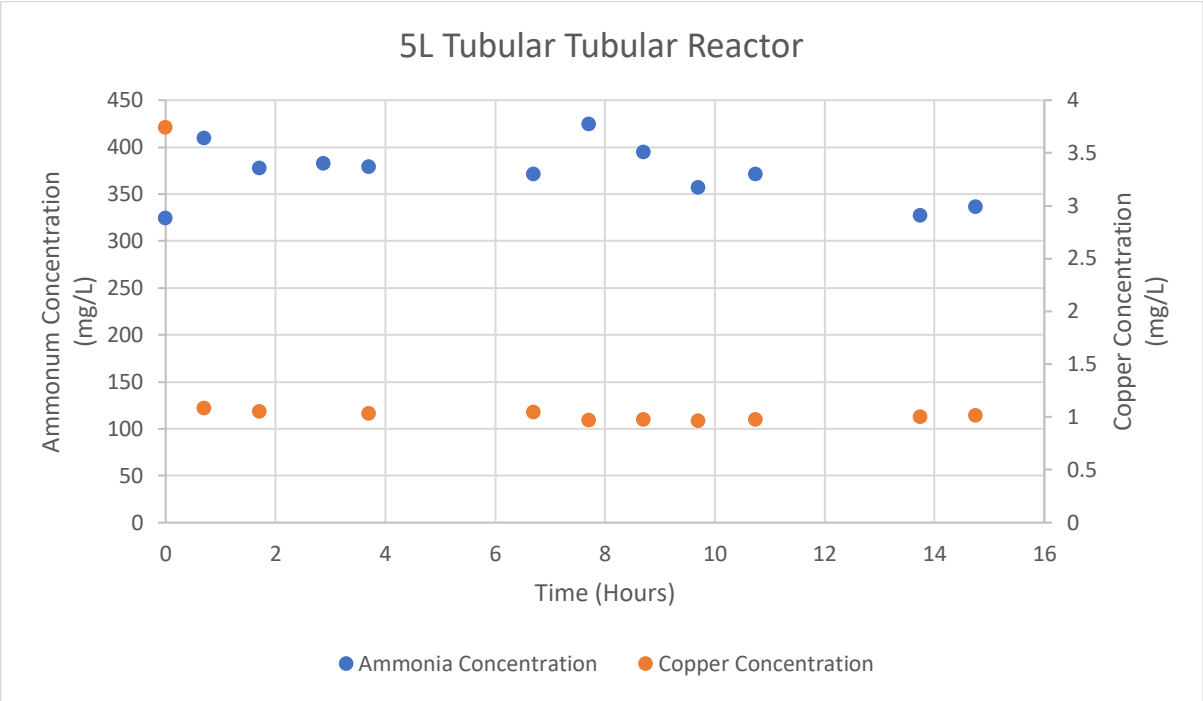

Figure 64: The concentration, time profiles of copper ions and ammonia being consumed by *Oocystis sp.* by a cultivation circulated in a 5L tubular reactor.

The data presented in Figure 64 suggests that the *Oocystis sp* was not proliferating within the 5L tubular reactor. The ammonium concentration was higher than that shown in Figure 63. The concentration of the centrate is dependent on the feed to the anaerobic digester which varies daily. The copper concentration was reduced during the first day, which was likely to have been caused by surface adsorption. The ammonium concentration did not reduce significantly, remaining around 350mg.L^{-1}.

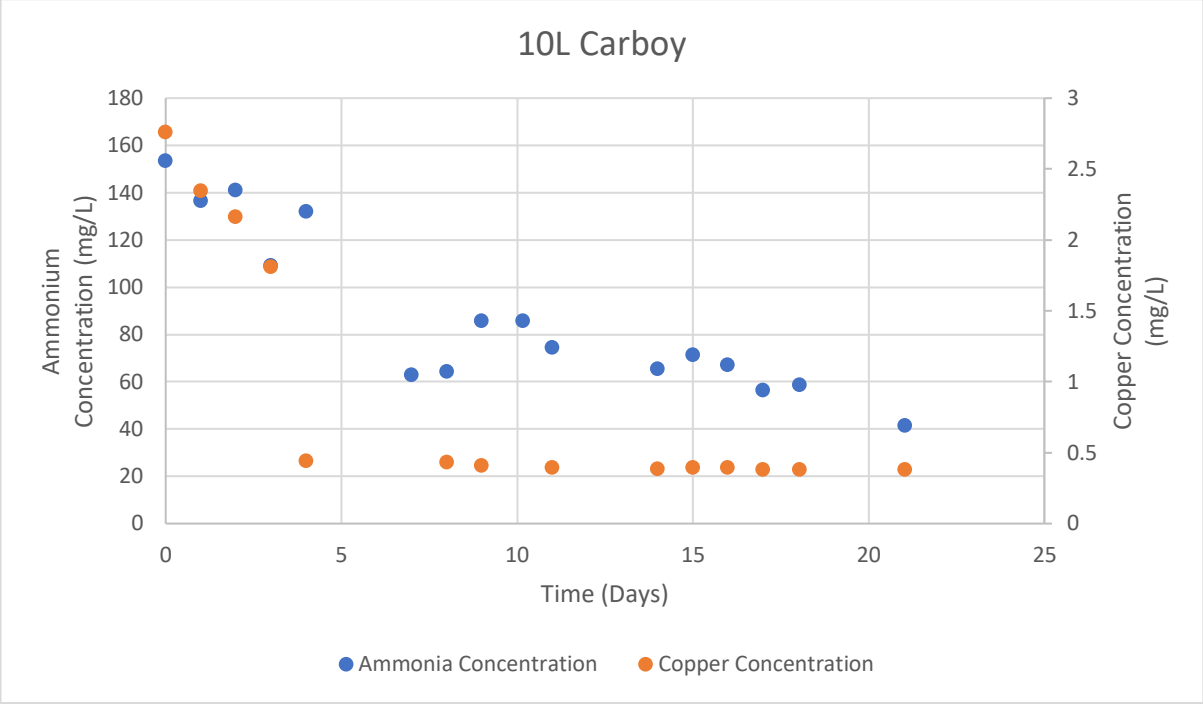

Figure 65: The concentration, time profiles of copper ions and ammonia being consumed by *Oocystis sp.* by a cultivation undertaken in a 10L carboy.

The final benchtop experiment produced the data displayed in Figure 65. This culture was exposed to lower concentrations compared to the studies displayed in Figure 63 and Figure 64. The copper removal in Figure 65 was more gradual compared to the other two experiments. In this experiment, mixing was supplied by aeration using a fish-tank pump, as it was for the 1L bottle experiment (Figure 63). The 5L tubular reactor was constantly circulated using a peristaltic pump at $1L.min^{-1}$, with additional aeration supplied using a fish-tank pump. The cultivation in the 10L carboy would not have been agitated to the same extent as the 1L bottle or the 5L tubular reactor, which will account for the slower uptake rate of the copper.

After three weeks, the ammonium concentration had dropped by 75%. This may not be quick enough for a functioning algae unit operation, but there is potential for optimisation.

In all experiments, the biomass concentration was unknown. Future optimisation experiments should investigate the effect of a higher initial biomass concentration and dilution factors for ammonia removal rate. It would be beneficial to investigate the ammonium removal rate, and growth rate of the *Oocystis sp*. by fitting Monod kinetics. This will assist in theoretical reactor design for upscaling the bioreactors.

8.1.2 Pilot Scale Study

The pilot scale experiments were conducted at a volume of approximately 160L. At this scale the biomass growth was monitored by measuring the dry weight of 100mL of sample taken from each reactor. This volume was filtered through a pre-weighed 0.22μm filter, which was dried for two hours at 80°C, and re-weighed. The difference in mass was multiplied by 10 to obtain the dry weight in units of $mg.L^{-1}$.

Initial experiments compared the two pilot scale bioreactors for algae cultivation. Freshwater F/2 medium was initially used to cultivate the *Oocystis sp.* for ten days, and on the tenth day the centrate was fed into each reactor at 250mL per hour. The effluent from the bioreactor was controlled by a solenoid valve, and the liquid level was maintained by addition of process water from the mains supply.

The effluent discharge of the HRAP failed on day 22 of the experiment, causing the reactor to be constantly diluted with process water from that day forward. There were no flow sensors on the process water or HRAP discharge at the time, so this went unnoticed during the first study. The biomass growth of both reactors are displayed in Figure 66. The photobioreactor appeared to be more effective when cultivating the sessile cell cultures. Initially the cultures were cultivated in freshwater f/2 medium, but after ten days the feed was switched on to add 250mL per hour feed. This resulted in an accelerated growth in the PBR, but the effect on the HRAP was less pronounced.

As with the bench scale experiments, the copper and the ammonium content of the reactors was also monitored over time. However after four and a half weeks the algae population within the PBR began to decline. It has since died and the trial needs to restart.

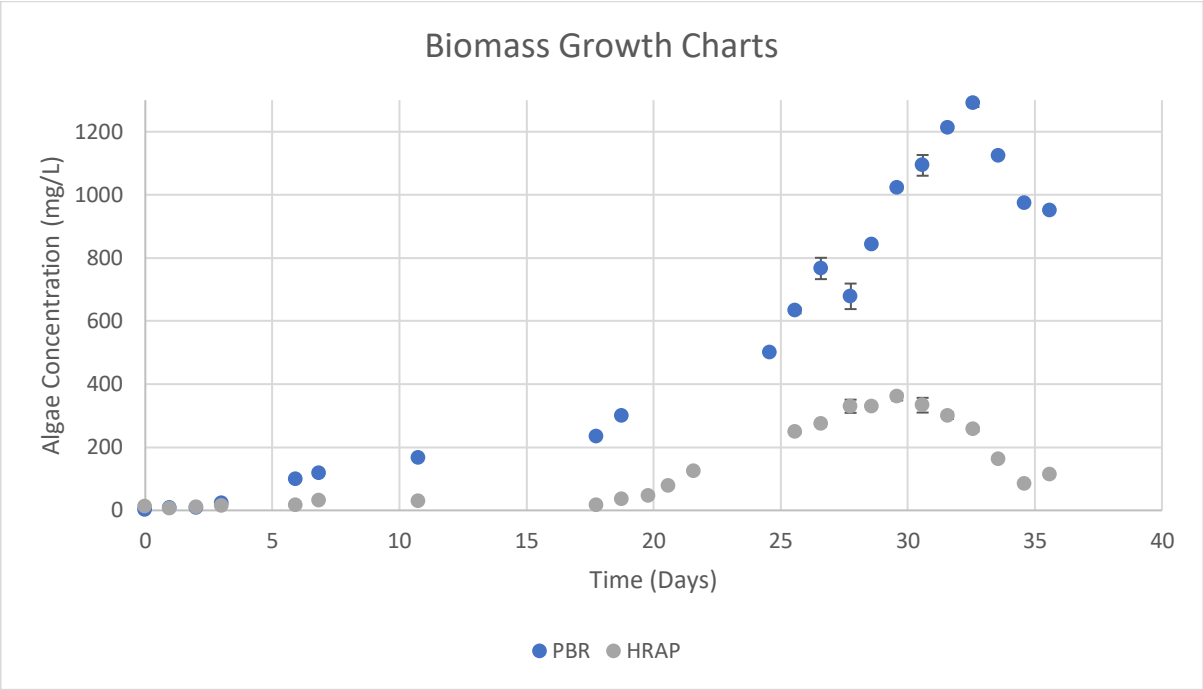

Figure 66: Comparison of the growth of *Oocystis sp*. in the tubular PBR (solid blue circles), and the HRAP (solid grey circles), over a thirty-six-day period. On the tenth day, the centrate feed was switched on at a feed rate of 250mL per hour.

The biomass growth appears to be more favourable in the PBR, with a greater increase of biomass following the initiation of the centrate feed into the reactors. However on day 22, it appears that the effluent discharge mechanism of the HRAP failed, so from this point onwards, the HRAP was discharging at a rate of 1L per hour. As the level in the HRAP was maintained with addition of mains water, from day 22 the reactor was being constantly diluted with freshwater.

The addition of the centrate promoted the biomass growth in both the HRAP and the PBR, although the two reactors cannot be directly compared due to the discharge failure of the HRAP. The biomass concentration within the PBR increased until the thirty second day, until the concentration began to decline. There are two possible reasons for this, the first is that the experiment was undertaken in winter, and the external temperature may have dropped too much for the heater to overcome the low temperatures, or the ammonia concentration within the reactor may have become too high from the centrate feed.

Figure 67 and Figure 68 display the charts that contain the time profile for ammonia and copper concentration within the PBR and the HRAP, respectively. The concentrations were recorded from day ten onwards, from the initiation of the feed.

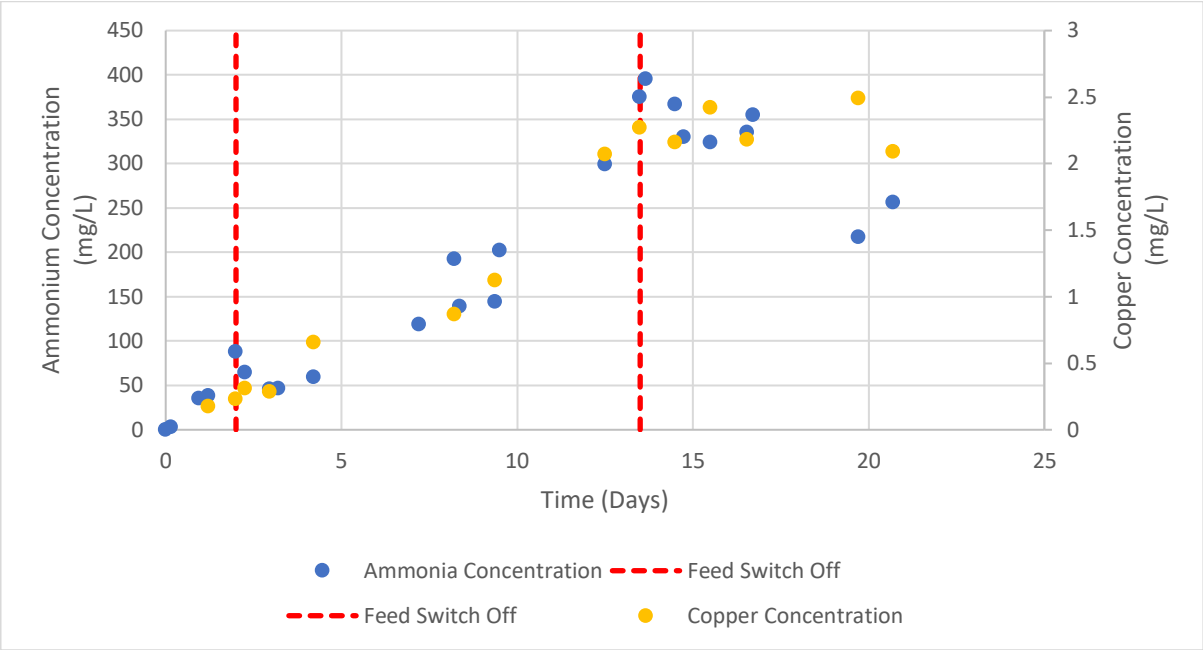

Figure 67: Variation of copper concentration and ammonium concentration over time in photo bioreactor fed at 250mL per minute.

The feed to the PBR was switched off at two periods of the investigation; the first switch off occurred on day two as the ammonium concentration reached 100mg.L^{-1}. The concentration rapidly decreased over the next twenty-four hours, so the feed was started again and maintained until the thirteenth day where the ammonia concentration reached 400mg.L^{-1}. The feed was switched off once more to allow for the culture to reduce the concentration ammonia, but before the feed was switched back on the temperature control encountered a fault and the culture within the PBR crashed and had to be recovered.

The feed for the high rate algal pond (HRAP), was kept at a constant flowrate of 250mL per hour and the concentration time profile is shown in Figure 68.

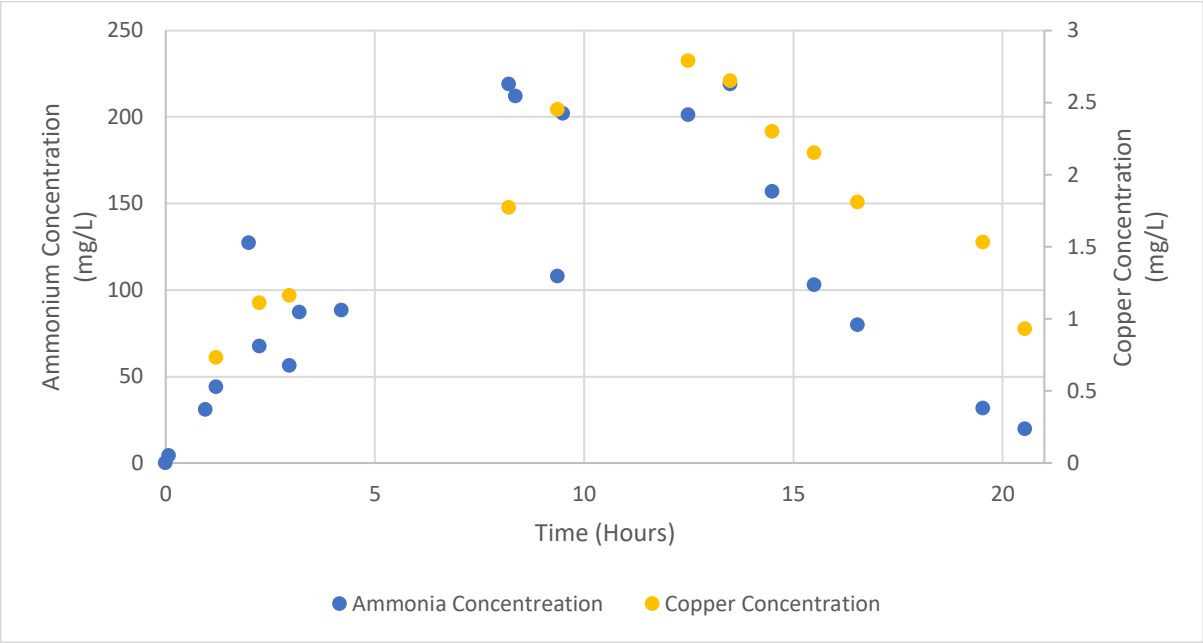

Figure 68: Variation of copper concentration and ammonium concentration over time in High Rate Algae Pond, fed at 250mL per minute. After 300 hours the filtration system failed.

The concentration of copper and ammonium present within the HRAP increased steadily until the twelfth day when the copper concentration reached a maximum of 7.79mg.L^{-1}, and the ammonia concentration was 201mg.L^{-1}. It is this day where it is likely that the solenoid valve that controlled the HRAP discharge failed open causing the HRAP to discharge effluent at a rate of 1L per hour. From this point forward the HRAP had a constant inlet stream of mains water that diluted the reactor. The discharge was through a cross-flow filter that retained the algae biomass and discharged the treated/diluted effluent only.

The data presented in Figure 67 and Figure 68 indicate that the removal rate of the ammonia and copper by the *Oocystis sp*. is too slow to overcome the feed rate of 250mL per hour. Comparing the two reactors, by design the PBR has the better temperature control due to the thin film flow in the HRAP. For this reason it is expected that optimal growth conditions are more easily maintained in the PBR. This is reflected in the growth data of Figure 66.

8.1.3 Summary of Chapter

This work was part of a project that was two technologies for wastewater treatment using microalgae. The results displayed were from a start-up trial to gain familiarity with the equipment, and also a bench scale investigation into ammonium removal

and copper removal from a batch process. This trial was conducted mid-winter so the environmental conditions were sub-optimal, but both the HRAP and the PBR were able to be used for cultivating the *Oocystis sp* using freshwater F/2 media.

The results from the batch scale experiments at a 1L volume and a 10L volume demonstrated rapid copper removal with copper removal after one day for the litre experiment and four days for the 10L experiment. The ammonium removal took longer, with the 1L experiment taking ten days and for the 10L experiment the ammonia concentration was still reducing by day 21.

There is still a lot of investigation to be undertaken with the treating of the centrifuged anaerobic digester effluent using *Oocystis sp*. In 10L bench-scale batch studies, the ammonium content is reduced by 60% after seven days. When investigating the concentration of the *Oocystis sp.* within the PBR, the biomass concentration peaked at approximately 1.3g.L^{-1}, while being continuously fed with digested centrate. It would have been beneficial to have run the PBR until the ammonium concentration levelled off and then subsequently measure the *Oocystis sp.* concentration. If this was possible, it would demonstrate the *Oocystis sp* could proliferate at a rate that equalled the feed input rate.

Chapter 9 Conclusions

The aim of this research was to investigate and model metal uptake by two species of microalgae from contaminated water. The algae selected were *Chlorella vulgaris* and *Scenedesmus obliquus*, and these were exposed to solutions contaminated with copper and cadmium ions.

In the initial stages of the project a procedure to investigate copper uptake by microalgae was developed. The preliminary studies mainly investigated copper sorption by *C. vulgaris*, but one study using *S. obliquus* was also performed. The initial experiments were performed at a 200mL batch scale, and produced one set of results that demonstrated a fast, initial metal uptake mechanism, followed by a slower secondary mechanism. The other results obtained from the 200mL batch experiments demonstrated difficulties with analysis using the ICP-OES. The sampling methodology was modified to ensure all samples had a similar pH to the calibration standards, and any future ICP analyses would require an internal standard to improve reliability of the analysis.

The focus of the investigation was directed to investigating the initial uptake mechanism of the microalgae. The procedure was modified so that small 4mL batches of microalgae solution and metal solution were contacted for short time intervals. This procedure investigated four different metal concentrations, which allowed for a rudimentary equilibrium study to be undertaken while investigating the effect of concentration on metal removal kinetics. The majority of these studies were undertaken using ICP-MS and the metal solution was created with deionised water as opposed to BG-11 medium.

The results demonstrated that adsorption capacity is a function of initial concentration of microalgae and initial concentration of metal ions in solution. A relationship was derived which showed that adsorption at equilibrium related linearly to the ration of the initial metal concentration to the initial algae biomass concentration. This relationship suggested that both species had a higher binding capacity to copper compared to cadmium, and that *C. vulgaris* has the highest binding capacity to copper, and *S. obliquus* has a highest capacity for cadmium. This

finding was proved false in later studies which demonstrated by direct comparison that *C. vulgaris* has a higher capacity to both copper and cadmium when adsorbed from a single metal solution, compared to *S. obliquus*. This is likely caused by experimental error caused by variations in algae biomass concentration during this analysis.

The adsorption capacity of the microalgae is greater when the metal ions are adsorbed from a pure solution than when the metal ions are adsorbed from growth medium, or from a binary metal solution. This would need to be taken into consideration when algae biomass is used to recover metals from real wastewater.

The extent of metal removal from the solution was not a function of biomass concentration, adsorption was driven by the concentration of adsorbate in solution. When copper was adsorbed by *C. vulgaris* biomass, the copper removal was approximately 90% of the copper ions present; this remained constant when the copper concentration was increased from 0.75mg.L^{-1} to 2.5mg.L^{-1}, and the *C. vulgaris* concentration was reduced from 500mg.L^{-1} to 240mg.L^{-1}. The cadmium removal by *C. vulgaris* was consistent for the three lower concentrations, but when the cadmium concentration increased from 0.75mg.L^{-1} to 2.5mg.L^{-1}, the extent of removal dropped from 95% to 84%. This suggests that the capacity of the *C. vulgaris* had been exceeded when the concentration of cadmium had increased to 2.5mg.L^{-1}.

The extent of metal removal by *S. obliquus* had a more complex pattern. The extent of copper and cadmium removal fell when the metal ion concentration was increased from 0.5mg.L^{-1} to 0.75mg.L^{-1}, but when the concentration was increased to 2.5mg.L^{-1}, the extent of removal increased. This is a mechanism that requires further investigation, but could suggest a cellular defence mechanism that is overwhelmed at higher metal concentrations.

Previous studies have fitted the Langmuir, Freundlich and Temkin Isotherms to equilibrium experimental data. In this study the adsorption was best described by the Freundlich Isotherm which returned an R^2 value for the linearised isotherm that was consistently above 0.98 for all datasets. The Langmuir Isotherm returned R^2

values greater than 0.9 for all datasets, however the parameters produced from the linear isotherm for the copper adsorption by *C. vulgaris* did not make physical sense; returning a negative value for the maximum adsorption capacity and the Langmuir constant. The Temkin Isotherm showed a poor fit for all datasets with the exception of the cadmium adsorption by *C. vulgaris*. The Temkin Isotherm is inappropriate for low and high adsorbate concentrations, while the Langmuir Isotherm works on assumptions that are not satisfied by the microalgae.

Kinetic data was then analysed and compared for the 2.5mg.L^{-1} copper and cadmium adsorption by *C. vulgaris* and *S. obliquus*. The three most common models found in literature were fitted to the experimental data, these were the pseudo-first order Lagergren model, the second order model and the Elovich model. All three models were fitted to the experimental data successfully by non-linear regression, but only the second order model and the Elovich model were able to be fitted by linearisation of the model. The second order model was considered to have the best fit, however the Lagergren model and the Second order model are often compared but rarely placed in theoretical context. Lui et al (2008) derived a form of the Langmuir kinetic equation that was a hybrid model containing both a first order term and a second order term.

When analysing the experimental data, the Langmuir kinetic equation could be simplified to the first order equation, where it shares its form with the Lagergren model, for the adsorption of copper and cadmium by *S. obliquus*. It wasn't possible to fit the Langmuir Isotherm to the experimental data for copper adsorption by *C. vulgaris*, but analysis of the data for the cadmium adsorption by *C. vulgaris* suggested that the Langmuir kinetic equation could not be simplified to either the first order or the second order model; for this data the hybrid model was successfully fitted to the experimental data. This suggests that the first order Lagergren model should not be discounted and when comparing the Lagergren model to the second order model, it is important to consider the theoretical background of the models when applying them to experimental data. It is not clear whether the Lagergren model or the second order model does have a theoretical basis, but this hybrid kenetic model that contains a first order and a second order component can be derived from both the Langmuir theory and the BET theory, but

previous researchers have acknowledged that information relating to the adsorption process cannot be directly interpreted from the rate equations.

There were two further preliminary studies undertaken during the PhD project.

1. The immobilisation of microalgae. Metal sorption by paper biocomposite was shown to improve with the presence of microalgae. This is a promising finding as immobilisation of the microalgae greatly increases the separation efficiency of algae from the treated wastewater.
2. A laboratory and a pilot scale study undertaken with an industrial partner, involving a species of *Oocystis* that was isolated from an industrial wastewater treatment plant. This species of microalgae was being investigated for its ability to remove ammonia from the wastewater, but it also was able to remove copper from batch solutions.

During the pilot-scale study a photobioreactor containing *Oocystis sp* had a continuous feed of anaerobic digestate. The feed rate in this study exceeded the rate of consumption of ammonia by the *Oocystis sp*, and also exceeded the rate of copper removal. Future studies should be undertaken to investigate the uptake rate of copper by *Oocystis sp*, so that the data can be compared to the data obtained for *Chlorella vulgaris*.

Overall it can be concluded that from a batch system, numerous species of microalgae are efficient metal chelators. The analysis undertaken demonstrates how the chelating properties of the microalgae can be compared so that suitable microalgae species can be selected when designing metal removal processes using microalgae. The metal uptake mechanism is very quick and can be modelled using a number of kinetic models, of which the Lagergren model and the Second order model are the most effective. These models are empirical, and their parameters are obtainable by using a variety of methods. These parameters have no bearing on the actual uptake mechanism of the microalgae.

Chapter 10 Further Work

This section summarises potential future studies arising from this PhD project. Detailed in this section are experimental plans to expand upon the investigations previously outlined within this thesis, and also other preliminary results of projects that could not be carried out to completion within the PhD period.

10.1 Adsorption Studies

The studies undertaken to date have mainly investigated a narrow biomass concentration range, and a low metal concentration, all at room temperature. In addition to these studies, a preliminary investigation was undertaken to immobilise *S. obliquus* and *C. vulgaris* in a paper biocomposite.

10.1.1 Sessile Algae

Future studies should involve repeating the experiments that were undertaken during this project, but varying the temperature and expanding the concentration range of the microalgae concentration and the copper and cadmium concentration. This will return parameters that will allow for the thermodynamics of adsorption to be calculated for each metal by each microalgae species.

The Van't Hoff equation is derived as follows:

$$\Delta G^{\circ} = \Delta H^{\circ} - T\Delta S^{\circ} \quad (1)$$

Where:

- ΔG° is the Gibbs free surface energy change (J).
- ΔH° is the change in system Enthalpy (J).
- T is the temperature (K).
- ΔS° is the change in Entropy (JK^{-1}).

The Gibbs free energy can be related to the equilibrium constant of the adsorption process is related to Gibbs free energy as follows:

$$\Delta G^{\circ} = -RT\ln(K_c) \quad (2)$$

Where:

- R is the universal gas constant ($Jmol^{-1}K^{-1}$)
- K_c is the equilibrium constant (dimensionless).

Equation 2 can be submitted in Equation 2, to produce the Van't Hoff equation:

$$\ln(K_c) = -\frac{\Delta H^{\circ}}{RT} + \frac{\Delta S^{\circ}}{R} \quad (3)$$

Previous studies have stated that K_c is equivalent to the Langmuir constant ($L.g^{-1}$) [90], the Freundlich constant ($mg.g^{-1}$)($mg.L^{-1}$)$^{-n}$ [189], and the Temkin constant ($L.g^{-1}$) [101, 113], at low concentrations. Although it may be true that they are numerically similar, K_c is a dimensionless constant so this is not without transforming the value to a dimensionless parameter [88, 90, 190]. Whereas some studies have just multiplied the isotherm equilibrium constants by values relating to density and concentration of pure water [88], others have concluded that the equilibrium constant is related to the activity of the adsorbate and the adsorption equilibrium constant [90, 190].

Another important thermodynamic parameter is the Isosteric heat of adsorption. This is derived from the Clausius-Clapeyron equation.

$$\frac{d\ln(C_e)}{dT} = -\frac{\Delta H_x}{RT^2} \quad (4)$$

$$\ln(C_e) = \frac{\Delta H_x}{R}.\frac{1}{T} + C \quad (5)$$

Where:

- ΔH_x is the isosteric heat of adsorption (J).
- C is a constant.
- C_e is the concentration at equilibrium ($mg.L^{-1}$)
- R is the universal gas constant ($Jmol^{-1}K^{-1}$)
- T is the temperature (K).

The isosteric enthalpy is the energy associated with the adsorption process. The isosteric enthalpy can give an indication of whether the process occurs via physisorption or chemisorption. If ΔH_x is less than $80kJmol^{-1}$, the process is physisorption, and if the process is between 80 and $400kJmol^{-1}$, the process is likely chemisorption [190]. The Gibbs free energy indicates the spontaneity of the adsorption process, if it is negative it indicates that the adsorption process occurs spontaneously [90].

10.1.2 Immobile Algae

Further experimentation can be undertaken to investigate the reusability of the algae-paper biocomposites by performing adsorption/desorption cycles and by creating the paper with *BG-11* medium instead of deionised water and perform tests to monitor the viability of the algae-paper biocomposites.

The adsorption of copper should be investigated in addition to cadmium, and the reusability of the biocomposite papers can be investigated by performing adsorption/desorption cycles, using EDTA to strip the bound metals.

The paper biocomposites were made using purchased, pre-purposed wood, future studies should investigate whether recycled wood chips or other lignocellulosic biomass to increase the sustainability of the production.

10.1.3 Continuous Removal Studies

The biocomposites, were potentially the basis a continuous system adsorption/desorption system. 64mm^2 discs were made using a hole punch, and these can be assembled into a series of units within specially 3D printed holders as shown in Figure 69.

Figure 69: 3D printed connector that can be disassembled to house the algae biocomposite paper, for continuous flow adsorption/desorption metal experiments.

The biocomposite disk would be housed in the centre, and the metal solution will be channelled through the paper. The connector was designed to join 8mm silicon tubing, and the units in principle could be arranged in series.

The idea behind this experiment was to produce a breakthrough curve as a first step in the design of an adsorption/desorption process.

10.2 Removal of Ammonium and Copper from Phase II centrate using a new *Chlorophyta, Oocystis sp.*

There are many avenues to explore with this study as there are numerous reactors being tested, at both a bench scale and a pilot scale. The most beneficial investigation would be a study into the maximum growth rate of the *Oocystis sp*. This would provide the means to select the feed rate of the reactors for future scale up projects.

The potential strategic outcomes for this study include:

1. Determination of the necessary retention time for an algae-based unit operation to reduce the pressure caused by ammonia concentration on the activated sludge process.
2. Determination of which reactor technology is most efficient and energy efficient.
3. Derivation of *Oocystis sp.* Monod growth kinetics with ammonia as the main substrate nutrient. Using synthetic wastewater, copper and cadmium ions could also be added to investigate the potential inhibitory effect on cell growth.
4. Adsorption experiments can be undertaken to compare the copper and cadmium capacity, and initial uptake rate of the metals by *Oocystis*.

10.3 Kinetics Studies

10.3.1 *S. elongatus* Comparison

The kinetics studies in this project have focussed on the metal uptake by *C. vulgaris* and *S. obliquus* which are both eucaryotic microalgae. Early on in the project, the cyanobacteria *Synechococcus elongatus* was also cultured with a view to investigate the cyanobacteria for its potential metal uptake properties. Due to issues with the ICP-OES, samples were sent for external analysis with ICP-MS. The budget could not accommodate all experiments so the focus was on *C. vulgaris* and *S. obliquus*. The uptake kinetics of *S. elongatus* (CCAP 1479/1A) would be an interesting comparison to the current study.

10.3.2 Long-term Metal Removal With Cell Growth

The experiments undertaken that investigated the secondary uptake mechanism of the microalgae were unsuccessful and incomplete. The relationship between adsorption at equilibrium and initial algae concentration and initial metal concentration is detailed already in this study. Experiments can be devised to now assume the first uptake kinetics, and the growth kinetics can then be monitored alongside with the nutrient and metal removal kinetics [191].

A 2^3 factorial design can be done to test for interaction between metal concentration and nutrient uptake. The test could investigate Nitrate, Phosphate and cadmium or copper uptake (metals tested separately), or a 2^4 factorial with the levels for each metal being 0 and 1mg.L^{-1}.

10.3.3 Kinetics Derived from Adsorption Isotherms

In Section 10.1.1, the hybrid form of the Langmuir Kinetic equation as derived by *Liu et al* (2008) [140], was applied to metal sorption data by microalgae. It was not possible to derive a model using this method for the copper adsorption by *C. vulgaris* as the Langmuir isotherm could not be fitted to the equilibrium data.

The adsorption isotherms were fitted using limited data in this study, and it would be valuable to repeat the adsorption equilibrium studies to obtain more accurate isotherms. The Langmuir kinetics has been rarely used and never to the author's knowledge has it been applied to metal sorption processes by microalgae.

A recent study by *Khomizov et al* (2018) [128] derived a hybrid kinetic model that had the same form as the model derived by *Liu et al*, from the BET isotherm. The authors of this study concluded that the adsorption mechanism could not be determined from the rate expressions stating that they are still classed as empirical. *Liu et al* [140, 142] and *Azizian* (2004) [138] have attempted to put the Lagergren model and the second order model into theoretical context, but further work in this area is necessary if this goal is to be achieved.

10.4 Life Cycle Assessment Study

The pilot project undertaken with Northumbrian Water Ltd (NWL), was funded with the intention for possible scale up to add a unit operation to relieve the ammonium load on the activated sludge (AS) process. The work described in this thesis was the beginning of a proof of concept study, however in addition to this study, prior to any scale up an environmental assessment and economic analysis should be undertaken to verify the theoretical feasibility of the process. Displayed in Figure 70 is the activated sludge process of Bran Sands, with a possible algae pre-treatment unit operation that will treat waste from the anaerobic digester prior to the AS process.

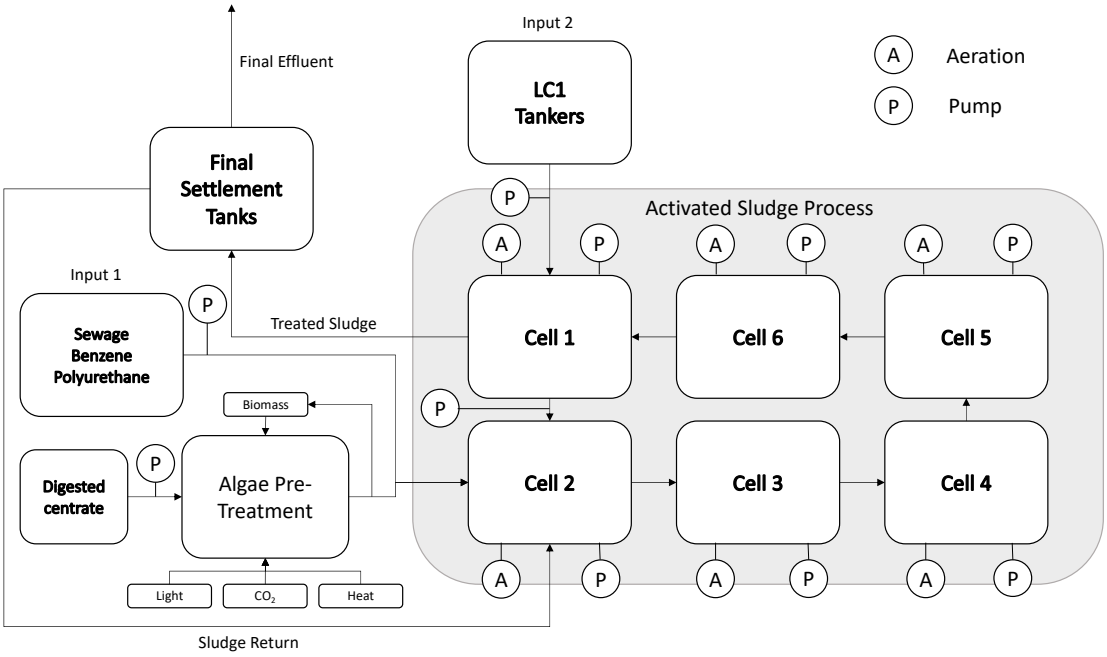

Figure 70: Flowsheet demonstrating the activated sludge process with a possible microalgae pre-treatment unit operation. Input streams, and numerous pumps and aeration duties are displayed.

This is a proposed boundary for the LCA study; only the treatment processes is examined. The anaerobic digestion and any primary settlement processes is not taken into consideration within this study.

What would be under investigation would be the energy usage, environmental impact and total capital cost and payback time of the process with the microalgae pre-treatment stage, compared to the AS process that is currently under operation, without modification.

References

[1]. Kaplan, D., *Absorption and adsorption of heavy metals by microalgae.* Handbook of microalgal culture: Applied phycology and biotechnology; Richmond A, Hu Q, Ed. John Wiley & Sons: Hoboken, 2013.

[2]. Lesmana, S.O., et al., *Studies on potential applications of biomass for the separation of heavy metals from water and wastewater.* Biochemical Engineering Journal, 2009. **44**(1): p. 19-41.

[3]. De Philippis, R., R. Paperi, and C. Sili, *Heavy metal sorption by released polysaccharides and whole cultures of two exopolysaccharide-producing cyanobacteria.* Biodegradation, 2007. **18**(2): p. 181-187.

[4]. Suresh Kumar, K., et al., *Microalgae – A promising tool for heavy metal remediation.* Ecotoxicology and Environmental Safety, 2015. **113**: p. 329-352.

[5]. Abdel-Raouf, N., A.A. Al-Homaidan, and I.B.M. Ibraheem, *Microalgae and wastewater treatment.* Saudi Journal of Biological Sciences, 2012. **19**(3): p. 257-275.

[6]. Eccles, H., *Treatment of metal-contaminated wastes: why select a biological process?* Trends in Biotechnology, 1999. **17**(12): p. 462-465.

[7]. Khosmanesh, A., F. Lawson, and I.G. Prince, *Cadmium uptake by unicellular green microalgae.* The Chemical Engineering Journal and the Biochemical Engineering Journal, 1996. **62**(1): p. 81-88.

[8]. Khummongkol, D., G. Canterford, and C. Fryer, *Accumulation of heavy metals in unicellular algae.* Biotechnology and Bioengineering, 1982. **24**(12): p. 2643-2660.

[9]. Mehta, S.K. and J.P. Gaur, *Use of Algae for Removing Heavy Metal Ions From Wastewater: Progress and Prospects.* Critical Reviews in Biotechnology, 2005. **25**(3): p. 113-152.

[10]. de-Bashan, L.E. and Y. Bashan, *Immobilized microalgae for removing pollutants: Review of practical aspects.* Bioresource Technology, 2010. **101**(6): p. 1611-1627.

[11]. Mallick, N., *Biotechnological potential of immobilized algae for wastewater N, P and metal removal: A review.* Biometals, 2002. **15**(4): p. 377-390.

[12]. Ting, Y., F. Lawson, and I. Prince, *Uptake of cadmium and zinc by the alga Chlorella vulgaris: Part 1. Individual ion species.* Biotechnology and Bioengineering, 1989. **34**(7): p. 990-999.

[13]. Ting, Y., I. Prince, and F. Lawson, *Uptake of cadmium and zinc by the alga Chlorella vulgaris: II. Multi-ion situation.* Biotechnology and Bioengineering, 1991. **37**(5): p. 445-455.

[14]. Edris, G., Y. Alhamed, and A. Alzahrani. *Cadmium and lead biosorption by Chlorella vulgaris*. in *Water Technol. Conf., IWTC*. 2012.

[15]. Edris, G., Y. Alhamed, and A. Alzahrani, *Biosorption of Cadmium and Lead from Aqueous Solutions by Chlorella vulgaris Biomass: Equilibrium and Kinetic Study.* Arabian Journal for Science and Engineering, 2014. **39**(1): p. 87-93.

[16]. Tüzün, I., et al., *Equilibrium and kinetic studies on biosorption of Hg(II), Cd(II) and Pb(II) ions onto microalgae Chlamydomonas reinhardtii.* J Environ Manage, 2005. **77**(2): p. 85-92.

[17]. Chen, C.-Y., et al., *Biosorption of cadmium by CO2-fixing microalga Scenedesmus obliquus CNW-N.* Bioresource technology, 2012. **105**: p. 74-80.

[18]. Maznah, W.W., A. Al-Fawwaz, and M. Surif, *Biosorption of copper and zinc by immobilised and free algal biomass, and the effects of metal biosorption on the growth and cellular structure of Chlorella sp. and Chlamydomonas sp. isolated from rivers in Penang, Malaysia.* Journal of Environmental Sciences, 2012. **24**(8): p. 1386-1393.

[19]. Aksu, Z. and G. Dönmez, *Binary biosorption of cadmium (II) and nickel (II) onto dried Chlorella vulgaris: Co-ion effect on mono-component isotherm parameters.* Process Biochemistry, 2006. **41**(4): p. 860-868.

[20]. Tien, C.-J., *Biosorption of metal ions by freshwater algae with different surface characteristics.* Process Biochemistry, 2002. **38**(4): p. 605-613.

[21]. Tam, N.F.Y., Y.-S. Wong, and C.G. Simpson, *Removal of Copper by Free and Immobilized Microalga, Chlorella vulgaris*, in *Wastewater Treatment with Algae*, Y.-S. Wong and N.F.Y. Tam, Editors. 1998, Springer Berlin Heidelberg: Berlin, Heidelberg. p. 17-36.

[22]. Dönmez, G.Ç., et al., *A comparative study on heavy metal biosorption characteristics of some algae.* Process biochemistry, 1999. **34**(9): p. 885-892.

[23]. Terry, P.A. and W. Stone, *Biosorption of cadmium and copper contaminated water by Scenedesmus abundans.* Chemosphere, 2002. **47**(3): p. 249-255.

[24]. Kumar, R., et al., *Accumulation of Cu by Microalgae Scenedesmus obliquus and Synechocystis sp. PCC 6803.* IOSR Journal of Environmental Science, Toxicology and Food Technology, 2014. **8**: p. 64-68.

[25]. Monteiro, C.M., P.M. Castro, and F.X. Malcata, *Use of the microalga Scenedesmus obliquus to remove cadmium cations from aqueous solutions.* World Journal of Microbiology and Biotechnology, 2009. **25**(9): p. 1573-1578.

[26]. Zhou, G.-J., et al., *Biosorption of zinc and copper from aqueous solutions by two freshwater green microalgae Chlorella pyrenoidosa and Scenedesmus obliquus.* Environmental Science and Pollution Research, 2012. **19**(7): p. 2918-2929.

[27]. MARINOVA, G., et al., *EFFECT OF HEAVY METALS ON THE GREEN ALGA Scenedesmus incrassatulus.* Oxidation Communications, 2018. **41**(2): p. 318-328.

[28]. Darnall, D.W., *A new biotechnology for removing and recovering heavy metals ions from groundwater and industrial wastewater.* Hazardous Waste Treatment: Biosystems for Pollution Control, 1989: p. 113-124.

[29]. Yang, J., et al., *Lipid production combined with biosorption and bioaccumulation of cadmium, copper, manganese and zinc by oleaginous microalgae Chlorella minutissima UTEX2341.* Bioresource technology, 2015. **175**: p. 537-544.

[30]. Rawat, I., et al., *Dual role of microalgae: phycoremediation of domestic wastewater and biomass production for sustainable biofuels production.* Applied energy, 2011. **88**(10): p. 3411-3424.

[31]. Zouboulis, A. and A. Tolkou, *Effect of climate change in wastewater treatment plants: reviewing the problems and solutions*, in *Managing water resources under climate uncertainty*. 2015, Springer. p. 197-220.

[32]. NATIONS, U., *The Sustainable Development Goals Report 2020*. 2020.

[33]. Parraviciniak, V., K. Svardala, and J. Krampea, *Greenhouse gas emissions from wastewater treatment plants.* Energy Procedia, 2016. **97**: p. 246-253.

[34]. Tam, N.F.Y. and Y.S. Wong, *Effect of ammonia concentrations on growth of Chlorella vulgaris and nitrogen removal from media.* Bioresource Technology, 1996. **57**(1): p. 45-50.

[35]. Weathers, P.J., *N2O evolution by green algae.* Applied and environmental microbiology, 1984. **48**(6): p. 1251-1253.

[36]. Sivakumar, G., et al., *Integrated green algal technology for bioremediation and biofuel.* Bioresource technology, 2012. **107**: p. 1-9.

[37]. Barakat, M., *New trends in removing heavy metals from industrial wastewater.* Arabian journal of chemistry, 2011. **4**(4): p. 361-377.

[38]. Law, Y., et al., *Nitrous oxide emissions from wastewater treatment processes.* Philosophical Transactions of the Royal Society B: Biological Sciences, 2012. **367**(1593): p. 1265-1277.

[39]. Johnston, J., T. LaPara, and S. Behrens, *Composition and dynamics of the activated sludge microbiome during seasonal nitrification failure.* Scientific reports, 2019. **9**(1): p. 1-15.

[40]. Razzak, S.A., et al., *Integrated CO2 capture, wastewater treatment and biofuel production by microalgae culturing—a review.* Renewable and sustainable energy reviews, 2013. **27**: p. 622-653.

[41]. Moral Pajares, E., L. Gallego Valero, and I.M. Román Sánchez, *Cost of urban wastewater treatment and ecotaxes: Evidence from municipalities in southern Europe.* Water, 2019. **11**(3): p. 423.

[42]. Alaswad, A., et al., *Technologies and developments of third generation biofuel production.* Renewable and Sustainable Energy Reviews, 2015. **51**: p. 1446-1460.

[43]. Brennan, L. and P. Owende, *Biofuels from microalgae—A review of technologies for production, processing, and extractions of biofuels and co-products.* Renewable and Sustainable Energy Reviews, 2010. **14**(2): p. 557-577.

[44]. Vidyashankar, S. and G. Ravishankar, *Algae-based bioremediation: bioproducts and biofuels for biobusiness*, in *Bioremediation and Bioeconomy*. 2016, Elsevier. p. 457-493.

[45]. Widjaja, A., C.-C. Chien, and Y.-H. Ju, *Study of increasing lipid production from fresh water microalgae Chlorella vulgaris.* Journal of the Taiwan Institute of Chemical Engineers, 2009. **40**(1): p. 13-20.

[46]. Islam, M.A. and F.A. Sobhani, *Determinants of outsourcing decision in the manufacturing industry in Bangladesh.* Business Review, 2010. **5**(2): p. 127-147.

[47]. Li, Y., et al., *Influence of industrialization and environmental protection on environmental pollution: a case study of Taihu Lake, China.* International journal of environmental research and public health, 2018. **15**(12): p. 2628.

[48]. Miazek, K., et al., *Effect of Metals, Metalloids and Metallic Nanoparticles on Microalgae Growth and Industrial Product Biosynthesis: A Review.* International Journal of Molecular Sciences, 2015. **16**(10): p. 23929.

[49]. Gray, N.F., *Biology of Wastewater Treatment*. 2 ed. Vol. 4. 2004: Imperial College Press.

[50]. Merck. *Nafion™ perfluorinated membrane*. 2021 [cited 2021 03/02/2021]; Available from: https://www.sigmaaldrich.com/catalog/product/aldrich/274674?lang=en&region=GB#productDetailSafetyRelatedDocs.

[51]. Zhang, T.-Y., et al., *Promising solutions to solve the bottlenecks in the large-scale cultivation of microalgae for biomass/bioenergy production.* Renewable and Sustainable Energy Reviews, 2016. **60**: p. 1602-1614.

[52]. Ritter, A. and R. Muñoz-Carpena, *Performance evaluation of hydrological models: Statistical significance for reducing subjectivity in goodness-of-fit assessments.* Journal of Hydrology, 2013. **480**: p. 33-45.

[53]. Afkar, E., H. Ababna, and A. Fathi, *Toxicological response of the green alga Chlorella vulgaris, to some heavy metals.* American Journal of Environmental Sciences, 2010. **6**(3): p. 230.

[54]. Blaby-Haas, C.E. and S.S. Merchant, *The ins and outs of algal metal transport.* Biochimica Et Biophysica Acta-Molecular Cell Research, 2012. **1823**(9): p. 1531-1552.

[55]. Milano, J., et al., *Microalgae biofuels as an alternative to fossil fuel for power generation.* Renewable and Sustainable Energy Reviews, 2016. **58**: p. 180-197.

[56]. Chinnasamy, S., et al., *Microalgae cultivation in a wastewater dominated by carpet mill effluents for biofuel applications.* Bioresource technology, 2010. **101**(9): p. 3097-3105.

[57]. Chew, K.W., et al., *Microalgae biorefinery: High value products perspectives.* Bioresource Technology, 2017. **229**: p. 53-62.

[58]. Zeng, X., et al., *Microalgae bioengineering: from CO2 fixation to biofuel production.* Renewable and Sustainable Energy Reviews, 2011. **15**(6): p. 3252-3260.

[59]. Kumar, K., et al., *Development of suitable photobioreactors for CO2 sequestration addressing global warming using green algae and cyanobacteria.* Bioresource Technology, 2011. **102**(8): p. 4945-4953.

[60]. Show, P.L., et al., *A holistic approach to managing microalgae for biofuel applications.* International journal of molecular sciences, 2017. **18**(1): p. 215.

[61]. Atomi, H., *Microbial enzymes involved in carbon dioxide fixation.* Journal of bioscience and bioengineering, 2002. **94**(6): p. 497-505.

[62]. Mohan, S.V., et al., *Heterotrophic microalgae cultivation to synergize biodiesel production with waste remediation: progress and perspectives.* Bioresource technology, 2015. **184**: p. 169-178.

[63]. Kaplan, D., D. Christiaen, and S.M. Arad, *Chelating properties of extracellular polysaccharides from Chlorella spp.* Applied and Environmental Microbiology, 1987. **53**(12): p. 2953-2956.

[64]. Wilde, E.W. and J.R. Benemann, *Bioremoval of heavy metals by the use of microalgae.* Biotechnology Advances, 1993. **11**(4): p. 781-812.

[65]. George, G., R. Prince, and S. Cramer, *The manganese site of the photosynthetic water-splitting enzyme.* Science, 1989. **243**(4892): p. 789-791.

[66]. Lane, T.W. and F.M. Morel, *A biological function for cadmium in marine diatoms.* Proceedings of the National Academy of Sciences, 2000. **97**(9): p. 4627-4631.

[67]. Wikfors, G., A. Neeman, and P. Jackson, *Cadmium-binding polypeptides in microalgal strains with laboratory-induced cadmium tolerance.* Marine Ecology-progress Series - MAR ECOL-PROGR SER, 1991. **79**: p. 163-170.

[68]. Perales-Vela, H.V., J.M. Peña-Castro, and R.O. Cañizares-Villanueva, *Heavy metal detoxification in eukaryotic microalgae.* Chemosphere, 2006. **64**(1): p. 1-10.

[69]. Filip, D.S., et al., *Residual heavy metal removal by an algae-intermittent sand filtration system.* Water Research, 1979. **13**(3): p. 305-313.

[70]. Cai, T., S.Y. Park, and Y. Li, *Nutrient recovery from wastewater streams by microalgae: status and prospects.* Renewable and Sustainable Energy Reviews, 2013. **19**: p. 360-369.

[71]. Hadjoudja, S., V. Deluchat, and M. Baudu, *Cell surface characterisation of Microcystis aeruginosa and Chlorella vulgaris.* Journal of colloid and interface science, 2010. **342**(2): p. 293-299.

[72]. Cheng, Y.-S., et al., *The impact of cell wall carbohydrate composition on the chitosan flocculation of Chlorella.* Process Biochemistry, 2011. **46**(10): p. 1927-1933.

[73]. Voigt, J., et al., *The cell-wall glycoproteins of the green alga Scenedesmus obliquus. The predominant cell-wall polypeptide of Scenedesmus obliquus is related to the cell-wall glycoprotein gp3 of Chlamydomonas reinhardtii.* Plant Science, 2014. **215**: p. 39-47.

[74]. Kikuchi, T. and S. Tanaka, *Biological Removal and Recovery of Toxic Heavy Metals in Water Environment.* Critical Reviews in Environmental Science and Technology - CRIT REV ENVIRON SCI TECHNOL, 2012. **42**.

[75]. Adey, W.H., P.C. Kangas, and W. Mulbry, *Algal Turf Scrubbing: Cleaning Surface Waters with Solar Energy while Producing a Biofuel.* BioScience, 2011. **61**(6): p. 434-441.

[76]. Kesaano, M. and R.C. Sims, *Algal biofilm based technology for wastewater treatment.* Algal Research, 2014. **5**: p. 231-240.

[77]. Yang, J., et al., *Co-contamination of Cu and Cd in paddy fields: Using periphyton to entrap heavy metals.* Journal of Hazardous Materials, 2016. **304**: p. 150-158.

[78]. Missirlis, F., et al., *Heavy Metal Accumulation by Periphyton Is Related to Eutrophication in the Hai River Basin, Northern China.* PLoS ONE, 2014. **9**(1): p. e86458.

[79]. Khatoon, H., et al., *Formation of periphyton biofilm and subsequent biofouling on different substrates in nutrient enriched brackishwater shrimp ponds.* Aquaculture, 2007. **273**(4): p. 470-477.

[80]. Berner, F., K. Heimann, and M. Sheehan, *Microalgal biofilms for biomass production.* Journal of Applied Phycology, 2015. **27**(5): p. 1793-1804.

[81]. Monteiro, C.M., P.M.L. Castro, and F.X. Malcata, *Metal uptake by microalgae: Underlying mechanisms and practical applications.* Biotechnology Progress, 2012. **28**(2): p. 299-311.

[82]. Mehta, S.K. and J.P. Gaur, *Removal of Ni and Cu from single and binary metalsolutions by free and immobilized Chlorella vulgaris.* European Journal of Protistology, 2001. **37**(3): p. 261-271.

[83]. Mehta, S., B. Tripathi, and J. Gaur, *Influence of pH, temperature, culture age and cations on adsorption and uptake of Ni by Chlorella vulgaris.* European Journal of Protistology, 2000. **36**(4): p. 443-450.

[84]. Abdel Ghafar, H.H., et al., *Lead biosorption from aqueous solution by raw and chemically modified green fresh water algae Scenedesmus obliquus.* Desalination and Water Treatment, 2014. **52**(40-42): p. 7906-7914.

[85]. Omar, H.H., *Adsorption of Zinc Ions by Scenedesmus Obliquus and S. Quadricauda and its Effect on Growth and Metabolism.* Biologia Plantarum, 2002. **45**(2): p. 261-266.

[86]. Travieso, L., et al., *Heavy metal removal by microalgae.* Bulletin of environmental contamination and toxicology, 1999. **62**(2): p. 144-151.

[87]. Langmuir, I., *The adsorption of gases on plane surfaces of glass, mica and platinum.* Journal of the American Chemical society, 1918. **40**(9): p. 1361-1403.

[88]. Tran, H.N., et al., *Mistakes and inconsistencies regarding adsorption of contaminants from aqueous solutions: A critical review.* Water Research, 2017. **120**: p. 88-116.

[89]. Foo, K.Y. and B.H. Hameed, *Insights into the modeling of adsorption isotherm systems.* Chemical engineering journal, 2010. **156**(1): p. 2-10.

[90]. Ghosal, P.S. and A.K. Gupta, *Determination of thermodynamic parameters from Langmuir isotherm constant-revisited.* Journal of Molecular Liquids, 2017. **225**: p. 137-146.

[91]. Sayadi, M.H., O. Rashki, and E. Shahri, *Application of modified Spirulina platensis and Chlorella vulgaris powder on the adsorption of heavy metals from aqueous solutions.* Journal of Environmental Chemical Engineering, 2019. **7**(3): p. 103169.

[92]. Dirbaz, M. and A. Roosta, *Adsorption, kinetic and thermodynamic studies for the biosorption of cadmium onto microalgae Parachlorella sp.* Journal of Environmental Chemical Engineering, 2018. **6**(2): p. 2302-2309.

[93]. Fraile, A., et al., *Biosorption of copper, zinc, cadmium and nickel by Chlorella vulgaris.* Chemistry and Ecology, 2005. **21**(1): p. 61-75.

[94]. Tuzen, M. and A. Sarı, *Biosorption of selenium from aqueous solution by green algae (Cladophora hutchinsiae) biomass: Equilibrium, thermodynamic and kinetic studies.* Chemical Engineering Journal, 2010. **158**(2): p. 200-206.

[95]. Akbari, M., et al., *Equilibrium and kinetic study and modeling of Cu(II) and Co(II) synergistic biosorption from Cu(II)-Co(II) single and binary mixtures on brown algae C. indica.* Journal of Environmental Chemical Engineering, 2015. **3**(1): p. 140-149.

[96]. Vijayaraghavan, K., et al., *Biosorption of nickel(II) ions onto Sargassum wightii: Application of two-parameter and three-parameter isotherm models.* Journal of Hazardous Materials, 2006. **133**(1): p. 304-308.

[97]. Lee, Y.-C. and S.-P. Chang, *The biosorption of heavy metals from aqueous solution by Spirogyra and Cladophora filamentous macroalgae.* Bioresource Technology, 2011. **102**(9): p. 5297-5304.

[98]. Solari∗, P., et al., *Removal of Toxic Metals by Biosorption onto Nonliving Sewage Sludge.* Separation Science and Technology, 1996. **31**(8): p. 1075-1092.

[99]. Araújo, C.S.T., et al., *Elucidation of mechanism involved in adsorption of Pb(II) onto lobeira fruit (Solanum lycocarpum) using Langmuir, Freundlich and Temkin isotherms.* Microchemical Journal, 2018. **137**: p. 348-354.

[100]. Inam, E., et al., *Process optimization for the application of carbon from plantain peels in dye abstraction.* Journal of Taibah University for Science, 2017. **11**(1): p. 173-185.

[101]. Ahmad, R. and S. Haseeb, *Adsorption of Pb(II) on Mentha piperita carbon (MTC) in single and quaternary systems.* Arabian Journal of Chemistry, 2017. **10**: p. S412-S421.

[102]. Guo, X. and J. Wang, *Comparison of linearization methods for modeling the Langmuir adsorption isotherm.* Journal of Molecular Liquids, 2019. **296**: p. 111850.

[103]. Liu, Y., *Is the free energy change of adsorption correctly calculated?* Journal of Chemical & Engineering Data, 2009. **54**(7): p. 1981-1985.

[104]. Zhou, X. and X. Zhou, *The unit problem in the thermodynamic calculation of adsorption using the Langmuir equation.* Chemical Engineering Communications, 2014. **201**(11): p. 1459-1467.

[105]. Milonjić, S.K., *A consideration of the correct calculation of thermodynamic parameters of adsorption.* Journal of the Serbian chemical society, 2007. **72**(12): p. 1363-1367.

[106]. Albadarin, A.B., et al., *Kinetic and thermodynamics of chromium ions adsorption onto low-cost dolomite adsorbent.* Chemical Engineering Journal, 2012. **179**: p. 193-202.

[107]. Tran, H.N., S.-J. You, and H.-P. Chao, *Thermodynamic parameters of cadmium adsorption onto orange peel calculated from various methods: a comparison study.* Journal of Environmental Chemical Engineering, 2016. **4**(3): p. 2671-2682.

[108]. Ross, J., *2.8 Non-Equilibrium Adsorption*, in *Heterogeneous CatalysisCatalysis - Fundamentals and Applications*. Elsevier.

[109]. Appel, J., *Freundlich's adsorption isotherm.* Surface Science, 1973. **39**(1): p. 237-244.

[110]. Yang, C., *Statistical Mechanical Study on the Freundlich Isotherm Equation.* J Colloid Interface Sci, 1998. **208**(2): p. 379-387.

[111]. Sparks, D.L., *5 - Sorption Phenomena on Soils*, in *Environmental Soil Chemistry (Second Edition)*, D.L. Sparks, Editor. 2003, Academic Press: Burlington. p. 133-186.

[112]. Selim, H.M. and M.C. Amacher, *Reactivity and transport of heavy metals in soils*. 1996: CRC Press.

[113]. Boulaiche, W., B. Hamdi, and M. Trari, *Removal of heavy metals by chitin: equilibrium, kinetic and thermodynamic studies.* Applied Water Science, 2019. **9**(2): p. 39.

[114]. Yang, C., *Statistical mechanical aspects of adsorption systems obeying the Temkin isotherm.* The Journal of Physical Chemistry, 1993. **97**(27): p. 7097-7101.

[115]. Elmorsi, T.M., *Equilibrium isotherms and kinetic studies of removal of methylene blue dye by adsorption onto miswak leaves as a natural adsorbent.* Journal of Environmental Protection, 2011. **2**(06): p. 817.

[116]. Langmuir, I., *THE CONSTITUTION AND FUNDAMENTAL PROPERTIES OF SOLIDS AND LIQUIDS. PART I. SOLIDS.* Journal of the American Chemical Society, 1916. **38**(11): p. 2221-2295.

[117]. Rangabhashiyam, S., et al., *Relevance of isotherm models in biosorption of pollutants by agricultural byproducts.* Journal of Environmental Chemical Engineering, 2014. **2**(1): p. 398-414.

[118]. Çelekli, A. and H. Bozkurt, *Bio-sorption of cadmium and nickel ions using Spirulina platensis: kinetic and equilibrium studies.* Desalination, 2011. **275**(1-3): p. 141-147.

[119]. Basha, S. and Z.V.P. Murthy, *Kinetic and equilibrium models for biosorption of Cr(VI) on chemically modified seaweed, Cystoseira indica.* Process Biochemistry, 2007. **42**(11): p. 1521-1529.

[120]. Montazer-Rahmati, M.M., et al., *Kinetics and equilibrium studies on biosorption of cadmium, lead, and nickel ions from aqueous solutions by intact and chemically modified brown algae.* Journal of Hazardous Materials, 2011. **185**(1): p. 401-407.

[121]. Zakhama, S., H. Dhaouadi, and F. M'Henni, *Nonlinear modelisation of heavy metal removal from aqueous solution using Ulva lactuca algae.* Bioresource Technology, 2011. **102**(2): p. 786-796.

[122]. Lagergren, s., *Zur theorie der sogenannten adsorption gelöster stoffe.* Kungliga Svenska Vetenskapsakademiens. Handlingar,, 1898. **24**(4): p. 1-39.

[123]. Aharoni, C. and D.L. Sparks, *Kinetics of soil chemical reactions—a theoretical treatment.* Rates of soil chemical processes, 1991. **27**: p. 1-18.

[124]. Ho, Y.S. and G. McKay, *A Comparison of Chemisorption Kinetic Models Applied to Pollutant Removal on Various Sorbents.* Process Safety and Environmental Protection, 1998. **76**(4): p. 332-340.

[125]. Ho, Y. and G. McKay, *The kinetics of sorption of basic dyes from aqueous solution by sphagnum moss peat.* The Canadian Journal of Chemical Engineering, 1998. **76**(4): p. 822-827.

[126]. Ho, Y.S. and G. McKay, *Kinetic Models for the Sorption of Dye from Aqueous Solution by Wood.* Process Safety and Environmental Protection, 1998. **76**(2): p. 183-191.

[127]. Ho, Y.S. and G. McKay, *Sorption of dye from aqueous solution by peat.* Chemical Engineering Journal, 1998. **70**(2): p. 115-124.

[128]. Khamizov, R.K., et al., *Kinetic Models of Batch Sorption in a Limited Volume.* Russian Journal of Physical Chemistry A, 2018. **92**(9): p. 1782-1789.

[129]. Tien, C. and B.V. Ramarao, *On the significance and utility of the Lagergren model and the pseudo second-order model of batch adsorption.* Separation Science and Technology, 2017. **52**(6): p. 975-986.

[130]. Yuh-Shan, H., *Citation review of Lagergren kinetic rate equation on adsorption reactions.* Scientometrics, 2004. **59**(1): p. 171-177.

[131]. Yusuff, A.S., L.T. Popoola, and E.O. Babatunde, *Adsorption of cadmium ion from aqueous solutions by copper-based metal organic framework: equilibrium modeling and kinetic studies.* Applied Water Science, 2019. **9**(4): p. 106.

[132]. Ahamad, K.U., et al., *Equilibrium and kinetics modeling of fluoride adsorption onto activated alumina, alum and brick powder.* Groundwater for Sustainable Development, 2018. **7**: p. 452-458.

[133]. Ritchie, A., *Alternative to the Elovich equation for the kinetics of adsorption of gases on solids.* Journal of the Chemical Society, Faraday Transactions, 1977. **73**: p. 1650-1653.

[134]. Khan, T.A., S.A. Chaudhry, and I. Ali, *Equilibrium uptake, isotherm and kinetic studies of Cd(II) adsorption onto iron oxide activated red mud from aqueous solution.* Journal of Molecular Liquids, 2015. **202**: p. 165-175.

[135]. Blanco, A., et al., *Biosorption of heavy metals to immobilised Phormidium laminosum biomass.* Journal of Biotechnology, 1999. **69**(2–3): p. 227-240.

[136]. Okpara, O.G., et al., *Kinetic and thermodynamic studies on adsorption of lead (ii) ions from aqueous solutions using polymer-modified coconut shell activated carbon (MCSAC).* 2020.

[137]. Gholami, L., G. Rahimi, and A. Khademi Jolgeh Nezhad, *Effect of thiourea-modified biochar on adsorption and fractionation of cadmium and lead in contaminated acidic soil.* International Journal of Phytoremediation, 2020. **22**(5): p. 468-481.

[138]. Azizian, S., *Kinetic models of sorption: a theoretical analysis.* Journal of colloid and Interface Science, 2004. **276**(1): p. 47-52.

[139]. Marczewski, A.W., *Analysis of kinetic Langmuir model. Part I: integrated kinetic Langmuir equation (IKL): a new complete analytical solution of the Langmuir rate equation.* Langmuir, 2010. **26**(19): p. 15229-15238.

[140]. Liu, Y. and L. Shen, *From Langmuir kinetics to first-and second-order rate equations for adsorption.* Langmuir, 2008. **24**(20): p. 11625-11630.

[141]. Liu, Y. and Y.-J. Liu, *Biosorption isotherms, kinetics and thermodynamics.* Separation and purification technology, 2008. **61**(3): p. 229-242.

[142]. Liu, Y., et al., *Biosorption kinetics of cadmium(II) on aerobic granular sludge.* Process Biochemistry, 2003. **38**(7): p. 997-1001.

[143]. Jianlong, W., et al., *Bioadsorption of lead(II) from aqueous solution by fungal biomass of Aspergillus niger.* J Biotechnol, 2001. **87**(3): p. 273-7.

[144]. Singh, S., B.N. Rai, and L.C. Rai, *Ni (II) and Cr (VI) sorption kinetics by Microcystis in single and multimetallic system.* Process Biochemistry, 2001. **36**(12): p. 1205-1213.

[145]. Blanchard, G., M. Maunaye, and G. Martin, *Removal of heavy metals from waters by means of natural zeolites.* Water Research, 1984. **18**(12): p. 1501-1507.

[146]. Salbitani, G. and S. Carfagna, *Ammonium Utilization in Microalgae: A Sustainable Method for Wastewater Treatment.* Sustainability, 2021. **13**(2): p. 956.

[147]. Mohammad Mirzaie, M.A., et al., *Investigation of mixotrophic, heterotrophic, and autotrophic growth of Chlorella vulgaris under agricultural waste medium.* Preparative Biochemistry & Biotechnology, 2016. **46**(2): p. 150-156.

[148]. Wang, L., et al., *Cultivation of Green Algae Chlorella sp. in Different Wastewaters from Municipal Wastewater Treatment Plant.* Applied Biochemistry and Biotechnology, 2010. **162**(4): p. 1174-1186.

[149]. Aslan, S. and I.K. Kapdan, *Batch kinetics of nitrogen and phosphorus removal from synthetic wastewater by algae.* Ecological Engineering, 2006. **28**(1): p. 64-70.

[150]. Mujtaba, G., et al., *Lipid production by Chlorella vulgaris after a shift from nutrient-rich to nitrogen starvation conditions.* Bioresource technology, 2012. **123**: p. 279-283.

[151]. Liu, J., et al., *Effects of light intensity on the growth and lipid accumulation of microalga Scenedesmus sp. 11-1 under nitrogen limitation.* Applied biochemistry and biotechnology, 2012. **166**(8): p. 2127-2137.

[152]. Stanier, R.Y., et al., *Purification and properties of unicellular blue-green algae (order Chroococcales).* Bacteriological reviews, 1971. **35**(2): p. 171-205.

[153]. Rippka, R., *Photoheterotrophy and chemoheterotrophy among unicellular blue-green algae.* Archiv für Mikrobiologie, 1972. **87**(1): p. 93-98.

[154]. Bhushan, B. and G.S. Hoondal, *Isolation, purification and properties of a thermostable chitinase from an alkalophilic Bacillus sp. BG-11.* Biotechnology letters, 1998. **20**(2): p. 157-159.

[155]. Jansson, C., et al., *[11] Use of Synechocystis 6803 to study expression of a psbA gene family*, in *Methods in enzymology*. 1998, Elsevier. p. 166-182.

[156]. Khan, M.I., J.H. Shin, and J.D. Kim, *The promising future of microalgae: current status, challenges, and optimization of a sustainable and renewable industry for biofuels, feed, and other products.* Microbial cell factories, 2018. **17**(1): p. 36.

[157]. Converti, A., et al., *Effect of temperature and nitrogen concentration on the growth and lipid content of Nannochloropsis oculata and Chlorella vulgaris for biodiesel production.* Chemical Engineering and Processing: Process Intensification, 2009. **48**(6): p. 1146-1151.

[158]. Wang, L., et al., *Chlorella vulgaris cultivation in sludge extracts from 2, 4, 6-TCP wastewater treatment for toxicity removal and utilization.* Journal of Environmental Management, 2017. **187**: p. 146-153.

[159]. Schmitt, D., et al., *The adsorption kinetics of metal ions onto different microalgae and siliceous earth.* Water Research, 2001. **35**(3): p. 779-785.

[160]. Todolí, J.L., et al., *Elemental matrix effects in ICP-AES.* Journal of analytical atomic spectrometry, 2002. **17**(2): p. 142-169.

[161]. Tunali, M., M.M. Tunali, and O. Yenigun, *Characterization of different types of electronic waste: heavy metal, precious metal and rare earth element content by comparing different digestıon methods.* Journal of Material Cycles and Waste Management, 2020: p. 1-9.

[162]. Nyika, J., et al., *A comparison of reproducibility of inductively coupled spectrometric techniques in soil metal analyses.* Air, Soil and Water Research, 2019. **12**: p. 1178622119869002.

[163]. Silva, F.V., et al., *Evaluation of inductively coupled plasma optical emission spectrometers with axially and radially viewed configurations.* Spectrochimica Acta Part B: Atomic Spectroscopy, 2002. **57**(12): p. 1905-1913.

[164]. Trevizan, L.C. and J.A. Nóbrega, *Inductively coupled plasma optical emission spectrometry with axially viewed configuration: an overview of applications.* Journal of the Brazilian Chemical Society, 2007. **18**(4): p. 678-690.

[165]. Barin, J.S., et al., *Determination of elemental impurities in pharmaceutical products and related matrices by ICP-based methods: a review.* Analytical and bioanalytical chemistry, 2016. **408**(17): p. 4547-4566.

[166]. Brenner, I. and A. Zander, *Axially and radially viewed inductively coupled plasmas—a critical review.* Spectrochimica Acta Part B: Atomic Spectroscopy, 2000. **55**(8): p. 1195-1240.

[167]. Silva, J.C., N. Baccan, and J.A. Nóbrega, *Analytical performance of an inductively coupled plasma optical emission spectrometry with dual view configuration.* Journal of the Brazilian Chemical Society, 2003. **14**(2): p. 310-315.

[168]. Drava, G. and V. Minganti, *Influence of an internal standard in axial ICP OES analysis of trace elements in plant materials.* Journal of Analytical Atomic Spectrometry, 2020. **35**(2): p. 301-306.

[169]. Sneddon, J. and M.D. Vincent, *ICP-OES and ICP-MS for the determination of metals: application to oysters.* Analytical Letters, 2008. **41**(8): p. 1291-1303.

[170]. Ekins-Coward, T., et al., *A Microalgae Biocomposite-Integrated Spinning Disk Bioreactor (SDBR): Toward a Scalable Engineering Approach for Bioprocess Intensification in Light-Driven CO2 Absorption Applications.* Industrial & Engineering Chemistry Research, 2019. **58**(15): p. 5936-5949.

[171]. Welschmeyer, N.A., *Fluorometric analysis of chlorophyll a in the presence of chlorophyll b and pheopigments.* Limnology and Oceanography, 1994. **39**(8): p. 1985-1992.

[172]. Da Rosa, A.P.C., et al., *Carbon dioxide fixation by microalgae cultivated in open bioreactors.* Energy Conversion and Management, 2011. **52**(8-9): p. 3071-3073.

[173]. Bajguz, A., *Suppression of Chlorella vulgaris Growth by Cadmium, Lead, and Copper Stress and Its Restoration by Endogenous Brassinolide.* Archives of Environmental Contamination and Toxicology, 2011. **60**(3): p. 406-416.

[174]. Bernal, O.I., J.J. Pawlak, and M.C. Flickinger, *Microbial Paper: Cellulose Fiber-based Photo-Absorber Producing Hydrogen Gas from Acetate using Dry-Stabilized Rhodopseudomonas palustris.* 2017, 2017. **12**(2): p. 18.

[175]. Vanhaecke, F., et al., *Applicability of High-Resolution ICP– Mass Spectrometry for Isotope Ratio Measurements.* Analytical Chemistry, 1997. **69**(2): p. 268-273.

[176]. Avery, S.V., G.A. Codd, and G.M. Gadd, *Microalgal removal of organic and inorganic metal species from aqueous solution*, in *Wastewater treatment with algae*. 1998, Springer. p. 55-72.

[177]. Al-Rikabey, M.N. and A.M. Al-Mayah, *Cultivation of Chlorella Vulgaris in BG-11 Media Using Taguchi Method.* 2018.

[178]. Marinova, G., et al., *Effect of heavy metals on the green alga scenedesmus incrassatulus.* Oxidation Communications, 2018. **41**: p. 318-328.

[179]. He, J. and J.P. Chen, *A comprehensive review on biosorption of heavy metals by algal biomass: Materials, performances, chemistry, and modeling simulation tools.* Bioresource Technology, 2014. **160**: p. 67-78.

[180]. Gok, Z. and E. Yel. *Heavy Metal Uptake Kinetics of Microalgae in Aquatic Media*. 2009.

[181]. Wu, F.-C., R.-L. Tseng, and R.-S. Juang, *Characteristics of Elovich equation used for the analysis of adsorption kinetics in dye-chitosan systems.* Chemical Engineering Journal, 2009. **150**(2): p. 366-373.

[182]. Juang, R.-S. and M.-L. Chen, *Application of the Elovich Equation to the Kinetics of Metal Sorption with Solvent-Impregnated Resins.* Industrial & Engineering Chemistry Research, 1997. **36**(3): p. 813-820.

[183]. Low, M.J.D., *Kinetics of Chemisorption of Gases on Solids.* Chemical Reviews, 1960. **60**(3): p. 267-312.

[184]. Pérez-Marín, A., et al., *Removal of cadmium from aqueous solutions by adsorption onto orange waste.* Journal of hazardous materials, 2007. **139**(1): p. 122-131.

[185]. Örnek, A., M. Özacar, and İ.A. Şengil, *Adsorption of lead onto formaldehyde or sulphuric acid treated acorn waste: equilibrium and kinetic studies.* Biochemical engineering journal, 2007. **37**(2): p. 192-200.

[186]. Malkoc, E. and Y. Nuhoglu, *Determination of kinetic and equilibrium parameters of the batch adsorption of Cr (VI) onto waste acorn of Quercus ithaburensis.* Chemical Engineering and Processing-Process Intensification, 2007. **46**(10): p. 1020-1029.

[187]. Anirudhan, T. and P. Radhakrishnan, *Chromium (III) removal from water and wastewater using a carboxylate-functionalized cation exchanger prepared from a lignocellulosic residue.* Journal of Colloid and Interface Science, 2007. **316**(2): p. 268-276.

[188]. Bernal, O.I., C.B. Mooney, and M.C. Flickinger, *Specific photosynthetic rate enhancement by cyanobacteria coated onto paper enables engineering of highly reactive cellular biocomposite "leaves".* Biotechnol Bioeng, 2014. **111**(10): p. 1993-2008.

[189]. Bhatt, A.S., et al., *Adsorption of an anionic dye from aqueous medium by organoclays: equilibrium modeling, kinetic and thermodynamic exploration.* RSC advances, 2012. **2**(23): p. 8663-8671.

[190]. Ghosal, P.S. and A.K. Gupta, *An insight into thermodynamics of adsorptive removal of fluoride by calcined Ca–Al–(NO3) layered double hydroxide.* RSC Advances, 2015. **5**(128): p. 105889-105900.

[191]. Eze, V.C., et al., *Kinetic modelling of microalgae cultivation for wastewater treatment and carbon dioxide sequestration.* Algal Research, 2018. **32**: p. 131-141.

[192]. (https://math.stackexchange.com/users/409/blue), B., *Combining and simplifying equations*. 2020, Mathematics Stack Exchange.

[193]. Fisher, M., A. Zamir, and U. Pick, *Iron uptake by the halotolerant alga Dunaliella is mediated by a plasma membrane transferrin.* Journal of biological chemistry, 1998. **273**(28): p. 17553-17558.

[194]. Folgar, S., et al., *Dunaliella salina as marine microalga highly tolerant to but a poor remover of cadmium.* Journal of Hazardous Materials, 2009. **165**(1): p. 486-493.

Appendix 1. BG-11 Medium Stock Creation

To create BG-11 medium, concentrated component salt solutions were created so that 1mL of each solution (1 to 7), is required per L of BG-11 medium. Solution 8 is the trace metal mixture, this is more concentrated that the other solutions, so only 100μL of Solution 8 is required per L of BG-11 medium.

Table 64: Components required to make BG-11 solution. Masses required to create 100mL stock solutions, of which 1mL stock solution is required to produce 1L BG-11 solution. The Trace Metal solution contained a mixture of all components, and requires 0.1mL stock solution per litre BG-11 medium.

Salt	Mass of Salt Required (g)	Stock Solution Volume (mL)	Stock Solution Concentration (g/L)	Stock Volume Required for 1L BG-11 Medium (mL)	Medium Concentration (g/L)
NaNO3	NA	NA	NA	NA	**1.5**
(1) K2HPO4	4	100	40	1	0.04
(2) MgSO4.7H2O	6.5	100	65	1	0.065
(3) CaCl2.2H2O	3.6	100	36	1	0.036
(4) Citric Acid	0.6	100	6	1	0.006
(5) Ammonium ferric citrate green	0.6	100	6	1	0.006
(6) EDTANa2	0.1	100	1	1	0.001
(7) Na2CO3	2	100	20	1	0.02
(8) Trace Metal Solution					
H3BO4	2.86	100	28.6	0.1	0.00286
MnCl2.4H2O	1.81		18.1		0.00181
ZnSO4.7H2O	0.22		2.2		0.00022
Na2MoO4.2H2O	0.39		3.9		0.00039
CuSO4.5H2O	0.08		0.8		0.00008
Co(NO3)2.6H2O	0.05		0.5		0.00005

Appendix 2. Lagergren Model Derivation

The Lagergren model claims that the rate of adsorption is directly proportional to a rate constant, multiplied by the difference between a maximum value of adsorption, and the adsorption at a particular time. This is shown in Equation 1a.

$$\frac{dQ_t}{dt} = k_t(Q_e - Q_t) \qquad (1a)$$

Where:

- Q_t is the adsorption at time t (mg.g^{-1}).
- Q_e is the adsorption at equilibrium (mg.g^{-1}).
- k_t is the first order rate constant (s^{-1}).
- t is elapsed time (s)

Equation 1a is integrated between the limits of Q_t = 0 and $Q_t = Q_t$, and t = 0 and $t = t$, as follows.

$$\int_0^{Q_t} dQ_t = \int_0^t k_t(Q_e - Q_t)dt$$

$$\int_0^{Q_t} \frac{dQ_t}{(Q_e - Q_t)} = k_t \int_0^t dt$$

$$-[\log_e(Q_e - Q_t)]_0^{Q_t} = k_t[t]_0^t$$

$$-\log_e\left(\frac{(Q_e - Q_t)}{Q_e}\right) = k_t.t$$

$$\frac{(Q_e - Q_t)}{Q_e} = e^{-k_t.t}$$

$$Q_t = Q_e(1 - e^{-k_t.t}) \qquad (1)$$

Appendix 3. Second Order Kinetics Derivation

The second order model claims that the rate of adsorption is directly proportional to a rate constant, multiplied by the square of the difference between a maximum value of adsorption, and the adsorption at a particular time. This is shown in Equation 2a.

$$\frac{dQ_t}{dt} = k_2(Q_e - Q_t)^2 \qquad (2a)$$

Where:

- Q_t is the adsorption at time t (mg.g^{-1}).
- Q_e is the adsorption at equilibrium (mg.g^{-1}).
- k_2 is the second order rate constant (g.mg^{-1}.s^{-1}).
- t is elapsed time (s).

Equation 2a is integrated between the limits of Q_t = 0 and Q_t = Q_t, and t = 0 and t = t, as follows.

$$\int_0^{Q_t} dQ_t = \int_0^t k_2(Q_e - Q_t)^2 dt$$

$$\int_0^{Q_t} \frac{dQ_t}{(Q_e - Q_t)^2} = k_2 \int_0^t dt$$

$$\left[\frac{1}{Q_e - Q_t}\right]_0^{Q_t} = k_2[t]_0^t$$

$$\frac{1}{Q_e - Q_t} - \frac{1}{Q_e} = k_2.t$$

$$\frac{Q_e}{Q_e(Q_e - Q_t)} - \frac{Q_e - Q_t}{Q_e(Q_e - Q_t)} = k_2.t$$

$$\frac{Q_t}{Q_e(Q_e - Q_t)} = k_2.t$$

$$Q_t = k_t.t(Q_e^2 - Q_eQ_t)$$

$$Q_t + Q_t Q_e k_t . t = Q_e^2 k_t . t$$

$$Q_t = \frac{Q_e^2 k_t . t}{1 + Q_e k_t . t} \quad (2)$$

Appendix 4. Elovich Model Derivation

The Elovich equation assumes that the maximum rate of adsorption occurs at the beginning of the process, and this rate reduces exponentially as the adsorption process proceeds. This is shown in Equation 3a:

$$\frac{dQ_t}{dt} = \alpha e^{-\beta Q_t} \qquad (3a)$$

Where:

- Q_t is the adsorption at time t (mg.g^{-1}).
- α is the maximum adsorption rate (mg.g^{-1}.s^{-1})
- β is the desorption constant (g.mg^{-1})
- t is elapsed time (s).

Equation 3a is integrated between the limits of Q_t = 0 and Q_t = Q_t, and t = 0 and t = t, as follows.

$$\int_0^{Q_t} e^{\beta Q_t} = \alpha \int_0^t dt$$

$$\left[\frac{e^{\beta Q_t}}{\beta}\right]_0^{Q_t} = \alpha [t]_0^t$$

$$\frac{e^{\beta Q_t} - 1}{\beta} = \alpha t$$

$$e^{\beta Q_t} = \alpha\beta t + 1$$

$$\beta Q_t = \log_e(\alpha\beta t + 1)$$

$$Q_t = \frac{1}{\beta}\log_e(\alpha\beta t + 1) \qquad (3)$$

Appendix 5. First-Order Rate Equation Derived from Langmuir [142]

This derivation begins with the Langmuir rate equation, which states that the rate of change of concentration is equal to the rate of adsorption, minus the rate of change of desorption.

$$-\frac{dC}{dt} = k_a C - k_d C_b \quad (1)$$

Where k_a is the adsorption rate, C is the concentration of the adsorbate in solution, C_b is the equivalent concentration of adsorbate bound to the adsorbent. C_b can be expressed as the difference between the initial concentration of adsorbate C_0 and C, and the equivalent concentration of adsorbate at equilibrium, C_{be} is the difference between the initial concentration C_0 and the concentration of adsorbate at equilibrium C_e.

$$C_b = C_0 - C \quad (2)$$

$$C_{be} = C_0 - C_e \quad (3)$$

At equilibrium, the rate of change of adsorption is equal to the rate of change of desorption.

$$k_a C_e = k_d C_{be} \quad (4)$$

Combining Equation 1,2 and 3, Equation 5 is obtained:

$$-\frac{dC}{dt} = k_a C - k_d (C_{be} + C_e - C) \quad (5)$$

Rearranging Equation 4 in terms of C_{be}, and collecting similar terms, the differential form of the first order equation in terms of concentration is obtained:

$$-\frac{dC}{dt} = k_1 (C - C_e) \quad (6)$$

Where:

$$k_1 = (k_a + k_d)$$

Appendix 6. Hybrid Langmuir Rate Equation Derivation [140, 192]

Langmuir kinetics are derived from the assumptions of Langmuir (1916) for surface coverage by gasses.

$$\theta_t = \frac{Q_t}{Q_{max}} \tag{3a}$$

$$Q_t = \frac{C_0 - C_t}{X_{Algae}} \tag{3b}$$

$$\theta_t = \frac{C_0 - C_t}{Q_{max} \cdot X_{Algae}} \tag{3c}$$

Where:

- θ_t is the fractional surface coverage at time t.
- Q_t is the adsorption at time t (mg.g^{-1}).
- Q_{max} is the maximum adsorption capacity of the adsorbent (mg.g^{-1}).
- C_0 is the initial concentration of adsorbate in solution (mg.L^{-1}).
- C_t is the concentration of adsorbate in solution at time t.

Rearranging Equation 3b to return C_t as the subject:

$$C_t = C_0 - Q_t . X_{Algae} \tag{3d}$$

Assuming the rate of adsorption is first order with respect to C_t and 1-θ_t and the rate of desorption was first order regarding the occupied binding sights:

$$r_a = k_a . C_t (1 - \theta_t) \tag{4d}$$

$$r_d = k_d \theta_t \tag{5d}$$

Where k_a is the adsorption rate constant and k_d is the desorption rate constant.

The rate of adsorption is defined by Langmuir as the rate of desorption subtracted from the rate of adsorption:

$$\frac{dQ_t}{dt} = r_a - r_d \tag{6d}$$

Substituting Equations 4d and 5d into Equation 6d, and substitution Equation 3a in for θ_t we have:

$$\frac{dQ_t}{dt} = k_a.C_t\left(1 - \frac{Q_t}{Q_{max}}\right) - k_d\frac{Q_t}{Q_{max}} \quad (7d)$$

The parameter, C_t is described by Equation 3d, and it can be substituted into Equation 7d:

$$\frac{dQ_t}{dt} = k_a.(C_0 - Q_t.X_{Algae})\left(1 - \frac{Q_t}{Q_{max}}\right) - k_d\frac{Q_t}{Q_{max}} \quad (8d)$$

Expanding the parentheses, and collecting terms we get:

$$\frac{dQ_t}{dt} = \frac{k_aX_{Algae}}{Q_{max}}.{Q_t}^2 - \left(k_a.X_{Algae} + \frac{k_aC_0}{Q_{max}} + \frac{k_d}{Q_{max}}\right).Q_t + k_aC_0 \quad (9d)$$

Equation 9d is a quadratic formula, and the expression is equal to 0 when $Q_t = Q_e$. The quadratic formula can be used to calculate the value of Q_e:

$$Q_e = \frac{-b - \sqrt{b^2 - 4ac}}{2a}$$

Where:

$$a = \frac{k_a.X_{Algae}}{Q_{max}}$$

$$b = -\left(k_a.X_{Algae} + \frac{k_aC_0}{Q_{max}} + \frac{k_d}{Q_{max}}\right)$$

$$c = k_aC_0$$

So Q_e can be expressed as:

$$Q_e = \frac{Q_{max}.\left(k_a.X_{Algae} + \frac{k_aC_0}{Q_{max}} + \frac{k_d}{Q_{max}} - \sqrt{B}\right)}{2k_aX_{Algae}} \quad (\#)$$

Where B is given by:

$$B = \left(k_a \,.X_{Algae} + \frac{k_a C_0}{Q_{max}} + \frac{k_d}{Q_{max}}\right)^2 - \frac{4{k_a}^2.C_0.X_{Algae}}{Q_{max}}$$

The expression for B can be rearranged to:

$$B = {k_a}^2\left(\frac{C_0}{Q_{max}} - X_{Algae}\right)^2 + 2k_a k_d\left(\frac{C_0}{{Q_{max}}^2} + \frac{X_{Algae}}{Q_{max}}\right) + \frac{{k_d}^2}{{Q_{max}}^2}$$

Now define:

$$k_1 = \sqrt{B} \qquad (10d)$$

$$k_2 = k_a X_{Algae} \qquad (11d)$$

Inserting the definitions 10d and 11d, the expression for B can be expanded and be rearranged to:

$$B = \frac{{k_a}^2{C_0}^2}{{Q_{max}}^2} - k_2\frac{2k_a C_0}{Q_{max}} + {k_2}^2 + \frac{2k_a k_d C_0}{{Q_{max}}^2} + k_2\frac{2k_d}{Q_{max}} + \frac{{k_d}^2}{{Q_{max}}^2}$$

Let:

$$\alpha = \frac{k_a C_0}{Q_{max}}$$

$$B = \alpha^2 - 2\alpha k_2 + {k_2}^2 + 2\alpha\frac{k_d}{Q_{max}} + 2k_2\frac{k_d}{Q_{max}} + \frac{{k_d}^2}{{Q_{max}}^2}$$

$$B = (\alpha - k_2)^2 + 2k_d\left(\frac{\alpha}{Q_{max}} + \frac{k_2}{Q_{max}}\right) + \frac{{k_d}^2}{{Q_{max}}^2}$$

$$B = -4\alpha k_2 + (\alpha + k_2)^2 + \frac{2k_d}{Q_{max}}(\alpha + k_2) + \frac{{k_d}^2}{{Q_{max}}^2}$$

$$B = -4\alpha k_2 + \left(\alpha + k_2 + \frac{k_d}{Q_{max}}\right)^2 = {k_1}^2 \qquad (12d)$$

Rearranging Equation 12d,

$$4\alpha k_2 = \left(\alpha + k_2 + \frac{k_d}{Q_{max}}\right)^2 - {k_1}^2 \qquad (13d)$$

Equation 13d can be rearranged to the form:

$$4\alpha k_2 = \left(\alpha + k_1 + k_2 + \frac{k_d}{Q_{max}}\right)\left(\alpha - k_1 + k_2 + \frac{k_d}{Q_{max}}\right) \qquad (14d)$$

Referring back to Equation #, and using the expressions given by Equation 10d and 11d:

$$Q_e = \frac{Q_{max}.\left(k_a\,.X_{Algae} + \frac{k_a C_0}{Q_{max}} + \frac{k_d}{Q_{max}} - \sqrt{B}\right)}{2k_a X_{Algae}} \qquad (\#)$$

Becomes:

$$\frac{Q_e}{Q_{max}} = \frac{\left(\alpha - k_1 + k_2 + \frac{k_d}{Q_{max}}\right)}{2k_2} \qquad (15d)$$

Equation 15d can be substituted into Equation 14d:

$$2\alpha = \frac{Q_e}{Q_{max}}\left(\alpha + k_1 + k_2 + \frac{k_d}{Q_{max}}\right) \qquad (16d)$$

Define a new constant, μ:

$$\mu = \alpha + k_2 + \frac{k_d}{Q_{max}}$$

Substitute μ into Equation 15d to obtain:

$$\frac{Q_e}{Q_{max}} = \frac{(\mu - k_1)}{2k_2} \qquad (17d)$$

Substitute μ into Equation 16d to obtain:

$$2\alpha = \frac{Q_e}{Q_{max}}(\mu + k_1) \qquad (18d)$$

Returning to Equation 9d, this expression can be simplified as follows:

$$\frac{dQ_t}{dt} = \frac{k_a X_{Algae}}{Q_{max}} . {Q_t}^2 - \left(k_a . X_{Algae} + \frac{k_a C_0}{Q_{max}} + \frac{k_d}{Q_{max}}\right). Q_t + k_a C_0 \qquad (9d)$$

$$\frac{dQ_t}{dt} = \frac{k_2}{Q_{max}} . {Q_t}^2 - \mu Q_t + \alpha Q_{max} \qquad (19d)$$

As:

$$\alpha = \frac{k_a C_0}{Q_{max}}$$

$$k_2 = k_a X_{Algae}$$

$$\mu = \alpha + k_2 + \frac{k_d}{Q_{max}}$$

Rearranging Equation 17d, the expression for μ can be obtained:

$$\mu = 2k_2 \frac{Q_e}{Q_{max}} + k_1 \qquad (20d)$$

The expression for α can be derived by rearranging Equation 18d:

$$\alpha = \frac{Q_e}{2Q_{max}} (\mu + k_1) \qquad (21d)$$

Substitution of Equation 20d and 21d into Equation 19d gives:

$$\frac{dQ_t}{dt} = \frac{k_2}{Q_{max}} . {Q_t}^2 - \left(2k_2 \frac{Q_e}{Q_{max}} + k_1\right). Q_t + \frac{Q_e}{2Q_{max}} \left(2k_2 \frac{Q_e}{Q_{max}} + k_1 + k_1\right). Q_{max} \qquad (22d)$$

Expanding the parentheses in Equation 22d, and collecting the terms containing k_2 and k_1, it can be seen that the terms containing k_2 are a quadratic.

$$\frac{dQ_t}{dt} = k_1 Q_e - k_1 Q_t + \frac{k_2}{Q_{max}} . {Q_e}^2 - 2\frac{k_2}{Q_{max}} Q_e Q_t + \frac{k_2}{Q_{max}} {Q_t}^2$$

This returns Langmuir kinetics that are a function of a first order term and a second order term:

$$\frac{dQ_t}{dt} = k_1 (Q_e - Q_t) + k_2{}' (Q_e - Q_t)^2 \qquad (23d)$$

Where:

$$k_2{}' = \frac{k_2}{Q_{max}}$$

Separating the variables and integrating Equation 23d between Q_t = 0 and Q_t = Q_t, and t = 0 and t = t:

$$\int_0^{Q_t} \frac{dQ_t}{k_1(Q_e - Q_t) + k_2{}'(Q_e - Q_t)^2} = \int_0^t dt$$

Let:

$$u = Q_e - Q_t$$

$$\frac{du}{dQ_t} = -1$$

$$\therefore dQ_t = -du$$

The integral becomes:

$$-\int_0^{Q_t} \frac{du}{k_1 u + k_2{}' u^2} = \int_0^t dt$$

The denominator can be rearranged by completing the square:

$$-\int_0^{Q_t} \frac{du}{\left(\frac{k_1}{2\sqrt{k_2{}'}} + \sqrt{k_2{}'}u\right)^2 - \frac{k_1{}^2}{4k_2{}'}} = \int_0^t dt$$

Let:

$$v = \frac{k_1}{2\sqrt{k_2{}'}} + \sqrt{k_2{}'}u$$

$$\frac{dv}{du} = \sqrt{k_2{}'}$$

$$\therefore du = \frac{dv}{\sqrt{k_2{}'}}$$

The integral now becomes:

$$-\frac{1}{\sqrt{k_2{}'}}\int_0^{Q_t}\frac{dv}{v^2-\frac{k_1{}^2}{4k_2{}'}}=\int_0^t dt$$

$$-\frac{1}{\sqrt{k_2{}'}}\int_0^{Q_t}\frac{4k_2{}'dv}{-k_1{}^2\left(1-\frac{4k_2{}'v^2}{k_1{}^2}\right)}=\int_0^t dt$$

$$\frac{4\sqrt{k_2{}'}}{k_1{}^2}\int_0^{Q_t}\frac{dv}{1-\frac{4k_2{}'v^2}{k_1{}^2}}=\int_0^t dt$$

Now let

$$p=\frac{2\boldsymbol{i}\sqrt{k_2{}'}v}{k_1}$$

$$\frac{dp}{dv}=\frac{2\boldsymbol{i}\sqrt{k_2{}'}}{k_1}$$

$$\therefore dv=\frac{k_1}{2\boldsymbol{i}\sqrt{k_2{}'}}dp$$

The integral becomes:

$$\frac{k_1}{2\boldsymbol{i}\sqrt{k_2{}'}}\times\frac{4\sqrt{k_2{}'}}{k_1{}^2}\int_0^{Q_t}\frac{dp}{p^2+1}=\int_0^t dt$$

$$-\frac{2\boldsymbol{i}}{k_1}\int_0^{Q_t}\frac{dp}{p^2+1}=\int_0^t dt$$

$$\left[-\frac{2\boldsymbol{i}\ \tan^{-1}(p)}{k_1}\right]_0^{Q_t}=t$$

$$\left[-\frac{2\boldsymbol{i}\ \tan^{-1}\left(\frac{2\boldsymbol{i}\sqrt{k_2{}'}v}{k_1}\right)}{k_1}\right]_0^{Q_t}=t \qquad (24d)$$

As

$$\tanh^{-1}(x) = \boldsymbol{i}\tan^{-1}(-\boldsymbol{i}x)$$

Equation 24d becomes

$$\left[\frac{2\ \tanh^{-1}\left(\frac{2\sqrt{k_2{}'}v}{k_1}\right)}{k_1}\right]_0^{Q_t} = t \qquad (25d)$$

Substituting in for v, Equation 25d becomes:

$$\left[\frac{2\ \tanh^{-1}\left(\frac{2\sqrt{k_2{}'}}{k_1} \times \left(\frac{k_1}{2\sqrt{k_2{}'}} + \sqrt{k_2{}'}u\right)\right)}{k_1}\right]_0^{Q_t} = t$$

$$\left[\frac{2\ \tanh^{-1}\left(1 + \frac{2k_2{}'}{k_1}u\right)}{k_1}\right]_0^{Q_t} = t \qquad (26d)$$

Substituting for u into Equation 26d:

$$\left[\frac{2\ \tanh^{-1}\left(1 + \frac{2k_2{}'}{k_1}(Q_e - Q_t)\right)}{k_1}\right]_0^{Q_t} = t \qquad (27d)$$

Let:

$$x = 1 + \frac{2k_2{}'}{k_1}(Q_e - Q_t)$$

Equation 23.3 becomes:

$$[2\ \tanh^{-1}(x)]_0^{Q_t} = k_1 t \qquad (28d)$$

For real values of x:

$$\tanh^{-1}(x) = \frac{1}{2}\ln\left(\frac{1+x}{1-x}\right)$$

Therefore Equation 27d becomes:

$$\left[\ln\left(\frac{1+1+\frac{2k_2{}'}{k_1}(Q_e - Q_t)}{1-\left(1+\frac{2k_2{}'}{k_1}(Q_e - Q_t)\right)}\right)\right]_0^{Q_t} = k_1 t \qquad (29d)$$

Equation 29d can be simplified as follows:

$$\left[\ln\left(-\frac{1}{\frac{k_2{}'}{k_1}(Q_e - Q_t)} - 1\right)\right]_0^{Q_t} = k_1 t \qquad (30d)$$

Applying the limits between Q_t = 0 and $Q_t = Q_t$, Equation 30d is expanded as follows:

$$\ln\left(-\frac{1}{\frac{k_2{}'}{k_1}(Q_e - Q_t)} - 1\right) - \ln\left(-\frac{1}{\frac{k_2{}'}{k_1}(Q_e)} - 1\right) = k_1 t$$

$$\ln\left(\frac{-\frac{k_1}{k_2{}'(Q_e - Q_t)} - 1}{-\frac{k_1}{k_2{}'Q_e} - 1}\right) = k_1 t$$

$$\frac{\frac{k_1}{k_2{}'(Q_e - Q_t)} + 1}{\frac{k_1}{k_2{}'Q_e} + 1} = e^{k_1 t}$$

$$\frac{\left(\frac{k_1}{k_2{}'(Q_e - Q_t)} + 1\right) \times k_2{}'Q_e}{k_1 + k_2{}'Q_e} = e^{k_1 t}$$

$$\frac{k_1 Q_e}{Q_e - Q_t} = (k_1 + k_2{}'Q_e)e^{k_1 t} - k_2{}'Q_e$$

Rearranging this expression, the integrated form of the Langmuir kinetic equation is obtained.

$$Q_t = Q_e \left(1 - \frac{k_1}{(k_1 + k_2{}' Q_e) e^{k_1 t} - k_2{}' Q_e}\right)$$

Appendix 7. *Chlorella vulgaris* Growth Curves

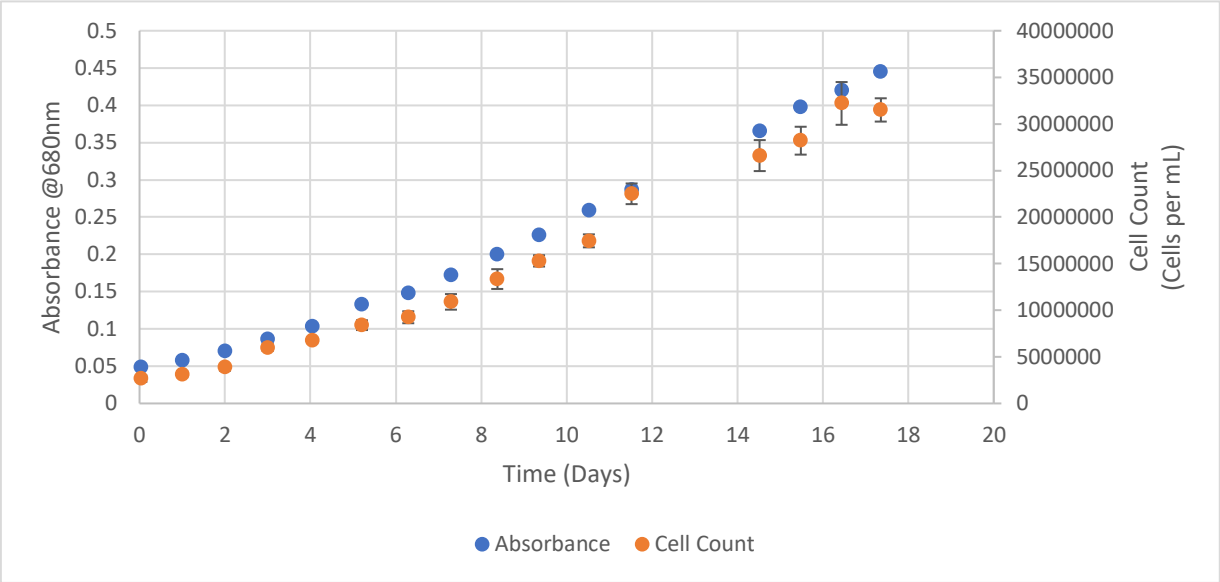

Figure 71: Growth of *Chlorella vulgaris* monitored using UV-Vis measured at 680nm and manual cell counting using a haemacytometer for cultivations in a 10 litre Carboy.

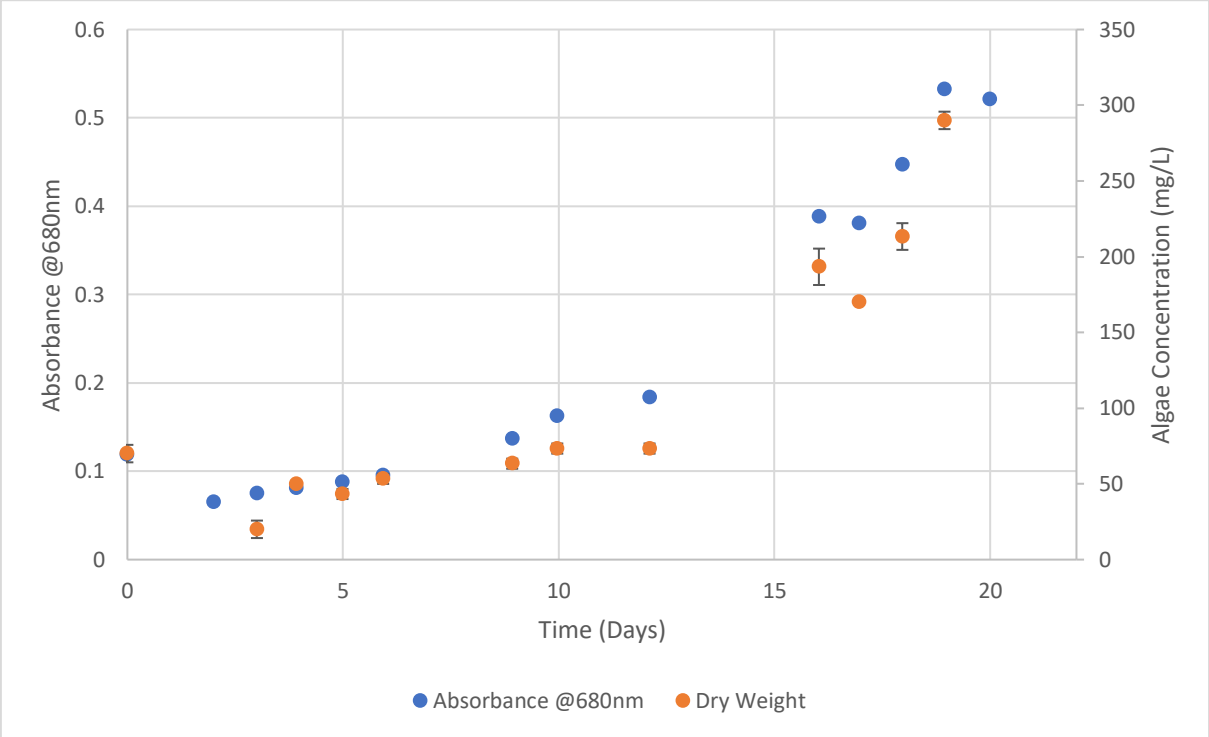

Figure 72: Growth of *Chlorella vulgaris* monitored using UV-Vis measured at 680nm and for dry weight for cultivations in a 10 litre Carboy.

Appendix 8. *Scenedesmus obliquus* Growth Curves

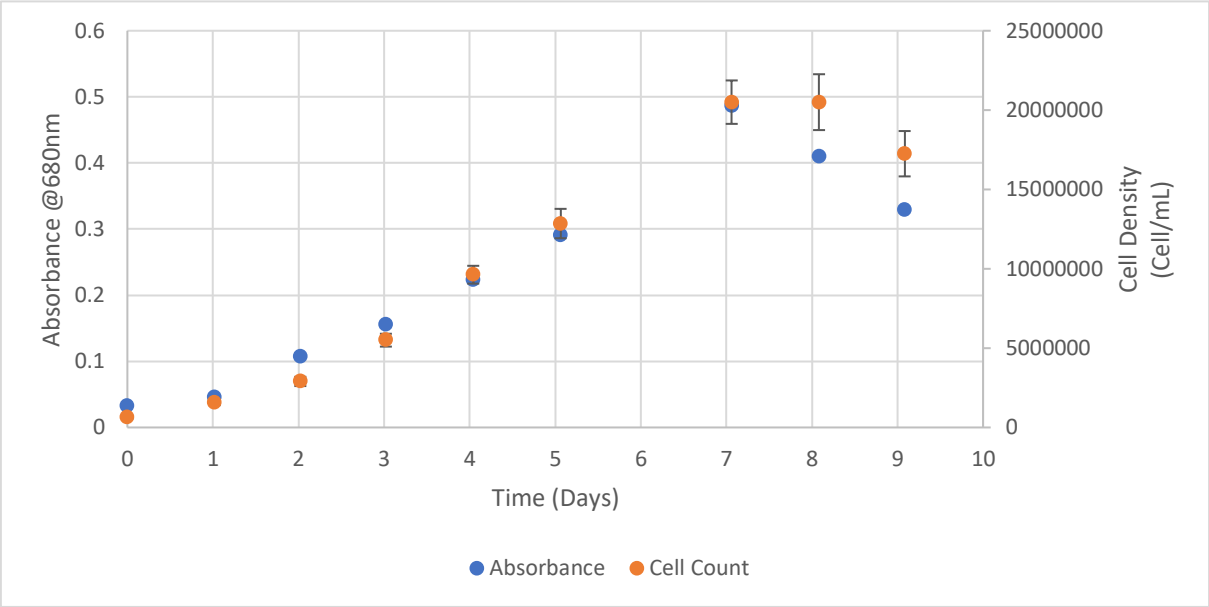

Figure 73: Growth of *Scenedesmus obliquus* monitored using UV-Vis measured at 680nm and manual cell counting using a haemacytometer for cultivations in a 1L bottle.

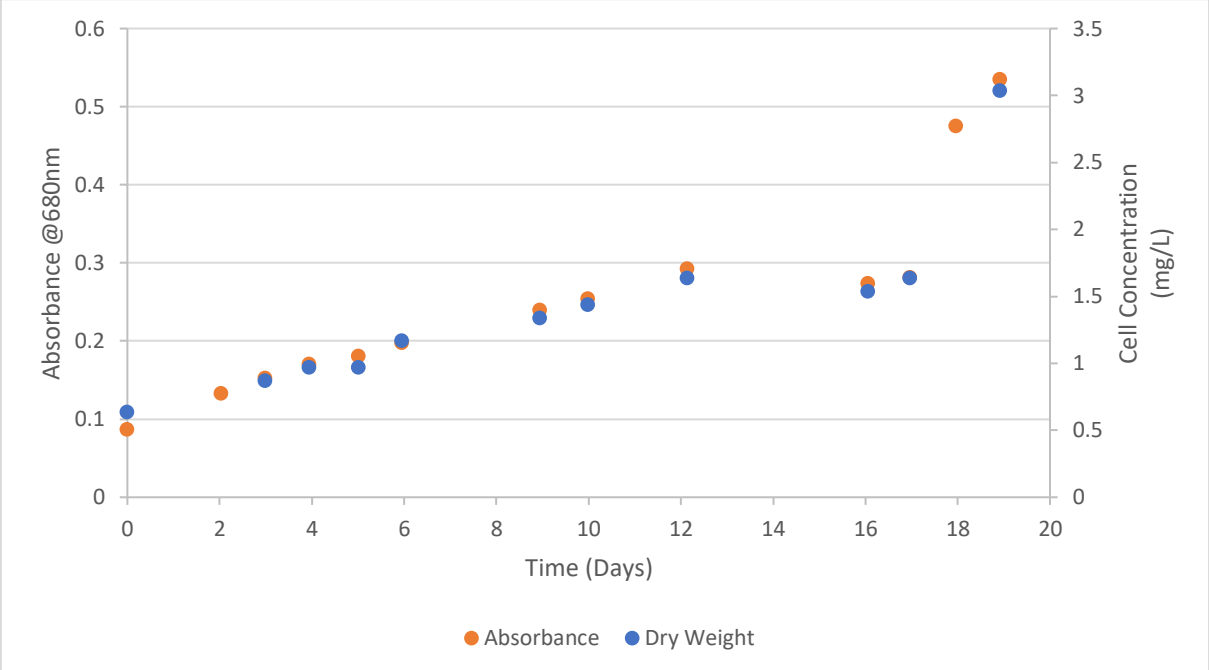

Figure 74: The Growth rate of *Scenedemus obliquus* cultivated in a 10L carboy recorded by absorbance at 680nm and algae concentration recorded by dry weight.

Appendix 9. *Synechococcus elongatus* Growth Curves

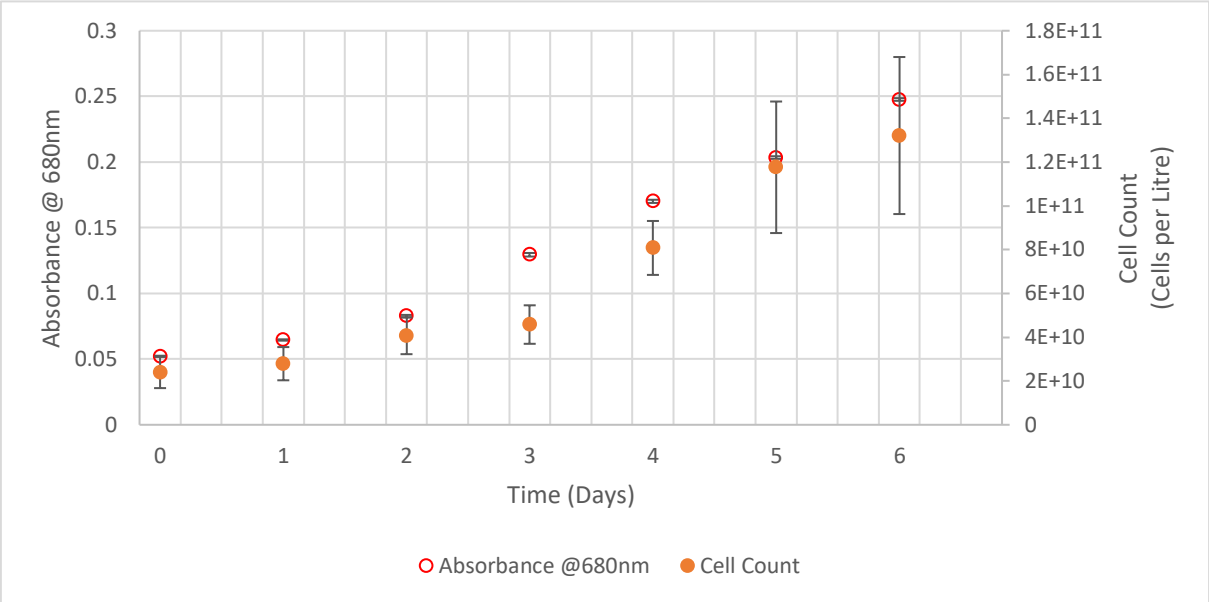

Figure 75: Growth of *Synechococcus elongatus* monitored using UV-Vis measured at 680nm and manual cell counting using a haemacytometer for cultivations in a 10 litre Carboy. For this analysis the errors in cell count became large very quickly. The cells were very small and would mover readily at the slightest knock.

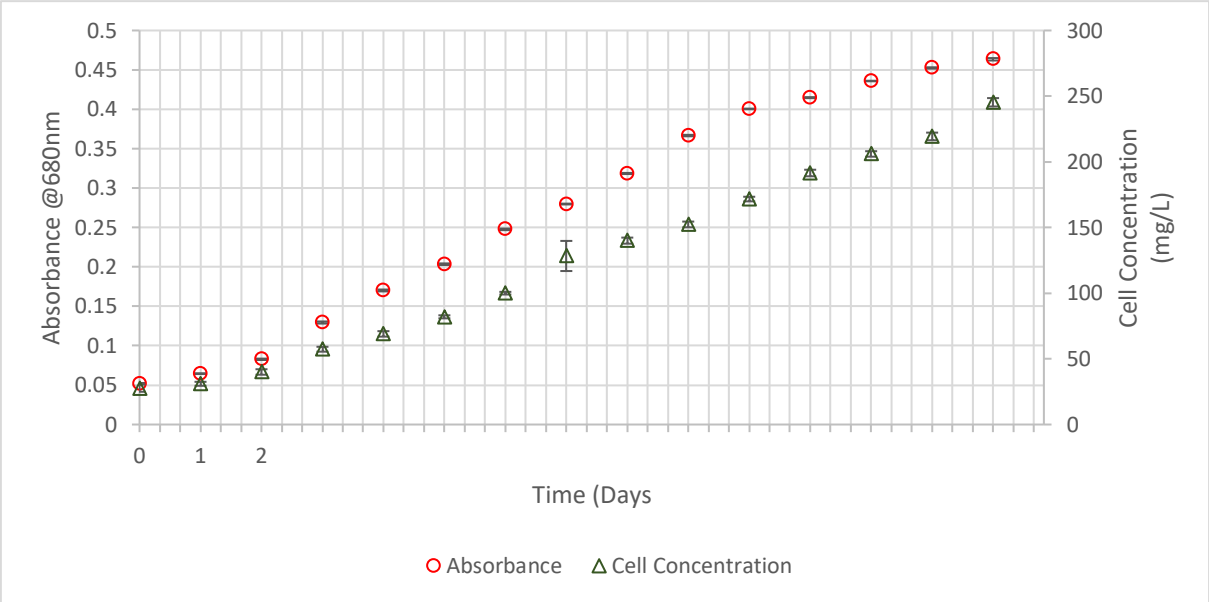

Figure 76: The Growth rate of *Synechococcus elongatus* cultivated in a 10L carboy recorded by absorbance at 680nm and algae concentration recorded by dry weight.

Appendix 10. Cell Count Standard Curves

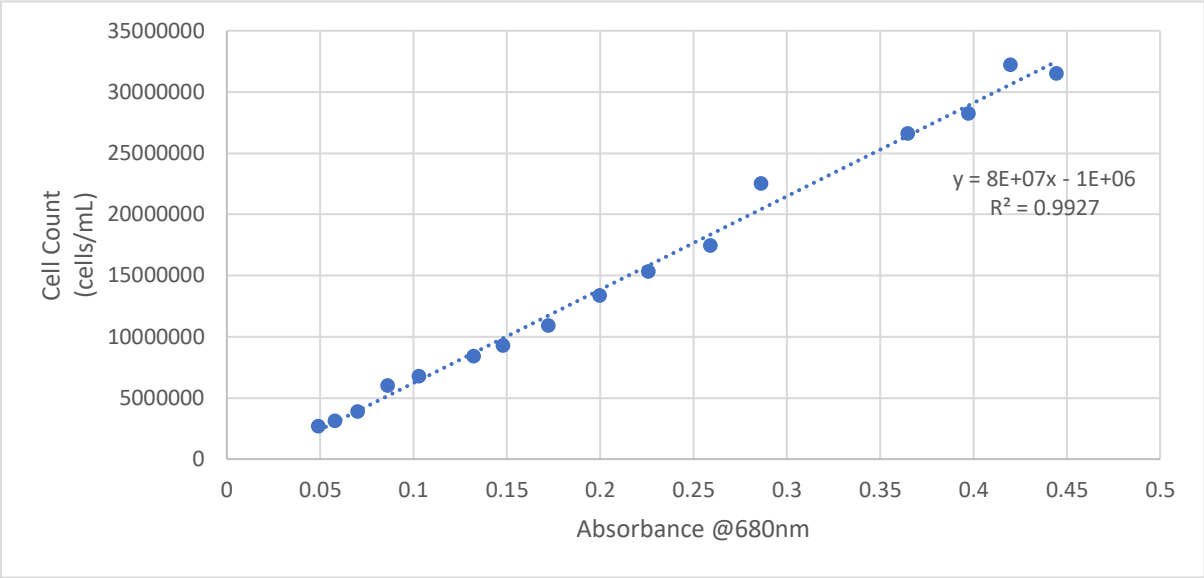

Figure 77: Standard curve of cell count of *Chlorella vulgaris* plotted against the optical density.

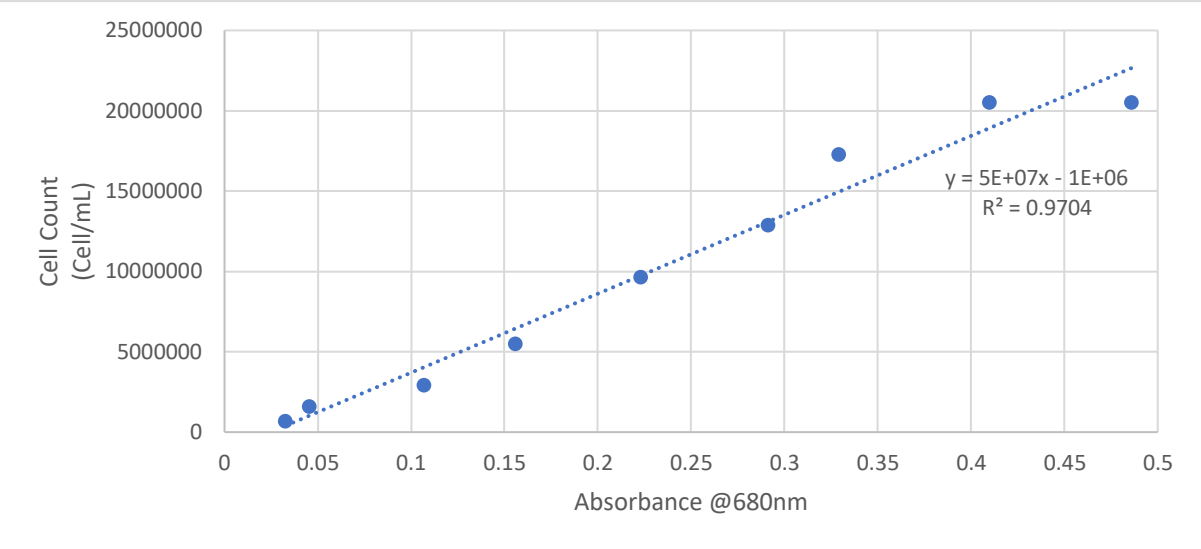

Figure 78: Standard curve of cell count of *Scenedesmus obliquus* plotted against the optical density.

Appendix 11. ICP-OES Copper Standard Curves

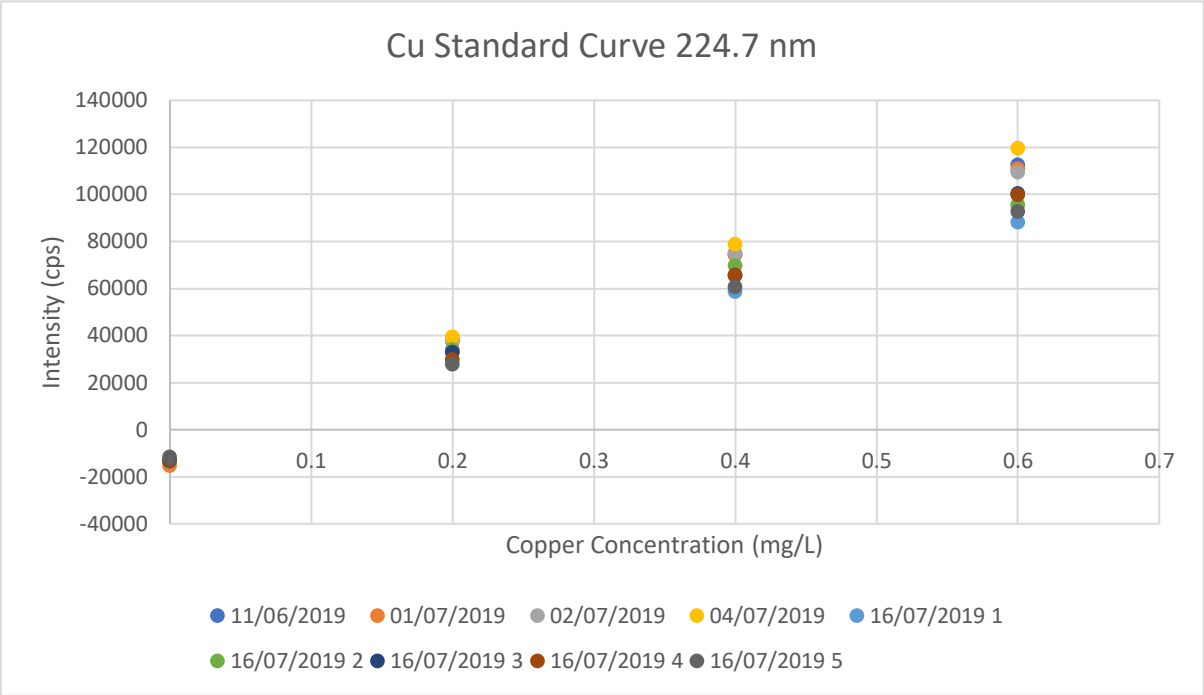

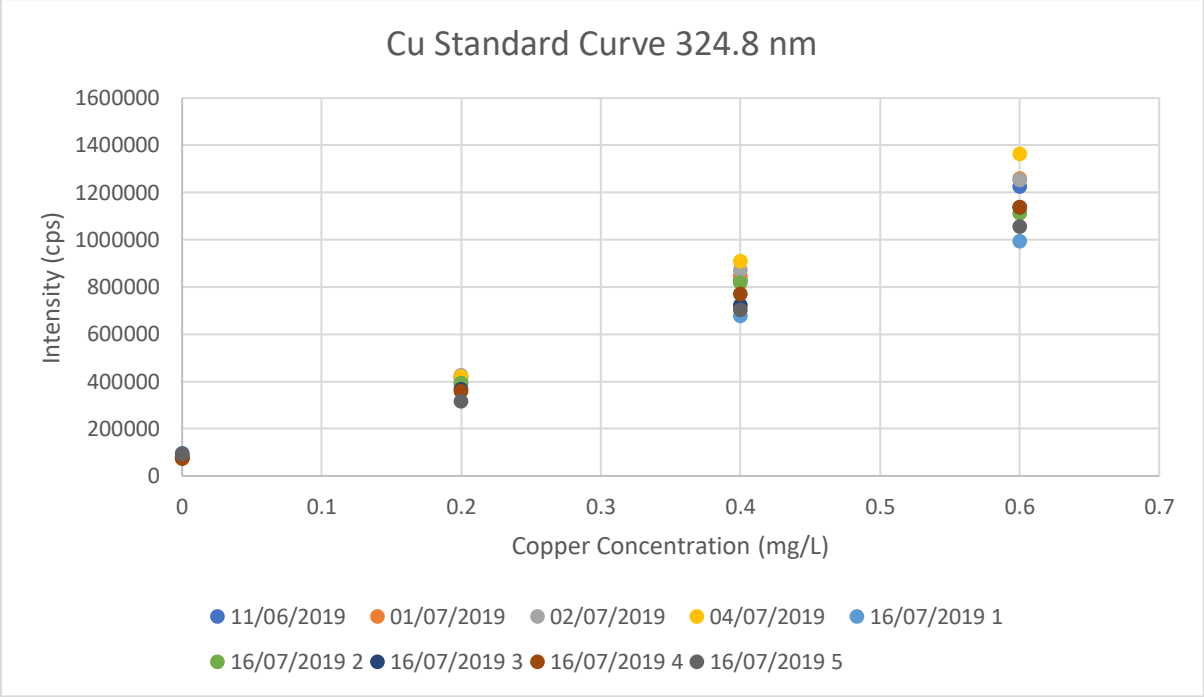

Appendix 12. ICP-OES Copper Peaks

The ICP-OES had calibration issues. The detector was measuring at a wavelength that was off-centre from the peak for copper analysis. This was an instrumentation issue that required resolving by members of the technical team.

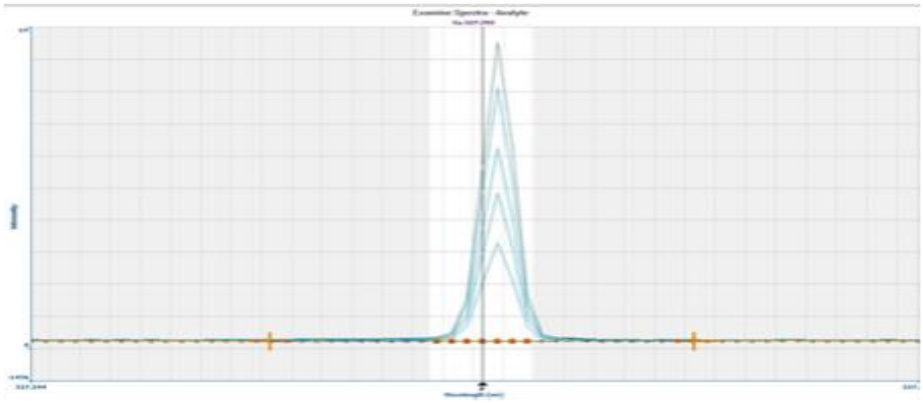

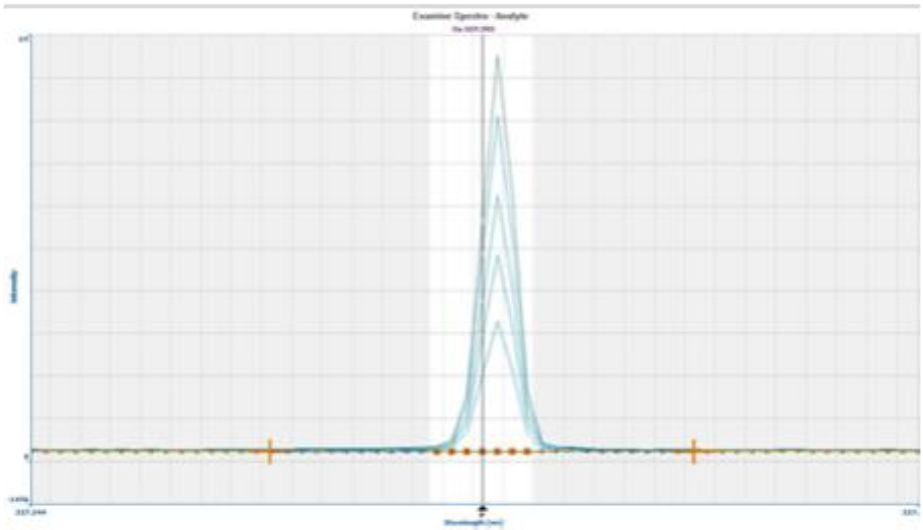

Appendix 13. *Chlorella vulgaris* concentration in presence of Cu^{2+}

During the first metal uptake experiment on a 200mL scale, the biomass concentration was monitored in BG-11 contaminated with copper ions, and in BG-11 without copper contamination. The test was over a three-day period and both the control cultivation and the experimental cultivation had the same biomass control profile over the three days.

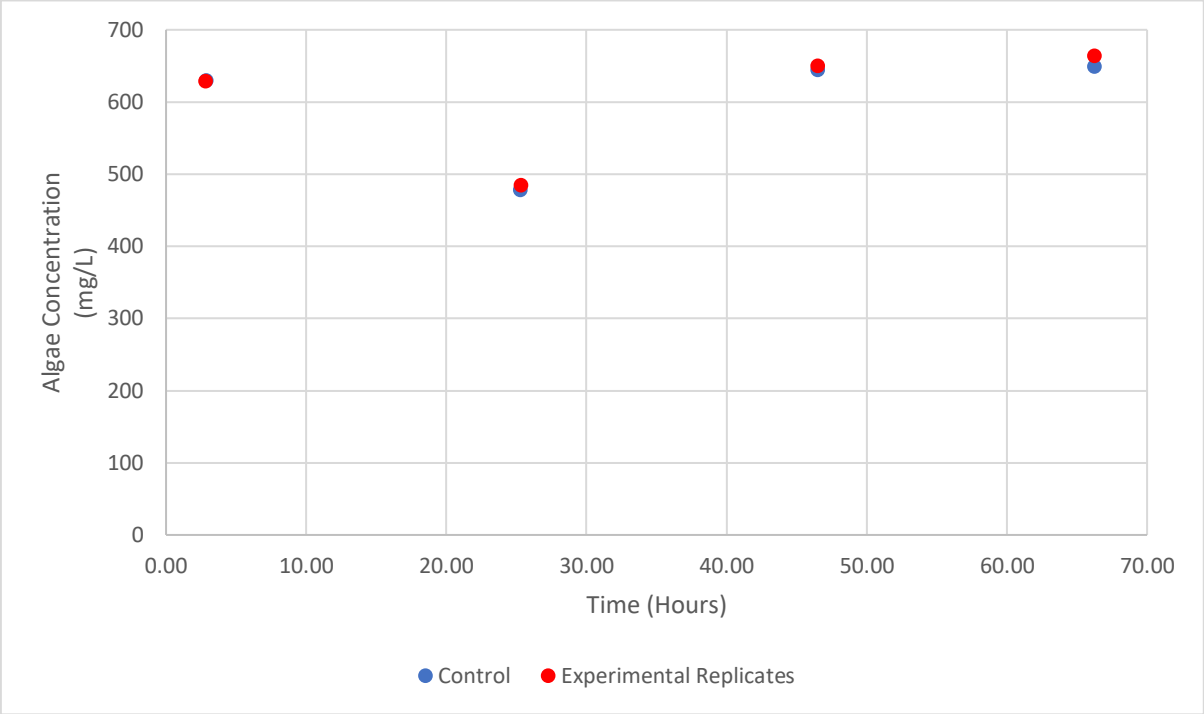

Appendix 14. ANOVA Charts for Section 4.2.1: 0.3mg.L^{-1} at pH 3

Analysis of variance was carried out to determine whether the concentrations returned by ICP-OES were equivalent for each wavelength. The wavelengths were 327.4nm, 324.8nm and 224.7nm. The analysis was split into two sets; analysis of samples at pH 3 and analysis of the samples at pH 7.

The charts produced in Minitab® for the ANOVA for the 0.3mg.L^{-1} samples obtained from the pH 3 experiments are displayed in Figure 79.

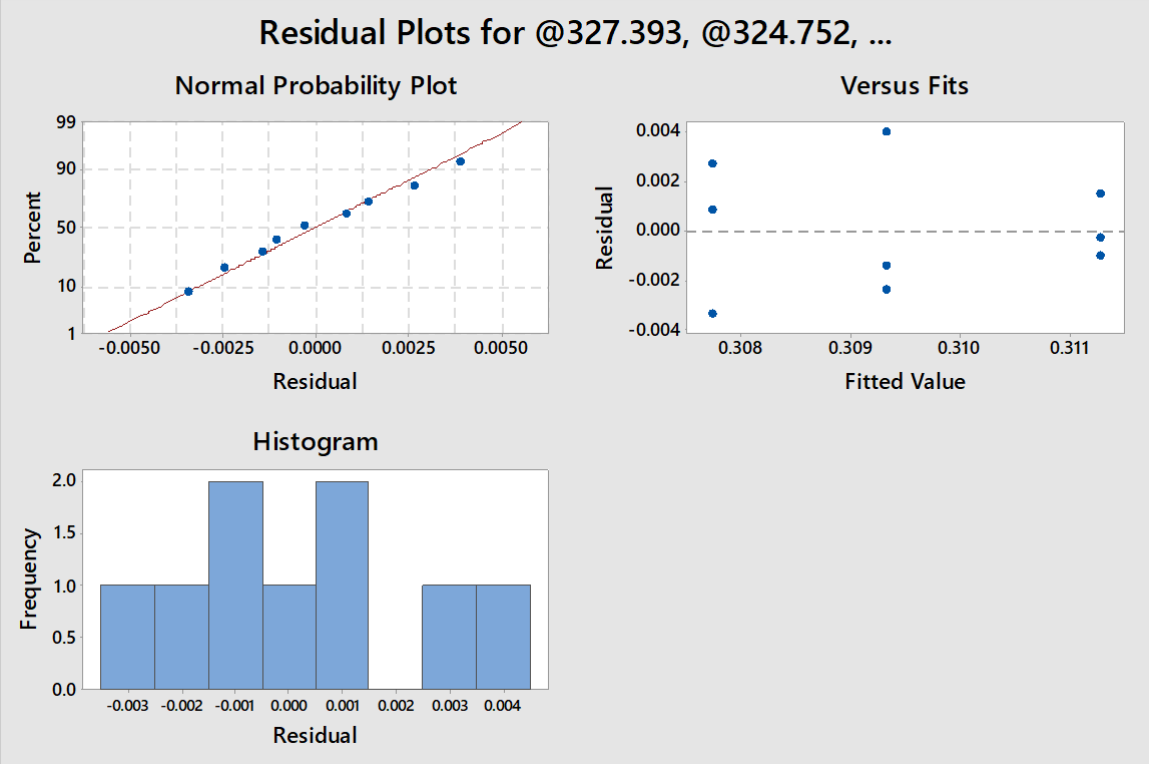

Figure 79: Normal probability plot, residuals vs fit and histogram of frequency vs residuals obtained for the ANOVA for the analysis of 0.3mg.L^{-1} samples analysed by ICP-OES at pH 3.

The normal probability plot indicates that the data is normally distributed and the vs. fits plot indicates the residuals are randomly distributed. In this case the histogram does indicate a normal distribution.

Appendix 15. ANOVA Charts for Section 4.2.1: 0.4mg.L^{-1} at pH 3

The charts produced in Minitab® for the ANOVA for the 0.4mg.L^{-1} samples obtained from the pH 3 experiments are displayed in Figure 80.

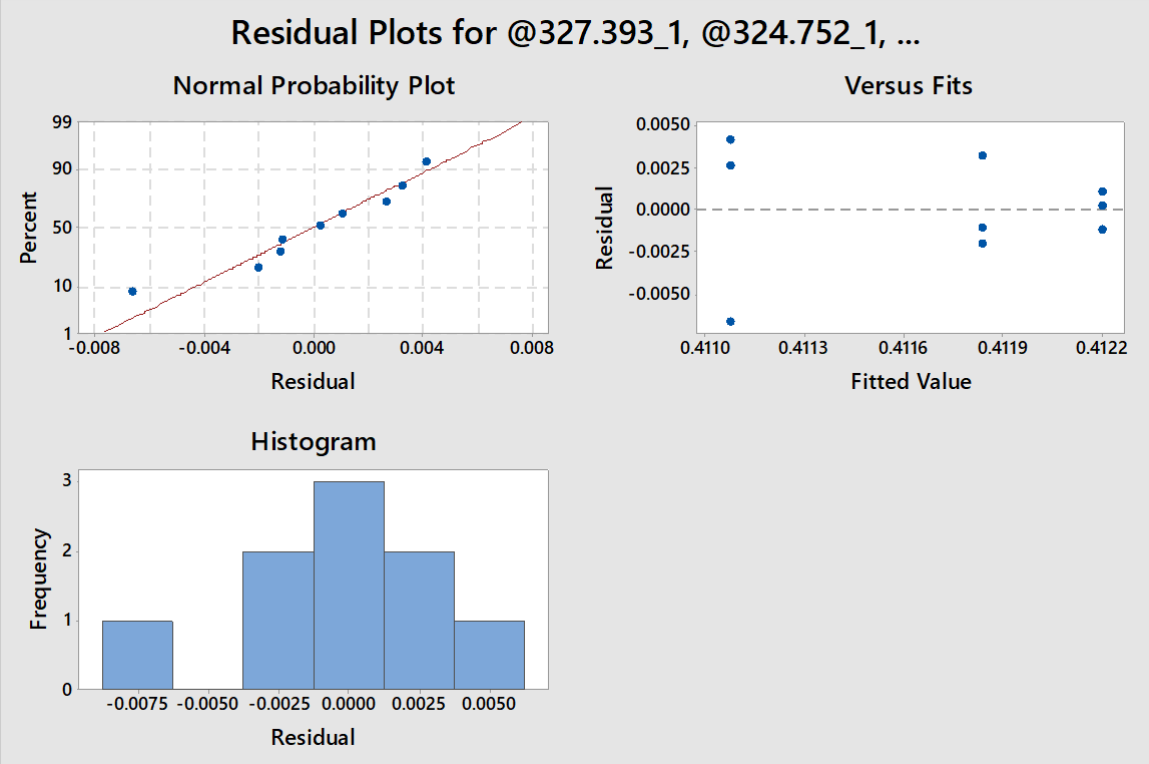

Figure 80: Normal probability plot, residuals vs fit and histogram of frequency vs residuals obtained for the ANOVA for the analysis of 0.4mg.L^{-1} samples analysed by ICP-OES at pH 3.

The normal probability plot indicates that the data is normally distributed and the vs. fits plot indicates the residuals are randomly distributed. In this case the histogram does indicate a normal distribution.

Appendix 16. ANOVA Charts for Section 4.2.1: 0.5mg.L^{-1} at pH 3

The charts produced in Minitab® for the ANOVA for the 0.5mg.L^{-1} samples obtained from the pH 3 experiments are displayed in Figure 81.

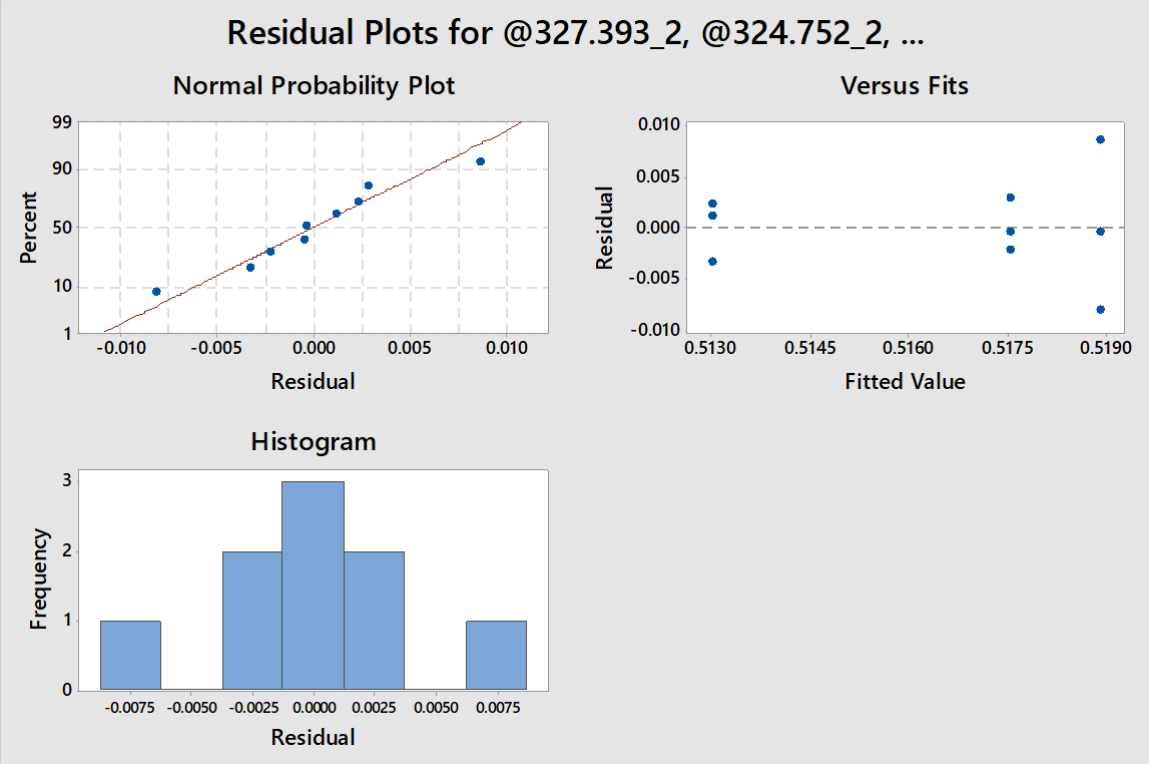

Figure 81: Normal probability plot, residuals vs fit and histogram of frequency vs residuals obtained for the ANOVA for the analysis of 0.5mg.L^{-1} samples analysed by ICP-OES at pH 3.

The normal probability plot indicates that the data is normally distributed and the vs. fits plot indicates the residuals are randomly distributed. In this case the histogram does indicate a normal distribution.

Appendix 17. ANOVA Charts for Section 4.2.1: 0.3mg.L^{-1} at pH 7

The charts produced in Minitab® for the ANOVA for the 0.3mg.L^{-1} samples obtained from the pH 7 experiments are displayed in Figure 82.

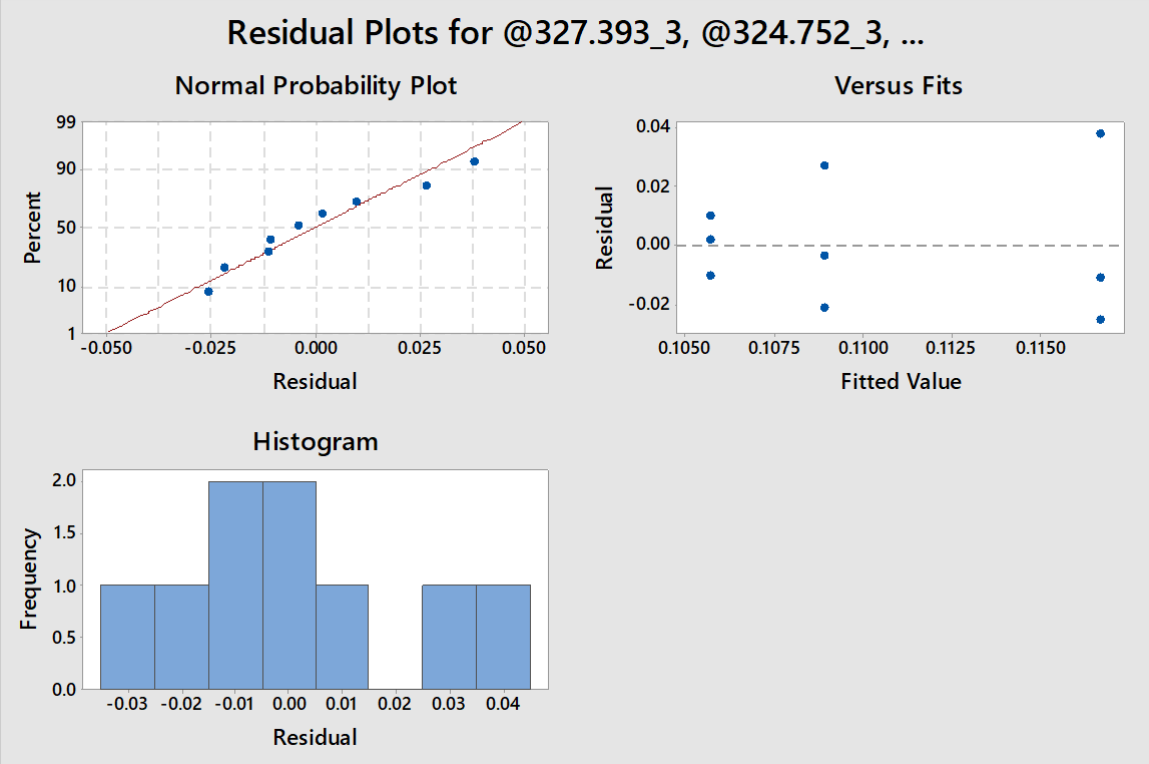

Figure 82: Normal probability plot, residuals vs fit and histogram of frequency vs residuals obtained for the ANOVA for the analysis of 0.3mg.L^{-1} samples analysed by ICP-OES at pH 7.

The normal probability plot indicates that the data is normally distributed and the vs. fits plot indicates the residuals are randomly distributed. In this case the histogram does indicate a normal distribution.

Appendix 18. ANOVA Charts for Section 4.2.1: 0.4mg.L^{-1} at pH 7

The charts produced in Minitab® for the ANOVA for the 0.4mg.L^{-1} samples obtained from the pH 7 experiments are displayed in Figure 83.

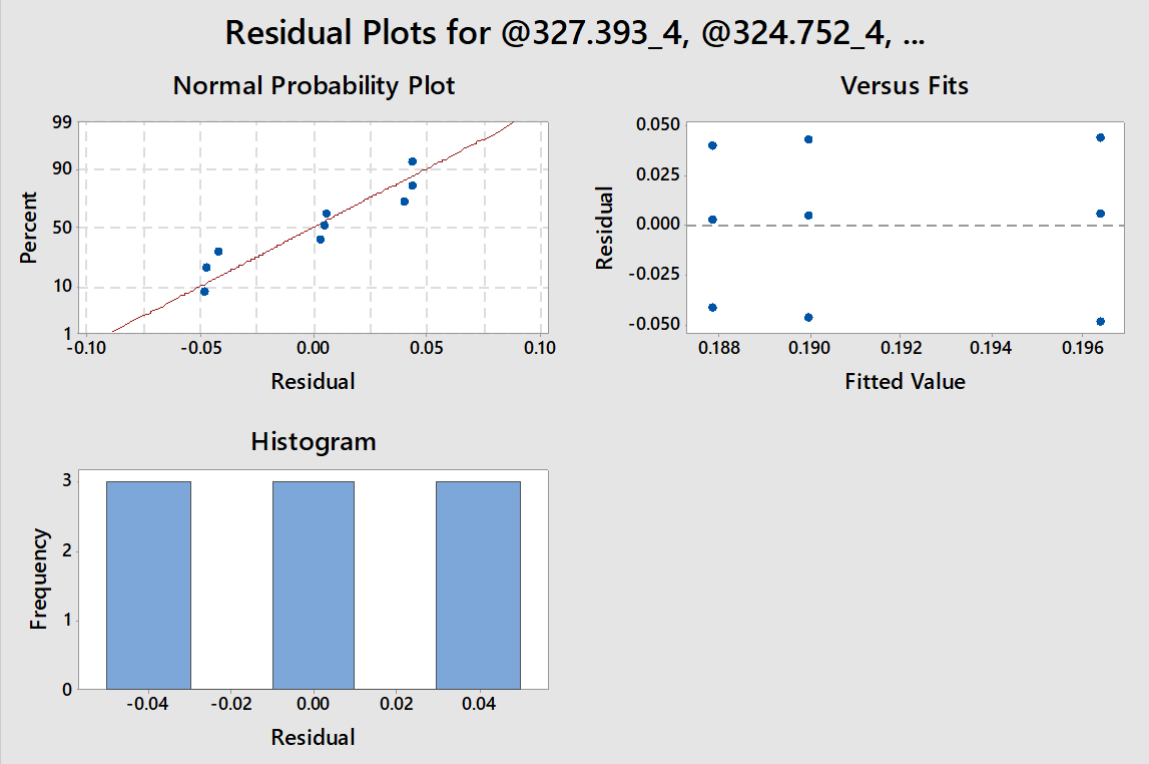

Figure 83: Normal probability plot, residuals vs fit and histogram of frequency vs residuals obtained for the ANOVA for the analysis of 0.4mg.L^{-1} samples analysed by ICP-OES at pH 7.

The normal probability plot indicates that the data is normally distributed and the vs. fits plot indicates the residuals are randomly distributed. In this case the histogram does not indicate a normal distribution.

Appendix 19. ANOVA Charts for Section 4.2.1: 0.5mg.L^{-1} at pH 7

The charts produced in Minitab® for the ANOVA for the 0.5mg.L^{-1} samples obtained from the pH 7 experiments are displayed in

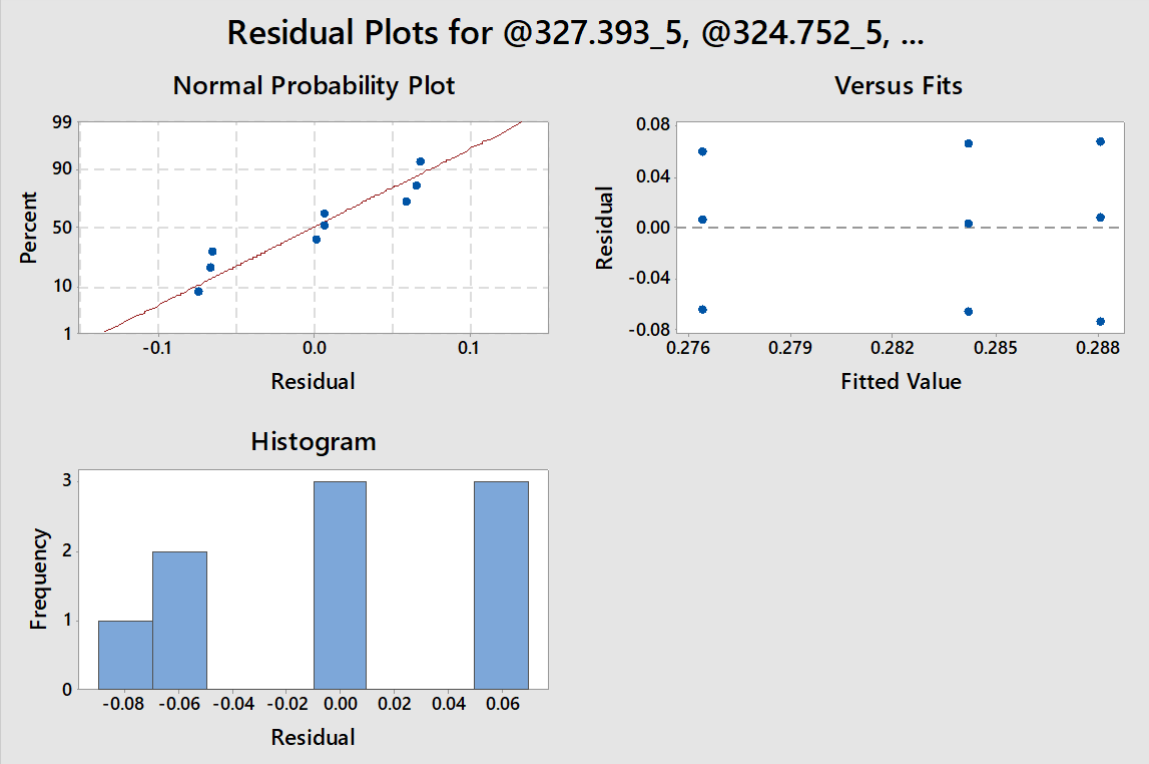

Figure 84: Normal probability plot, residuals vs fit and histogram of frequency vs residuals obtained for the ANOVA for the analysis of 0.5mg.L^{-1} samples analysed by ICP-OES at pH 7.

The normal probability plot indicates that the data is normally distributed and the vs. fits plot indicates the residuals are randomly distributed. In this case the histogram does not indicate a normal distribution.

Appendix 20. ANOVA Charts for Section 4.2.1: pH and Cu^{2+} stability

In this section the charts produced during the ANOVA for investigating the stability of the copper ions with varying pH. The scatter plot displayed in Figure 16 appear to show little difference between the data obtained for pH 3 and pH 5. However on analysis of the ANOVA, there was no significant difference in the data obtained between the four datasets. Residual plots are displayed in Figure 85.

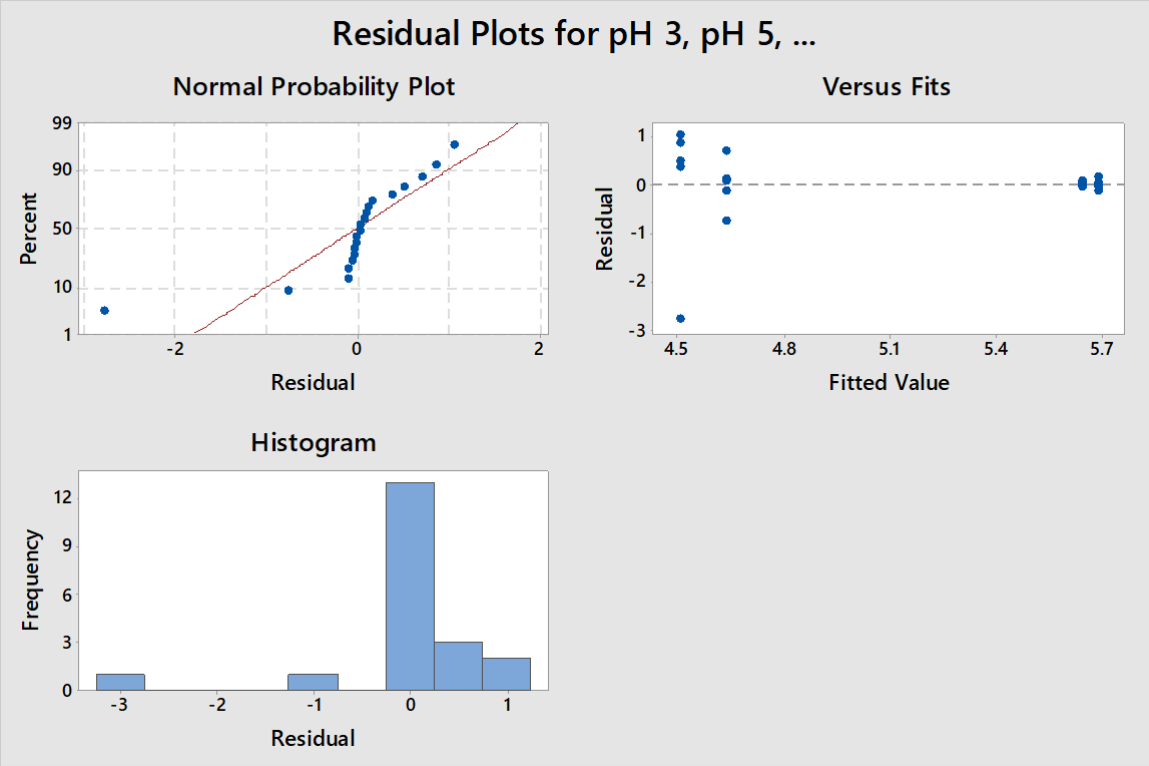

Figure 85: Normal probability plot, residuals vs fit and histogram of frequency vs residuals obtained for the ANOVA for the analysis of the copper samples obtained from solutions maintained at pH 3, pH 5, pH 7 and pH 9.

In this analysis there is an observable outlier in the normal probability plot and the histogram. The residuals vs. fits do not show randomised residuals. A Tuckey analysis was performed to determine whether there was a significant difference between the means of each dataset. This is displayed in Figure 86.

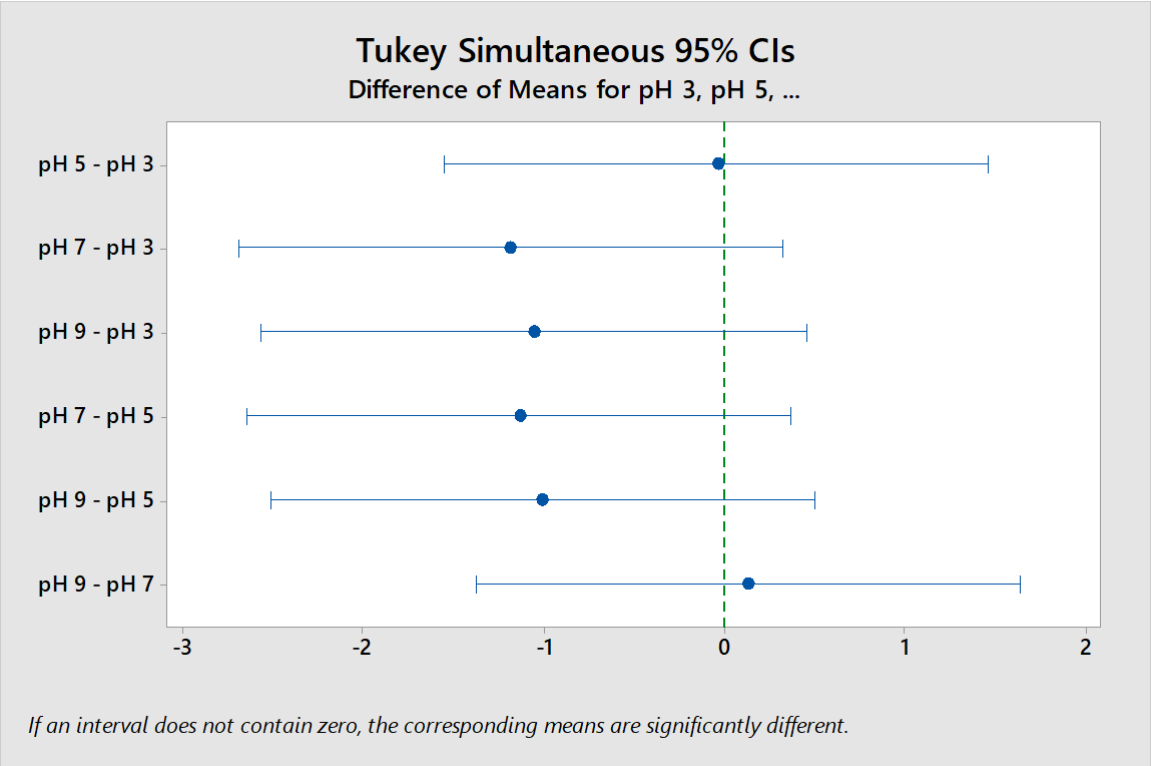

Figure 86: Tukey analysis of the copper samples obtained from solutions maintained at pH 3, pH 5, pH 7 and pH 9.

The Tukey analysis indicates that there is no significant difference in the means of each dataset.

Appendix 21. Linearising Langmuir Isotherms

There are four methods of linearising the Langmuir Isotherm.

Hanes-Woolf linearisation:

$$\frac{C_e}{Q_e} = \left(\frac{1}{Q_{max}}\right) C_e + \frac{1}{Q_{max} b_L}$$

Lineweaver-Burk Linearization:

$$\frac{1}{Q_e} = \left(\frac{1}{Q_{max} b_L}\right) \frac{1}{C_e} + \frac{1}{Q_{max}}$$

Eadie-Hoffsiee linearisation:

$$Q_e = \left(-\frac{1}{b_L}\right) \frac{Q_e}{C_e} + Q_{max}$$

Scatchard Linearisation

$$\frac{Q_e}{C_e} = -b_L Q_e + Q_{max} b_L$$

The data for copper adsorption by *C. vulgaris* was not represented by the Langmuir isotherm when the Lineweaver-Burk method of linearisation was used. Linearisation using the other three methods produced Langmuir parameters as shown in

Table 65: Langmuir Parameters calculated using the Hanes-Woolf, Eadie-Hoffsiee and Scatchard linearisation methods. As with the Lineweaver-Burk method, the other three linearisation methods did not produce Langmuir parameters that made physical sense.

Linearisation Method	Q_{max}	b_L
Hanes-Woolf	-0.13	-1.18
Eadie-Hoffsiee	-0.04	-16.06
Scatchard	0.65	-0.06

Appendix 22. Other Adsorption Isotherms

The BET isotherm has the following form for adsorption from an aqueous solution.

$$\frac{C_e}{Q_e(C_s - C_e)} = \left[\frac{K_{BET} - 1}{K_{BET} Q_{max}}\right] \cdot \left(\frac{C_e}{C_s}\right) + \frac{1}{K_{BET} Q_{max}}$$

K_{BET} is found from the linear BET plot by dividing the gradient by the y-axis intercept, plus 1. Q_{max} is calculated by taking the reciprocal of the y-axis intercept multiplied by K_{BET}. C_s is the saturation concentration of the adsorbate.

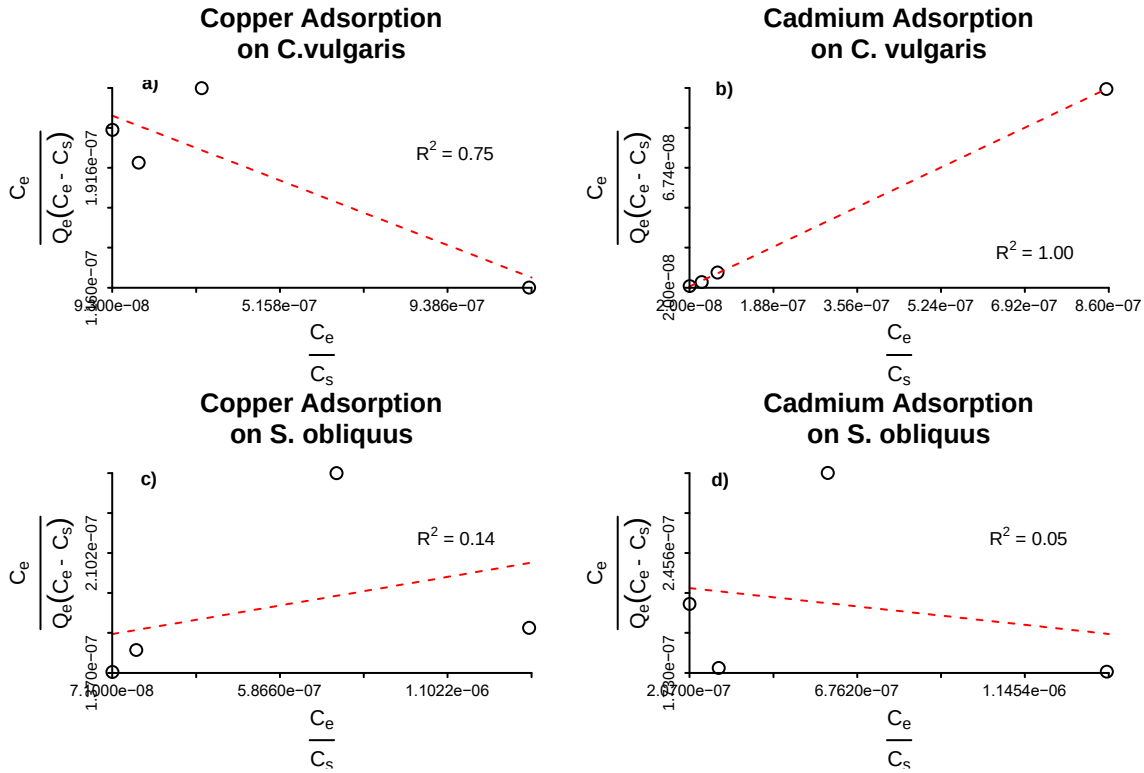

Figure 87: BET Isotherms

Table 66: BET isotherm model parameters for copper and cadmium adsorption by *C. vulgaris* and *S. obliquus*.

Microalgae	Metal	Q_{max} (mg.g^{-1})	K_{BET} (L.mg^{-1})
C. vulgaris	Copper	-10.35	-4.1×10^{5}
C. vulgaris	Cadmium	10.69	5.0×10^{6}
S. obliquus	Copper	29.52	2.1×10^{5}
S. obliquus	Cadmium	-42.19	-1.0×10^{5}

The Dubinin-Radushkevich has the following form

$$\ln(Q_e) = \ln(Q_s) - K_{ad}\varepsilon^2$$

Where:

$$\varepsilon = RT\ln\left(1 + \frac{1}{C_e}\right)$$

K_{ad} is calculated from the negative value of the gradient of the linear plot, and the adsorbate saturation value (Q_s) is found by taking the exponential of the y-axis intercept.

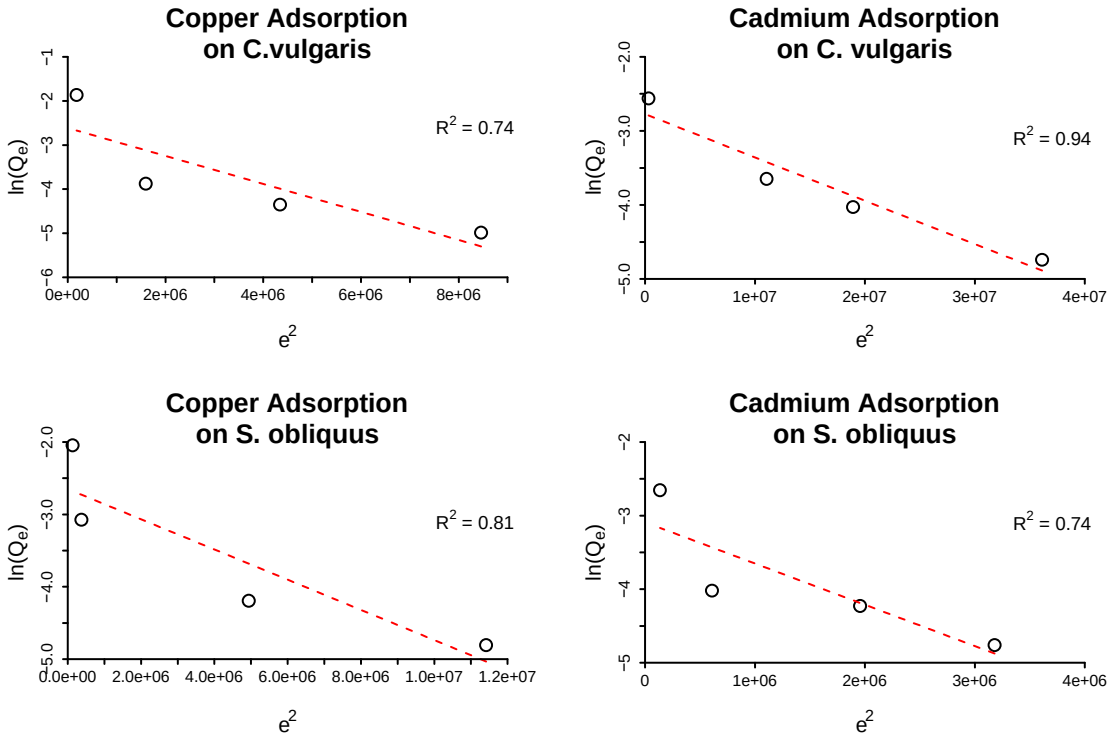

Figure 88: Dubinin-Radushkevich Isotherms

Table 67: Dubinin-Radushkevich isotherm model parameters for copper and cadmium adsorption by *C. vulgaris* and *S. obliquus*.

Microalgae	Metal	Q_s (mg.g^{-1})	K_{ad} (mol^2.kJ^{-2})
C. vulgaris	Copper	1.15	3.2×10^{-7}
C. vulgaris	Cadmium	0.56	5.9×10^{-8}
S. obliquus	Copper	1.11	2.1×10^{-7}
S. obliquus	Cadmium	0.40	5.6×10^{-7}

The Elovich Isotherm has the following linear form:

$$\ln\left(\frac{Q_e}{C_e}\right) = \ln(K_e Q_m) - \frac{Q_e}{Q_m}$$

Q_m is calculated by multiplying the reciprocal of the gradient by negative one. K_e is calculated by dividing the exponential of the y-axis intercept by Q_m.

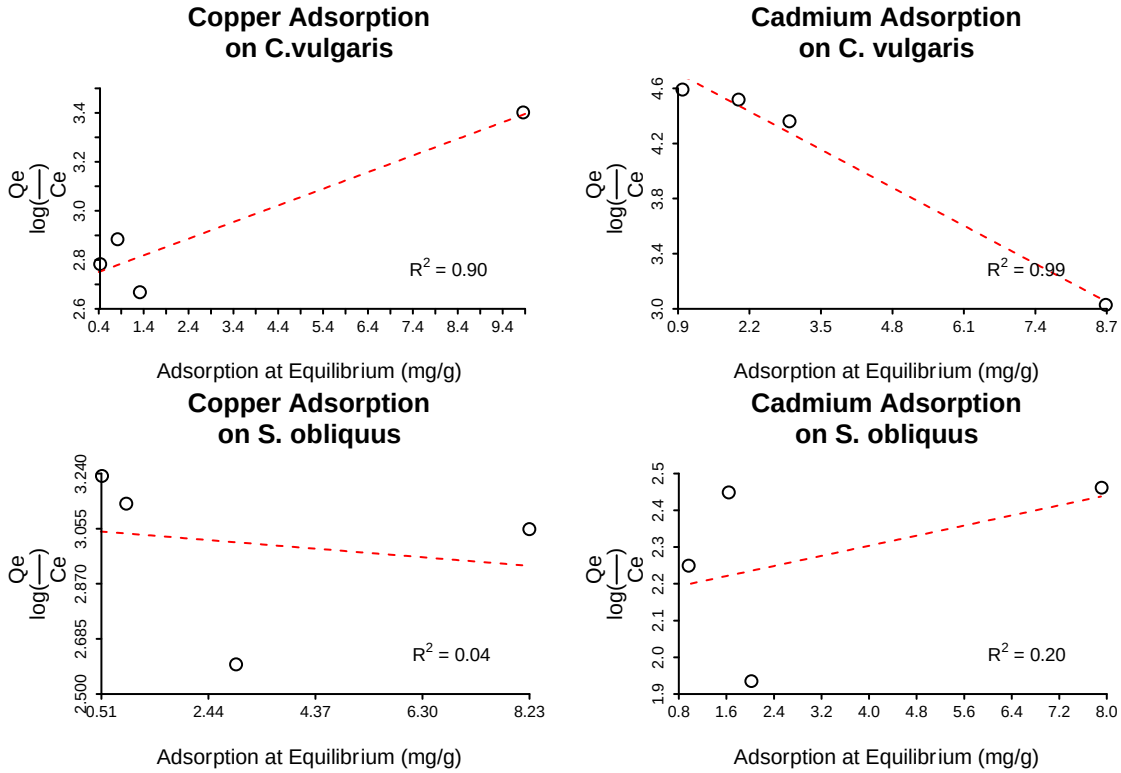

Figure 89: Elovich Isotherm

Table 68: Elovich isotherm model parameters for copper and cadmium adsorption by *C. vulgaris* and *S. obliquus*.

Microalgae	Metal	Q_m (mg.g^{-1})	K_e (L.mg^{-1})
C. vulgaris	Copper	-14.7	-1.0
C. vulgaris	Cadmium	4.7	28.5
S. obliquus	Copper	67.0	0.3
S. obliquus	Cadmium	-29.1	-0.3

The Flory-Huggins isotherm has the following linear form:

$$\log\left(\frac{\theta}{C_0}\right) = \log(K_{FH}) + n_{FH}\log(1 - \theta)$$

Where

$$\theta = 1 - \frac{C_e}{C_0}$$

Where θ is the fraction of adsorbate removal. n_{FH} is equivalent to the gradient of the linear Flory-Huggins plot. K_{FH} is calculated by rising ten to the power of the value of the y-axis intercept.

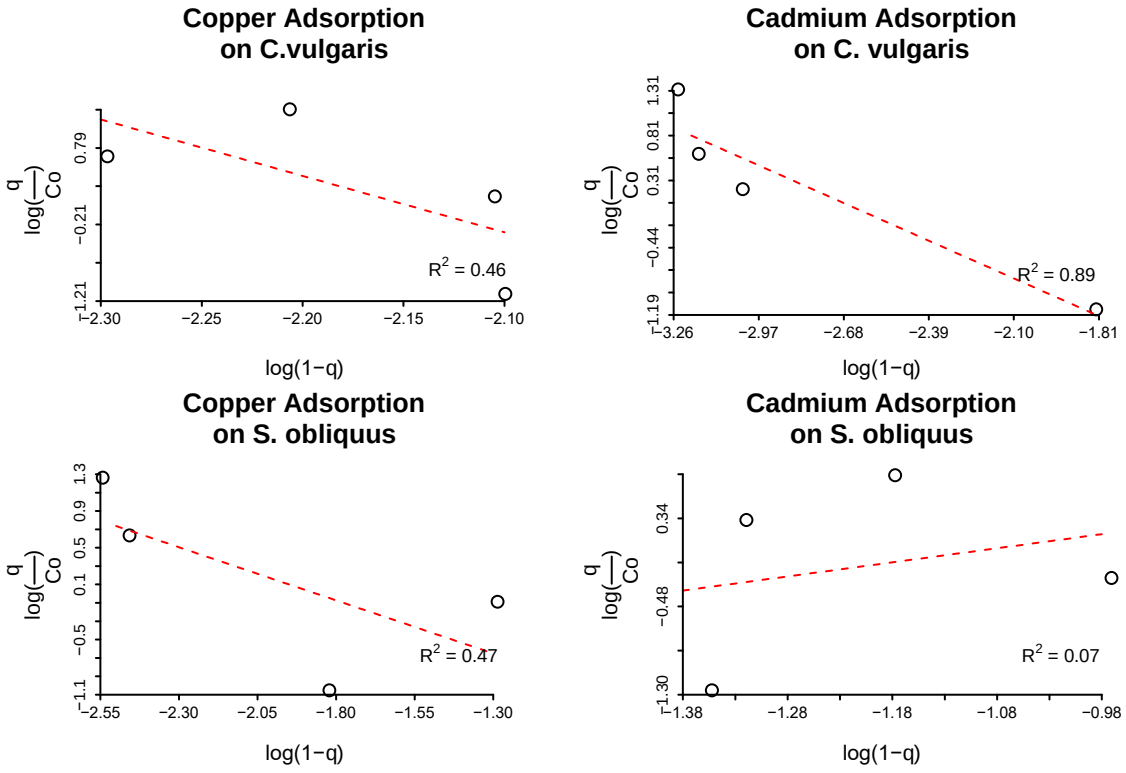

Figure 90: Flory-Huggins Isotherms

Table 69: Flory-Huggins isotherm model parameters for copper and cadmium adsorption by *C. vulgaris* and *S. obliquus*.

Microalgae	Metal	K_F (L.mg^{-1})	n_F
C. vulgaris	Copper	1.4×10^{-7}	-7.4
C. vulgaris	Cadmium	28.5	-1.4
S. obliquus	Copper	0.1	-1.2
S. obliquus	Cadmium	4.4	1.3

The Kiselev isotherm has the following linear form:

$$\frac{1}{C_e(1-\theta)} = K_{1K}\theta^{-1} + K_{1K}K_n$$

Where K_{1K} is the equilibrium constant (L.mg^{-1}), equivalent to the gradient of the linear Flory-Huggins plot. K_n is a constant associated with the formation of adsorbate, adsorbent complexes. This is calculated by dividing the y-axis intercept by K_{1K}.

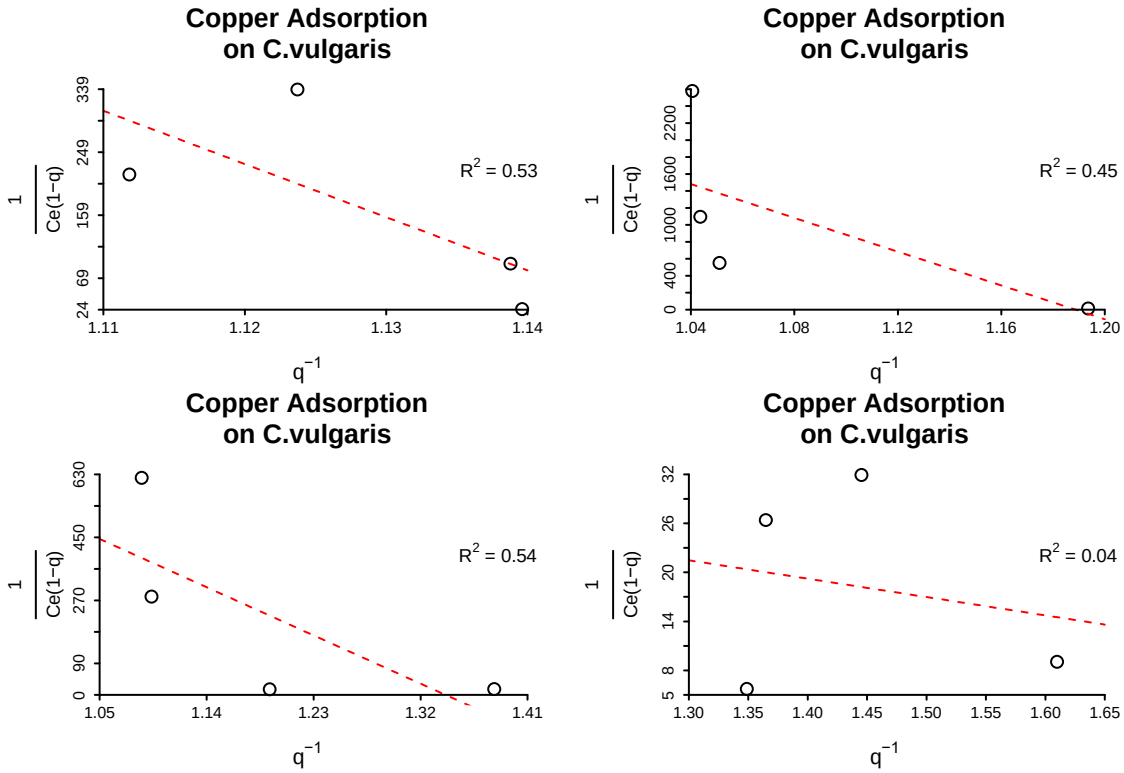

Figure 91: Kiselev Isotherm

Table 70: Kiselev isotherm model parameters for copper and cadmium adsorption by *C. vulgaris* and *S. obliquus*.

Microalgae	Metal	K_{1K} (L.mg^{-1})	K_n
C. vulgaris	Copper	-7600.9	-1.2
C. vulgaris	Cadmium	-9957.1	-1.2
S. obliquus	Copper	-1530.7	-1.3
S. obliquus	Cadmium	-22.5	-2.3

Appendix 23. Lagergren Model Parameters Various Concentrations

Table 71: Parameters derived for the pseudo-first order model. C0 represents the initial metal concentration (mg/L), Qe0 represents the extent of adsorption at equilibrium determined from the linearized model (mg/L), and k0 is the first order rate constant determined from the linearized model (s^{-1}). Qe and k were determined by least squares method.

Algae Species	Algae Concentration (mg/L)	Metal	C0 (mg/L)	Qe0 (mg/g)	k0	Qe	k
Scenedesmus obliquus	236.83	Cadmium	0.33	0.39	-0.08	0.94	-0.26
Scenedesmus obliquus	236.83	Cadmium	0.53	0.33	-0.05	1.61	-0.32
Scenedesmus obliquus	236.83	Cadmium	0.77	0.09	0.01	NA	NA
Scenedesmus obliquus	244.55	Cadmium	2.61	2.48	-0.09	7.93	-0.24
Scenedesmus obliquus	462.47	Copper	0.26	0.06	-0.09	0.52	-0.70
Scenedesmus obliquus	462.47	Copper	0.49	0.17	-0.10	0.95	-0.44
Scenedesmus obliquus	194.59	Copper	0.79	1.35	-0.05	2.80	-0.19
Scenedesmus obliquus	244.55	Copper	2.40	1.82	-0.09	8.19	-0.39
Chlorella vulgaris	250	Cadmium	0.26	0.04	-0.08	NA	NA
Chlorella vulgaris	250	Cadmium	0.52	0.16	-0.08	NA	NA
Chlorella vulgaris	250	Cadmium	0.77	0.24	-0.06	NA	NA
Chlorella vulgaris	250	Cadmium	2.59	1.26	-0.07	NA	NA
Chlorella vulgaris	500	Copper	0.24	0.03	-0.06	NA	NA
Chlorella vulgaris	500	Copper	0.46	0.08	-0.06	0.81	-0.46
Chlorella vulgaris	500	Copper	0.75	0.19	-0.05	1.30	-0.50
Chlorella vulgaris	238.58	Copper	2.68	1.27	-0.09	9.89	-0.59

Appendix 24. Lagergren and Elovich modified model for mixed metal uptake.

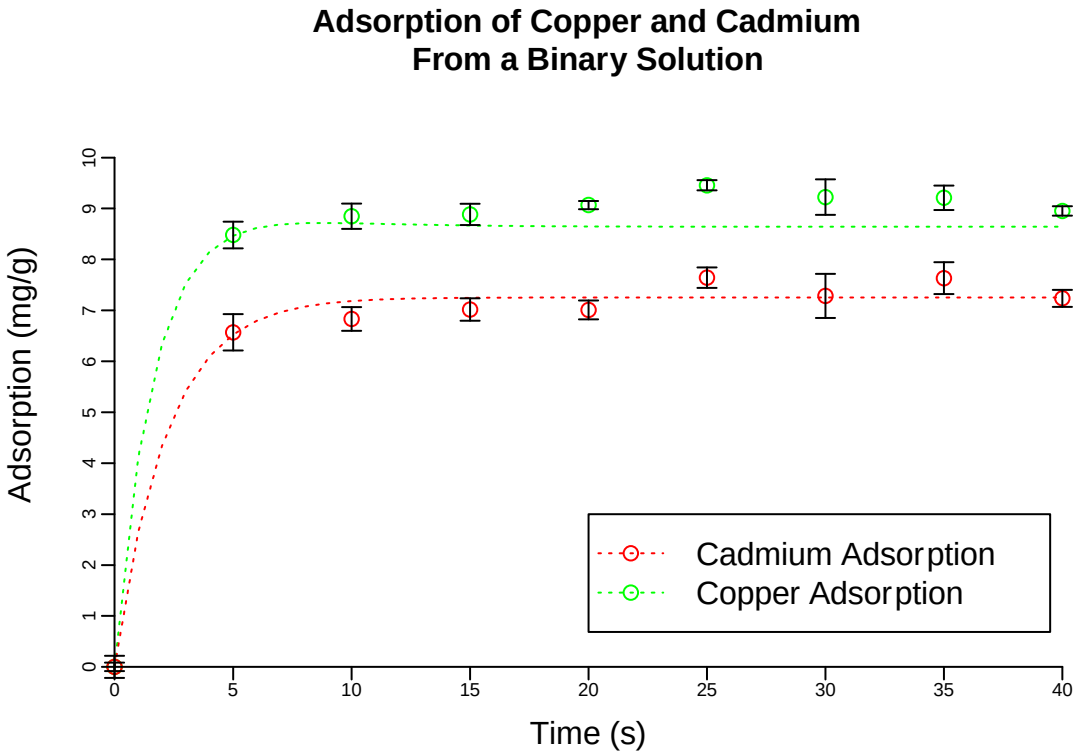

Figure 92: Adsorption-time profiles for copper and cadmium uptake by *C. vulgaris* from a binary metal solution (green open circles – copper, red open circles - cadmium), vs additive, Lagergren predictions using parameters fitted to the experimental data (dashed green line – copper predictions; dashed red line – cadmium uptake predictions).

The combined Lagergren model has the form:

$$Q_t = Q_{e,s}(1 - e^{-k_s t}) - Q_{-1}(1 - e^{-k_{-1} t})$$

The values of $Q_{e,s}$ and k_s were calculated in Section 6.1.1, and these represent the adsorption at equilibrium and the first order uptake rate for metal uptake from a single metal mixture, respectively.

Table 72: Model parameters derived for an additive Lagergren model that incorporates an inhibition term to the model for metal uptake from a single mixture to fit the model to the data obtained from a binary metal mixture.

Metal Species	$Q_{e,s}$	k_s	Q_{-1}	k_{-1}
Copper	9.89	0.59	1.25	0.26
Cadmium	9.13	0.48	1.87	0.57

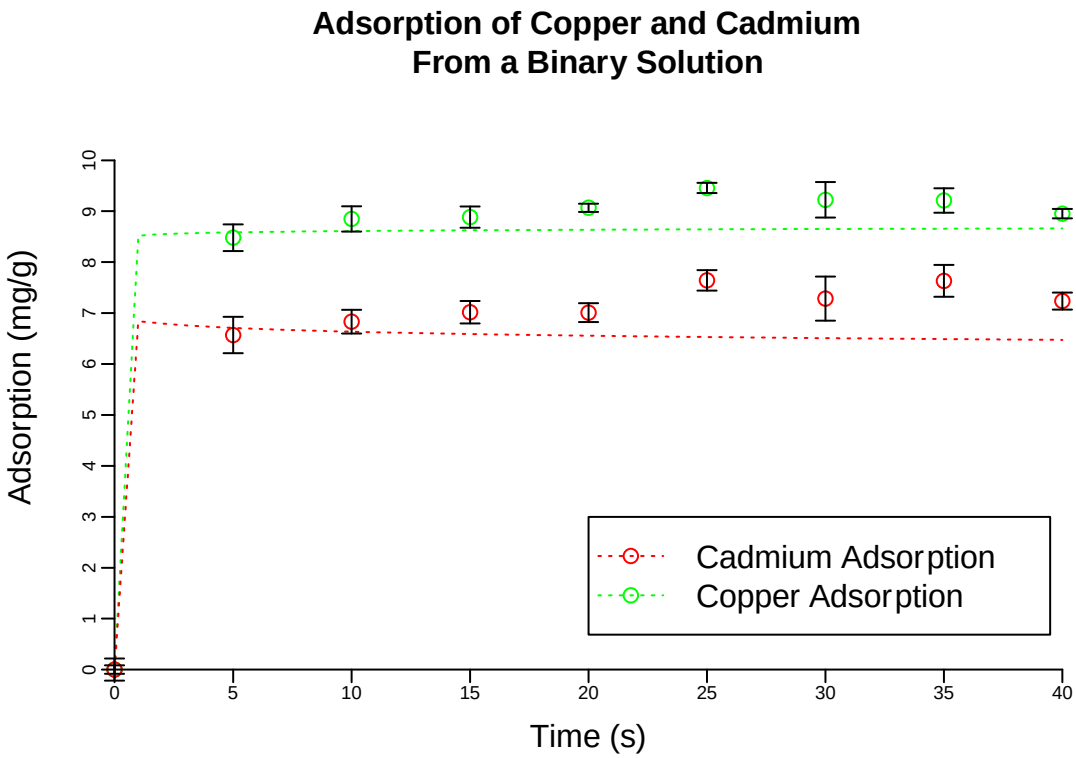

Figure 93: Adsorption-time profiles for copper and cadmium uptake by *C. vulgaris* from a binary metal solution (green open circles – copper, red open circles - cadmium), vs additive, Elovich predictions using parameters fitted to the experimental data (dashed green line – copper predictions; dashed red line – cadmium uptake predictions).

The combined Elovich model has the form

$$Q_t = \frac{1}{\beta_s}\ln(\alpha_s\beta_s t + 1) - \frac{1}{\beta_{-1}}\ln(\alpha_{-1}\beta_{-1}t + 1)$$

The values of α_s and β_s were calculated in Section 6.2.3.1 and these represent the maximum adsorption rate and desorption constant for metal sorption from a single metal solution.

Table 73: Model parameters derived for an additive Elovich model that incorporates an inhibition term to the model for metal uptake from a single mixture to fit the model to the data obtained from a binary metal mixture.

Metal Species	α_s	β_s	α_{-1}	β_{-1}
Copper	1.4×10^{18}	4.7	8.0	5.7
Cadmium	1.1×10^{8}	2.5	3.14	1.9

Appendix 25. Second Order Model Parameters Mixed Concentrations

Table 74: Parameters calculated and fitted to the pseudo-second order model. Calculated parameters, *'0'* were similar to those fitted by the non-linear least squares method.

Algae Species	Algae Concentration	Metal	C0	Qe0 mg/g	k0	Qe	k
Scenedesmus obliquus	236.83	Cadmium	0.33	1.00	0.50	1.00	0.48
Scenedesmus obliquus	236.83	Cadmium	0.53	1.68	0.44	1.68	0.41
Scenedesmus obliquus	236.83	Cadmium	0.77	2.03	2.08	2.06	1.44
Scenedesmus obliquus	244.55	Cadmium	2.61	8.59	0.05	8.72	0.04
Scenedesmus obliquus	462.47	Copper	0.26	0.52	6.89	0.52	6.66
Scenedesmus obliquus	462.47	Copper	0.49	0.99	1.28	0.99	1.26
Scenedesmus obliquus	194.59	Copper	0.79	2.97	0.13	3.09	0.09
Scenedesmus obliquus	244.55	Copper	2.40	8.57	0.11	8.60	0.11
Chlorella vulgaris	250	Cadmium	0.26	0.99	5.43	0.99	5.46
Chlorella vulgaris	250	Cadmium	0.52	2.01	1.70	2.01	1.66
Chlorella vulgaris	250	Cadmium	0.77	2.93	5.29	2.93	5.24
Chlorella vulgaris	250	Cadmium	2.59	8.69	1.55	8.75	1.15
Chlorella vulgaris	500	Copper	0.24	0.44	4.06	0.44	4.06
Chlorella vulgaris	500	Copper	0.46	0.83	1.89	0.83	1.88
Chlorella vulgaris	500	Copper	0.75	1.32	1.28	1.33	1.22
Chlorella vulgaris	238.58	Copper	2.68	10.02	0.32	10.02	0.33

Appendix 26. ANOVA Comparing Lagergren, Second-order and Elovich predictions for Adsorption at Equilibrium Copper Adsorbed by *C. vulgaris*

ANOVA analysis for comparing the models fitted to the adsorption kinetics of Cu^{2+} adsorbed by *C. vulgaris* are displayed in Figure 94.

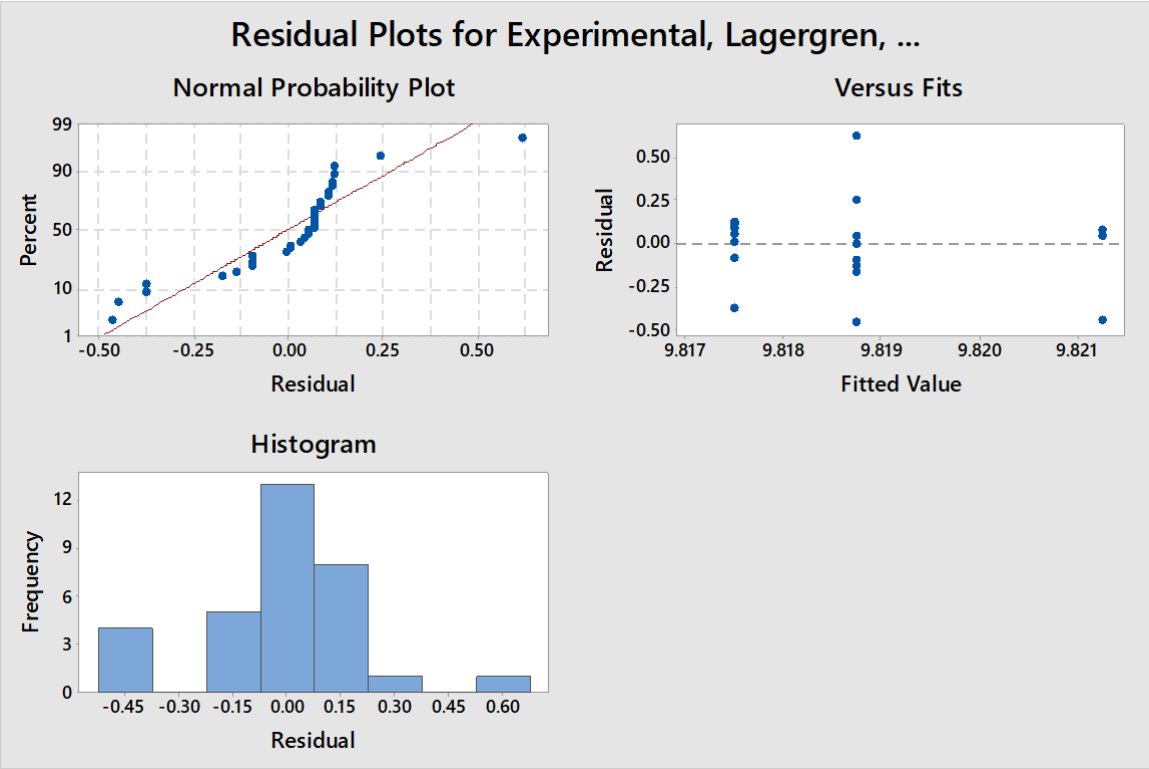

Figure 94: Normal probability plot, residuals vs fit and histogram of frequency vs residuals obtained for the ANOVA for the adsorption at equilibrium values predicted by the Lagergren model, second-order model and Elovich model for Cu^{2+} adsorption by *C. vulgaris*.

The residuals are normally distributed and randomised.

```
Analysis of Variance

Source  DF   Adj SS    Adj MS  F-Value  P-Value
Factor   3  0.00008  0.000025     0.00    1.000
Error   28  1.35888  0.048531
Total   31  1.35895


Model Summary

        S   R-sq  R-sq(adj)  R-sq(pred)
0.220298  0.01%      0.00%       0.00%

Means

Factor         N    Mean   StDev        95% CI
Experimental   8   9.819   0.322  ( 9.659,  9.978)
Lagergren      8  9.8213  0.1826  (9.6617, 9.9808)
second order   8  9.8175  0.1689  (9.6580, 9.9770)
Elovich        8  9.8175  0.1689  (9.6580, 9.9770)
```

Appendix 27. ANOVA Comparing Lagergren, Second-order and Elovich predictions for Adsorption at Equilibrium Cadmium Adsorbed by *C. vulgaris*

ANOVA analysis for comparing the models fitted to the adsorption kinetics of Cd^{2+} adsorbed by *C. vulgaris* are displayed in Figure 95.

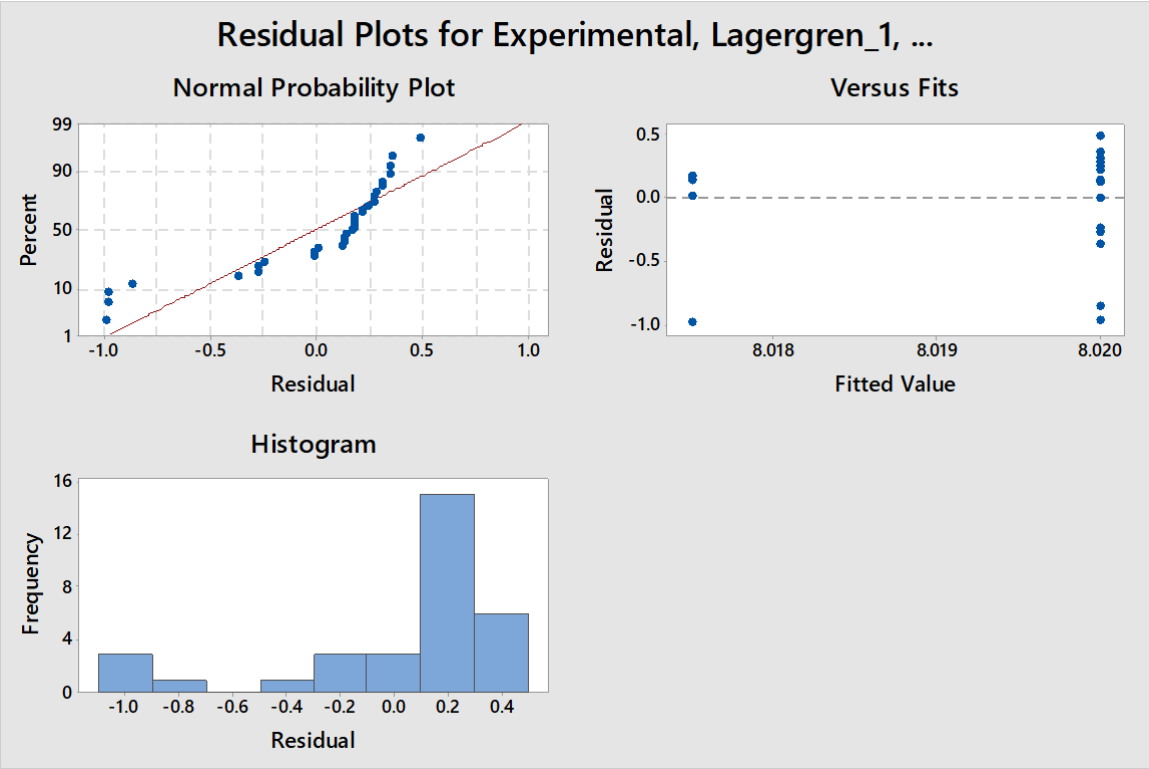

Figure 95: Normal probability plot, residuals vs fit and histogram of frequency vs residuals obtained for the ANOVA for the adsorption at equilibrium values predicted by the Lagergren model, second-order model and Elovich model for Cd^{2+} adsorption by *C. vulgaris*.

The residuals are normally distributed and randomised.

```
Analysis of Variance

Source  DF   Adj SS    Adj MS  F-Value  P-Value
Factor   3  0.00004  0.000013     0.00    1.000
Error   28  5.41995  0.193570
Total   31  5.41999


Model Summary

        S   R-sq  R-sq(adj)  R-sq(pred)
0.439966  0.00%      0.00%       0.00%

Means

Factor          N   Mean  StDev      95% CI
Experimental_1  8  8.020  0.459  (7.701, 8.339)
Lagergren_1     8  8.018  0.407  (7.699, 8.336)
second order_1  8  8.020  0.446  (7.701, 8.339)
Elovich_1       8  8.020  0.446  (7.701, 8.339)
```

Appendix 28. ANOVA Comparing Lagergren, Second-order and Elovich predictions for Adsorption at Equilibrium Copper Adsorbed by *S. obliquus*

ANOVA analysis for comparing the models fitted to the adsorption kinetics of Cu^{2+} adsorbed by *S. obliquus* are displayed in Figure 96.

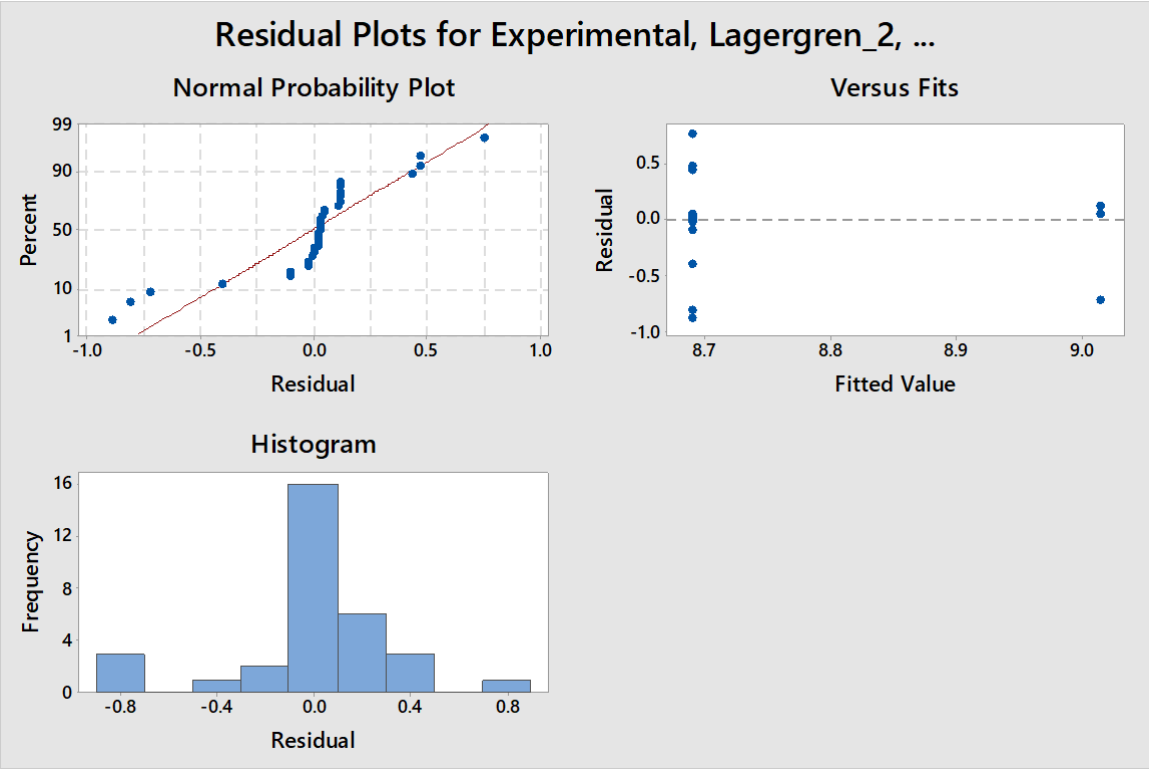

Figure 96: Normal probability plot, residuals vs fit and histogram of frequency vs residuals obtained for the ANOVA for the adsorption at equilibrium values predicted by the Lagergren model, second-order model and Elovich model for Cu^{2+} adsorption by *S. obliquus*.

The residuals are normally distributed and randomised.

```
Analysis of Variance

Source  DF  Adj SS  Adj MS  F-Value  P-Value
Factor   3  0.6289  0.2096     1.70    0.189
Error   28  3.4440  0.1230
Total   31  4.0729


Model Summary

       S    R-sq  R-sq(adj)  R-sq(pred)
0.350713  15.44%      6.38%       0.00%

Means

Factor          N    Mean   StDev        95% CI
Experimental_2  8   8.690   0.633  ( 8.436,  8.944)
Lagergren_2     8   9.014   0.294  ( 8.760,  9.268)
second order_2  8  8.6900  0.0496  (8.4360, 8.9440)
Elovich_2       8  8.6900  0.0496  (8.4360, 8.9440)
```

Appendix 29. ANOVA Comparing Lagergren, Second-order and Elovich predictions for Adsorption at Equilibrium Cadmium Adsorbed by *S. obliquus*

ANOVA analysis for comparing the models fitted to the adsorption kinetics of Cd^{2+} adsorbed by *S. obliquus* are displayed in Figure 97.

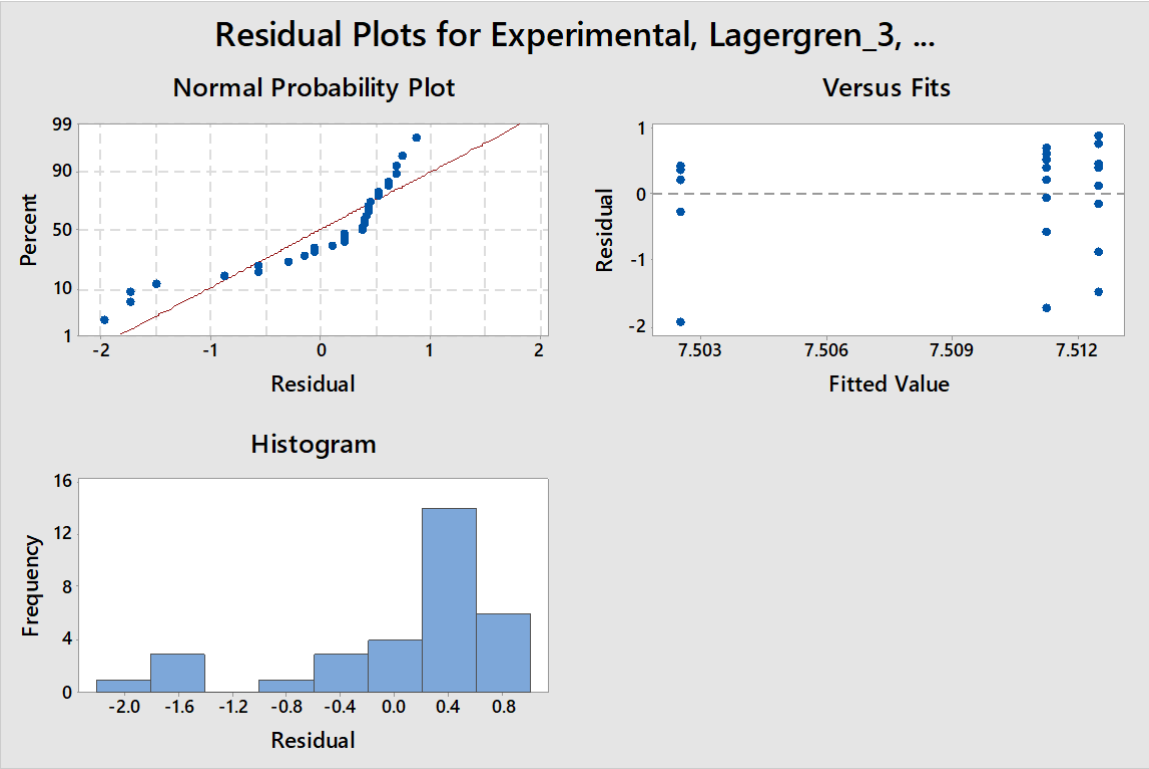

Figure 97: Normal probability plot, residuals vs fit and histogram of frequency vs residuals obtained for the ANOVA for the adsorption at equilibrium values predicted by the Lagergren model, second-order model and Elovich model for Cd^{2+} adsorption by *S. obliquus*.

The residuals are normally distributed and randomised.

```
Analysis of Variance

Source  DF   Adj SS    Adj MS  F-Value  P-Value
Factor   3   0.0005  0.000171     0.00    1.000
Error   28  19.0285  0.679588
Total   31  19.0290


Model Summary

       S   R-sq  R-sq(adj)  R-sq(pred)
0.824372  0.00%      0.00%       0.00%

Means

Factor          N   Mean  StDev      95% CI
Experimental_3  8  7.512  0.824  (6.915, 8.110)
Lagergren_3     8  7.503  0.834  (6.905, 8.100)
second order_3  8  7.511  0.820  (6.914, 8.108)
Elovich_3       8  7.511  0.820  (6.914, 8.108)
```

Appendix 30. Examples of Metal Sorption by Microalgae

Table 75: List of algae and their known metals that they can sequester. Unless stated otherwise, all information obtained from Mehta et al [9]

Algae Species	Algae Type	Metal
Anacystis nidulans	Cyanobacteria	Chromium[10]
Anabaena Doliolum	Cyanobacteria	Nickel[10], Cadmium[10], Iron[10]
Anabaena Nodosum	Cyanobacteria	Cadmium[9]
Chlamydomonas Reinhardtii	Chlorophyta	Mercury[10], Cadmium[10], Lead[10]
Chlorella Emersonii	Chlorophyta	Mercury[10]
Chlorella Homosphaera	Chlorophyta	Gold[10], Nickel[10], Zinc[10]
Chlorella Miniata	Chlorophyta	Nickel[9], Zinc[9]
Chlorella Minimata	Chlorophyta	Nickel[9]
Chlorella Sorokiniana	Chlorophyta	Nickel[9, 10], Zinc, Lead[10], Cadmium[10]
Chlorella Vulgaris	Chlorophyta	Copper[9, 10], Gold[9], Cadmium[9, 10], Mercury[10] Nickel[9, 10], Lead[10], Zinc[9], Chromium (VI)[10], Iron[10]
Chlorella salina	Chlorophyta	Cobalt[10]
Cladophora Crispata	Chlorophyta	Zinc[9]
Lyngbya Taylorii	Cyanobacteria	Cadmium[9], Nickel[9], Lead[9], Zinc[9]
Microcystis Aeruginosa	Cyanobacteria	Copper[9], Nickel[9]
Microcystis Sp	Cyanobacteria	Copper[9], Zinc[9]
Nannochloropsis Oculata	Ochrophyta	Cadmium[9]
Oscillatoria Angustissima	Cyanobacteria	Copper[9], Zinc[9], Cobalt[9]
Phaeodactylum Tricornutum	Bacillariophyta	Cadmium[9]
Porphyridium Cruentum	Rhodophyta	Cadmium[9]
Scenedesmus *various*	Chlorophyta	Uranium[10], copper[10], cadmium[10] and zinc[10].
Scenedesmus Obliquus	Chlorophyta	Nickel[9], Cobalt[10], Chromium[10].
Scenedesmus Quadricauda	Chlorophyta	Nickel[9], Zinc[9]
Scenedesmus Acutus	Chlorophyta	Cadmium[10]
Schizomeris leibleinii	Chlorophyta	Lead[9]
Spirulina Platensis	Cyanobacteria	Copper[9], Cadmium[9], Lead[9], Zinc[9]
Spirulina Sp	Cyanobacteria	Copper[9], Aluminium[9], Cadmium[9], Chromium (III)[9], Mercury[9], Nickel[9], Lead[9], Zinc[9], Cobalt[9]

Algae Species	Algae Type	Metal
Spirulina Maxima	Cyanobacteria	Cadmium[10]
Synechococcus Sp	Cyanobacteria	Copper[9], Cadmium[9], Chromium (III)[9], Nickel[9], Lead[9]
Tetraselmis Chui	Chlorophyta	Cadmium[10], Copper[10]
Dunaliella Salina	Chlorophyta	Iron[193], Cadmium[194]